GEORGIA INSTITUTE OF TECHNOLOGY — OFFICE OF CONTRACT ADMINISTRATION

PROJECT ADMINISTRATION DATA SHEET

[X] ORIGINAL [ ] REVISION NO. ______

Project No./(Center No.) E-21-603 (R6239-0A0) GTRC/~~GIT~~ DATE 11 / 25 / 86

Project Director: A. Rohatgi School/~~Lab~~ EE

Sponsor: Sandia National Laboratories

Agreement No.: Contract No. 02-2255

Award Period: From 10/28/86 To ~~10/27/87~~ 2/28/88 (Performance) ______ Reports

Sponsor Amount:

	New With This Change	Total to Date
Contract Value:	$	$ 32,383
Funded:	$	$ 32,383

Cost Sharing No./(Center No.) ______ Cost Sharing: $ ______

Title: Research on AlGaAs/GaAs Interfaces in GaAs Solar Cells

ADMINISTRATIVE DATA

OCA Contact John B. Schonk X4820

1) Sponsor Technical Contact:

J. Gee
Sandia National Laboratories
P. O. Box 5800
Albuquerque, NJ 87185-5800
505-844-7812

2) Sponsor Issuing Office:

J. B. Romano
Sandia National Laboratories
Purchasing Organization 3716
P. O. Box 5800
Albuquerque, NJ 87185-5800
505/844-5174

Military Security Classification: ______
(or) Company/Industrial Proprietary: ______

ONR Resident Rep. is ACO: ______ Yes ______ No
Defense Priority Rating: ______

RESTRICTIONS

See Attached ______ Supplemental Information Sheet for Additional Requirements.

Travel: Foreign travel must have prior approval — Contact OCA in each case. Domestic travel requires sponsor approval where total will exceed greater of $500 or 125% of approved proposal budget category.

Equipment: Title vests with Gov't

COMMENTS:

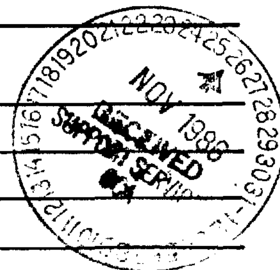

SPONSOR'S I.D. NO. 02.240.003.87.001

COPIES TO:

Project Director
Research Administrative Network
Research Property Management
Accounting

Procurement/GTRI Supply Services
~~Research Security Services~~
Contract Support Div.(OCA)(2) AH

GTRC
Library
Project File

GEORGIA INSTITUTE OF TECHNOLOGY OFFICE OF CONTRACT ADMINISTRATION

SPONSORED PROJECT TERMINATION/CLOSEOUT SHEET

Date 7/6/88

Project No. E-21-603 School/Lab EE

Includes Subproject No.(s) N/A

Project Director(s) A. Rohatgi GTRC/GIT

Sponsor Sandia National Laboratories

Title Research on AlGaAs/GaAs Interfaces in GaAs Solar Cells

Effective Completion Date: 7/1/88 (Performance) 7/1/88 (Reports)

Grant/Contract Closeout Actions Remaining:

- [ ] None
- [XX] Final Invoice or Copy of Last Invoice Serving as Final
- [XX] Release and Assignment
- [XX] Final Report of Inventions and/or Subcontract: Patent and Subcontract Questionnaire sent to Project Director [XX]
- [XX] Govt. Property Inventory & Related Certificate
- [ ] Classified Material Certificate
- [ ] Other ____

Continues Project No. ____ Continued by Project No. ____

COPIES TO:

Project Director
Research Administrative Network
Research Property Management
Accounting
Procurement/~~GTRI Supply Services~~
~~Research Security Services~~
~~[illegible]~~
~~Program Administration Division~~
Contract Support Division (2)

~~Facilities Management - ERB~~
Library
GTRC
Project File
Other Angela
File
Lynn

E-21-603

CONTRACTOR: Complete all spaces and the bottom block.

PURCHASING ORGANIZATION Georgia Tech

ALBUQUERQUE, NEW MEXICO 87185
LIVERMORE, CALIFORNIA 94550

J. Gee
Sandia Contracting Representative

MONTHLY COST STATUS REPORT

CONTRACT NO. 02-2255

PERIOD ENDING (1) 12/31/86

Contractor must forecast as a minimum the first three months, Balance of Fiscal Year, and Subsequent Fiscal Years when costs will be incurred in these months and years.

Contractor must forward this report to reach the Sandia Contracting Representative by the 15th of the month following the Report Period or at such other time as requested by the Sandia Contracting Representative.

TOTAL FUNDS AUTHORIZED .... $ 32,383

ACTUAL COST INCURRED TO DATE (2) .... -0-

ESTIMATED COST TO COMPLETE: (3)

1st MONTH FOLLOWING "PERIOD ENDING" as specified above	3,238.30
2nd MONTH	3,238.30
3rd MONTH	3,238.30
4th MONTH	3,238.30
5th MONTH	3,238.30
6th MONTH	3,238.30
BALANCE OF FISCAL YEAR (4)	9,714.90
SUBSEQUENT FISCAL YEARS	3,238.30

TOTAL ESTIMATE TO COMPLETE 32,383

TOTAL ESTIMATED COST AT COMPLETION .... $ 32,383

NOTES:
(1) Last full month for which actual costs are available.
(2) Cost includes applicable fee.
(3) Estimates for costs to be incurred (Do not include commitments), including applicable fee.
(4) Fiscal year is 10/1 through 9/30. Balance of fiscal year means all months remaining in the fiscal year following the 6th month shown on the line above. If the 6th month is September, then balance of fiscal year is 10/1 through 9/30 of the next fiscal year.

Contractor (name and address)	Signature of Contractor's Representative, Date and Phone
Georgia Tech Research Corporation School of Electrical Engineering Georgia Institute of Technology Atlanta, GA 30332	Pam Majors 404-894-7337 1/27/87

(6432-CS(1-85)

E-21-603

GEORGIA INSTITUTE OF TECHNOLOGY
SCHOOL OF ELECTRICAL ENGINEERING
ATLANTA, GEORGIA 30332

LEPHONE: (404) 894-7337

February 16, 1987

Mr. J. Gee
Sandia National Laboratories
P. O. Box 5800
Albuquerque, NM 87185-5800

Re: Contract No. 02-2255

Dear Mr. Gee:

Enclosed please find a copy of the Monthly Cost Status Report for the period 1/1/87-1/31/87.

If you have any questions, please feel free to contact me.

Sincerely yours,

Pam Majors
Administrative Assistant

pm
Enclosure

A UNIT OF THE UNIVERSITY SYSTEM OF GEORGIA
AN EQUAL EDUCATION AND EMPLOYMENT OPPORTUNITY INSTITUTION

ONTRACTOR: Complete all spaces and the bottom block.

PURCHASING ORGANIZATION Georgia Tech

ALBUQUERQUE, NEW MEXICO 87185
LIVERMORE, CALIFORNIA 94550

J. Gee
Sandia Contracting Representative

MONTHLY COST STATUS REPORT

CONTRACT NO. 02-2255

PERIOD ENDING [1] 1/31/87

›ntractor must forecast as a minimum the first three months, Balance of Fiscal Year, and Subsequent Fiscal Years when costs will incurred in these months and years.

›ntractor must forward this report to reach the Sandia Contracting Representative by the 15th of the month llowing the Report Period or at such other time as requested by the Sandia Contracting Representative.

)TAL FUNDS AUTHORIZED .... $ 32,383

:TUAL COST INCURRED TO DATE[2] .... -0-

;TIMATED COST TO COMPLETE:[3]

1st MONTH FOLLOWING "PERIOD ENDING" as specified above	3,598.11
2nd MONTH	3,598.11
3rd MONTH	3,598.11
4th MONTH	3,598.11
5th MONTH	3,598.11
6th MONTH	3,598.11
ıLANCE OF FISCAL YEAR[4]	7,196.22
JBSEQUENT FISCAL YEARS	3,598.11

TOTAL ESTIMATE TO COMPLETE 32,383

)TAL ESTIMATED COST AT COMPLETION .... $ 32,383

)TES:

) Last full month for which actual costs are available.
) Cost includes applicable fee.
) Estimates for costs to be incurred (Do not include commitments), including applicable fee.
) Fiscal year is 10/1 through 9/30. Balance of fiscal year means all months remaining in the fiscal year following the 6th month own on the line above. If the 6th month is September, then balance of fiscal year is 10/1 through 9/30 of the next fiscal year.

ontractor (name and address)	Signature of ... r's Representative, Date and Phone
Georgia Tech Research Corporation School of Electrical Engineering Georgia Institute of Technology Atlanta, GA 30332	Paul Majors 404-894-7337 2/16/87

432-CS(1-85)

E-21-603

GEORGIA INSTITUTE OF TECHNOLOGY
SCHOOL OF ELECTRICAL ENGINEERING
ATLANTA, GEORGIA 30332

LEPHONE: (404) 894- 7337

March 13, 1987

Mr. J. Gee
Sandia National Laboratories
P. O. Box 5800
Albuquerque, NM 87185-5800

SUBJECT: Contract No. 02-2255
Project Director - A. Rohatgi

Dear Mr. Gee:

Enclosed please find a copy of the Monthly Cost Status Report for the period 2/1/87-2/28/87.

If you have any questions, please feel free to contact me.

Sincerely yours,

Pam Majors
Administrative Assistant

pm
Enclosure

A UNIT OF THE UNIVERSITY SYSTEM OF GEORGIA
AN EQUAL EDUCATION AND EMPLOYMENT OPPORTUNITY INSTITUTION

ONTRACTOR: Complete all spaces and the bottom block.

Sandia National Laboratories

PURCHASING ORGANIZATION Georgia Tech

ALBUQUERQUE, NEW MEXICO 87185

LIVERMORE, CALIFORNIA 94550

J. Gee
Sandia Contracting Representative

MONTHLY COST STATUS REPORT

CONTRACT NO. 02-2255

PERIOD ENDING (1) 2/28/87

ontractor must forecast as a minimum the first three months, Balance of Fiscal Year, and Subsequent Fiscal Years when costs will
incurred in these months and years.

**ontractor must forward this report to reach the Sandia Contracting Representative by the 15th of the month
llowing the Report Period or at such other time as requested by the Sandia Contracting Representative.**

OTAL FUNDS AUTHORIZED		$ 32,383
CTUAL COST INCURRED TO DATE(2)		3,041
STIMATED COST TO COMPLETE:(3)		
1st MONTH FOLLOWING "PERIOD ENDING" as specified above	3,667.75	
2nd MONTH	3,667.75	
3rd MONTH	3,667.75	
4th MONTH	3,667.75	
5th MONTH	3,667.75	
6th MONTH	3,667.75	
ALANCE OF FISCAL YEAR(4)	3,667.75	
UBSEQUENT FISCAL YEARS	3,667.75	
TOTAL ESTIMATE TO COMPLETE		29,342
OTAL ESTIMATED COST AT COMPLETION		$ 32,383

OTES:

) Last full month for which actual costs are available.

) Cost includes applicable fee.

) Estimates for costs to be incurred (Do not include commitments), including applicable fee.

) Fiscal year is 10/1 through 9/30. Balance of fiscal year means all months remaining in the fiscal year following the 6th month
own on the line above. If the 6th month is September, then balance of fiscal year is 10/1 through 9/30 of the next fiscal year.

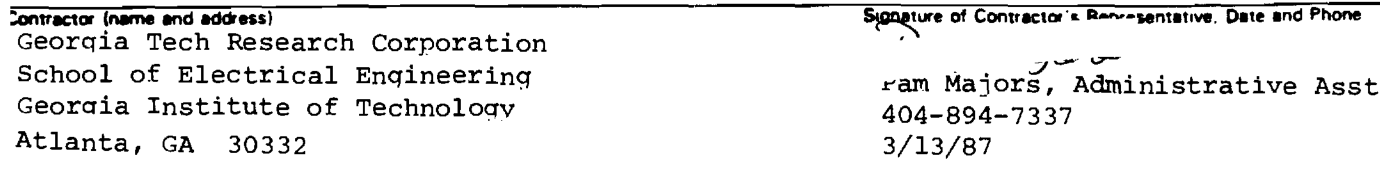
Contractor (name and address)
Georgia Tech Research Corporation
School of Electrical Engineering
Georgia Institute of Technology
Atlanta, GA 30332

Signature of Contractor's Representative, Date and Phone
ram Majors, Administrative Asst.
404-894-7337
3/13/87

6432-CS(1-85)

E-21-603

GEORGIA INSTITUTE OF TECHNOLOGY
SCHOOL OF ELECTRICAL ENGINEERING
ATLANTA, GEORGIA 30332

.EPHONE: (404) 894-7337

April 15, 1987

Mr. J. Gee
Sandia National Laboratories
P. O. Box 5800
Albuquerque, NM 87185-5800

SUBJECT: Contract No. 02-2255
Project Director - A. Rohatgi

Dear Mr. Gee:

Enclosed please find a copy of the Monthly Cost Status Report for the period 3/1/87-3/31/87.

If you have any questions, please feel free to contact me.

Sincerely yours,

Pam Majors
Administrative Assistant

pm
Enclosure

ONTRACTOR: Complete all spaces and the bottom block.

PURCHASING ORGANIZATION Georgia Tech

ALBUQUERQUE, NEW MEXICO 87185
LIVERMORE, CALIFORNIA 94550

J. Gee
Sandia Contracting Representative

MONTHLY COST STATUS REPORT

CONTRACT NO. 02-2255

PERIOD ENDING (1) 3/31/87

ntractor must forecast as a minimum the first three months, Balance of Fiscal Year, and Subsequent Fiscal Years when costs will incurred in these months and years.

ntractor must forward this report to reach the Sandia Contracting Representative by the 15th of the month lowing the Report Period or at such other time as requested by the Sandia Contracting Representative.

TAL FUNDS AUTHORIZED .... $ 32,383

TUAL COST INCURRED TO DATE(2) 4,562

TIMATED COST TO COMPLETE:(3)

1st MONTH FOLLOWING "PERIOD ENDING" as specified above	3,974.42
2nd MONTH	3,974.42
3rd MONTH	3,974.42
4th MONTH	3,974.42
5th MONTH	3,974.42
6th MONTH	3,974.42
LANCE OF FISCAL YEAR(4)	
BSEQUENT FISCAL YEARS	3,974.42

TOTAL ESTIMATE TO COMPLETE 27,821

TAL ESTIMATED COST AT COMPLETION .... $ 32,383

TES:

Last full month for which actual costs are available.
Cost includes applicable fee.
Estimates for costs to be incurred (Do not include commitments), including applicable fee.
Fiscal year is 10/1 through 9/30. Balance of fiscal year means all months remaining in the fiscal year following the 6th month own on the line above. If the 6th month is September, then balance of fiscal year is 10/1 through 9/30 of the next fiscal year.

ntractor (name and address)	Signature ... presentative, Date and Phone
Georgia Tech Research Corporation School of Electrical Engineering Georgia Institute of Technology Atlanta, GA 30332	Pam Majors, Administrative Assist. 404-894-7337 4/15/87

132-CS(1-85)

E-21-603

GEORGIA INSTITUTE OF TECHNOLOGY
SCHOOL OF ELECTRICAL ENGINEERING
ATLANTA, GEORGIA 30332

.EPHONE: (404) 894-7337

May 14, 1987

Mr. J. Gee
Sandia National Laboratories
P. O. Box 5800
Albuquerque, NM 87185-5800

SUBJECT: Contract No. 02-2255
Project Director - A. Rohatgi

Dear Mr. Gee:

Enclosed please find a copy of the Monthly Cost Status Report for the period 4/1/87-4/30/87.

If you have any questions, please feel free to contact me.

Sincerely yours,

Pam Majors
Administrative Assistant

pm
Enclosure

ONTRACTOR: Complete all spaces and the bottom block.

Sandia National Laboratories

PURCHASING ORGANIZATION Georgia Tech

ALBUQUERQUE, NEW MEXICO 87185

LIVERMORE, CALIFORNIA 94550

J. Gee
Sandia Contracting Representative

MONTHLY COST STATUS REPORT

CONTRACT NO. 02-2255

PERIOD ENDING (1) April 30, 1987

ntractor must forecast as a minimum the first three months, Balance of Fiscal Year, and Subsequent Fiscal Years when costs will incurred in these months and years.

ntractor must forward this report to reach the Sandia Contracting Representative by the 15th of the month llowing the Report Period or at such other time as requested by the Sandia Contracting Representative.

TAL FUNDS AUTHORIZED		$ 32,383
TUAL COST INCURRED TO DATE(2)		6,082
TIMATED COST TO COMPLETE:(3)		
1st MONTH FOLLOWING "PERIOD ENDING" as specified above	4,383.50	
2nd MONTH	4,383.50	
3rd MONTH	4,383.50	
4th MONTH	4,383.50	
5th MONTH	4,383.50	
6th MONTH		
LANCE OF FISCAL YEAR(4)		
BSEQUENT FISCAL YEARS	4,383.50	
TOTAL ESTIMATE TO COMPLETE		26,301
TAL ESTIMATED COST AT COMPLETION		$ 32,383

OTES:

(1) Last full month for which actual costs are available.

(2) Cost includes applicable fee.

(3) Estimates for costs to be incurred (Do not include commitments), including applicable fee.

(4) Fiscal year is 10/1 through 9/30. Balance of fiscal year means all months remaining in the fiscal year following the 6th month own on the line above. If the 6th month is September, then balance of fiscal year is 10/1 through 9/30 of the next fiscal year.

ontractor (name and address)	Signature of Contractor's Representative, Date and Phone
Georgia Tech Research Corporation School of Electrical Engineering Georgia Institute of Technology Atlanta, GA 30332	Pam Majors, Administrative Asst. 404-894-7337 5/14/87

432-CS(1-85)

GEORGIA INSTITUTE OF TECHNOLOGY
SCHOOL OF ELECTRICAL ENGINEERING
ATLANTA, GEORGIA 30332

EPHONE: (404) 894-7337

June 15, 1987

Mr. J. Gee
Sandia National Laboratories
P. O. Box 5800
Albuquerque, NM 87185-5800

SUBJECT: Contract No. 02-2255
Project Director: A. Rohatgi

Dear Mr. Gee:

Enclosed please find a copy of the Monthly Cost Status Report for the period 5/1/87-5/31/87.

If you have any questions, please feel free to contact me.

Sincerely yours,

Pam Majors
Administrative Assistant

pm
Enclosure

A UNIT OF THE UNIVERSITY SYSTEM OF GEORGIA
AN EQUAL EDUCATION AND EMPLOYMENT OPPORTUNITY INSTITUTION

ONTRACTOR: Complete all spaces and the bottom block.

PURCHASING ORGANIZATION Georgia Tech

ALBUQUERQUE, NEW MEXICO 87185
LIVERMORE, CALIFORNIA 94550

J. Gee
Sandia Contracting Representative

MONTHLY COST STATUS REPORT

CONTRACT NO. 02-2255

PERIOD ENDING [1] May 31, 1987

ntractor must forecast as a minimum the first three months, Balance of Fiscal Year, and Subsequent Fiscal Years when costs will incurred in these months and years.

ntractor must forward this report to reach the Sandia Contracting Representative by the 15th of the month lowing the Report Period or at such other time as requested by the Sandia Contracting Representative.

TAL FUNDS AUTHORIZED .... $ 32,383

TUAL COST INCURRED TO DATE[2] 7,603

TIMATED COST TO COMPLETE:[3]

1st MONTH FOLLOWING "PERIOD ENDING" as specified above	4,956.00
2nd MONTH	4,956.00
3rd MONTH	4,956.00
4th MONTH	4,956.00
5th MONTH	
6th MONTH	
LANCE OF FISCAL YEAR[4]	
BSEQUENT FISCAL YEARS	4,956.00

TOTAL ESTIMATE TO COMPLETE 24,780

TAL ESTIMATED COST AT COMPLETION .... $ 32,383

OTES:

1. Last full month for which actual costs are available.
2. Cost includes applicable fee.
3. Estimates for costs to be incurred (Do not include commitments), including applicable fee.
4. Fiscal year is 10/1 through 9/30. Balance of fiscal year means all months remaining in the fiscal year following the 6th month own on the line above. If the 6th month is September, then balance of fiscal year is 10/1 through 9/30 of the next fiscal year.

ontractor (name and address)	Signature of Contractor's Representative, Date and Phone
Georgia Tech Research Corporation School of Electrical Engineering Georgia Institute of Technology Atlanta, GA 30332	Pam Majors, Administrative Asst. 404-894-7337 6/15/87

432-CS(1-85)

GEORGIA INSTITUTE OF TECHNOLOGY
SCHOOL OF ELECTRICAL ENGINEERING
ATLANTA, GEORGIA 30332

:PHONE: (404) 894-7337

July 24, 1987

Mr. J. Gee
Sandia National Laboratories
P. O. Box 5800
Albuquerque, NM 87185-5800

SUBJECT: Contract No. 02-2255
Project Director: A. Rohatgi

Dear Mr. Gee:

Enclosed please find a copy of the Monthly Cost Status Report for the period 6/1/87-6/30/87.

If you have any questions, please feel free to contact me.

Sincerely yours,

Pam Majors
Administrative Assistant

pm
Enclosure

ONTRACTOR: Complete all spaces and the bottom block.

Sandia National Laboratories

PURCHASING ORGANIZATION Georgia Tech

ALBUQUERQUE, NEW MEXICO 87185

LIVERMORE, CALIFORNIA 94550

J. Gee

Sandia Contracting Representative

MONTHLY COST STATUS REPORT

CONTRACT NO. 02-2255

PERIOD ENDING (1) June 30, 1987

ontractor must forecast as a minimum the first three months, Balance of Fiscal Year, and Subsequent Fiscal Years when costs will incurred in these months and years.

ontractor must forward this report to reach the Sandia Contracting Representative by the 15th of the month llowing the Report Period or at such other time as requested by the Sandia Contracting Representative.

OTAL FUNDS AUTHORIZED		$ 32,383
CTUAL COST INCURRED TO DATE(2)		9,123
STIMATED COST TO COMPLETE:(3)		
1st MONTH FOLLOWING "PERIOD ENDING" as specified above	5,815.00	
2nd MONTH	5,815.00	
3rd MONTH	5,815.00	
4th MONTH		
5th MONTH		
6th MONTH		
ALANCE OF FISCAL YEAR(4)		
UBSEQUENT FISCAL YEARS	5,815.00	
TOTAL ESTIMATE TO COMPLETE		23,260
OTAL ESTIMATED COST AT COMPLETION		$ 32,383

OTES:

) Last full month for which actual costs are available.

) Cost includes applicable fee.

) Estimates for costs to be incurred (Do not include commitments), including applicable fee.

) Fiscal year is 10/1 through 9/30. Balance of fiscal year means all months remaining in the fiscal year following the 6th month own on the line above. If the 6th month is September, then balance of fiscal year is 10/1 through 9/30 of the next fiscal year.

Contractor (name and address)	Signature of C... ...epresentative, Date and Phone
Georgia Tech Research Corporation School of Electrical Engineering Georgia Institute of Technology Atlanta, GA 30332	Pam Majors, Administrative Asst. 404-894-7337 7/24/87

-6432-CS(1-85)

E-21-603

GEORGIA INSTITUTE OF TECHNOLOGY
SCHOOL OF ELECTRICAL ENGINEERING
ATLANTA, GEORGIA 30332

.EPHONE: (404) 894-7337

August 10, 1987

Mr. J. Gee
Sandia National Laboratories
P. O. Box 5800
Albuquerque, NM 87185-5800

SUBJECT: Contract No. 02-2255
Project Director: A. Rohatgi

Dear Mr. Gee:

Enclosed please find a copy of the Monthly Cost Status Report for the period 7/1/87-7/31/87 on the above reference contract.

If you have any questions, please feel free to contact me.

Sincerely yours,

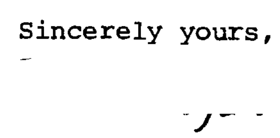

Pam Majors
Administrative Assistant

pm
Enclosure

ONTRACTOR: Complete all spaces and the bottom block.

PURCHASING ORGANIZATION Georgia Tech

J. Gee
Sandia Contracting Representative

ALBUQUERQUE, NEW MEXICO 87185
LIVERMORE, CALIFORNIA 94550

MONTHLY COST STATUS REPORT

CONTRACT NO. 02-2255

PERIOD ENDING [1] July 31, 1987

ntractor must forecast as a minimum the first three months, Balance of Fiscal Year, and Subsequent Fiscal Years when costs will incurred in these months and years.

ntractor must forward this report to reach the Sandia Contracting Representative by the 15th of the month lowing the Report Period or at such other time as requested by the Sandia Contracting Representative.

TAL FUNDS AUTHORIZED		$ 32,383
TUAL COST INCURRED TO DATE[2]		14,824
TIMATED COST TO COMPLETE:[3]		
1st MONTH FOLLOWING "PERIOD ENDING" as specified above	5,866.33	
2nd MONTH	5,866.33	
3rd MONTH		
4th MONTH		
5th MONTH		
6th MONTH		
LANCE OF FISCAL YEAR[4]		
IBSEQUENT FISCAL YEARS	5,866.34	
TOTAL ESTIMATE TO COMPLETE		17,559
TAL ESTIMATED COST AT COMPLETION		$ 32,383

OTES:
Last full month for which actual costs are available.
Cost includes applicable fee.
Estimates for costs to be incurred (Do not include commitments), including applicable fee.
Fiscal year is 10/1 through 9/30. Balance of fiscal year means all months remaining in the fiscal year following the 6th month own on the line above. If the 6th month is September, then balance of fiscal year is 10/1 through 9/30 of the next fiscal year.

ontractor (name and address)	Signature of Contractor's Representative, Date and Phone
Georgia Tech Research Corporation School of Electrical Engineering Georgia Institute of Technology Atlanta, GA 30332	Pam Majors, Administrative Asst. 404-894-7337 8/10/87

432-CS(1-85)

E-21-603

GEORGIA INSTITUTE OF TECHNOLOGY
SCHOOL OF ELECTRICAL ENGINEERING
ATLANTA, GEORGIA 30332

-EPHONE: (404) 894-7337

September 16, 1987

Mr. J. Gee
Sandia National Laboratories
P. O. Box 5800
Albuquerque, NM 87185-5800

SUBJECT: Contract No. 02-2255
Project Director: A. Rohatgi

Dear Mr. Gee:

Enclosed please find a copy of the Monthly Cost Status Report for the period 8/1/87-8/31/87 on the above referenced contract.

If you have any questions, please feel free to contact me.

Sincerely yours,

Pam Majors
Administrative Assistant

pm
Enclosure

A UNIT OF THE UNIVERSITY SYSTEM OF GEORGIA
AN EQUAL EDUCATION AND EMPLOYMENT OPPORTUNITY INSTITUTION

ONTRACTOR: Complete all spaces and the bottom block.

PURCHASING ORGANIZATION Georgia Tech

ALBUQUERQUE, NEW MEXICO 87185

LIVERMORE, CALIFORNIA 94550

J. Gee

Sandia Contracting Representative

MONTHLY COST STATUS REPORT

CONTRACT NO. 02-2255

PERIOD ENDING (1) August 31, 1987

ontractor must forecast as a minimum the first three months, Balance of Fiscal Year, and Subsequent Fiscal Years when costs will incurred in these months and years.

ontractor must forward this report to reach the Sandia Contracting Representative by the 15th of the month llowing the Report Period or at such other time as requested by the Sandia Contracting Representative.

)TAL FUNDS AUTHORIZED		$ 32,383
:TUAL COST INCURRED TO DATE(2)		20,527
TIMATED COST TO COMPLETE:(3)		
1st MONTH FOLLOWING "PERIOD ENDING" as specified above	5,928	
2nd MONTH		
3rd MONTH		
4th MONTH		
5th MONTH		
6th MONTH		
LANCE OF FISCAL YEAR(4)		
IBSEQUENT FISCAL YEARS	5,928	
TOTAL ESTIMATE TO COMPLETE		11,856
TAL ESTIMATED COST AT COMPLETION		$ 32,383

)TES:

Last full month for which actual costs are available.

Cost includes applicable fee.

Estimates for costs to be incurred (Do not include commitments), including applicable fee.

Fiscal year is 10/1 through 9/30. Balance of fiscal year means all months remaining in the fiscal year following the 6th month own on the line above. If the 6th month is September, then balance of fiscal year is 10/1 through 9/30 of the next fiscal year.

ontractor (name and address)
eorgia Tech Research Corporation
chool of Electrical Engineering
eorgia Institute of Technology
tlanta, GA 30332

Signature of C[illegible] Representative, Date and Phone
Pam Majors, Adm. Assistant
404-894-7337
9/16/87

132-CS(1-85)

E-21-603

GEORGIA INSTITUTE OF TECHNOLOGY
SCHOOL OF ELECTRICAL ENGINEERING
ATLANTA, GEORGIA 30332

EPHONE: (404) 894-7337

October 14, 1987

Mr. J. Gee
Sandia National Laboratories
P. O. Box 5800
Albuquerque, NM 87185-5800

SUBJECT: Contract No. 02-2255
Project Director: A. Rohatgi

Dear Mr. Gee:

Enclosed please find a copy of the Monthly Cost Status Report for the period 9/1/87-9/30/87 on the above referenced contract.

If you have any questions, please feel free to contact me.

Sincerely,

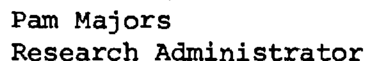

Pam Majors
Research Administrator

pm
Enclosure

A UNIT OF THE UNIVERSITY SYSTEM OF GEORGIA
AN EQUAL EDUCATION AND EMPLOYMENT OPPORTUNITY INSTITUTION

)NTRACTOR: Complete all spaces and the bottom block.

PURCHASING ORGANIZATION Georgia Tech

ALBUQUERQUE, NEW MEXICO 87185
LIVERMORE, CALIFORNIA 94550

J. Gee
Sandia Contracting Representative

MONTHLY COST STATUS REPORT

CONTRACT NO. 02-2255

PERIOD ENDING (1) September 30, 1987

ıtractor must forecast as a minimum the first three months, Balance of Fiscal Year, and Subsequent Fiscal Years when costs will incurred in these months and years.

ntractor must forward this report to reach the Sandia Contracting Representative by the 15th of the month ıowing the Report Period or at such other time as requested by the Sandia Contracting Representative.

TAL FUNDS AUTHORIZED		$ 32,383
TUAL COST INCURRED TO DATE(2)		27,644
TIMATED COST TO COMPLETE:(3)		
1st MONTH FOLLOWING "PERIOD ENDING" as specified above		
2nd MONTH		
3rd MONTH		
4th MONTH		
5th MONTH		
6th MONTH		
LANCE OF FISCAL YEAR(4)		
BSEQUENT FISCAL YEARS	4,739	
TOTAL ESTIMATE TO COMPLETE		4,739
TAL ESTIMATED COST AT COMPLETION		$ 32,383

ITES:
Last full month for which actual costs are available.
Cost includes applicable fee.
Estimates for costs to be incurred (Do not include commitments), including applicable fee.
Fiscal year is 10/1 through 9/30. Balance of fiscal year means all months remaining in the fiscal year following the 6th month ɔwn on the line above. If the 6th month is September, then balance of fiscal year is 10/1 through 9/30 of the next fiscal year.

ntractor (name and address)	Signature of Contractor's Representative, Date and Phone
;eorgia Tech Research Corporation ;chool of Electrical Engineering ;eorgia Institute of Technology ıtlanta, GA 30332	Pam Majors, Research Adm. 404-894=7337 10/14/87

132-CS(1-85)

E-21-603

GEORGIA INSTITUTE OF TECHNOLOGY
SCHOOL OF ELECTRICAL ENGINEERING
ATLANTA, GEORGIA 30332

.EPHONE: (404) 894-7337

November 10, 1987

Mr. J. Gee
Sandia National Laboratories
P. O. Box 5800
Albuquerque, NM 87185-5800

SUBJECT: Contract No. 02-2255
Project Director: A. Rohatgi

Dear Mr. Gee:

Enclosed please find a copy of the Monthly Cost Status Report for the period 10/1/87-10/27/87 on the above referenced contract. Please note that the project terminated on 10/27/87. Some orders were placed during the month of October and expenditures will not appear until next month. I will submit a final cost report in November for all expenditures.

If you have any questions, please feel free to contact me.

Sincerely,

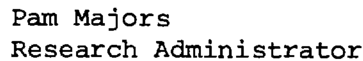

Pam Majors
Research Administrator

pm
Enclosure

ONTRACTOR: Complete all spaces and the bottom block.

Sandia National Laboratories

PURCHASING ORGANIZATION Georgia Tech

ALBUQUERQUE, NEW MEXICO 87185

LIVERMORE, CALIFORNIA 94550

J. Gee
Sandia Contracting Representative

MONTHLY COST STATUS REPORT

CONTRACT NO. 02-2255

PERIOD ENDING (1) October 31, 1987

ontractor must forecast as a minimum the first three months, Balance of Fiscal Year, and Subsequent Fiscal Years when costs will incurred in these months and years.

ontractor must forward this report to reach the Sandia Contracting Representative by the 15th of the month llowing the Report Period or at such other time as requested by the Sandia Contracting Representative.

)TAL FUNDS AUTHORIZED		$ 32,383
:TUAL COST INCURRED TO DATE(2)		28,220
;TIMATED COST TO COMPLETE:(3)		
1st MONTH FOLLOWING "PERIOD ENDING" as specified above		
2nd MONTH		
3rd MONTH		
4th MONTH		
5th MONTH		
6th MONTH		
\LANCE OF FISCAL YEAR(4)		
JBSEQUENT FISCAL YEARS	4,163	
TOTAL ESTIMATE TO COMPLETE		4,163
)TAL ESTIMATED COST AT COMPLETION		$ 32,383

)TES:

) Last full month for which actual costs are available.

) Cost includes applicable fee.

) Estimates for costs to be incurred (Do not include commitments), including applicable fee.

) Fiscal year is 10/1 through 9/30. Balance of fiscal year means all months remaining in the fiscal year following the 6th month own on the line above. If the 6th month is September, then balance of fiscal year is 10/1 through 9/30 of the next fiscal year.

ontractor (name and address)
Georgia Tech Research Corporation
School of Electrical Engineering
Georgia Institute of Technology
Atlanta, GA 30332

Signature of Contractor's Representative, Date and Phone
Pam Majors, Research Adm.
404-894-7337
11/10/87

1432-CS(1-85)

E-21-603

GEORGIA INSTITUTE OF TECHNOLOGY
SCHOOL OF ELECTRICAL ENGINEERING
ATLANTA, GEORGIA 30332

EPHONE: (404) 894-7337

June 2, 1988

Mr. J. Gee
Sandia National Laboratories
P. O. Box 5800
Albuquerque, NM 87185-5800

SUBJECT: Contract No. 02-2255
Project Director: A. Rohatgi

Dear Mr. Gee:

Enclosed please find the final Monthly Cost Status Report through 2/28/88 on the above referenced contract. Please note there is a balance of $34.27 on the contract.

If you have any questions, please feel free to contact me.

Sincerely,

Pam Majors
Research Administrator

pm
Enclosure

ONTRACTOR: Complete all spac(.nd the bottom block.

PURCHASING ORGANIZATION Georgia Tech

ALBUQUERQUE, NEW MEXICO 87185

LIVERMORE, CALIFORNIA 94550

J. Gee

Sandia Contracting Representative

MONTHLY COST STATUS REPORT

CONTRACT NO. 02-2255

PERIOD ENDING (1) February 28, 1988

ntractor must forecast as a minimum the first three months, Balance of Fiscal Year, and Subsequent Fiscal Years when costs will incurred in these months and years.

ntractor must forward this report to reach the Sandia Contracting Representative by the 15th of the month lowing the Report Period or at such other time as requested by the Sandia Contracting Representative.

TAL FUNDS AUTHORIZED .... $ 32,383.00

TUAL COST INCURRED TO DATE(2) 32,348.73

TIMATED COST TO COMPLETE:(3)

1st MONTH FOLLOWING "PERIOD ENDING" as specified above ______

2nd MONTH ______

3rd MONTH ______

4th MONTH ______

5th MONTH ______

6th MONTH ______

.ANCE OF FISCAL YEAR(4) ______

3SEQUENT FISCAL YEARS ______

TOTAL ESTIMATE TO COMPLETE 34.27

TAL ESTIMATED COST AT COMPLETION .... $ 32,383.00

TES:

Last full month for which actual costs are available.

Cost includes applicable fee.

Estimates for costs to be incurred (Do not include commitments), including applicable fee.

Fiscal year is 10/1 through 9/30. Balance of fiscal year means all months remaining in the fiscal year following the 6th month wn on the line above. If the 6th month is September, then balance of fiscal year is 10/1 through 9/30 of the next fiscal year.

ntractor (name and address)	Signature of Contractor's Representative, Date and Phone
eorgia Tech Research Corporation chool of Electrical Engineering eorgia Institute of Technology .tlanta, GA 30332	Pam Majors, Research Adm. 404-894-7337 6/2/88

2-CS(1-85)

E-21-603

RESEARCH ON AlGaAs/GaAs INTERFACES IN GaAs SOLAR CELLS

A. Rohatgi

First Monthly Report for the Period

December 1 to December 31, 1986

Sandia National Laboratories

Contract No. 02-2255

GEORGIA INSTITUTE OF TECHNOLOGY
SCHOOL OF ELECTRICAL ENGINEERING
ATLANTA, GEORGIA 30332

Technical Progress

The major objective of this program is to develop techniques and methodology to characterize AlGaAs/GaAs interfaces and provide guidelines for improving GaAs heteroface or heterojunction solar cells.

The first month of work on this project entailed an extensive literature search on electrical characterization techniques for heterojunctions, particulary the GaAs/AlGaAs System. As a result of our findings, we have devised a number of experiments which we feel would aid in clearing some of the ambiguity in the electrical properties of the GaAs/AlGaAs interface. We are proposing a specialized test structure (see Figure 1) to measure both the valence band edge and conduction band edge discontinuities. We feel that this is necessary due to the controversy surrounding the correct assignment of these values. Also, to the best of our knowledge, this question has not been addressed for structures with high Al content as the cells in this study have. The method we will use is described by Kroemer, et al. Devices of various Al content and doping levels will be tested to ascertain the dependence of the band edge discontinuities on these parameters. In conjunction with this, the Al diffusion across the interface will be studied as a function of the above parameters using photovoltage spectroscopy along with electrochemical depth profiling. Dopant profiles will be measured as well.

In the next month, we plan to run DLTS measurements on the Hughes mesa diodes provided by Sandia National Labs to probe the depletion region of the pn junction of the cell. Based on the initial results, we will devise test structures which will allow us to ascertain the contribution, if any, from the GaAs/AlGaAs

interface to the pn junction. Also, we will obtain dopant profiles for the "dead" Hughes cells and measure the photovoltage spectrum as a function of depth to determine if any Al diffusion is the cause of failure. We will try to correlate the results with the solar cell performance data that we have already received. In addition, a request for a series of test structures have been sent to Dr. J. Gee. These structures will provide a data base that will aid in the basic understanding of the AlGaAs/GaAs heteroface.

The author would like to acknowledge the assistance of Steve Ringel (GRA) who is conducting the experimental research for this program.

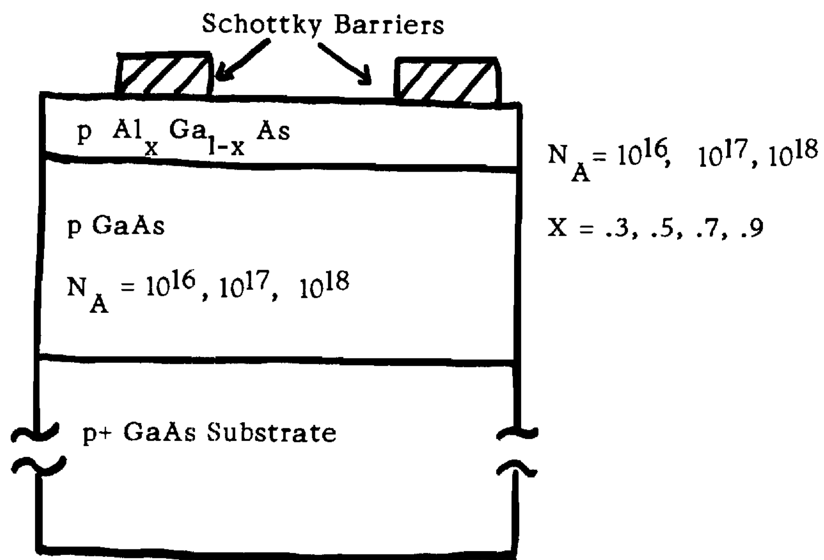

Figure 1: Test structure for measuring valence band edge discontinuity as a function of Al content and doping (n-type samples are also proposed to confirm the accuracy of the measurement).

RESEARCH ON AlGaAs/GaAs INTERFACES IN GaAs SOLAR CELLS

A. Rohatgi

Second Monthly Report for the Period
January 1 to January 30, 1987

Sandia National Laboratories
Contract No. 02-2255

GEORGIA INSTITUTE OF TECHNOLOGY
SCHOOL OF ELECTRICAL ENGINEERING
ATLANTA, GEORGIA 30332

RESEARCH ON $AlGaAs/GaAs$ INTERFACES IN $GaAs$ SOLAR CELLS

A. Rohatgi

Second Monthly Report for the Period
January 1 to January 30, 1987

Sandia National Laboratories
Contract No. 02-2255

GEORGIA INSTITUTE OF TECHNOLOGY
SCHOOL OF ELECTRICAL ENGINEERING
ATLANTA, GEORGIA 30332

Technical Progress

The major objective of this program is to develop techniques and methodology to characterize AlGaAs/GaAs interfaces and provide guidelines for improving GaAs heterojunction solar cells.

In the second month of this program we made attempts to characterize LPE grown GaAs solar cells and mesa diode structures (see Fig. 1) supplied by Hughes. After extensive testing and manipulation, a methodology to run DLTS on these devices was determined. The DLTS parameters used in the experiment are shown in Figure la. It is assumed that the region the DLTS was probing is the n-type GaAs layer since essentially all of the depletion region under reverse bias is there. The results obtained generally agree with what is commonly reported for LPE n-type GaAs. There is evidence of only a hole trap in n-GaAs as indicated by DLTS spectra in Figure 2a. The Arrhenius plot (Figure 2B) of this deep level indicates the level exists approximately 0.86 eV below the conduction band with a density on the order of $10^{14}cm^{-3}$, both of which agree well with outside reports. A shoulder adjacent to the DLTS peak suggests the possibility of another hole trap, but it is difficult to deconvolute this data to obtain the exact energy level, which is expected to be close to the first one. No evidence of any kind for the presence of electron traps was found, which is consistent with the DLTS behavior of the LPG GaAs. We may try to study the annealing behavior of the trap level to find a way of getting rid of it.

Surface photovoltage measurements, both at the cell surface (beneath the contacts) and as a function of depth into the device, were attempted. Since we were not supplied with contact-less devices, it was necessary to chemically etch away both the contact grid and antire flection coating of an actual cell. This was, however, not possible since after numerous tries with different etching recipes we were unable to find an etchant which would remove the metal and AR coating without adversely affecting the high AlGaAs layer with high aluminum content.

We have recently received MOCVD grown high quality GaAs heteroface solar cells ($\geq$ 21% efficient) from Spire Corporation. In addition to the cells, they have provided us with mesa diodes for DLTS measurements and an unprocessed piece for doping, surface photovoltage, and FTIR measurements. We also have I-V and photoluminescence data from Spire Corporation. Experiments have just begun and the results will be reported in the third monthly report. We will also make an attempt to run DLTS measurements on the finished solar cells. If this succeeds then we can have a more definite correlation between the material properties and cell efficiency. These measurements will provide us with a first look at the differences between the deep levels in Hughes LPE GaAs and Spire's MOCVD GaAs layers.

The author would like to acknowledge the assistance of Steve Ringel (GRA) who is conducting the experimental research for this program.

FIGURE 1 HUGHES MESA DIODE STRUCTURE USED FOR DLTS MEASUREMENTS

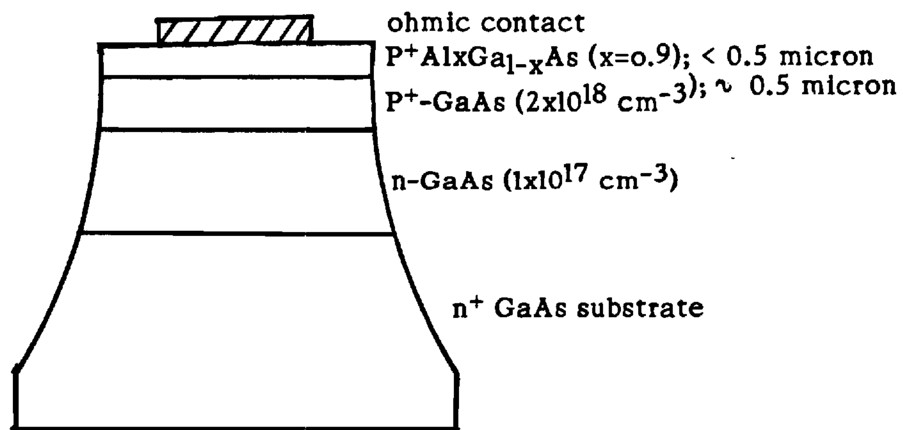

FIGURE 2   a - DLTS SPECTRUM FOR HUGHES MESA DIODE

b - ARRHENIUS PLOT FOR DEEP LEVEL INDICATED IN DLTS SPECTRUM

(A)

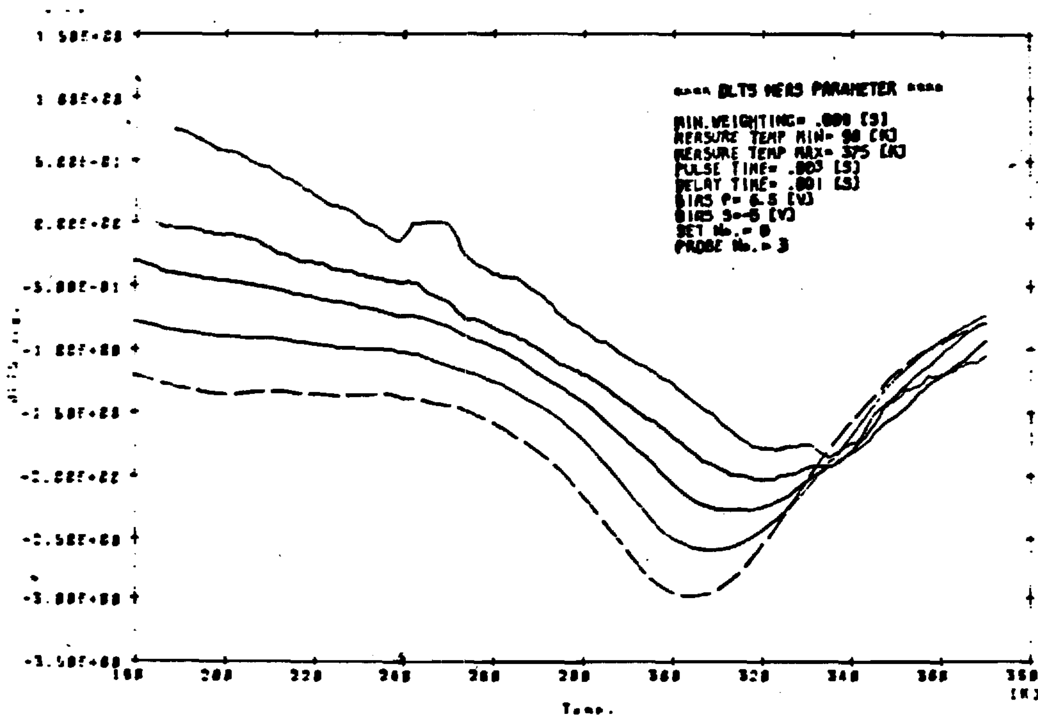

(B)

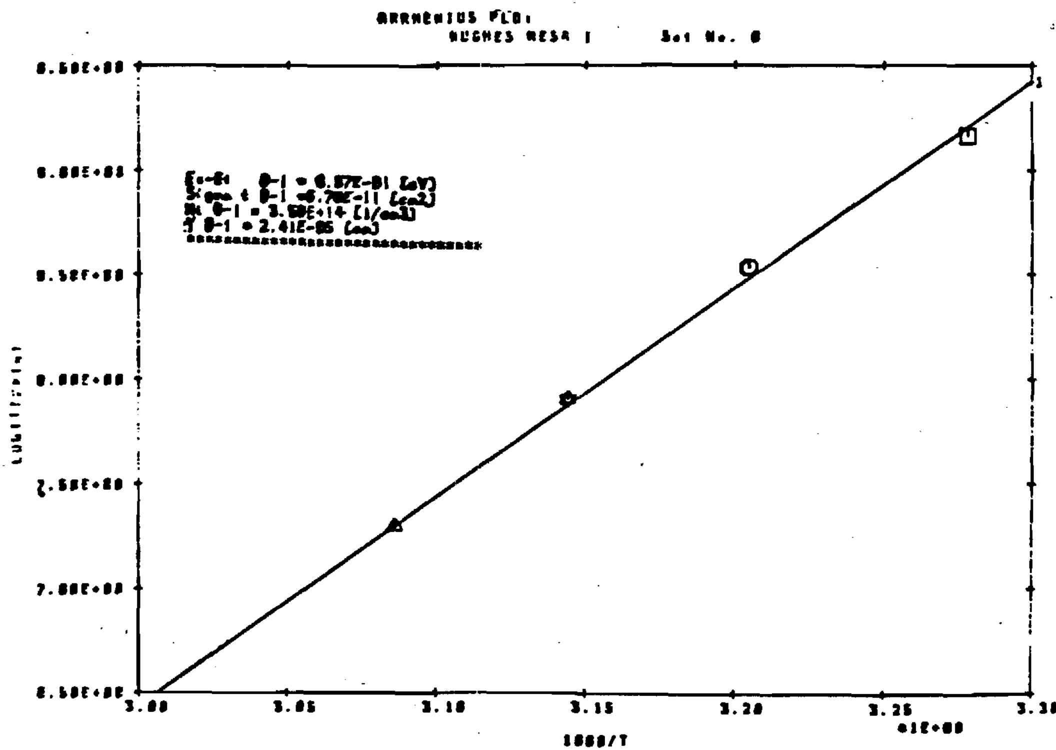

E-21-[illegible]

GEORGIA INSTITUTE OF TECHNOLOGY
SCHOOL OF ELECTRICAL ENGINEERING
ATLANTA, GEORGIA 30332

EPHONE: (404) 894-7337

May 11, 1987

Mr. J. Gee
Sandia National Laboratories
P. O. Box 5800
Albuquerque, NM 87185-5800

Re: Contract No. 02-5800
Project Director: A. Rohatgi

Dear Mr. Gee:

Enclosed please find a copy of the Monthly Technical Progress Report for the period 2/1/87-2/28/87.

If you have any questions, please feel free to contact me.

Sincerely yours,

Pam Majors
Administrative Assistant

pm
Enclosure

RESEARCH ON AlGaAs/GaAs INTERFACES IN GaAs SOLAR CELLS

A. Rohatgi

Third Monthly Report for the Period
February 1 to February 28, 1987

Sandia National Laboratories

Contract No. 02-2255

GEORGIA INSTITUTE OF TECHNOLOGY
SCHOOL OF ELECTRICAL ENGINEERING
ATLANTA, GEORGIA 30332

Technical Progress

The major objective of this program is to develop techniques and methodology to characterize AlGaAs/GaAs interfaces and provide guidelines for improving GaAs heterojunction solar cells.

During the past month we have successfully obtained dopant profiles and photovoltage spectra as a function of depth for high efficiency MOCVD-grown GaAs solar cell structures. Before presenting some preliminary results however, it is useful to briefly describe the characterization technique used here since we feel it can be a very powerful method for electronic and optical materials characterization.

A Biorad Polaron Pn4200 electrochemical dopant profiler with a Polaron PN 4250 photovoltage spectrometer accessory was used for our experiments. The heart of the system is an electrochemical cell (see Figure 1) which houses an electrolyte solution that wets a precisely determined contact area of a sample to be characterized. The function of the electrolyte is twofold. First, it forms an electrically rectifying (Schottky) contact with the sample, and second, it acts to dissolve the sample through an electrochemical dissolution process. Since a Schottky contact can be formed, capacitance and hence net doping level can be measured. And since the material can be dissolved, a sequential process of measure, etch, measure, etc., can be realized. This cycle is accurately controlled and monitored via a user-controlled computer work station where one chooses the correct parameters (electrode bias, etch current, etc.) to obtain accurate data. We have the ability to measure net dopant concentrations ranging from $\sim 10^{13}$-10^{20} cm^{-3} with a depth accuracy in the tens of angstroms. The only restriction on sample material is that for some, a suitable electrolyte may not be available.

As mentioned above, we also have a photovoltage spectrometer accessory to the profiler. The spectrometer can operate from $\sim$400 - 1600 nm. and is coupled to the sample via an optical fiber and a prism as shown in figure 2. The software is arranged such that one can interrupt the dopant profile cycle at any time and

make a photovoltage measurement at that etch depth. Hence it is able to obtain photovoltage spectra as a function of depth at steps as small as 10 angstroms.

Doping profile and depth resolved SPV measurements were performed on the GaAs solar cell grown by MOCVD at Spire Corporation shown in Figure 3. The heavily Zn doped GaAs cap layer presented some problems in choosing a good electrolyte since the one most favorable for working with GaAs (Tiron - $C_6H_2(OH)_2(NaSO_3)_2.2H_20$) happens to readily react with Zn to form a surface residue layer. After some trial and error, a suitable electrolyte, .2M NaOH + .1M EDTA by dry weight per unit volume, was found.

Figure 4 shows the doping profile obtained for this structure up to 0.6 microns. The peak at $\sim$0.55 microns is not real and is due to the crossing of the p-n junction region. The doping levels in the depletion region are meaningless due to the high conductance condition that occurs when the material conduction type is changed (by forward bias condition) before the applied measuring bias can bc adjusted. Measurements in the profile were taken at 50 angstrom intervals. In comparison with the supplied data from Spire, the sample profile is somewhat different, with the GaAs cap layer being thinner and the p-n junction being shallower than expected.

Figure 5 displays photovoltage spectra obtained at various etch depths during the dopant profile. The peaks at $\sim$550 and $\sim$730 nm are due to the optics of the PVS (Photovoltage Spectroscopy) System and will be subtracted out of all data taken in the future. Note that the absorption edge at $\sim$880 nm is indicative of GaAs but there is no edge present at $\sim$450 nm to reveal the presence of $Al_{.87}Ga_{.13}As$. It is quite possible that the signal is being masked by the GaAs and spectrometer since it would be expected that the AlGaAs response would be small considering its layer thickness ($\sim$.05 micron).

Note the trends in photovoltage response as a function of etch depth (Figure 5). The spectra in the heavily doped cap layer is essentially zero with only the spectrometer contributing any structure. This would be expected since the diffusion length is greatly reduced by the presence of heavy doping so photogenerated carriers do not "live" long enough to be collected. As the cap layer is etched, the photons can "see" the lower doped p-GaAs region where the

photogenerated carriers live longer to get to the collecting junction at the surface, hence the magnitude of the PVS signal increases. This effect is seen in Figure 5 where the magnitude of the PVS response continues to increase until the cap layer is completely removed at which point it stabilizes for a few hundred angstroms. As the etch profile continues, toward the p-n junction, the magnitude of the response steadily decreases (see Figure 6). This is a result of competition for photogenerated carriers between the Schottky barrier at the electrolyte/GaAs inteface and the p-n junction, which are aligned back to back and hence decrease the overall PVS response. A dramatic change occurs at an etch depth of 0.44 micron (Figure 7) apparently due to the p-n junction. There is no response for the higher energy photons indicating that the carriers generated close the Schottky barrier, which at this etch depth are just outside the depletion region on the p-side of the p-n junction, are being lost, possibly by a defective layer of material underneath. As the etch is continued 100 angstroms deeper, at 0.45 microns (Figure 8), a similar spectrum results except that the response is increased somewhat. This spatially dependent change in SPV response suggests the presence of a region of defects which the profiler is slowly stepping through. It is not yet certain, however, that if there is a defective region close to the Schottky barrier, how carriers generated deeper in the sample by the longer wavelength photons are able to return across a high trap density layer and be collected by the Schottky barrier. As the etch process is stepped toward and into the n-GaAs, the response continues to increase as the lower doped n-layer becomes the dominant and eventually the sole remaining layer. A typical PVS spectrum for this region is shown in Figure 9.

In conclusion we have successfully used photovoltage spectroscopy in a depth profiling mode in conjunction with electrochemical dopant profiling to study spatially varying properties of a GaAs solar cell structure. We plan to extract the contribution of the optics set-up from the existing data to determine what, if anything, has been masked out. We also plan to subtract two PVS spectra which are spatially separated by a very small difference and compare the difference between these two spectra with the difference between the next two

spectra, and thus allowing us to get a measure of the optical quality of the material as a function of the depth; i.e., if the two differences are equal, then the material is uniform in quality, otherwise there is a variation which may be process-induced. We plan to repeat these studies on another Spire sample of the same structure. We also plan to finish DLTS measurements on these samples to see if there is a correlation between the DLTS signature and PVS behavior on the same wafer. In addition, we will look into the correlation between the DLTS and SPV data and the cell efficiency.

The author would like to acknowledge the assistance of Steven A. Ringel (GRA) who is conducting the experimental research for this program.

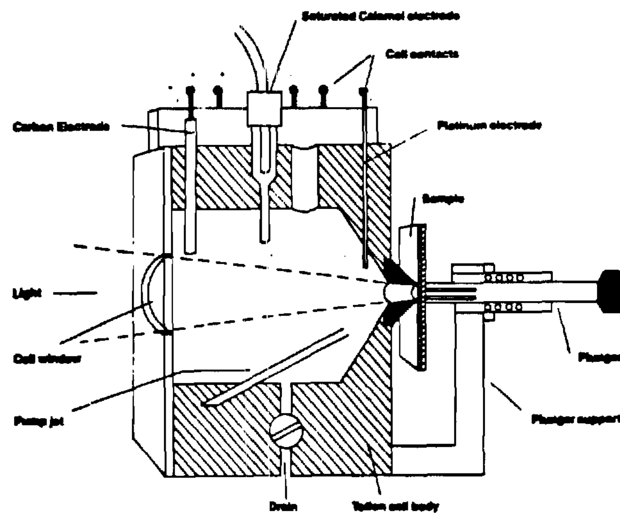

Figure 1: Schematic of electrochemical cell used in the Polaron system.

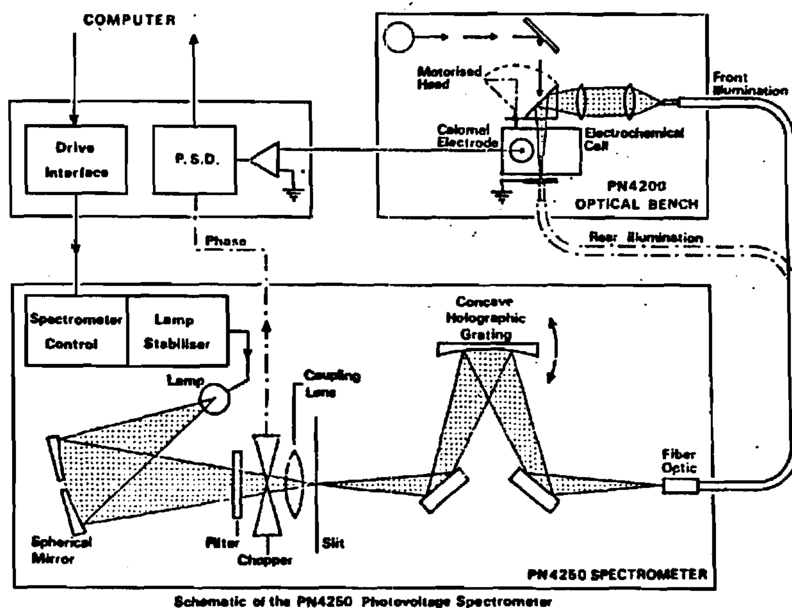

Figure 2: Schematic of coupling between spectrometer for photovoltage measurements and electrochemical cell.

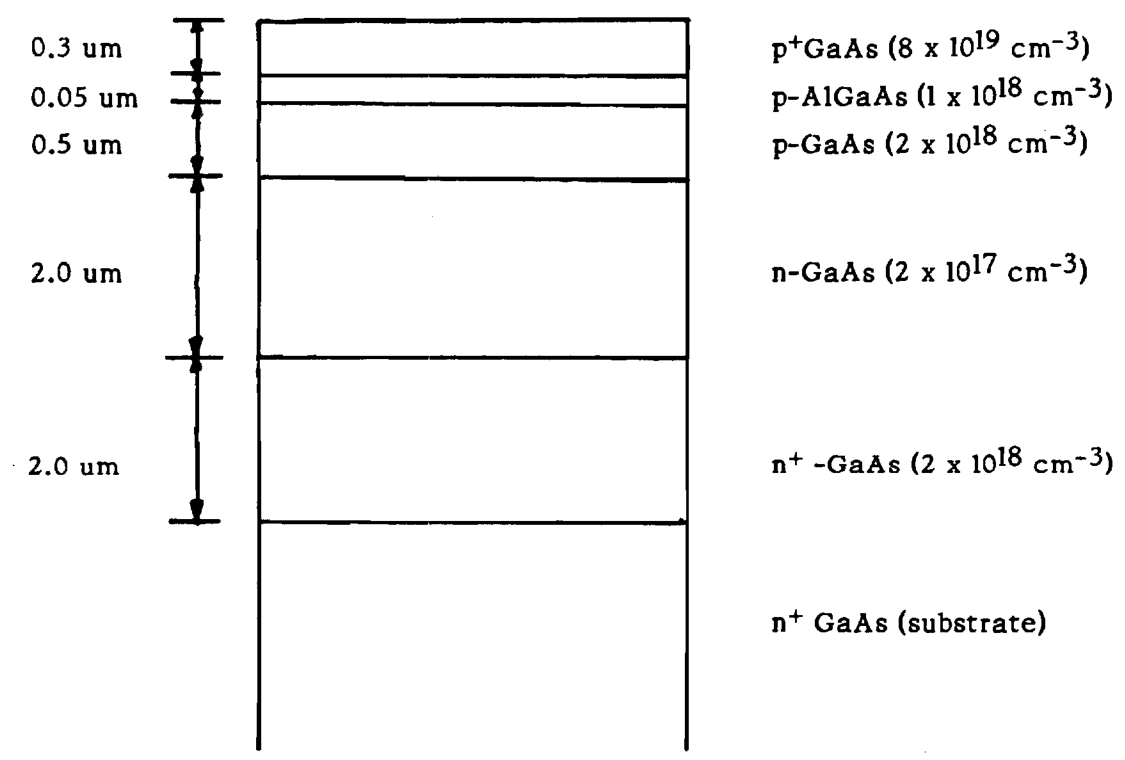

Figure 3: GaAs solar cell structure used in these experiments.

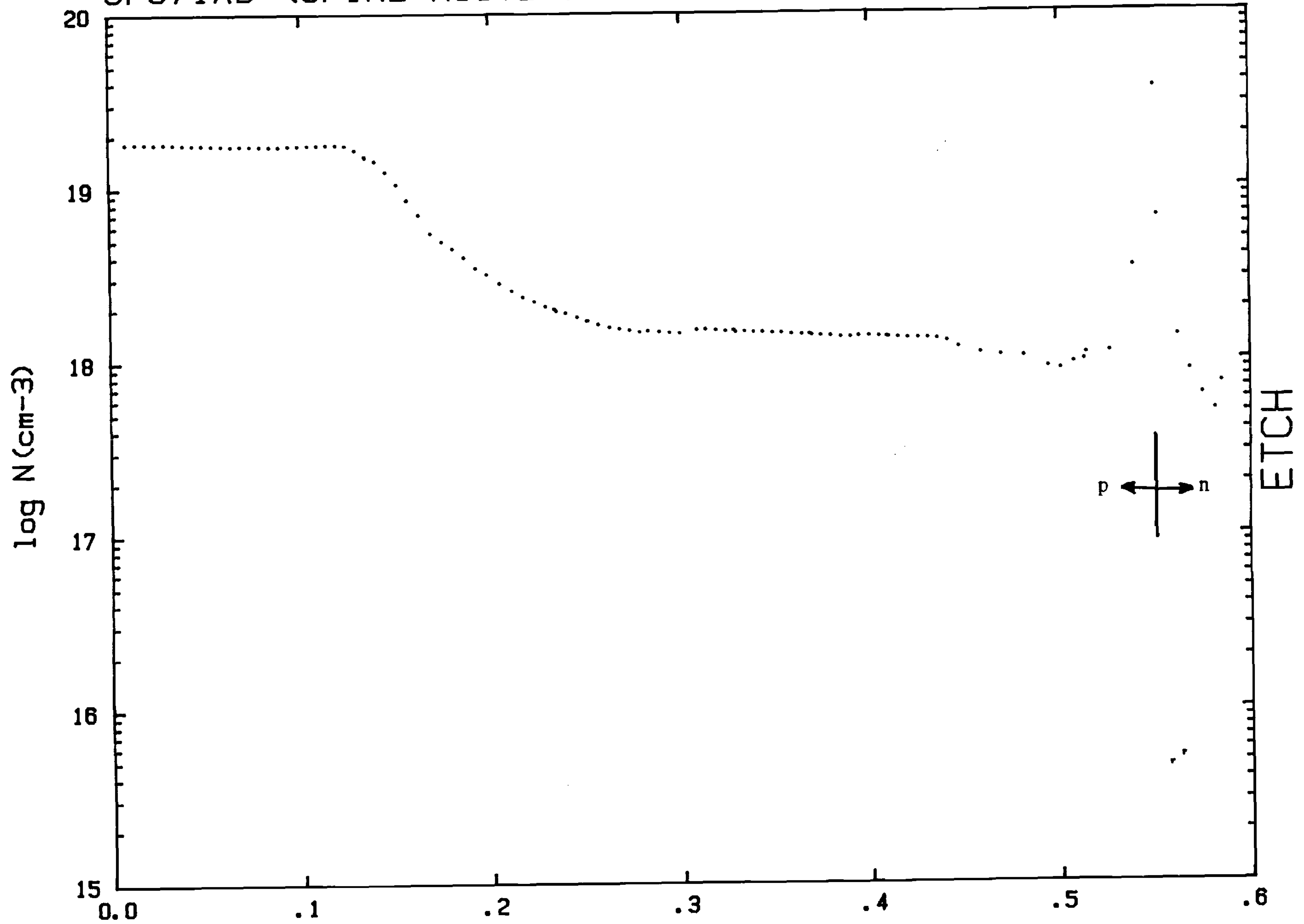

Figure 4: Doping profile of solar cell structure through the p-n junction. Spike at ∿0.55 micron is the p-n junction; to the left is p-type and to the right is n-type, as indicated.

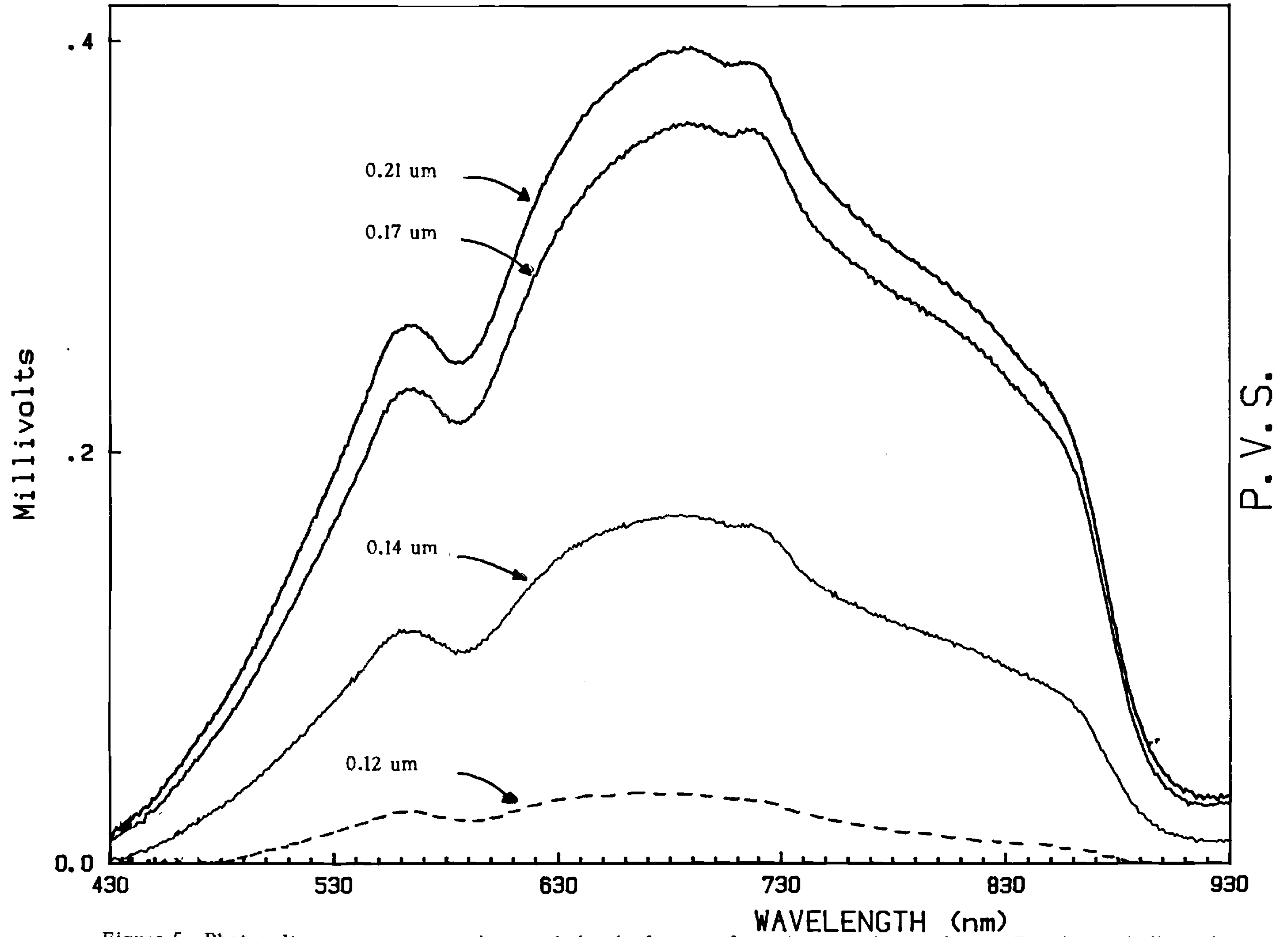

Figure 5: Photovoltage spectra at various etch depths from surface through the cap layer. Depths are indicated.

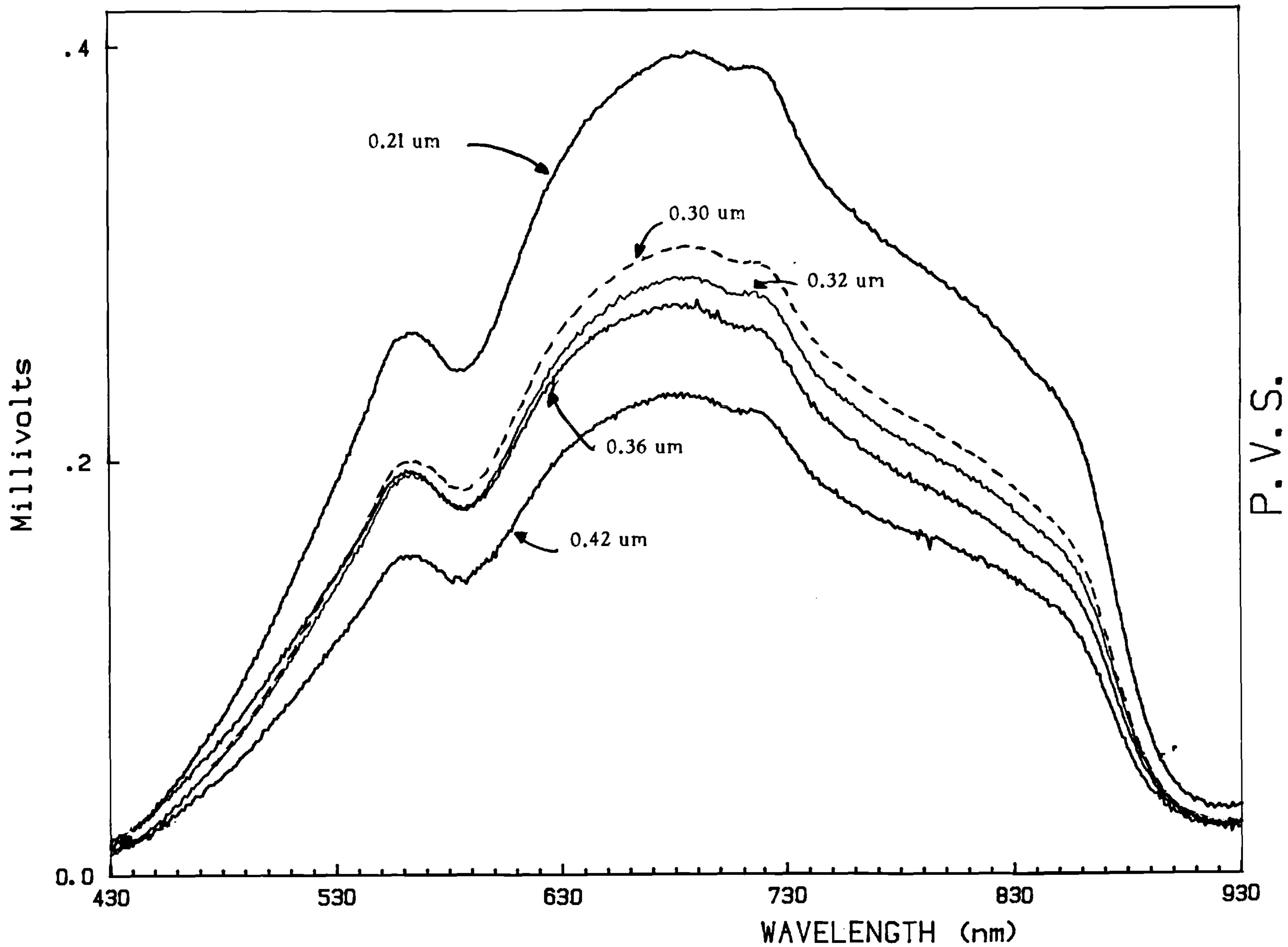

Figure 6: Photovoltage spectra at various etch depths from edge of cap layer toward the p-n junction.

SP571AB (SPIRE MOCVD CELL) SAR 4/16/87

.4

.2

0.0

Millivolts

P. V. S.

43■ .44 um 530 630 730 830 930

WAVELENGTH (nm)

Figure 7: Photovoltage spectrum near p-n junction indicating dramatic effect of p-n junction region on response.

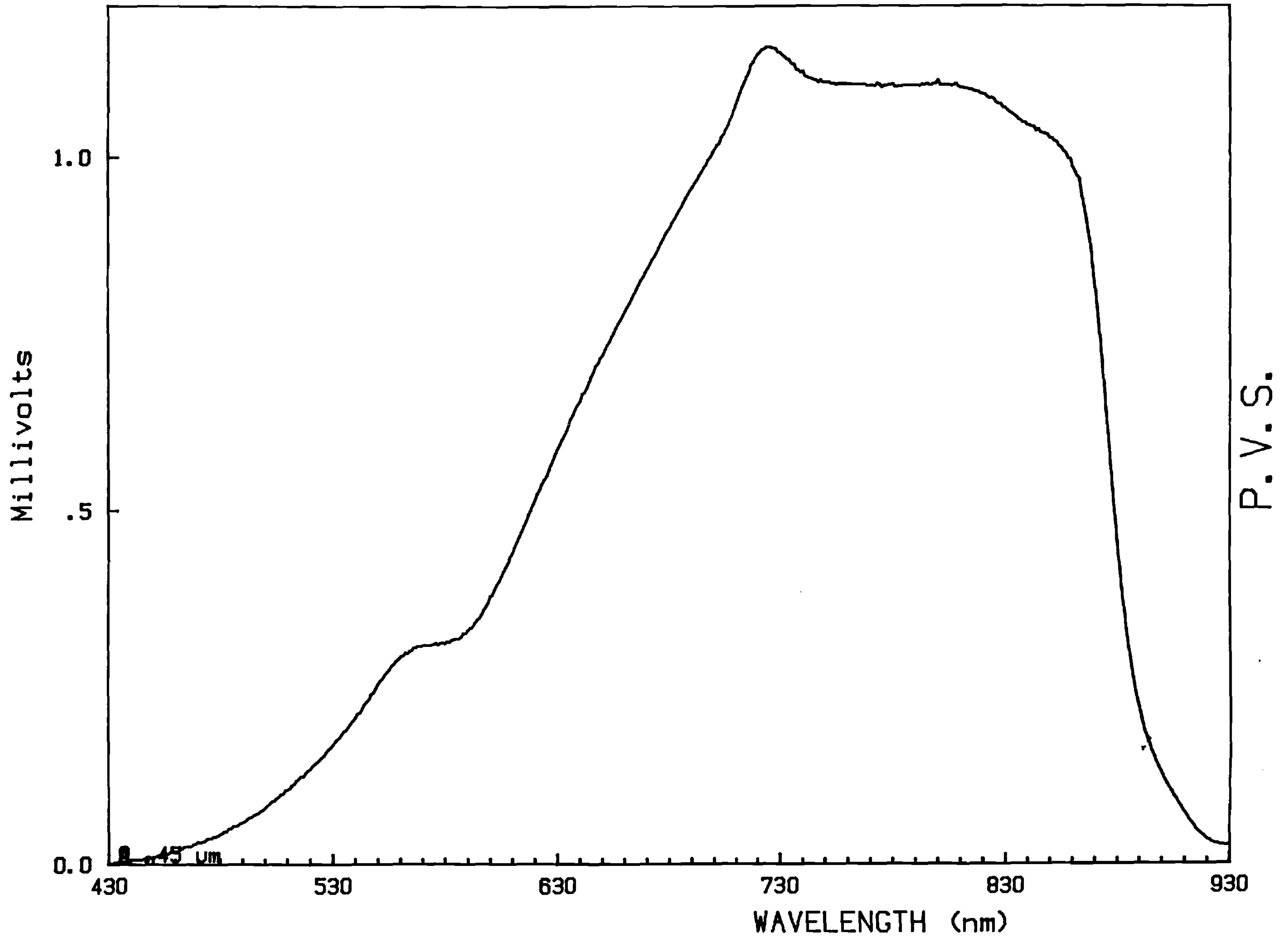

Figure 8: Photovoltage spectrum 100 angstroms beneath Figure 7 indicating a gradual recovery of unperturbed response.

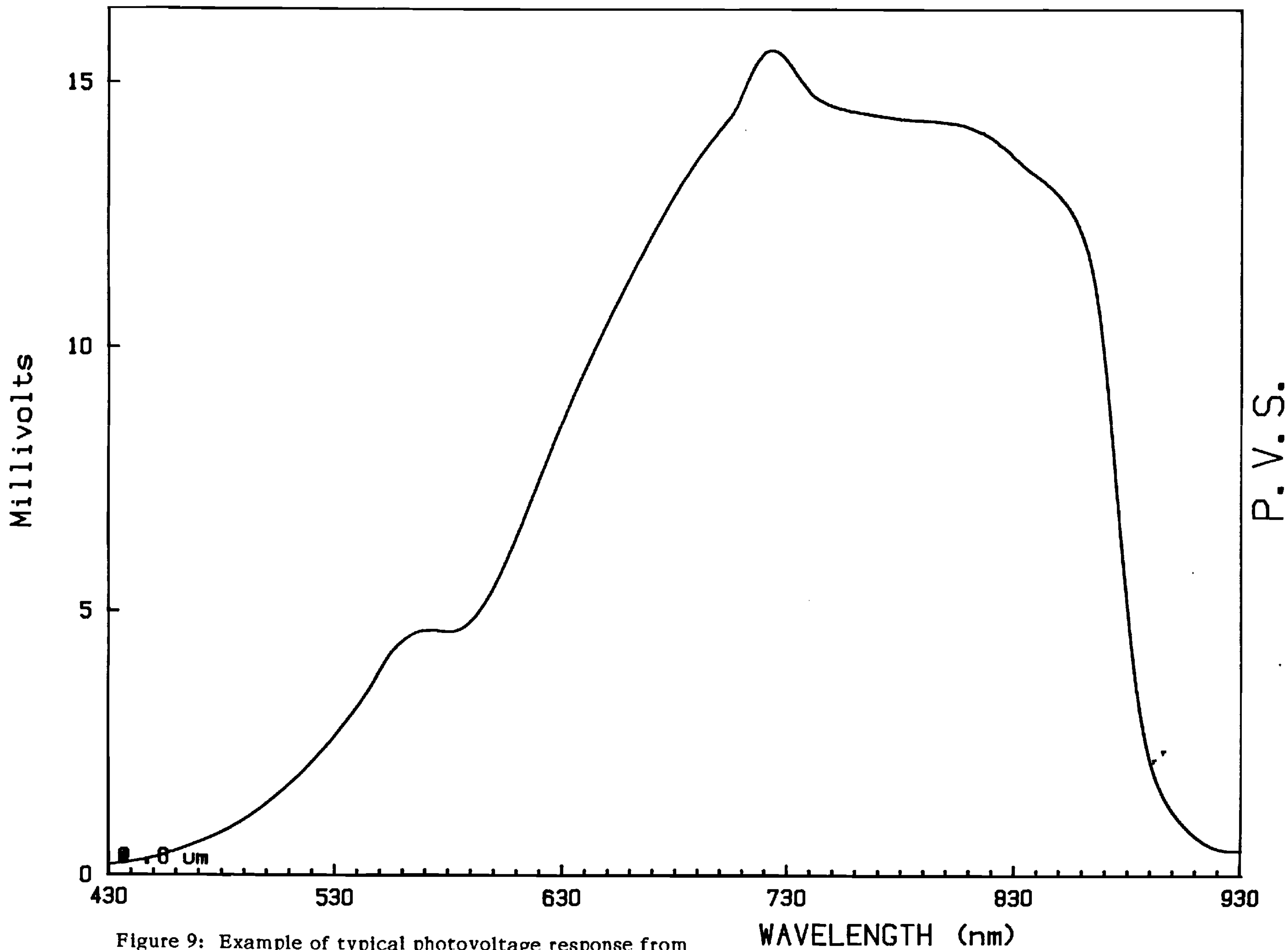

Figure 9: Example of typical photovoltage response from lower doped n-layer.

RESEARCH ON $AlGaAs/GaAs$ INTERFACES IN GaAs SOLAR CELLS

A. Rohatgi

Fourth Monthly Report for the Period

March 1 to March 31, 1987

Sandia National Laboratories

Contract No. 02-2255

GEORGIA INSTITUTE OF TECHNOLOGY
SCHOOL OF ELECTRICAL ENGINEERING
ATLANTA, GEORGIA 30332

Technical Progress

The major objective of this program is to develop techniques and methodology to characterize AlGaAs/GaAs interfaces and provide guidelines for improving GaAs solar cells.

During the past month, we have studied depth-resolved photovoltage responses of a MOCVD-grown GaAs solar cell structure supplied by Spire Corporation (see Figure 1a; the doping profile obtained experimentally is shown in Figure 1b). The photovoltage measurements were done using an automated photovoltage spectroscopy (PVS) system. We have also obtained some preliminary infrared reflection measurements on the same sample.

An attempt was made to assess the quality and uniformity of the material in the structure by comparing PVS spectra at different etch depths. This was accomplished by dividing the PVS spectrum at one depth by a spectrum taken at another depth. These divisions were done periodically to ascertain any material variations. Ideally, if one were comparing two spectra from the same material with the same doping level, the PVS ratio should be unity over the entire wavelength range. But in this case, there is a doping variation normal to the surface so the ratio will not be unity (since the signal strength is inversely proportional to the doping) but should still remain flat throughout the wavelength range if the material quality is perfect. If another material, such as AlGaAs, is present in one spectrum but not another, then a division of the two should result in the AlGaAs response alone. Figure 2 shows the result of a division of SPV at 0.30 micron by an SPV at 0.28 micron. The deviation from unity indicates a material variation between 0.28 and 0.30 micron. Figure 3 shows the division of SPV at 0.38 micron by SPV at 0.36 micron where it is now observed that the result is flat (although the ratio is no longer one since the doping is changing through this region). Figure 4 shows the division of SPV at 0.44 micron by SPV at 0.42 micron indicating a large difference between the SPV response at these depth values. It is not clear at this point as to the cause of this variation. However, upon comparison with the doping profile in Figure 1B and considering

the penetration depth of the incoming photon flux, it would appear that the p-n junction area is introducing, possibly through an extended spatial layer of defects, the deviation. Figure 5 shows a return to a basically flat ratio after the junction has been etched through. Hence, although correlations must be made with other characterization methods, SPV profiling seems to be a useful and capable tool for assessing material quality and uniformity. PVS data analysis is not fully understood at this time, specifically quantitative analysis of the data.

Infrared (IR) reflection measurements in the range 50-450 cm^{-1} have been taken at 300K and 6K (Figures 6 and 7, respectively). The spectrum at 300K shows sharp peaks at 250, 270, and 365 cm^{-1}. At 6K all peaks sharpen, a characteristic behavior of phonons. The peak at 270cm-1 corresponds to GaAs transverse optical phonon mode, and the peaks at 365 and 256 cm^{-1} correspond to the AlGaAs layer. Below 200 cm^{-1} the reflectivity increases with decreasing frequency at 300K and 6K. At 300K increasing reflectivity below 200 cm is a clear indication of free carriers in the sample, but the increasing reflectivity below 200 cm^{-1} at 6K cannot be explained by the same argument. Further experiments like measuring reflectivity after removing the AlGaAs layer, and measuring reflectivity in the range 20-240 cm^{-1} may give some clue to understanding the 6K data.

In conclusion, we have been able to profile the photovoltage response with depth and make accurate comparisons at various depths to study changes in the response. The variations could be directly related to process-induced fluctuations in material quality. Interpretation of the PVS data is tricky and will be studied carefully. We have successfully performed IR measurements on this sample and have identified the AlGaAs layer which the SPV measurement could not resolve. Future work will include additional reflectivity measurements as mentioneed above. We will be studying the effects of atomic hydrogen (introduced by low-energy (<.5 KeV) ion implantation) on the PVS response and DLTS signature of the structure studied here since it is well known that hydrogen has a beneficial effect on materials with electronically active defects such as Si and GaAs. We will also be studying the bulk properties of AlGaAs at different x values since

the quality of this layer in a GaAs solar cell is becoming widely acknowledged as major contributor in limiting solar cell efficiency.

The author would like to acknowledge the assistance of Steven A. Ringel (GRA) who is conducting the experimental research for this program. I would also like to acknowledge the assistance of R. Sudharsanan and S. Perkowitz of Emory University for the help in IR measurements.

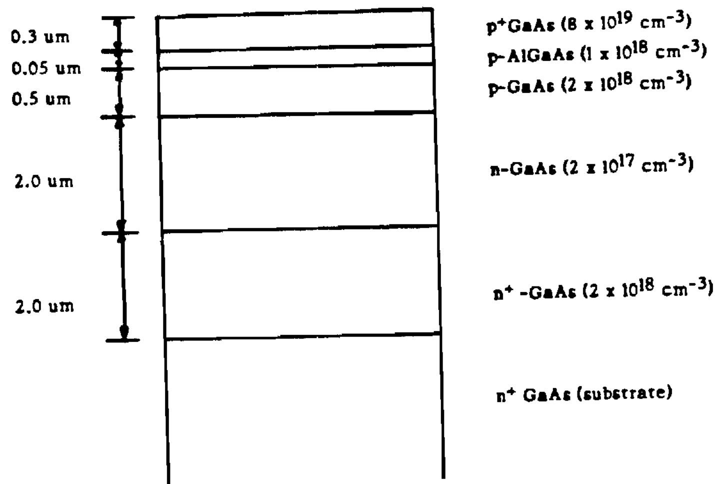

Figure 1 a) GaAs solar cell structure used here

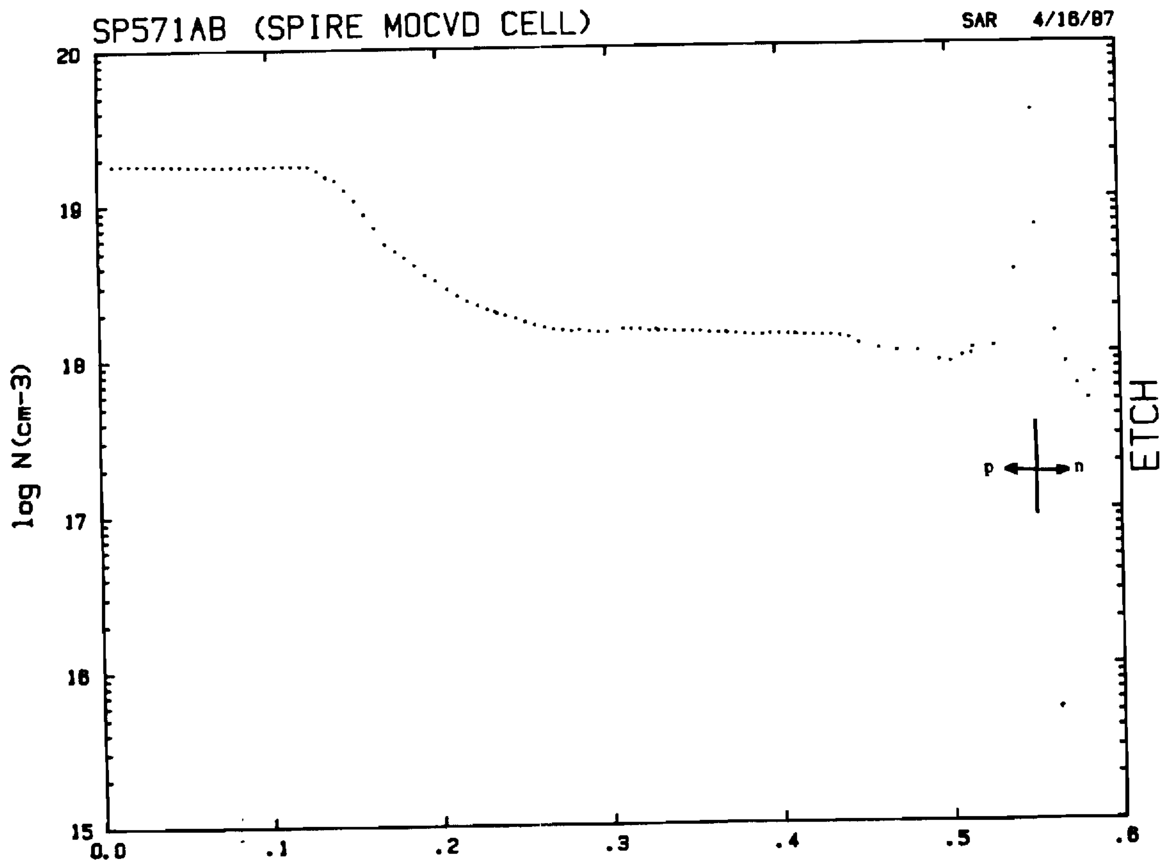

b) Doping profile of solar cell through p-n junction. The spike at a55 micron is the p-n junction; to the left is p-type and to the right is n-type, as indicated.

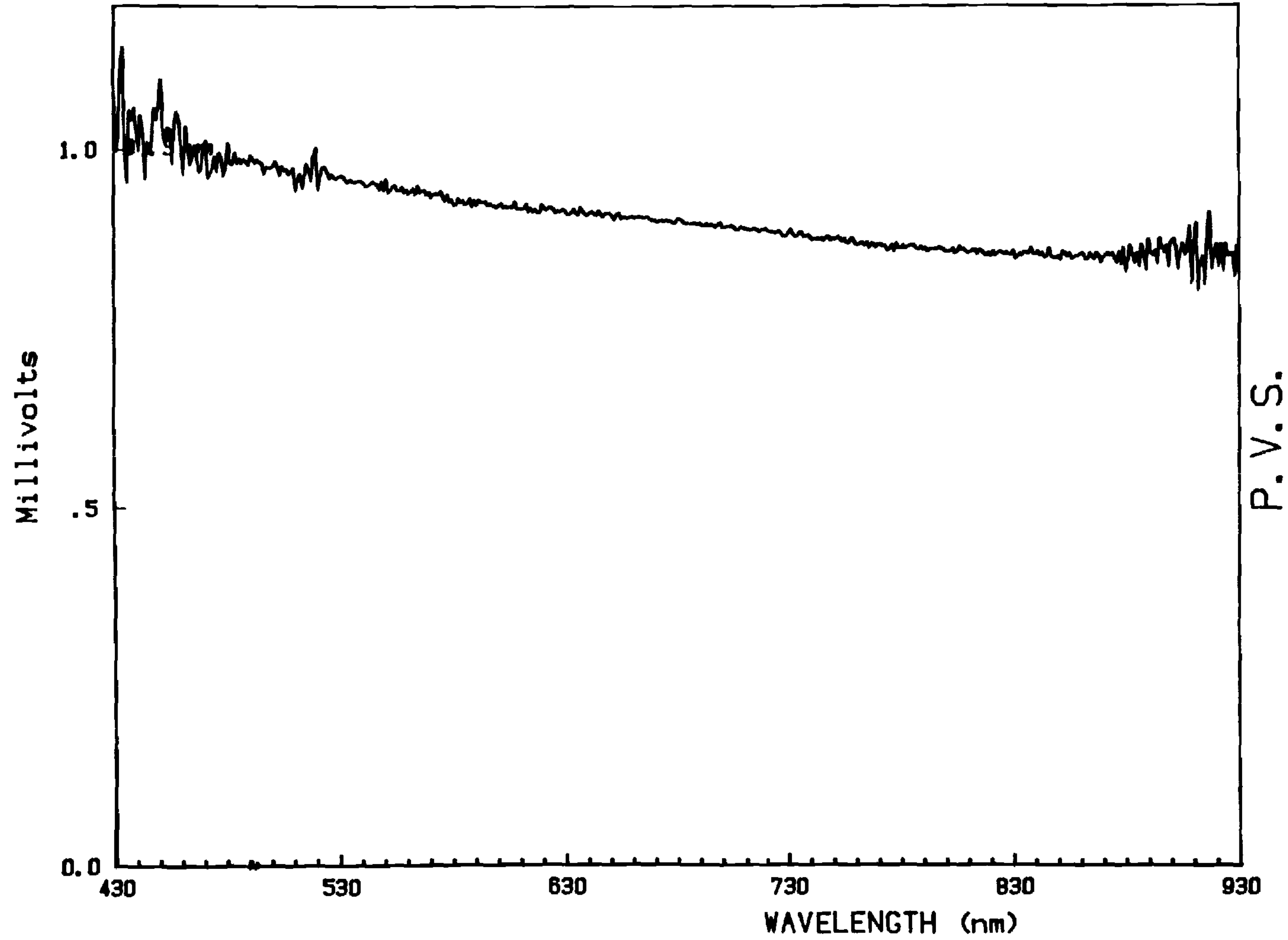

Figure 2: Ratio of SPV spectrum at 0.30 micron to SPV spectrum at 0.28 micron

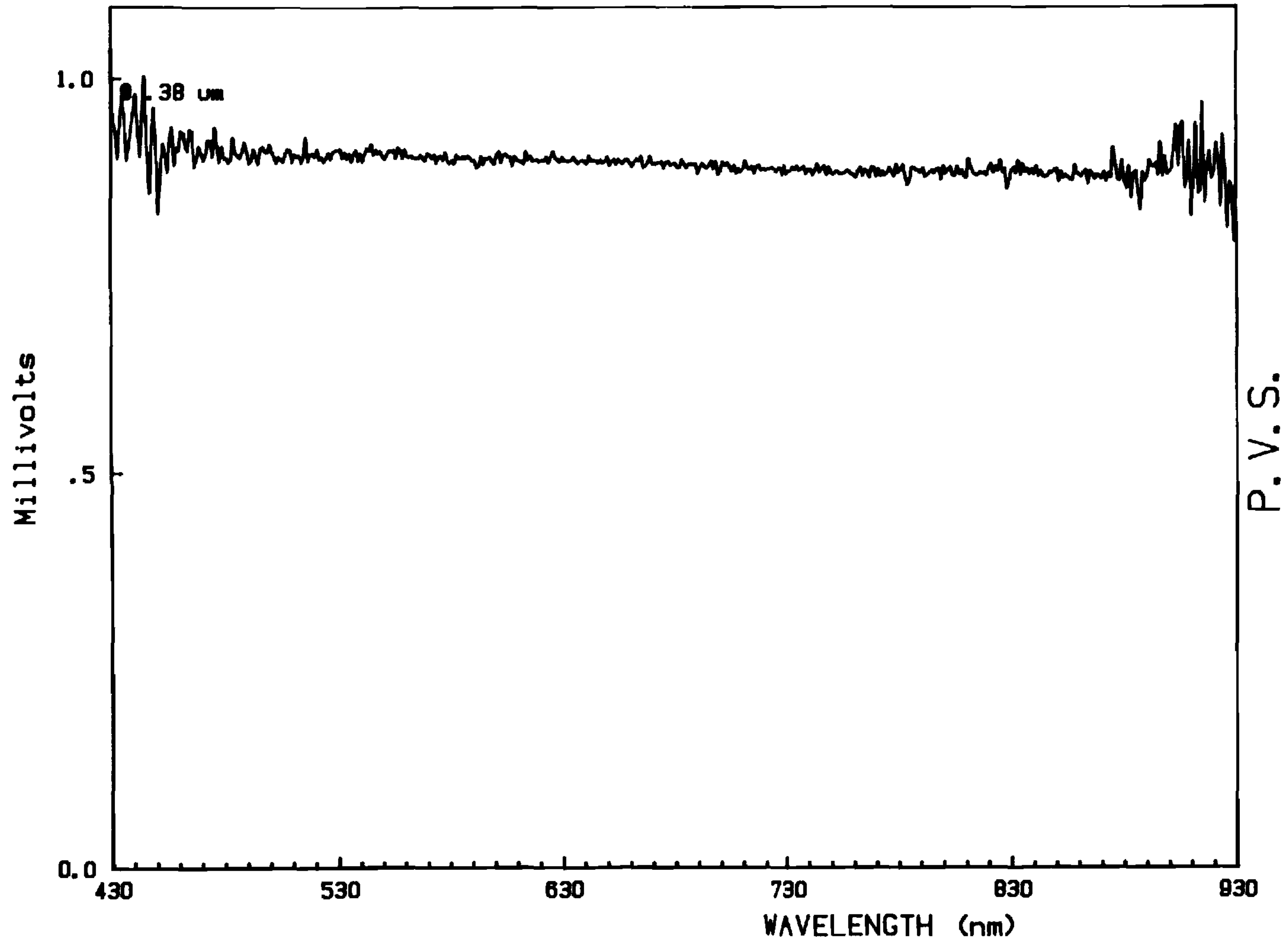

Figure 3: Ratio of SPV spectrum at 0.38 micron to SPV spectrum at 0.36 micron

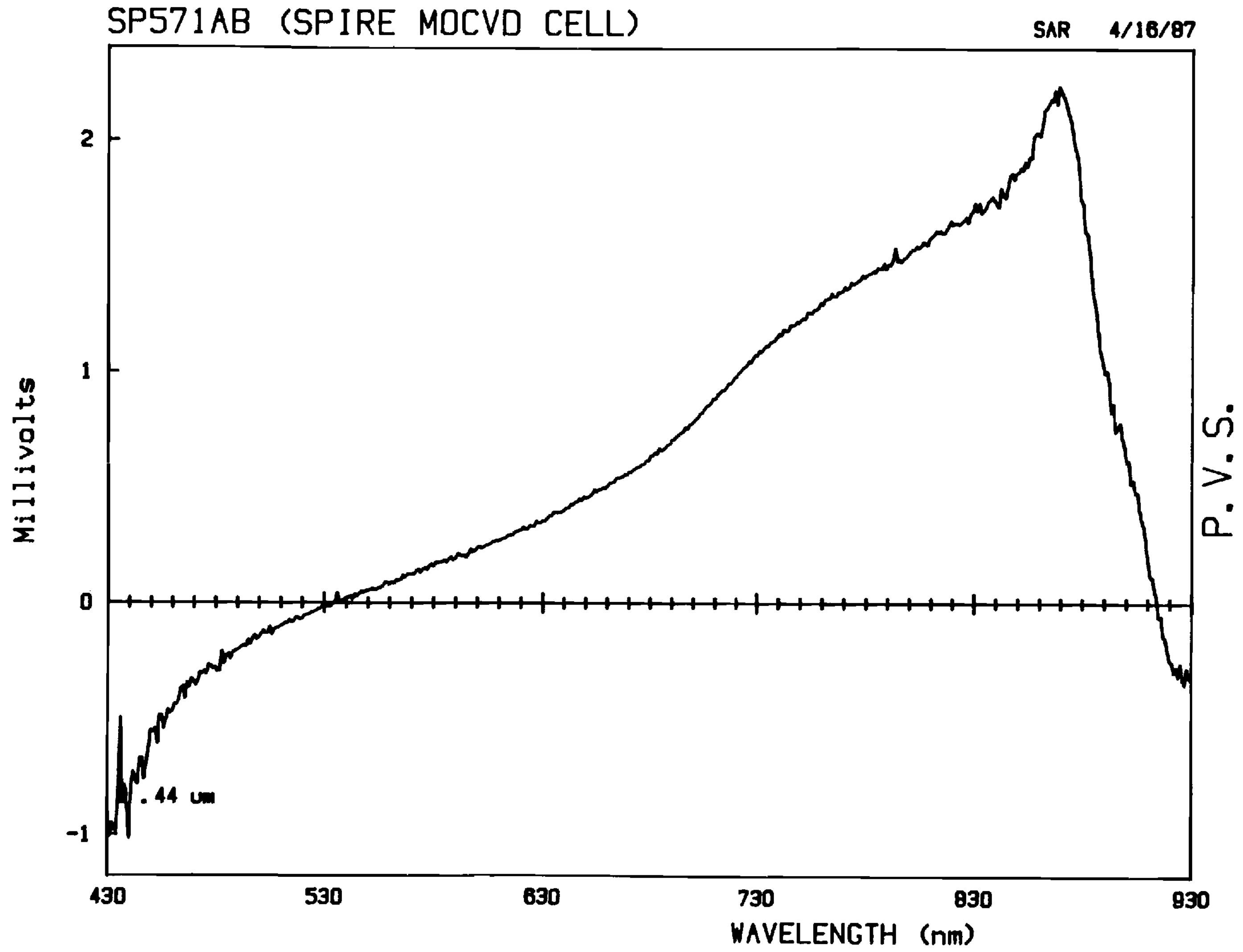

Figure 4: Ratio of SPV spectrum at 0.44 micron to SPV spectrum at 0.42 micron

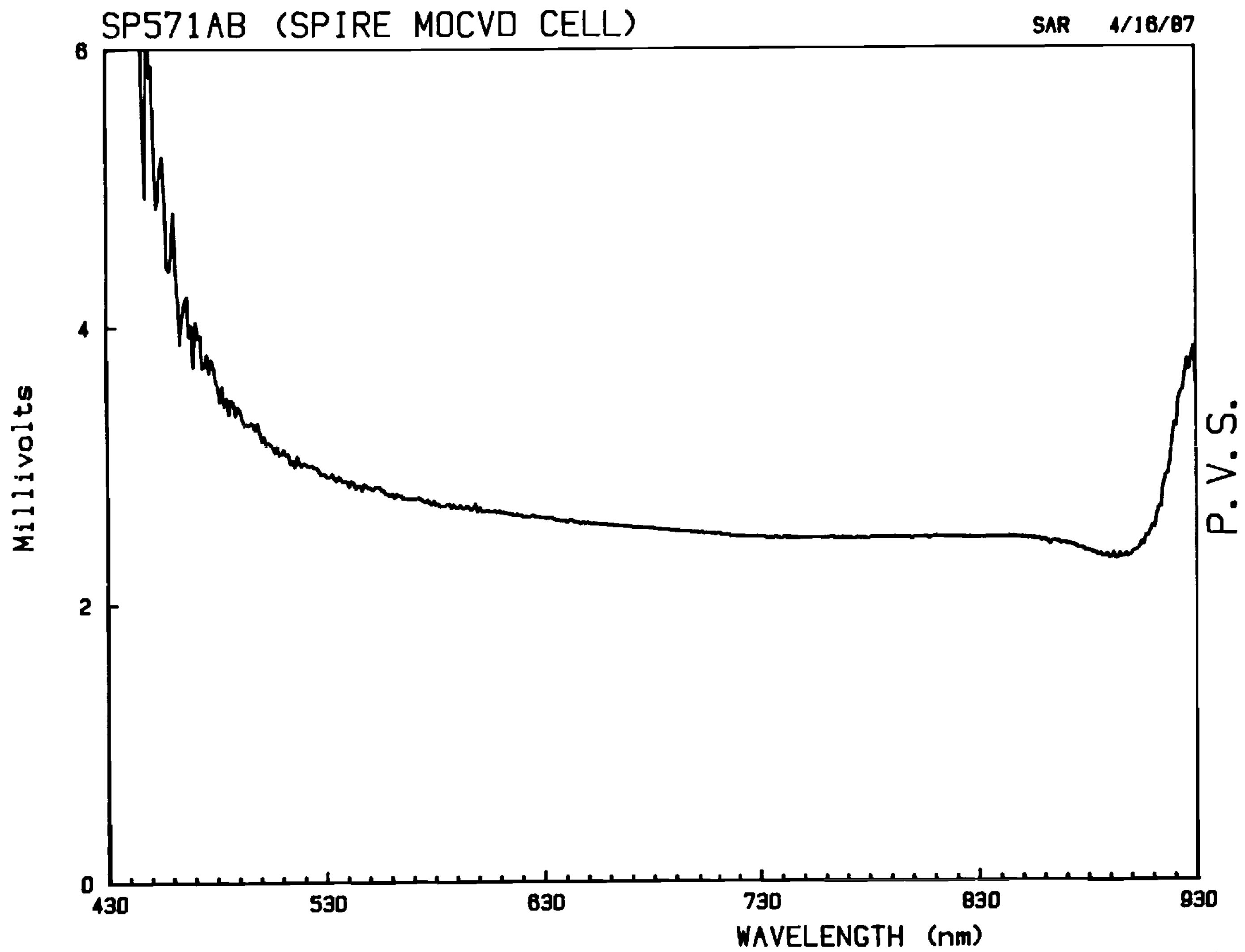

Figure 5: Ratio of SPV spectrum at 0.47 micron to SPV spectrum at 0.45 micron

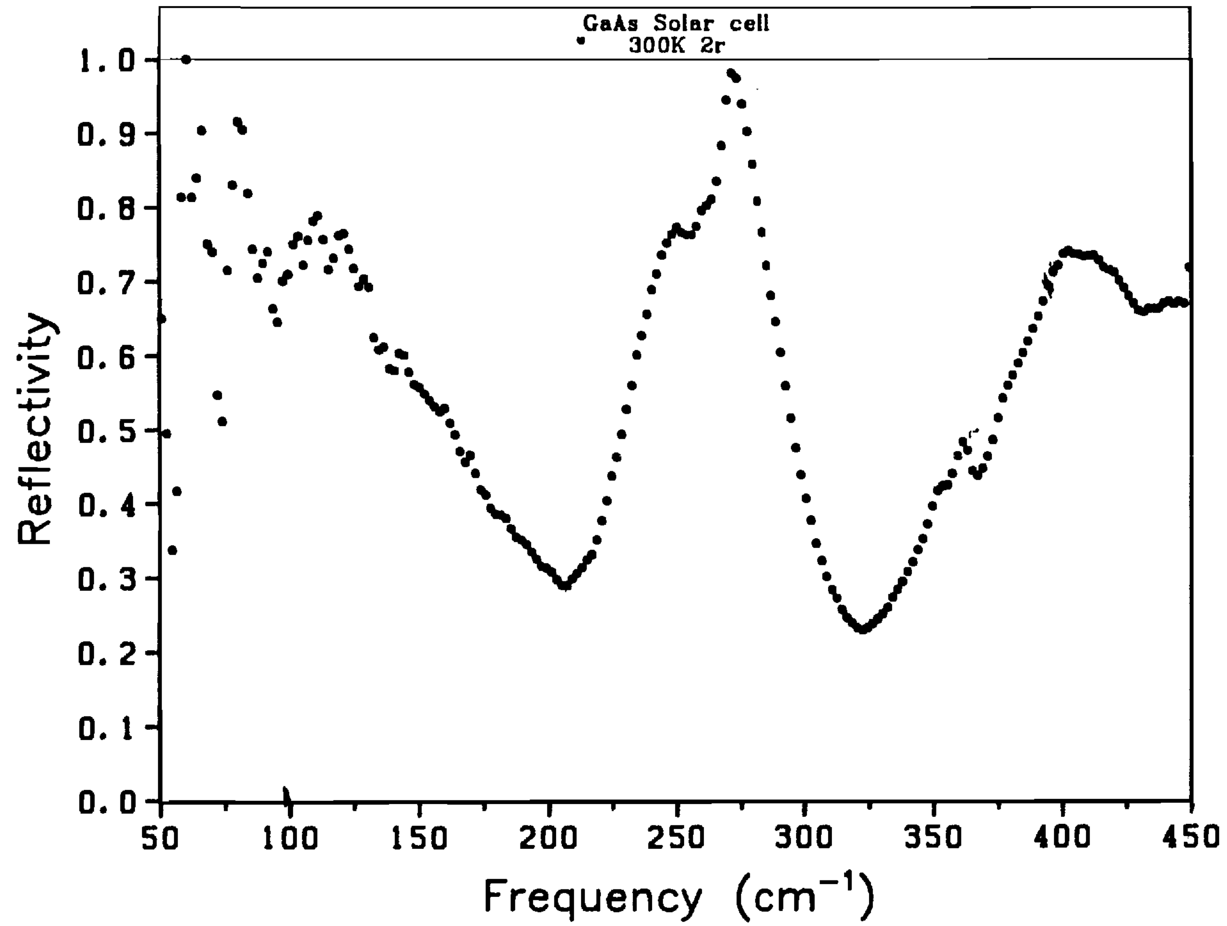

Figure 6: IR reflection measurement at 300K of the GaAs cell

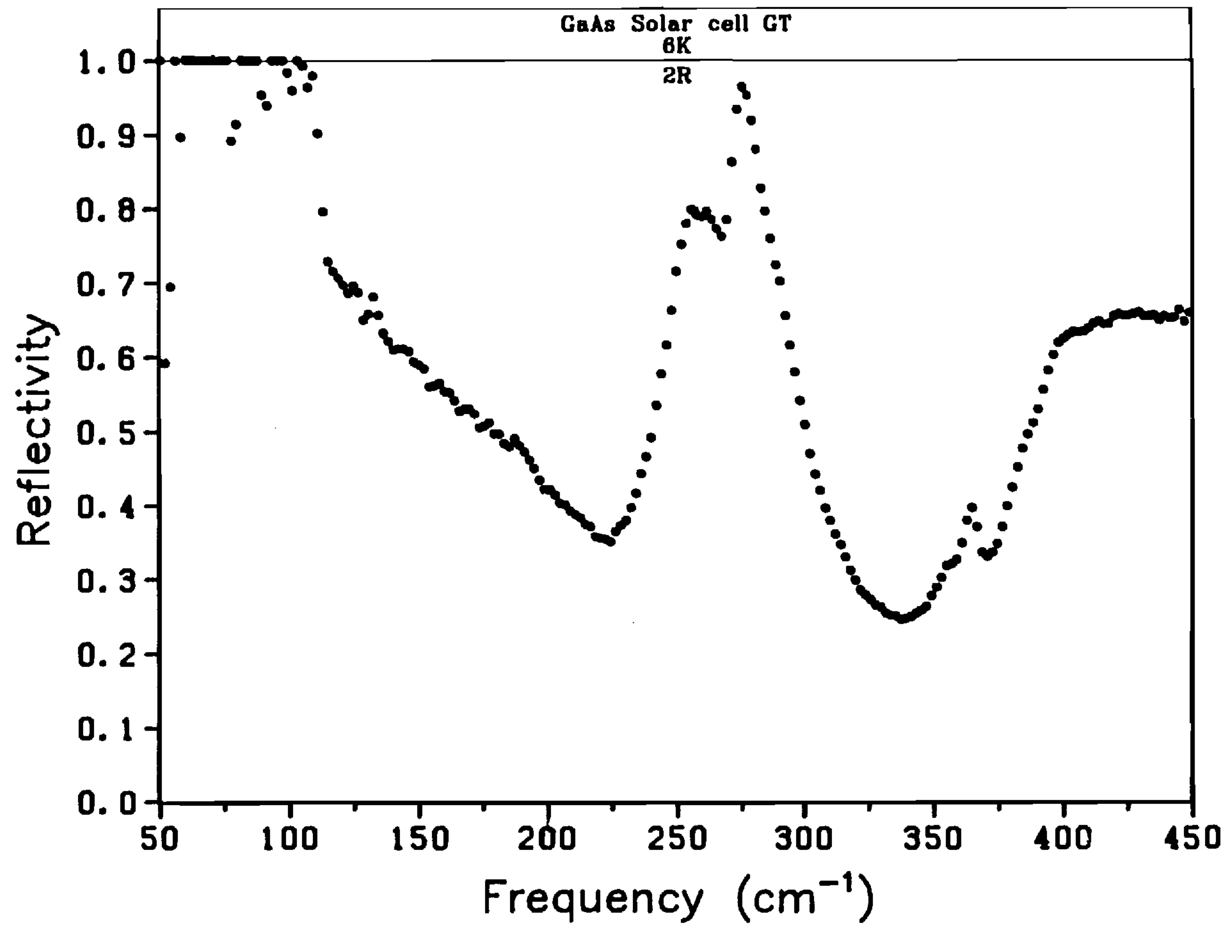

Figure 7: IR reflection measurement at 6K of the GaAs cell

RESEARCH ON AlGaAs/GaAs INTERFACES IN GaAs SOLAR CELLS

A. Rohatgi

Fifth Monthly Report for the Period

April 1 to April 30, 1987

Sandia National Laboratories

Contract No. 02-2255

GEORGIA INSTITUTE OF TECHNOLOGY
SCHOOL OF ELECTRICAL ENGINEERING
ATLANTA, GEORGIA 30332

Technical Progress

The major objective of this program is to develop techniques and methodology to characterize AlGaAs/GaAs interfaces and provide guidelines for improving GaAs heterojunction solar cells.

During the past month we have investigated some properties of LPE-grown AlGaAs, supplied by Hughes, at two different x values, x=0.20 and x=0.38. Photovoltage spectroscopy measurements, dopant profiling, and Hall effect measurements as a function of temperature were all successfully run on these samples.

Figure 1 shows the photovoltage spectrum for both AlGaAs samples (x=0.20 and x=0.38). Each spectrum was taken after etching somewhat into the epilayer to insure no contribution from surface effects. Note the difference in the absorption edge of each trace indicating the bandgap change with x value. The cutoff wavelengths determined at the half-maximum points give energy gaps of 1.97 eV and 1.71 eV for x=0.38 and x=0.20, respectively. These values agree with those independently found by Dr. Bob Loo of Hughes using other measurement techniques. The difference in the magnitude of the responses may be attributed to the difference in the absorption coefficient (α) since α goes as $(h\nu - E_G)^{\frac{1}{2}}$. With a lower α (larger bandgap energy) a photon will travel farther into the layer to generate an electron-hole-pair. This carrier then would have a more difficult time of making it back to the surface to be collected than had it been generated closer to the surface (which is the case for higher α, or lower bandgap material. This explanation would suggest a decrease in the photovoltage response of the higher bandgap material with respect to that of the lower bandgap material. This is precisely what is observed here. Another possible factor is the increase in alloy scattering events in the x=0.38 AlGaAs as compared to the x=0.20 AlGaAs which greatly decreases the diffusion length and hence makes carrier collection, particularly from electron-hole-pairs generated deeper into the epilayer, less probable. As Figure 2 indicates, free carrier effects are not a factor in changing the absorption coefficient here since the net doping levels of the two samples

are virtually identical. One other point of interest in Figure 1 is the broadening of the absorption edge just below the bandgap in both samples. While we are not certain at this point, this feature is possibly due to shallow levels contributing the absorption as has been observed and reported elsewhere.

Hall effect measurements were successfully made on the x=0.20 sample (we did not have a Hall sample available for the x=0.38 piece) as a function of temperature from room temperature to 80 K. Figure 3 is a plot of doping concentration and Hall mobility versus 1000/T as derived from the Hall data, indicating typical results.

In conclusion, we have successfully demonstrated the ability to use depth-resolved photovoltage spectroscopy to study ternary compounds. We have clearly demonstrated the changes in optical properties of AlGaAs at two different x values by this method. We have also successfully performed automated Hall measurements on these samples. Future work will involve studying the effect of the implantation of atomic Hydrogen on AlGaAs since it is well known to have a beneficial effect on the electrical properties of Si and GaAs. We will resume the study of the GaAs solar cell structure which is presently undergoing Hydrogen implantation to see what change this may produce in DLTS and photovoltage measurements.

The author would like to acknowledge the assistance of Steven A. Ringel (GRA) who is conducting the experimental research for this program.

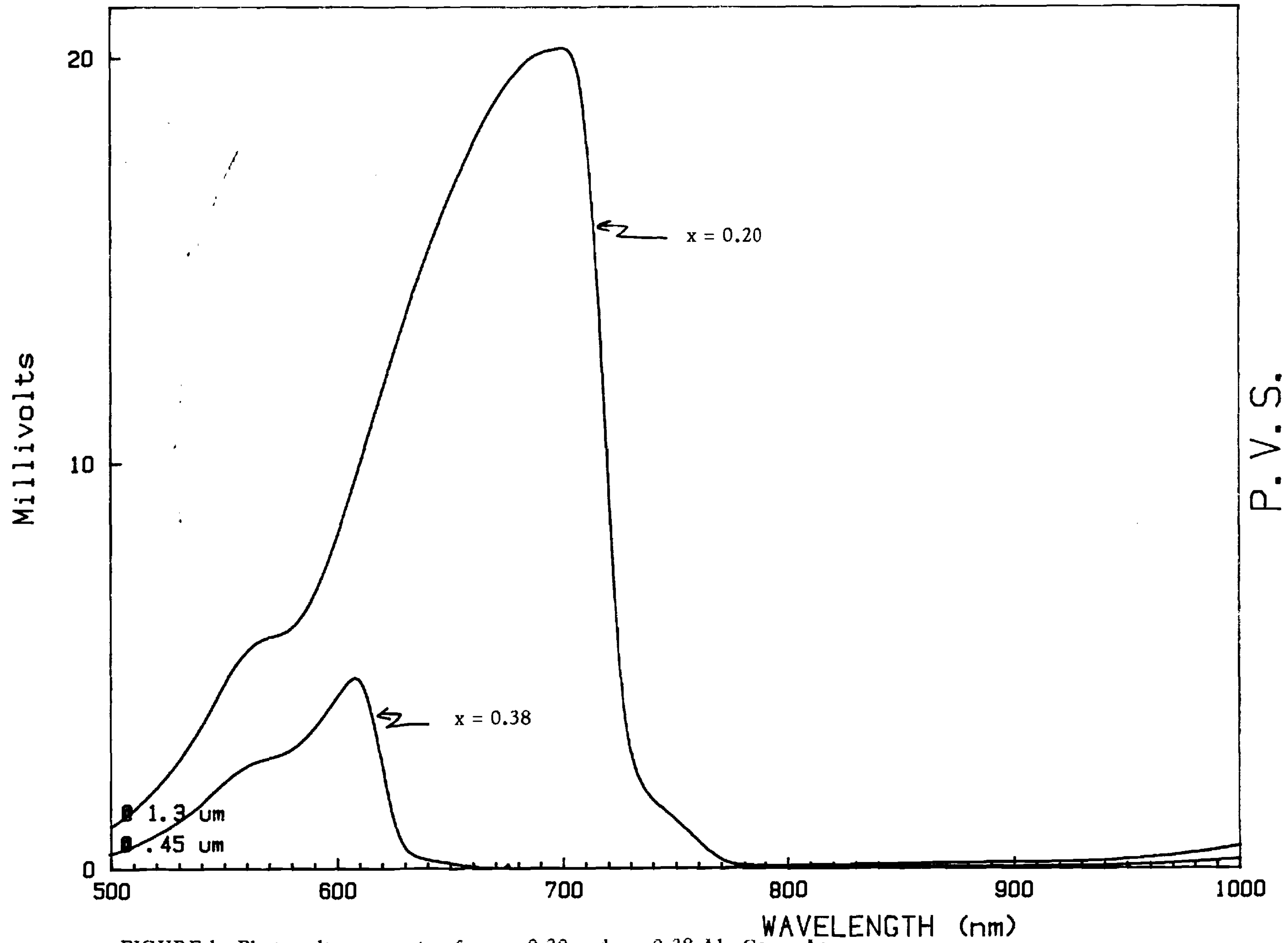

FIGURE 1: Photovoltage spectra for x = 0.20 and x = 0.38 $Al_x Ga_{1-x} As$

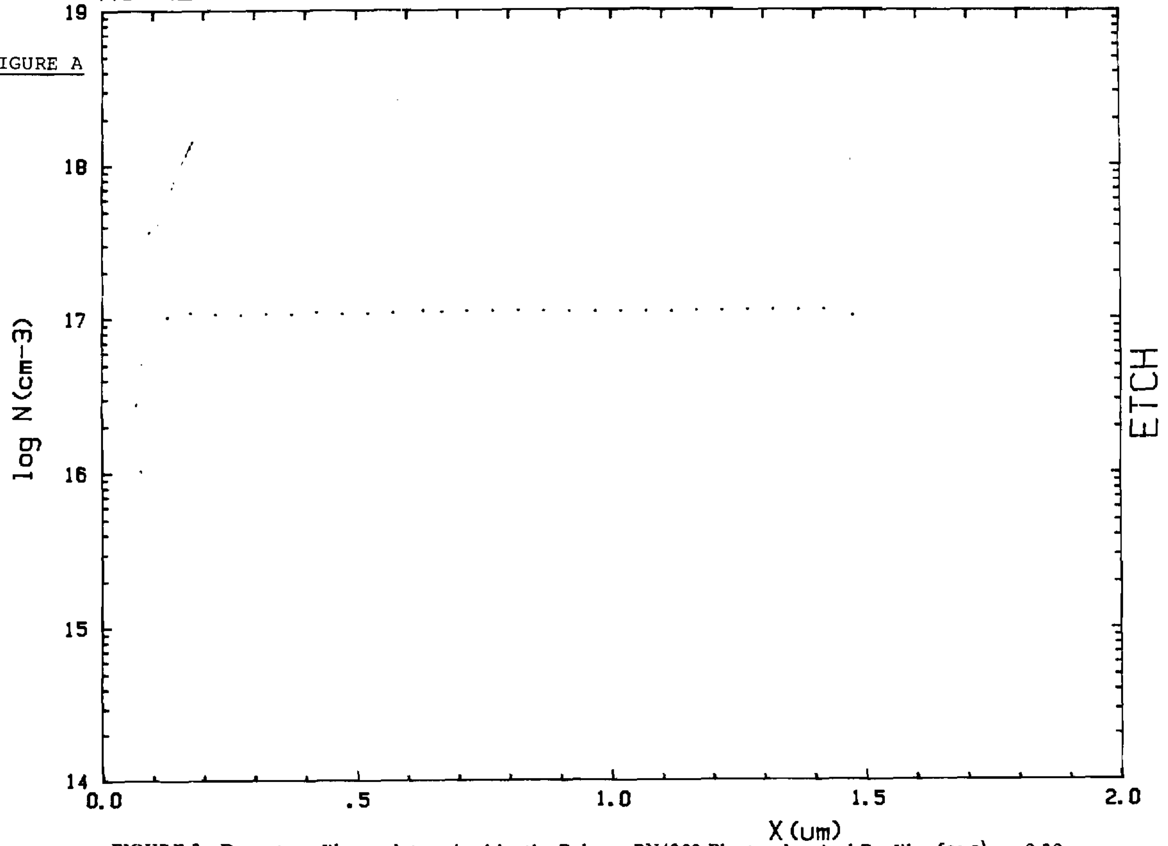

FIGURE 2: Dopant profiles as determined by the Polaron PN4200 Electrochemical Profiler for a) x = 0.20 and b) x = 0.38 AlGaAs

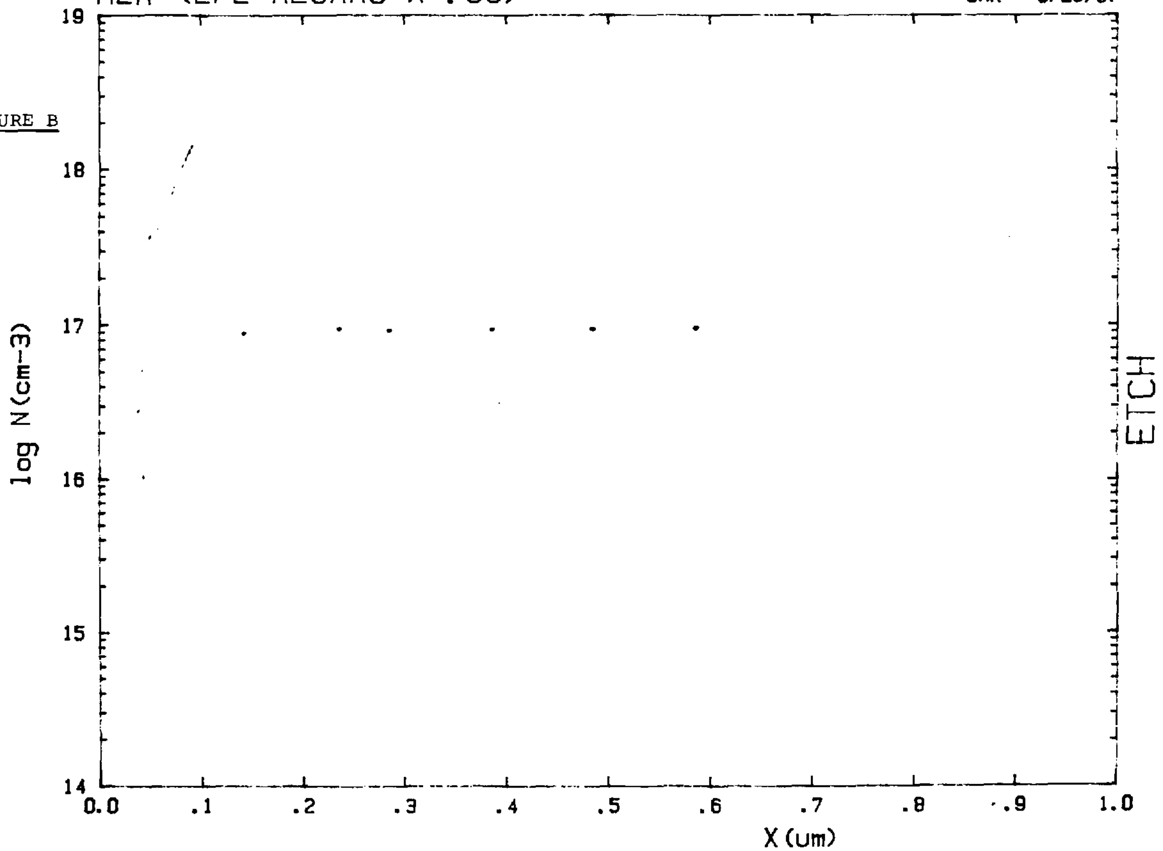

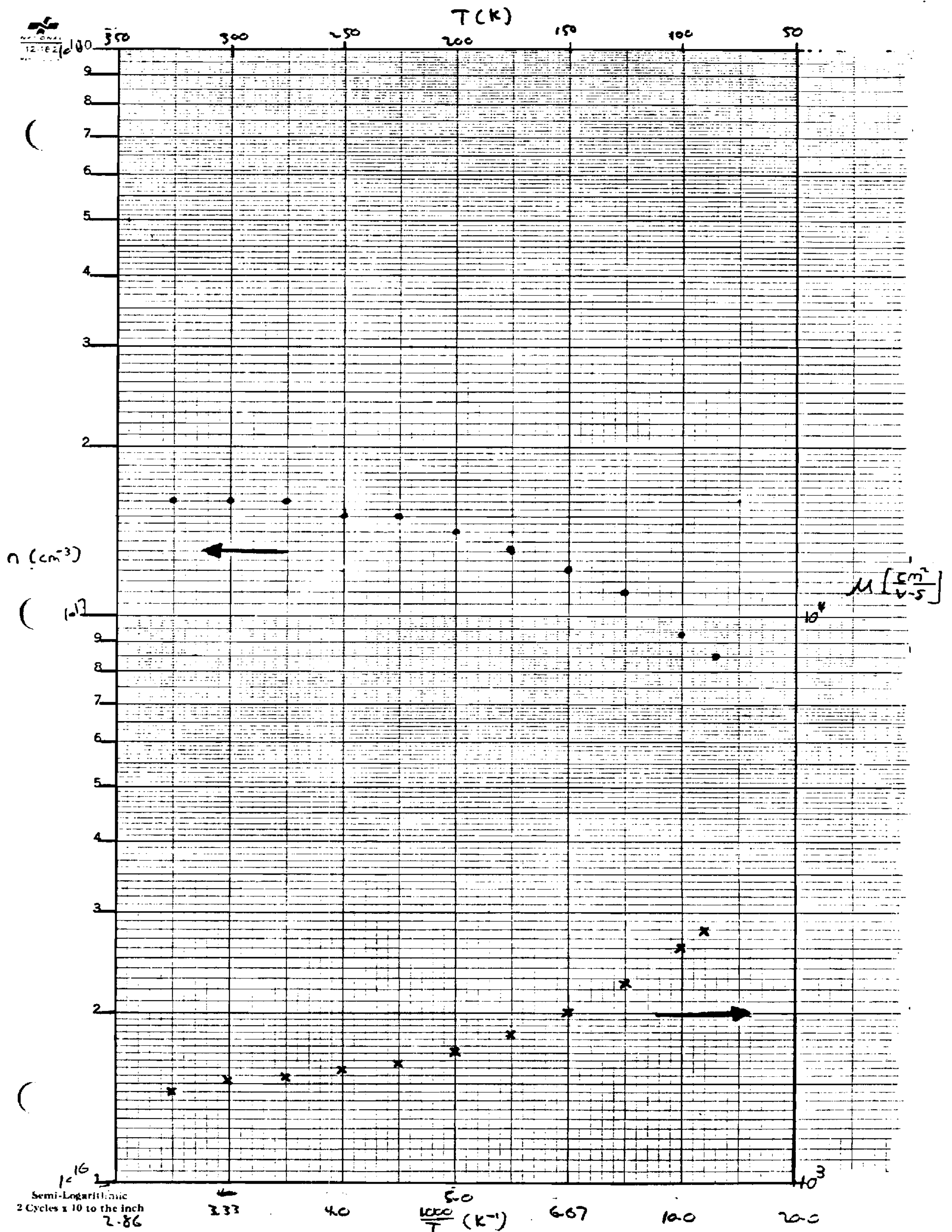

FIGURE 3: Plot of doping vs. $1000/_T$ derived from Hall measurement

RESEARCH ON AlGaAs/GaAs INTERFACES IN

GaAs SOLAR CELLS

A. Rohatgi

Sixth Monthly Report for the Period

May 1 to May 31, 1987

Sandia National Laboratories

Contract No. 02-2255

GEORGIA INSTITUTE OF TECHNOLOGY
SCHOOL OF ELECTRICAL ENGINEERING
ATLANTA, GEORGIA 30332

Technical Progress

The major objective of this program is to develop techniques and methodology to characterize AlGaAs/GaAs interfaces and provide guidelines for improving GaAs heterojunction solar cells.

During the past month we have attempted to profile the p/n junction region of a high efficiency GaAs MOCVD p/n heteroface solar cell structure supplied by Spire Corporation for electrically active deep levels by Deep Level Transient Spectroscopy (DLTS). Mesa diodes were fabricated onto a piece of wafer and a schematic of the test device is shown in Figure 1. The C/V characteristics of the p/n junction (Figure 2a) indicates that the n-GaAs side is being probed (voltage scale polarity is with respect to the gate contact) and the corresponding dopant profile derived from this C/V (Figure 2b) indicates good agreement with the target value of 2×10^{17} cm^{-3}.

Depth-resolved DLTS measurements were made by a systematic variation of the depletion bias and pulse bias while keeping the sum of these voltages constant. In this way, the spatial region of sensitivity is changed. In the DLTS setup at Georgia Tech, it is possible to perform five such runs (each with a different depletion width) per each temperature cycle and is referred to as the multi-bias mode. A description of the technique is most easily seen pictorially in Figure 3. Here, Figure 3a shows the multi-bias condition for electron (majority) traps in a $p^{+}n$ diode with a standard filling pulse while Figure 3b is the condition for multibias profiling of hole (minority) and electron traps using an injection pulse. The lock-in amplifier technique is used here with five different weighting functions for each bias condition being analyzed during a single temperature scan.

I/V data measurements taken on the mesa diode indicated a reverse breakdown voltage of -9.5 volts and hence the initial multi-bias measurement was made by varying the steady depletion bias (Vs) from -8.0 to -1.0 volts, and shrinking the depletion width to a thickness corresponding to a bias of -0.5 volts with each filling pulse (Vp). The results are shown in Figure 4 where each grouping

of traces corresponds to a different weighting function and there are five traces due to the five bias conditions in each grouping. No outstanding features indicative of the presence of deep levels are discernable. To probe the region in the vicinity of the p/n junction, multi-bias DLTS was done by varying Vs from -1.0 to -0.2 volts while keeping Vs + Vp = -0.1 volts, constant. The multibias spectrum was again featureless but upon closer scrutinization a small possible peak was detected for the three bias condition conditions closest to the junction. The peak was the largest for the smallest bias indicating a possible non-uniform distribution of a defect near the junction. The DLTS scan at this bias was separated from the multi-bias plot for each weighting function to study its character more closely and is shown in Figure 5. Multi-bias DLTS was also run using injection pulses (see Figure 3b) to determine the presence of hole traps in the n-GaAs but none were detected.

The difficulty in finding deep levels in MOCVD n-GaAs is somewhat surprising given the abundance of traps reported in this material. However, the high efficiency of the p/n heteroface cells fabricated on this structure by Spire Corporation indicate that the concentration of traps should be small. This fact, coupled with the high doping level in the region being probed (n-GaAs doping is 2×10^{17} cm^{-3}), suggests that the number of deep levels present are simply below the detection limit of conventional DLTS which is at best one hundredth of 1% of the background doping level. Hence, traps with a density of less than 2×10^{13} cm^{-3}, which is a reasonably large number, will go undetected by DLTS. It is interesting to compare this result with the DLTS data found on the LPE GaAs p/n heteroface solar cell supplied by Hughes, which we studied earlier. The doping levels are essentially the same as the MOCVD cell. Here one hole trap of reasonably large density was found and the DLTS scan is shown in Figure 6.

In the next month we will run single bias DLTS close to the p/n junction of the MOCVD cell in an attempt to discern any more information by increasing the signal to noise ratio of the measurement. We will also attempt to detect traps by I/V techniques since ideally there is no detection limit to the sensitivity

of the experiment. We also hope to extract the minority carrier lifetimes from the I/V and possibly correlate this with information we are presently obtaining from photoluminescence, Raman, and FTIR spectroscopic measurements.

In addition, we hope to receive the MOCVD cell structure which was sent out for atomic Hydrogen implantation to study the effects of this process on the above data.

The author would like to acknowledge the assistance of Steven A. Ringel (GRA) who is conducting the experimental research for this program.

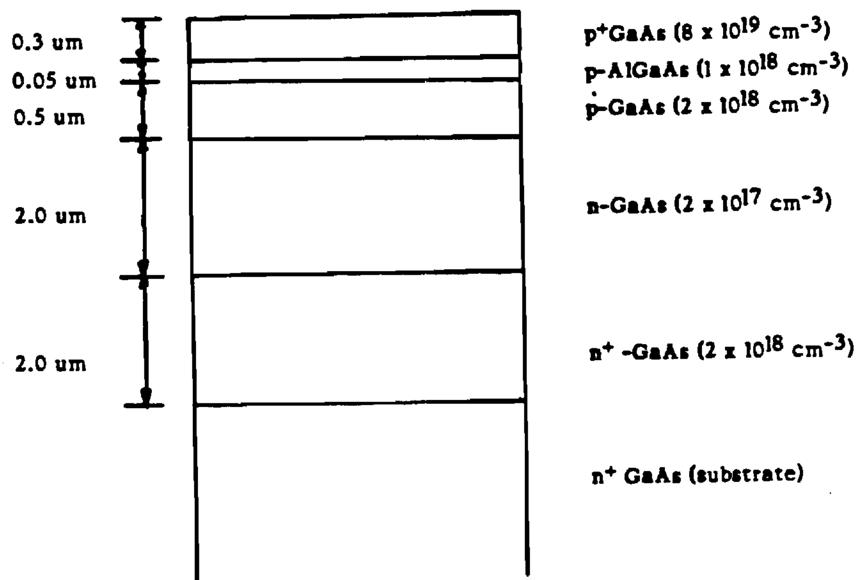

FIGURE 1: GaAs solar cell structure used in these experiments

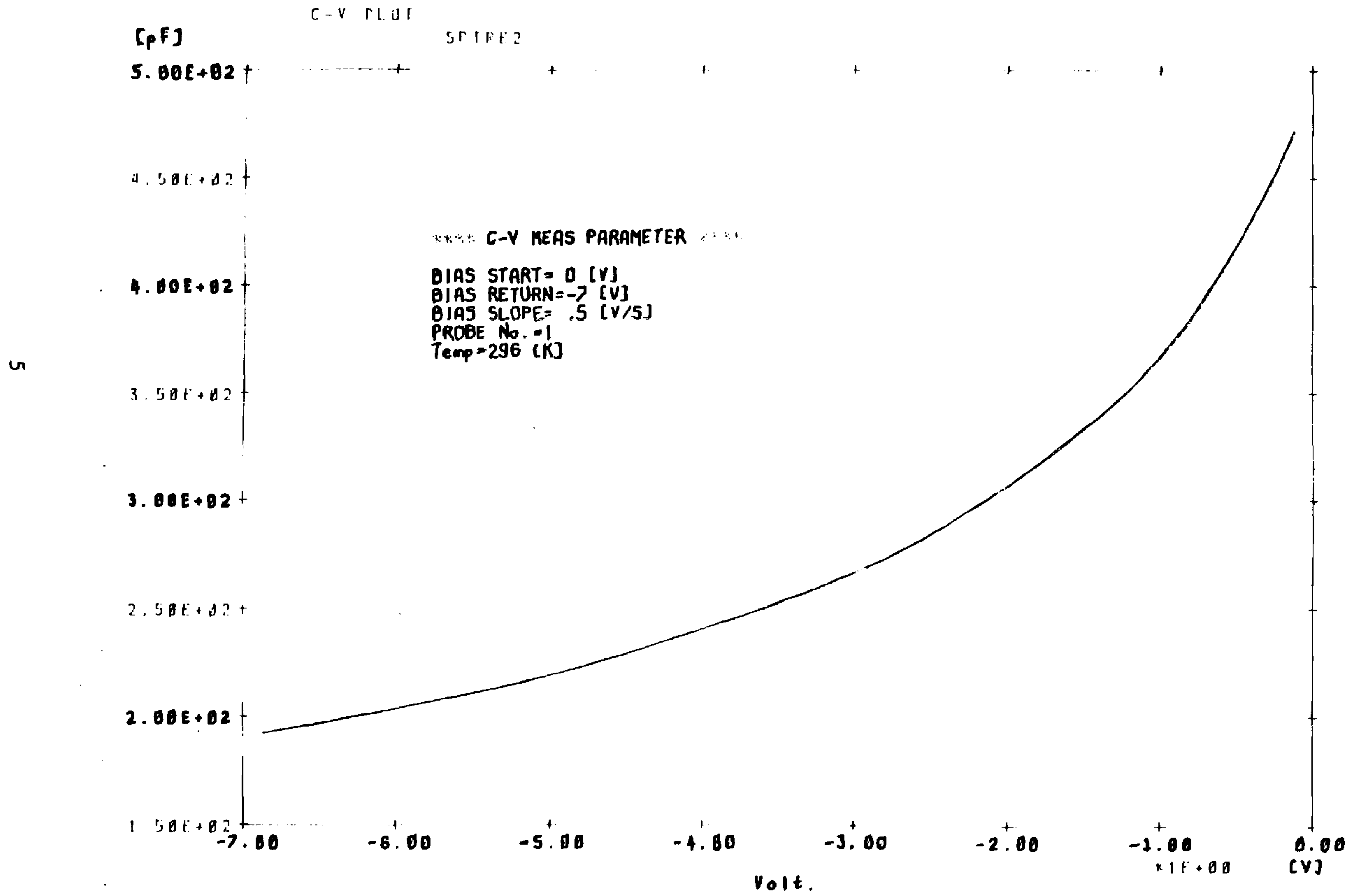

FIGURE 2 (a) C/V characteristic of the GaAs cell structure.

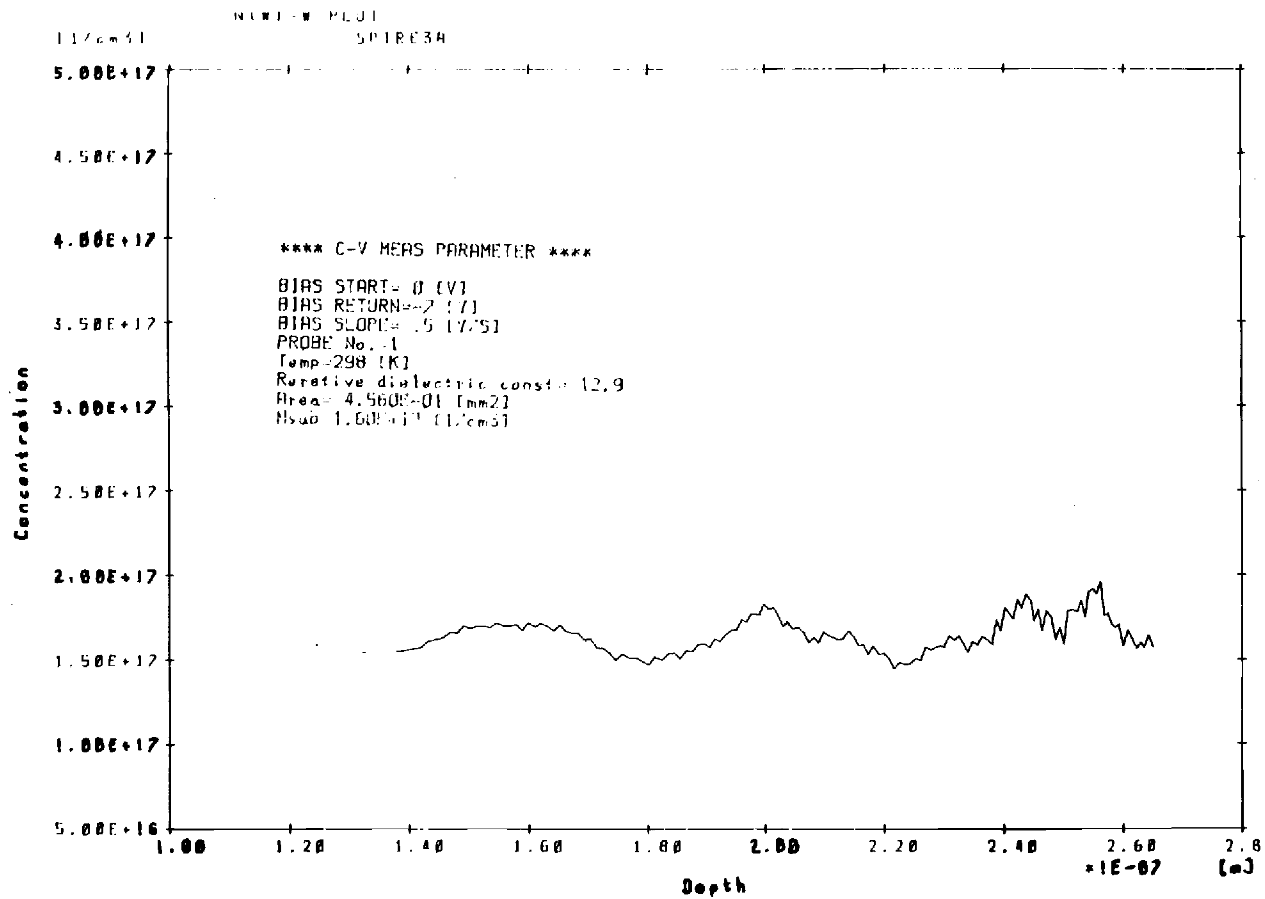

FIGURE 2 (b) Doping profile determined from C/V measurement.

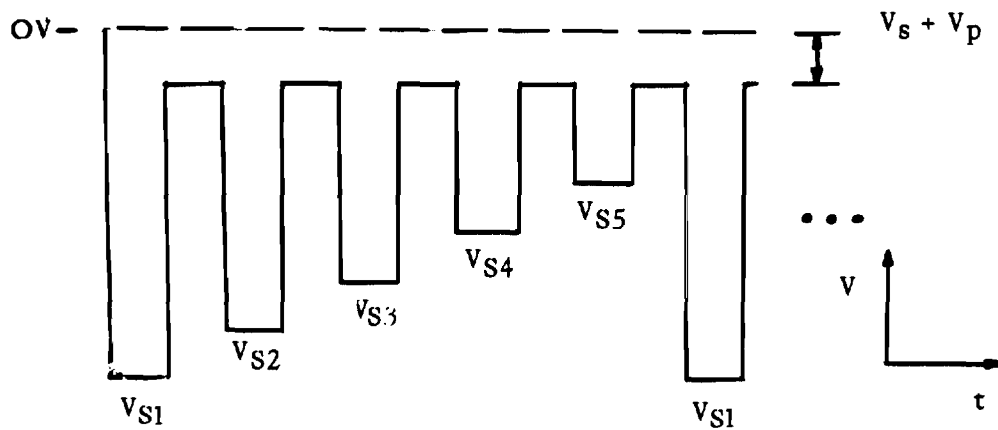

FIGURE 3 (a) Bias configuration and sequence for a standard DLTS filling pulse.

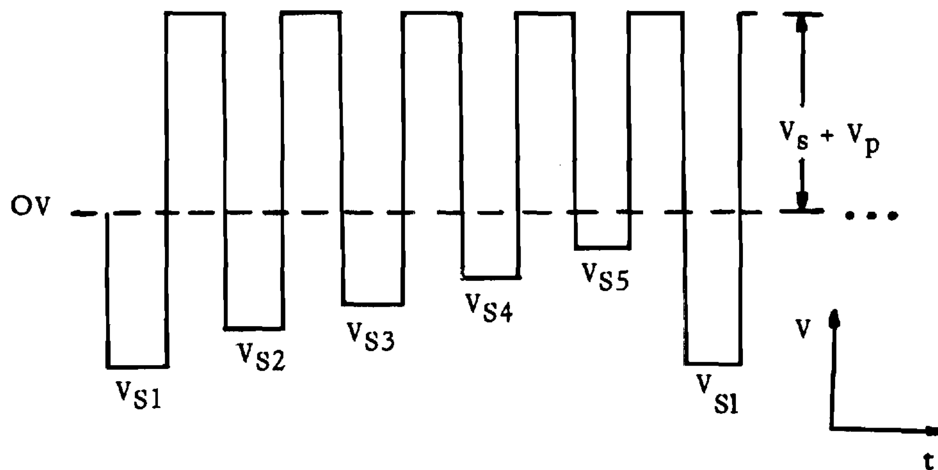

FIGURE 3 (b) Bias configuration and sequence for a minority carrier injection pulse.

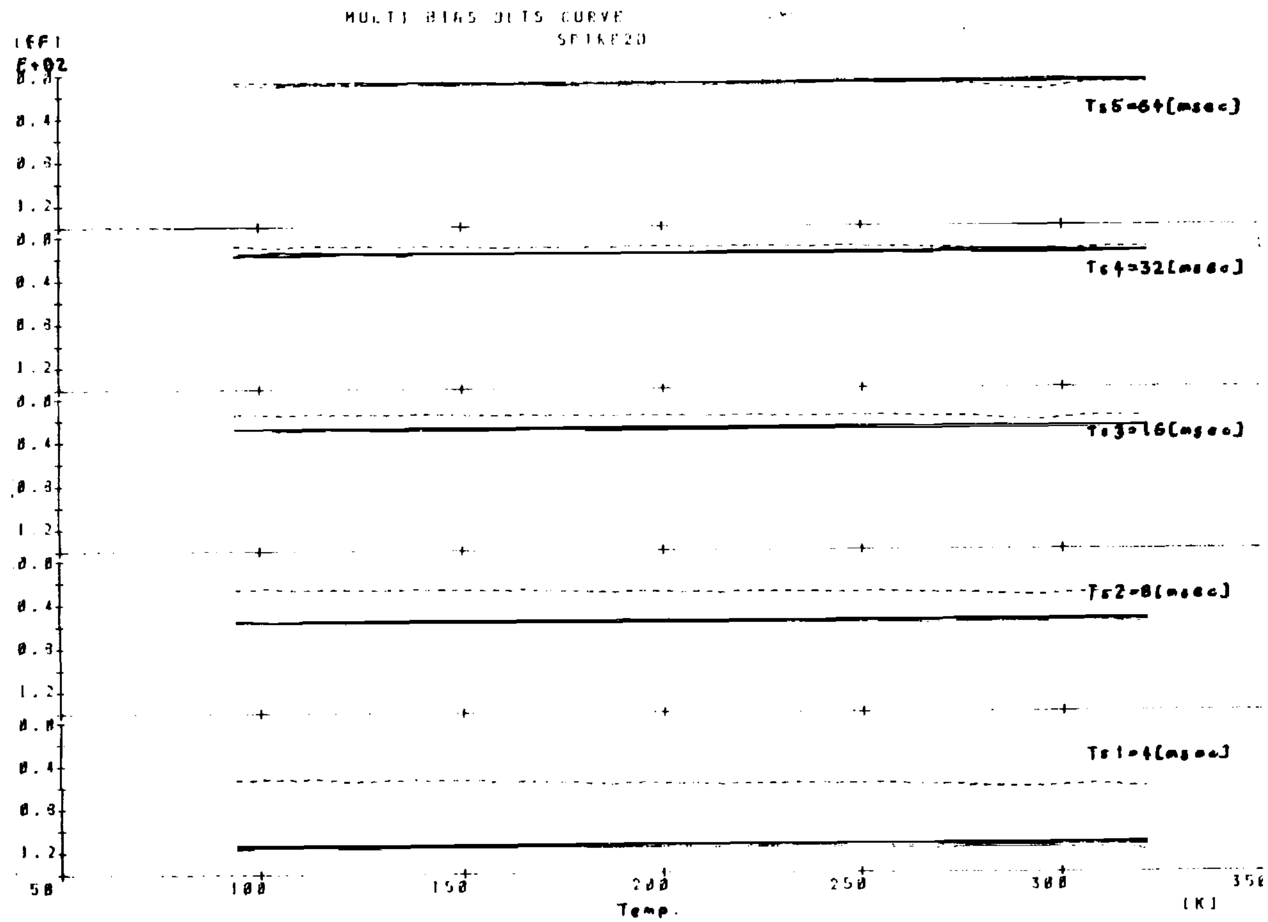

FIGURE 4: Multi-bias DLTS spectrum with five different biases for each weighting function.

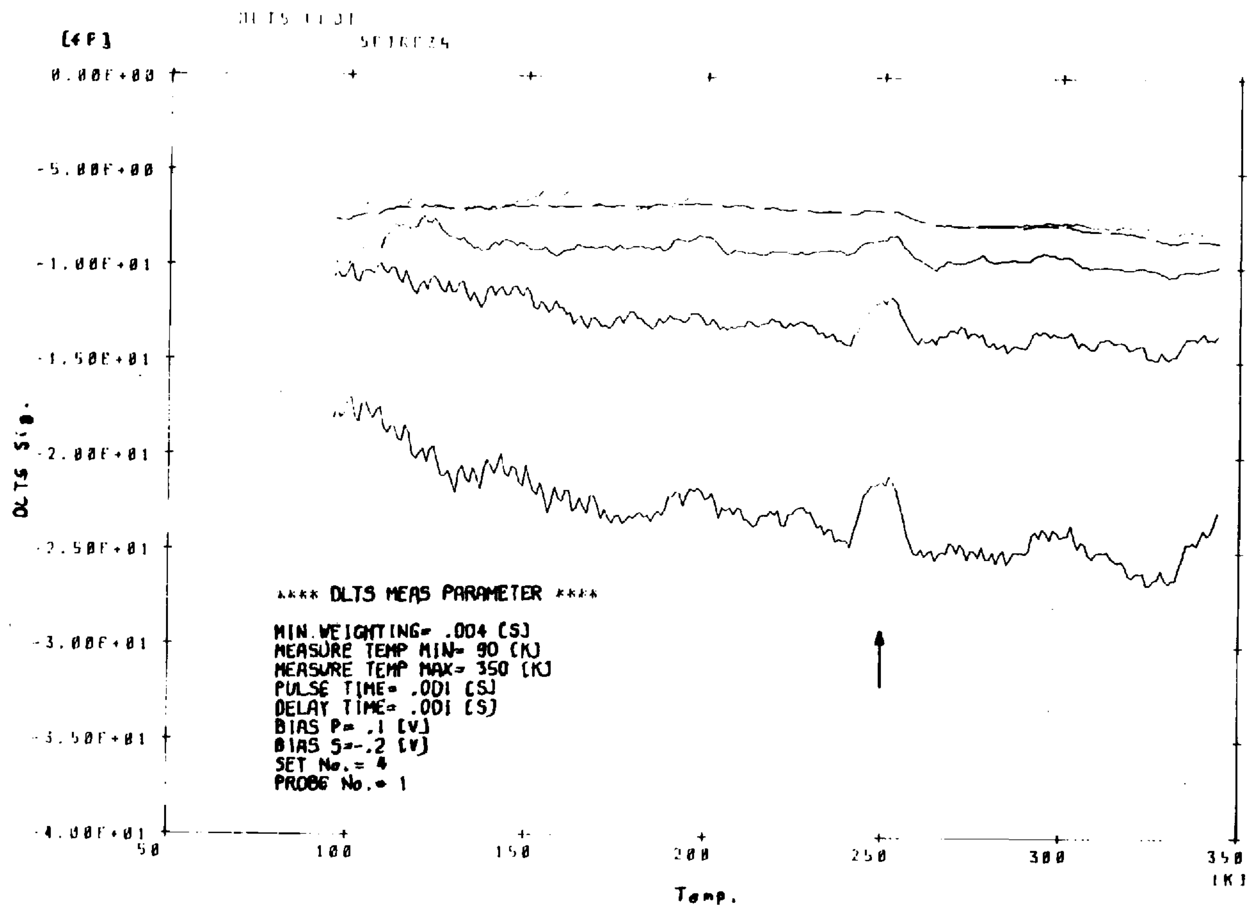

FIGURE 5: Separated DLTS scan for bias condition closest to p/n junction.

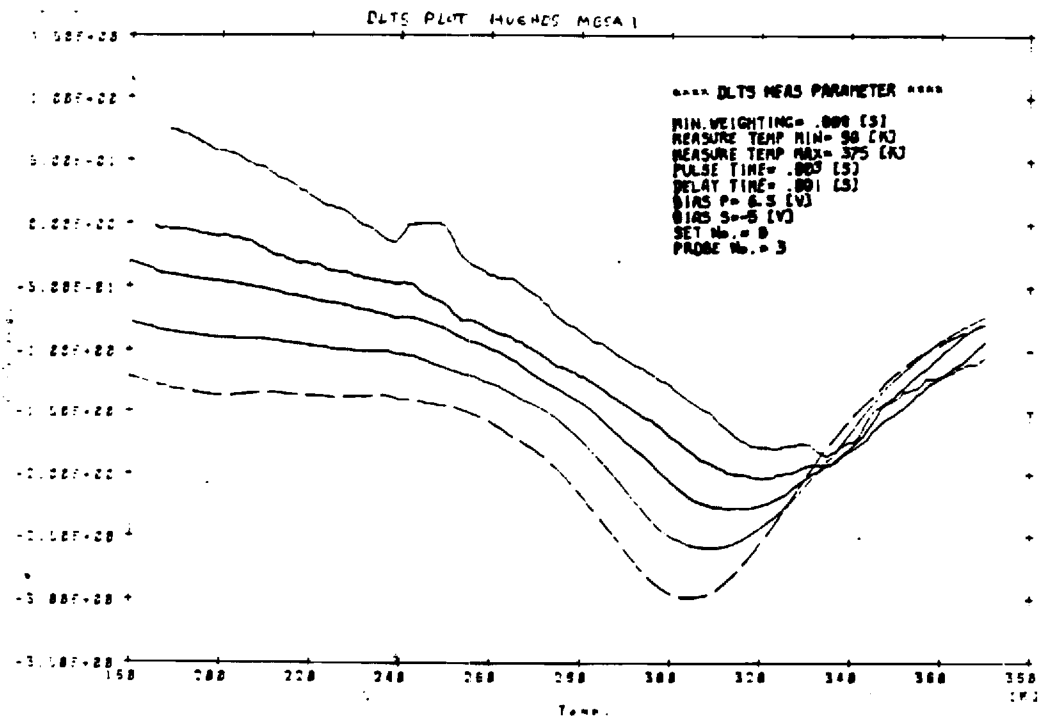

FIGURE 6: DLTS scan of an LPE-grown cell of similar structure indicating the presence of a hole trap.

RESEARCH ON AlGaAs/GaAs INTERFACES IN GaAs SOLAR CELLS

A. Rohatgi

Seventh Monthly Report for the Period
June 1 to June 30, 1987

Sandia National Laboratories

Contract No. 02-2255

GEORGIA INSTITUTE OF TECHNOLOGY
SCHOOL OF ELECTRICAL ENGINEERING
ATLANTA, GEORGIA 30332

Technical Progress

The major objective of this program is to develop techniques and methodology to characterize AlGaAs/GaAs interfaces and provide guidelines for improving GaAs solar cells.

During the past month we performed detailed measurements and analyses of deep levels near the p/n junction of the MOCVD GaAs p/n heteroface solar cell structure shown in Figure 1. Current/voltage measurements as a function of temperature (I-V-T) were used to reveal deep levels when the DLTS sensitivity became a limiting factor.

The device was etched into mesa form and ohmic contacts were deposited on front and back surfaces. DLTS measurements were made under "normal" conditions (versus the multibias configuration as we previously reported) to increase detection sensitivity. A deep level was detected using an injection pulse (into forward bias) and is shown in Figure 2a for three different weighting functions (lock-in amplifier technique is used). This level is identified as a hole (minority carrier) trap in the n-type base. The corresponding Arrhenius plot giving a deep level activation energy of E_v+0.912 eV is shown in Figure 2b. However, due to the difficulty in detecting deep levels in high quality GaAs, particularly when the doping is fairly high as is the case here (the detection limit is one hundredth of 1% of the background doping), an I-V-T technique was used which does not suffer from this limit.

This technique is based on the assumption that the reverse leakage density $J_o = (J_{o1} + J_{02})$ is dominated by J_{02}, the space charge generation current under reverse bias conditions. From Schockly-Read-Hall (SRH) theory, the recombination rate, R, is given by $R = -n_i/T_g$ where

$T_g = T_{po}\{\exp[(E_t-E_i)/kT]\} + T_{no}\{\exp[-(E_t-E_i)/kT]\}$

and

$T_{po} = 1/\sigma_p N_T V_{TH})$; $Tno = 1/(\sigma_n N_T V_{TH})$

If $T_{no} = T_{po}$ and $|Et - Ei| >> kT$ then T_g can be written as

$T_g = T_{po}(\exp[(E_t-E_i)/kT]\}$ for $E_t>E_i$

or $T_g = T_{no}\{\exp[-(E_t-E_i)/kT]\}$ for $E_t<E_i$

and knowing that the space charge generation current, J_{02} is given by

$$Jo_2 = (qn_iW/T_g)$$

then

$$J_{02} \propto \exp[-(E_t)/kT] \text{ for } E_t>E_i$$

or

$$J_{02} \propto \exp[-(E_c-E_t)/kT] \text{ for } E_t<E_i.$$

Hence, by plotting $\ln(J_{02})$ vs. 1000/T, the activation energy of the level which limits the leakage current can be determined. It is important to note that the I-V-T method cannot determine which of the above activation energies is correct and hence must be supplemented by other methods to find the exact location of the level in energy. If more than one level competes for dominance of the

leakage current the plot may have more than one linear region or it may not be linear at all.

In the case of our device, the above approximation that $T_{no} \sim T_{po}$ cannot be made. This is simply seen by considering that the deep level, which was detected in the upper half of the GaAs bandgap (as determined from DLTS), is behaving as a hole trap even though from a strictly probabilistic viewpoint the electron capture and emission processes should dominate. The only explanation for this is that σ_p, the capture cross-section of this deep level for holes, is much greater than σ_n, the capture cross-section of this deep level for electrons. Therefore, by the definitions of Tno and Tpo, Tno >> Tpo so Tg must be treated in a general fashion as in equation (2).

Figure 3 shows the results of such an I-V-T experiment on the same device as the DLTS scan of Figure 2 was taken from. At higher temperatures (above room temperature or below 3.33 on the 1000/T axis) the relation is roughly linear and gives a value of Ea = 0.4523 eV. We note that E_G (GaAs) = 1.42 eV is roughly equal to $E_a|_{IVT} + (E_t - E_v)|$ DLTS. Hence we assume the levels in DLTS and I-V-T are the same. We then obtain

$$(E_t - E_i) = 0.257 \text{ eV (since } E_t > E_I)$$

and from equation (4) we find that

$$T_g = 1.83 \times 10^{-10} \text{ sec.}$$

DLTS gives

$$T_{po} = 6.2 \times 10^{-17} \text{ sec.}$$

so that Tno can be calculated from equation (2) to be

$$T_{no} = 5.2 \times 10^{-7} \text{ sec.}$$

The above values assume a cross-section independent of temperature. The effect this has will be considered later.

In conclusion, we have shown that deep levels in high quality, highly doped devices can be detected by an I-V-T technique which does not suffer from the same limitations as does DLTS. In addition, the I-V-T method will reveal the deep level or deep levels which control the reverse saturation current, while DLTS cannot specify the dominant levels involved in the carrier transport mechanisms. Hence the I-V-T method can fully characterize the J_{02} component of the dark leakage current. In follow-up experiments, we will test this method on other devices and then pursue the analysis of the J_{01} component from transformed I-V measurements. Using this information, we plan to model the solar cell structure by varying an effective recombination velocity throughout the device so that calculated currents and external solar cell parameters can be matched to measured values. In this way, the importance and values of interface recombination velocities can be estimated and the quality of the material throughout a device structure can be mapped.

The author would like to acknowledge the assistance of Steven A. Ringel (GRA) who is conducting the experimental research for this program.

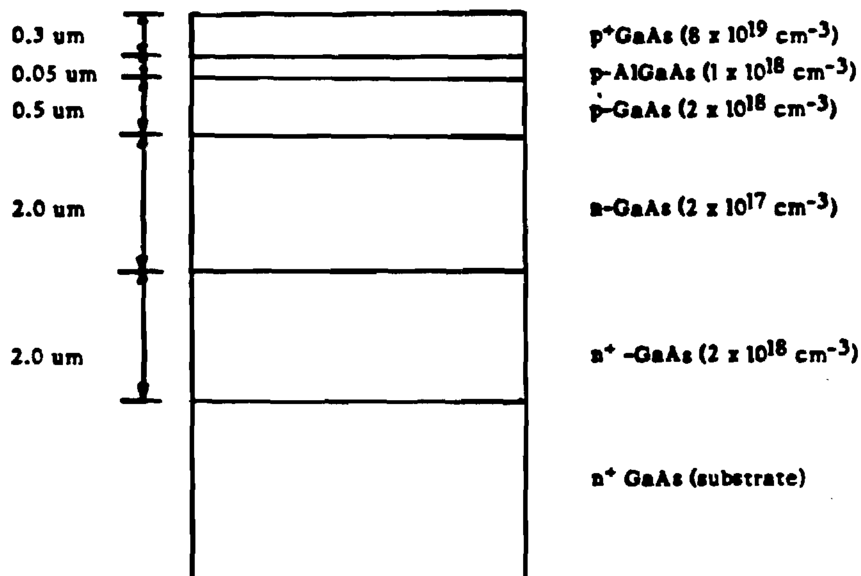

FIGURE 1: GaAs solar cell structure used in these experiments

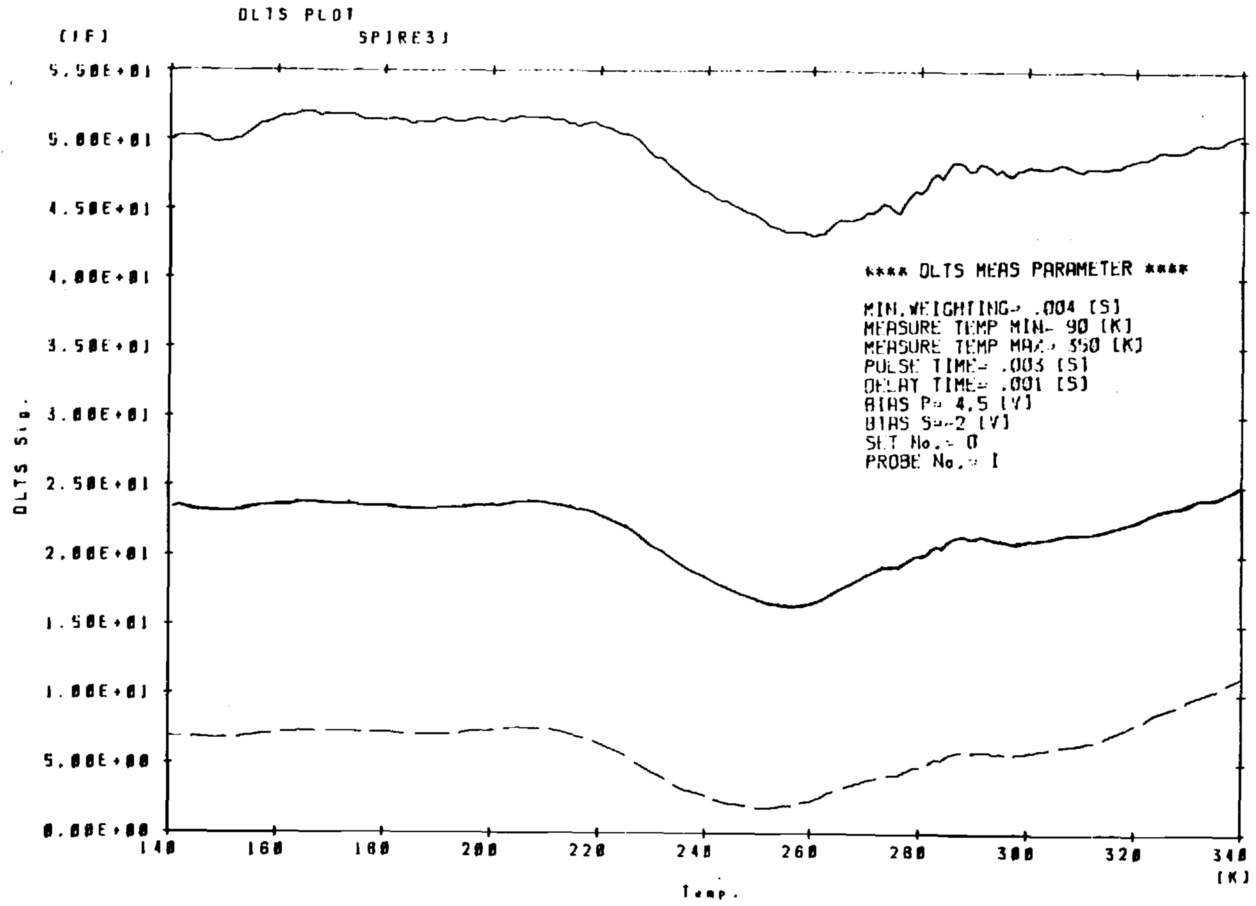

FIGURE 2a: DLTS scan of GaAs p/n heteroface cell

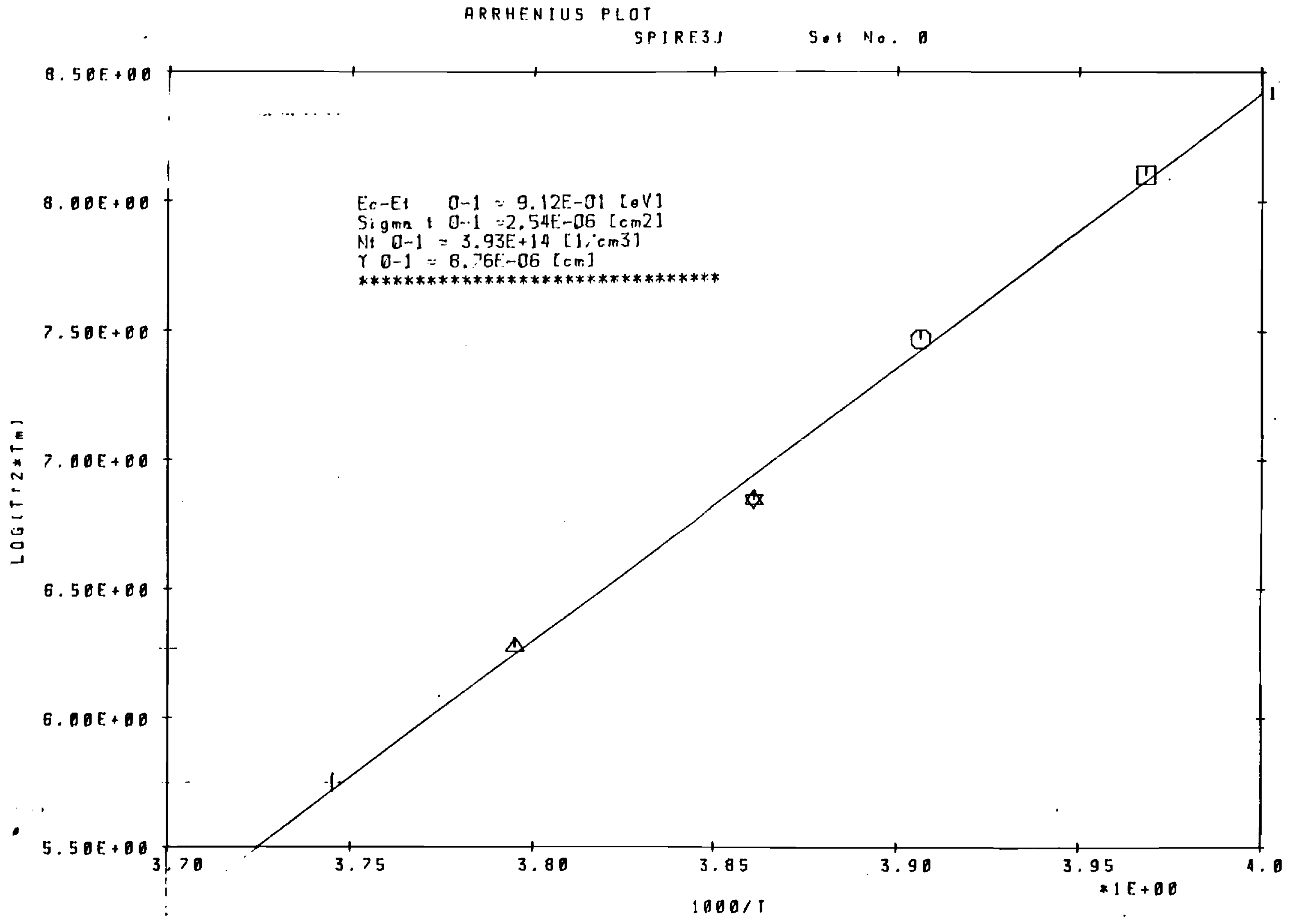

FIGURE 2b: Arrhenius plot for deep level found in GaAs p/n heteroface cell

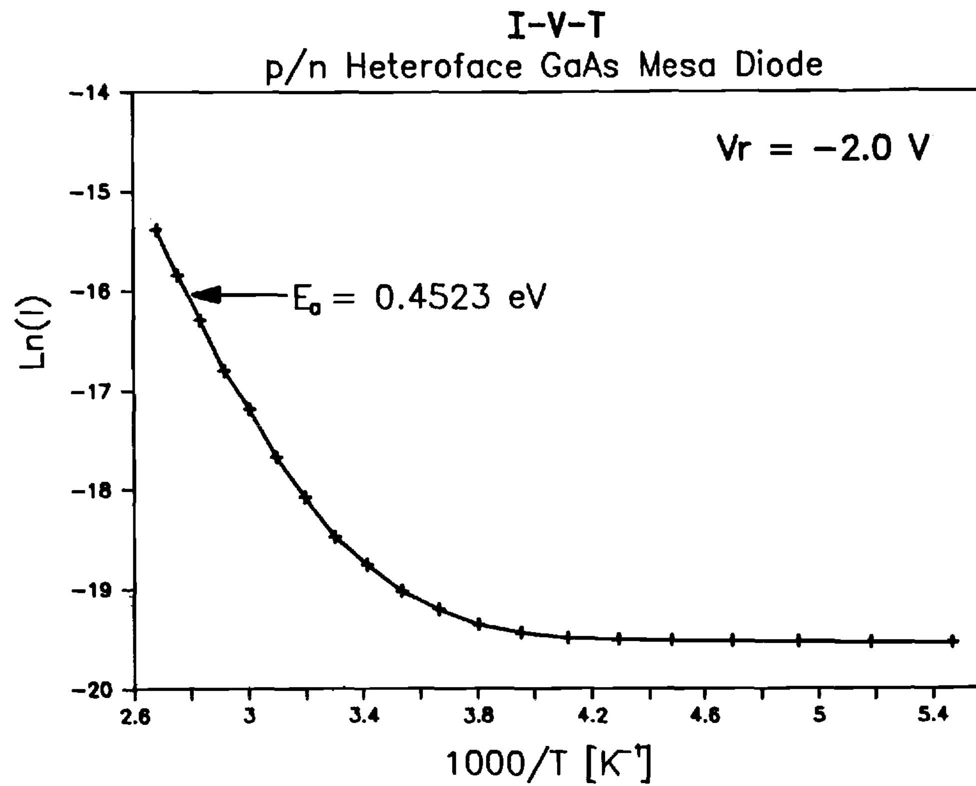

FIGURE 3: I-V-T results of GaAs p/n heteroface cell

E-21-603

GEORGIA INSTITUTE OF TECHNOLOGY
SCHOOL OF ELECTRICAL ENGINEERING
ATLANTA, GEORGIA 30332

(404) 894-7337

October 23, 1987

Mr. J. Gee
Sandia National Laboratories
P. O. Box 5800
Albuquerque, NM 87185-5800

Re: Contract No. 02-5800
Project Director: A. Rohatgi

Dear Mr. Gee:

Enclosed please find a copy of the Monthly Technical Progress Report for the period 7/1/87-7/31/87 on the above referenced contract.

If you have any questions, please feel free to contact me.

Sincerely,

Pam Majors
Research Administrator

pm
Enclosure

RESEARCH ON AlGaAs/GaAs INTERFACES IN

GaAs SOLAR CELLS

A. Rohatgi

Eighth Monthly Report for the Period
July 1 to July 31, 1987

Sandia National Laboratories
Contract No. 02-2255

GEORGIA INSTITUTE OF TECHNOLOGY
SCHOOL OF ELECTRICAL ENGINEERING
ATLANTA, GEORGIA 30332

Technical Progress

The major objective of this work is to develop techniques and methodology to characterize AlGaAs/GaAs interfaces and provide guidelines for improving GaAs solar cells.

During the eighth month of this program we have characterized two GaAs p/n heteroface solar cell structures, one grown by MOCVD (Figure 1a) and the other by LPE (Figure 1B), by current/voltage (I/V) measurements. Deep level detection by the I-V-T method introduced in the seventh monthly report was repeated on another device structure (Figure 1b: the device of Figure 1A was tested previously) and yielded reasonable results. Using information from the I-V measurements, we were able to model the effective recombination velocity throughout a device as well as match the overall solar cell data supplied by the manufacturer (Spire Corp.).

The I-V-T behavior of the LPE device in Figure 1b is shown in Figure 2. The steady reverse bias of the measurement of 8 V is well below the measured value of the breakdown voltage (13 V). Two linear regions are observed indicating that two different deep levels are limiting the reverse leakage (generation) current over the temperature range shown (0 to 140°C).

As explained in the seventh monthly report, there is some ambiguity associated with the activation energies shown since it cannot be determined without other experimental confirmation if they represent (Ec - Et) or (Et - Ev). Upon comparison with the DLTS spectrum obtained for this device (Figure 3a) and the associated Arrhenius plot (Figure 3b) we see that $(E_t - E_v)|_{DLTS} + E_a$ (=0.480 eV) = Eg (GaAs) indicating that the DLTS level and the higher temperature I-V-T level are the same. It is apparent however, that the level at Ea = 0.264 eV (either (Ec - Et) or (Et - Ev)) controls the leakage current over the operating temperature of the device.

The I-V characteristics of both devices in Figure 1 were measured and transformed into the n=1 and n=2 current components by an automated and computer-controlled I-V measurement and analysis set-up. The plotted results for the MOCVD cell of Figure 1a is shown in Figure 4 where J_1 is the diffusion controlled component and J_2 is the space charge generation component of the total current, J, and are given under forward bias by

$$J = J_1 + J_2$$

$$J_1 = J_{01} e^{\left(\frac{qV}{kT}\right)}$$

$$J_2 = J_{02} e^{\left(\frac{qV}{2kT}\right)}$$

J_{01} and J_{02} are the leakage current components for each mechanism. By neglecting the interface recombination velocity at the n/n+ (base/buffer) junction and assuming that J_{01} is dominated by J_{0B} so that J_{0E} can be neglected, the base bulk lifetime can be determined from

$$J_{01} = \frac{q n_i^2}{N_D} \cdot \frac{D}{T}$$

resulting in T_B = 4.07 nsec. The SRH (Schockley-Read-Hall) lifetime, To, can be found from

$$\frac{1}{T_B} = \frac{1}{T_o} + BN_D + CN_D^2$$

where B is the radiative recombination coefficient and C is the Auger recom bination coefficient for GaAs. The calculation results in To = 10 nsec. This lifetime is characteristic of the deep level or levels which control the leakage current in the bulk material. Recalling the generation lifetime, Tg, deduced from the I-V-T measurements of this device in the seventh monthly report, one can write Tg as

$$T_g = T_r \left(\frac{e^{|E_t - E_i|}}{kT} \right)$$

where Tr is the recombination lifetime due to deep levels in the space charge region of the device since this relation is derived from the determination of J_{02}. Using the experimental values of Tg and |Et - Ei|, Tr = 5E-15 sec. which is much less than To found in the bulk. This indicates that the level detected by I-V-T (and also by DLTS) does not limit the bulk lifetime or J_{01}. This result also suggests that the level found by I-V-T and DLTS may be spatially localized in the space charge region since these two techniques are sensitive only in this region while J_{01} is a bulk property. This question is being addressed at the present time.

It should be noted that even though the I-V-T deep level does not contribute to J_{01} it is still important in the device operation and can play a role in limiting its performance. This is clear from Figure 4 where J_{01} and J_{02} are of comparable magnitude near the operating pt ($\sim$1 V) at the cell. The magnitude of J_{02} current component at the operating point is essentially equal to the current that does not make it to the external load.

Using the base bulk lifetime obtained from the I-V above, the recombination velocity anywhere within the device was calculated using a computer model. The model is based on the division of the device into a particular number of slices of constant thickness. The surface recombination velocity is either known or assumed at the front and back surfaces of the device and an effective recombination velocity is calculated at the opposite end of the slice based on this initial value. This process is iterated throughout the structure. The value of S at one end of a slice, Se_2, is given in terms of the value at the other end of the slice, S_{e2}, by

$$S_{e2} = \frac{N_2}{N_1}\frac{D}{L}\left[\frac{S_{e1}\frac{L}{D} + \tanh\left(\frac{W}{L}\right)}{1 + S_{e1}\frac{L}{D}\tanh\left(\frac{W}{L}\right)}\right]e^{\left(\frac{\Delta E_{C2}-\Delta E_{C1}}{kT}\right)}$$

where

W = slice thickness

D = diffusion coefficient within slice

L = diffusion length within slice

N_2 = doping density at end of slice

N_1 = doping density at beginning of slice

exponential term = band gap narrowing effect

An example of the iteration results is shown in Figure 5 for various S values at the back of the buffer layer and at the window/emitter interface (right hand side of plot). It should be noted that the bulk lifetime used in the base, and hence the emitter lifetime which was determined from this, rely on the assumption that $J_{01} = J_{0B}$ and that S at the buffer/base interface does not affect J_{0B}. The latter assumption appears to be valid from Figure 5 which shows that Sejb, the recombination velocity at the base side of the p/n junction, is pinned for all values of S at the back of the buffer. The first assumption can be checked by calculating J_{0B} and J_{0E} using

$$J_{0B} = \frac{qn_i^2}{N_D} \cdot S_{ejb} = 1.09X10^{-19} A/cm^2$$

$$J_{0E} = \frac{qn_i^2}{N_a} \cdot S_{eje} = 0.2X10^{-19} A/cm^2$$

giving a modeled value of J_{01} (= J_{0B} + J_{0E}) = 1.29E-19 A/cm^2. The measured (experimental) value of J_{01} from the transformed I-V data also yielded a value of 1.29E-19 A/cm^2. Thus the model supports the experimental data.

A number of conclusions can be made from the plot in Figure 5. The passivation at the emitter surface has little effect of the value of Seje (and hence J_{0E}) if the interface recombination velocity if the value is kept below 10^4 cm/s for this emitter thickness. Also, the value of the interface recombination velocity at the buffer/base interface has little effect on J_{0B} with the a base thickness of 2 microns. Hence cell performance and its relation to device geometry and material quality can be extracted from this type of model.

the effect of modifying the emitter thickness will be checked since according to our dopant profile of this structure, the emitter thickness is actually less than what has been used in the calculations thus far.

The author would like to acknowledge the assistance of Steven A. Ringel (GRA), who is conducting the experimental research for this program and A. Smith who is helping in the solar cell modelling.

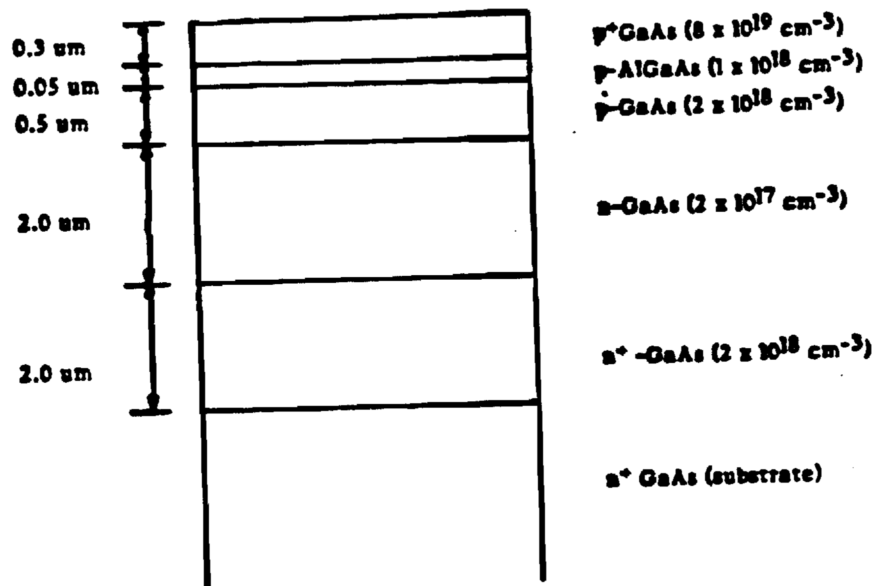

Figure la: MOCVD p/n heteroface cell structure.

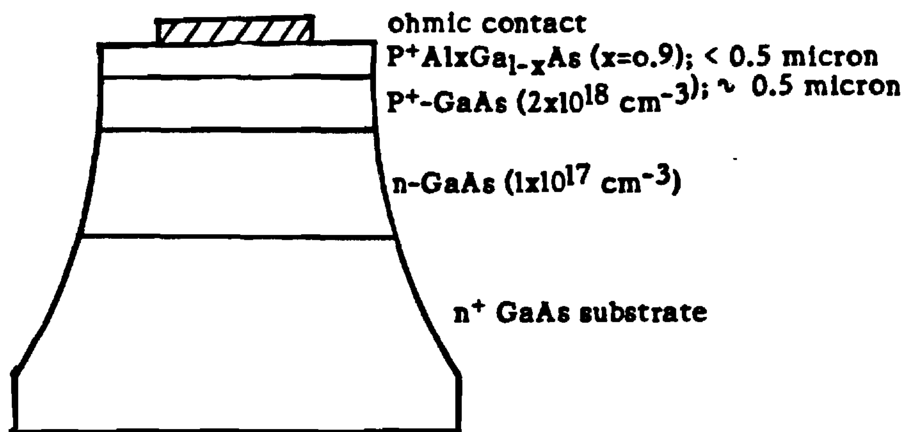

Figure 1b: LPE GaAs p/n heteroface cell structure.

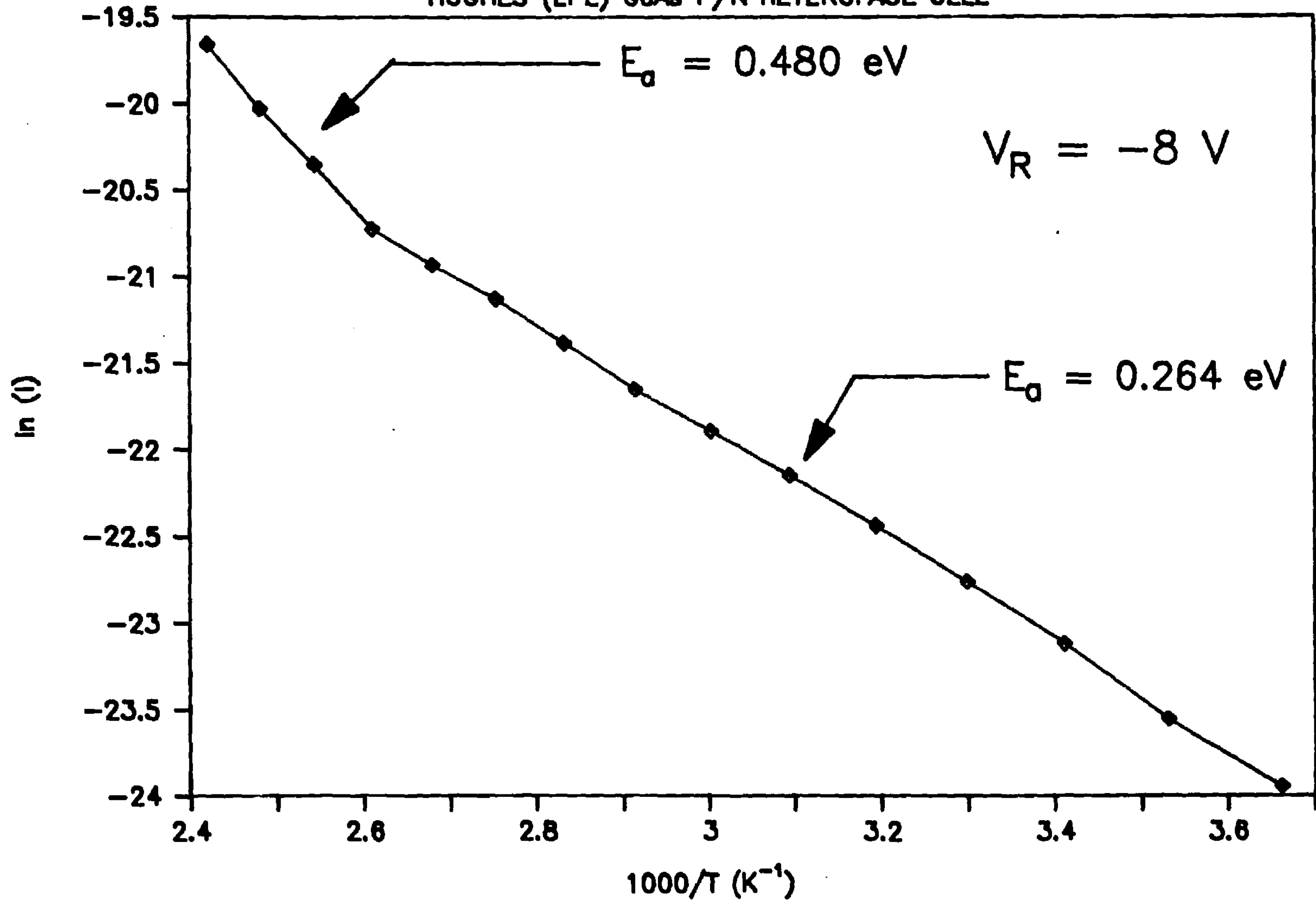

Figure 2: I-V-T plot for LPE GaAs heteroface cell indicating transport dominance by two generation levels.

FIGURE 3 a - DLTS SPECTRUM FOR HUGHES MESA DIODE

b - ARRHENIUS PLOT FOR DEEP LEVEL INDICATED IN DLTS SPECTRUM

(A)

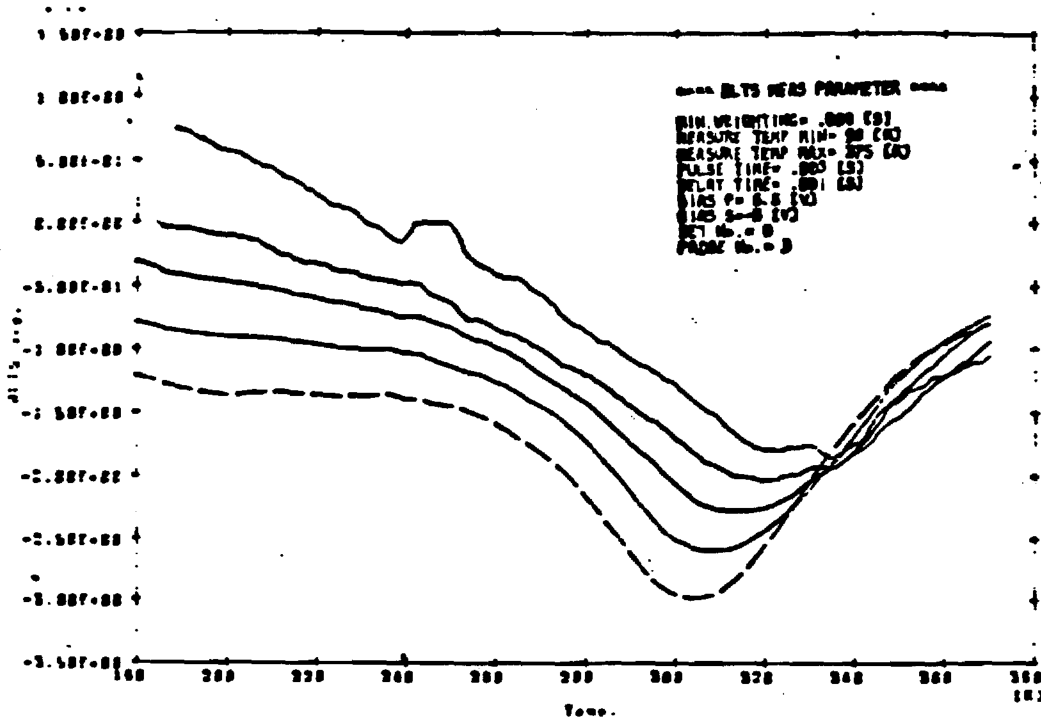

(B)

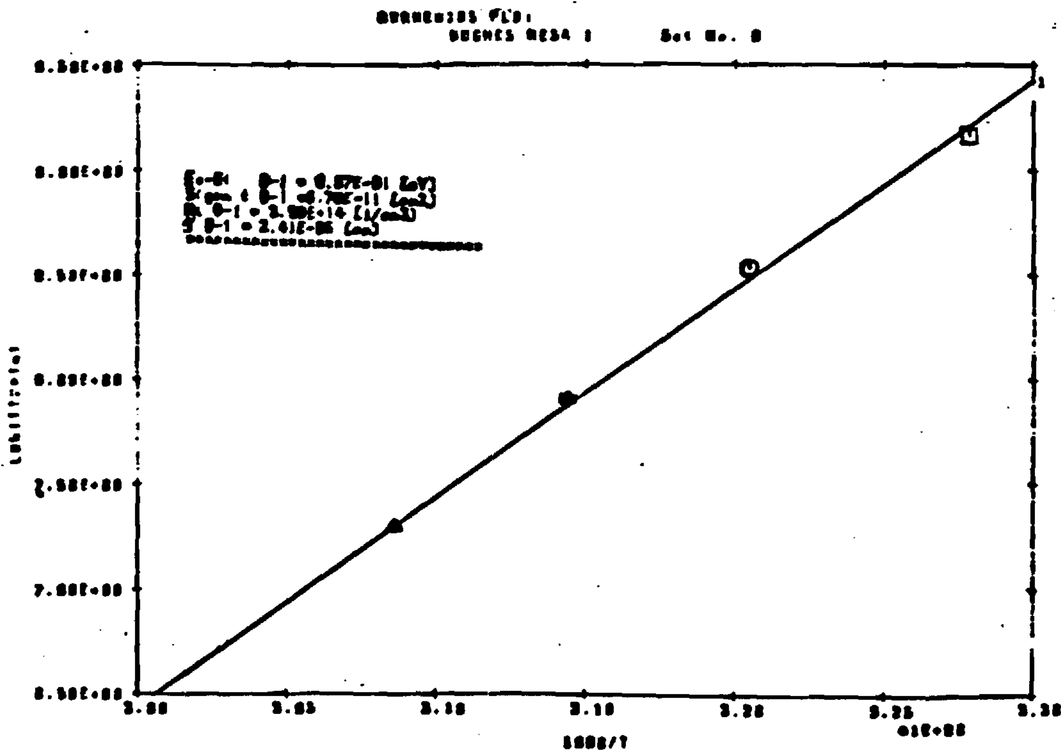

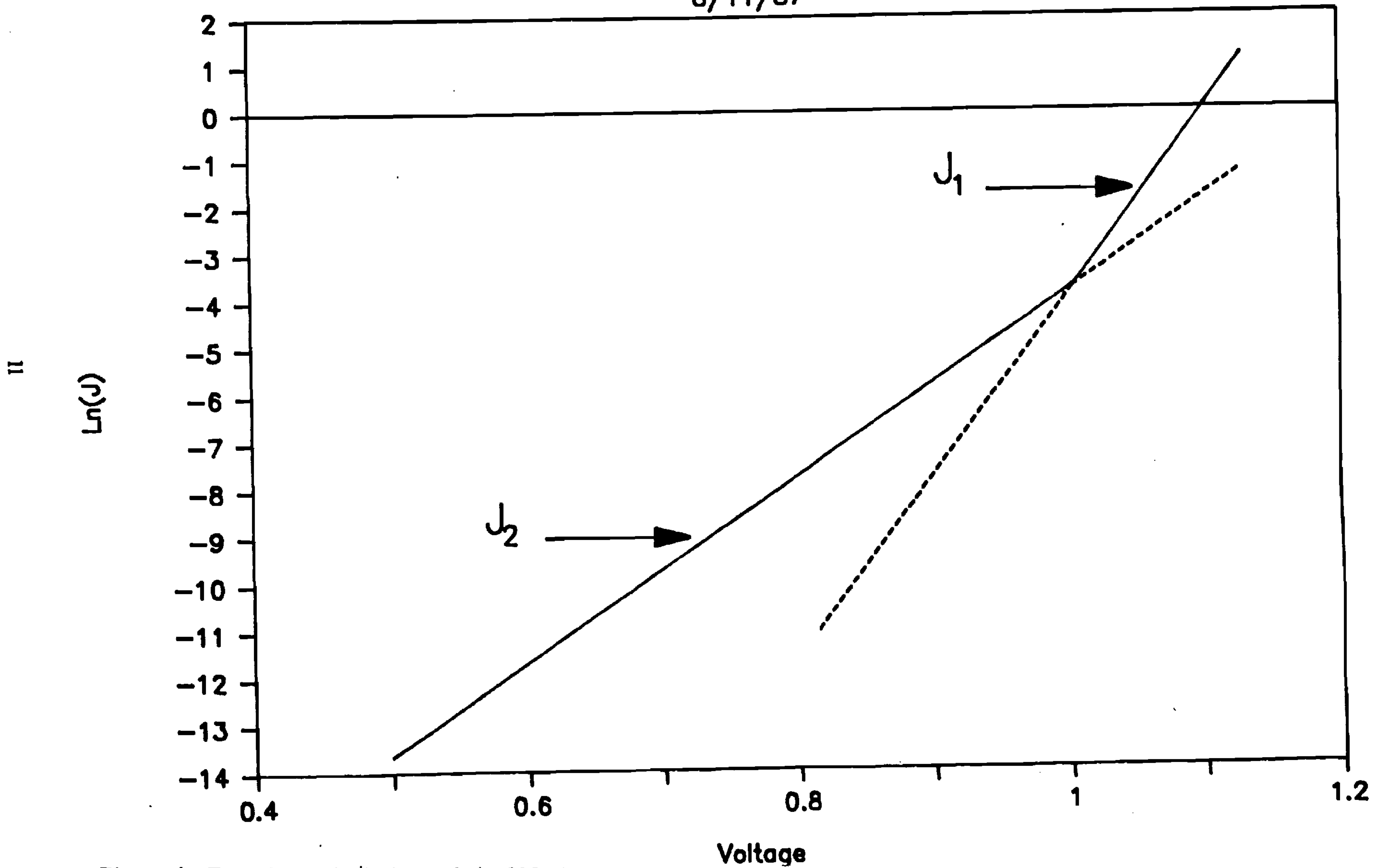

Figure 4: Transformed I/V data of the MOCVD cell. J_1 refers to the diffusion current component and J_2 refers to the space charge generation current.

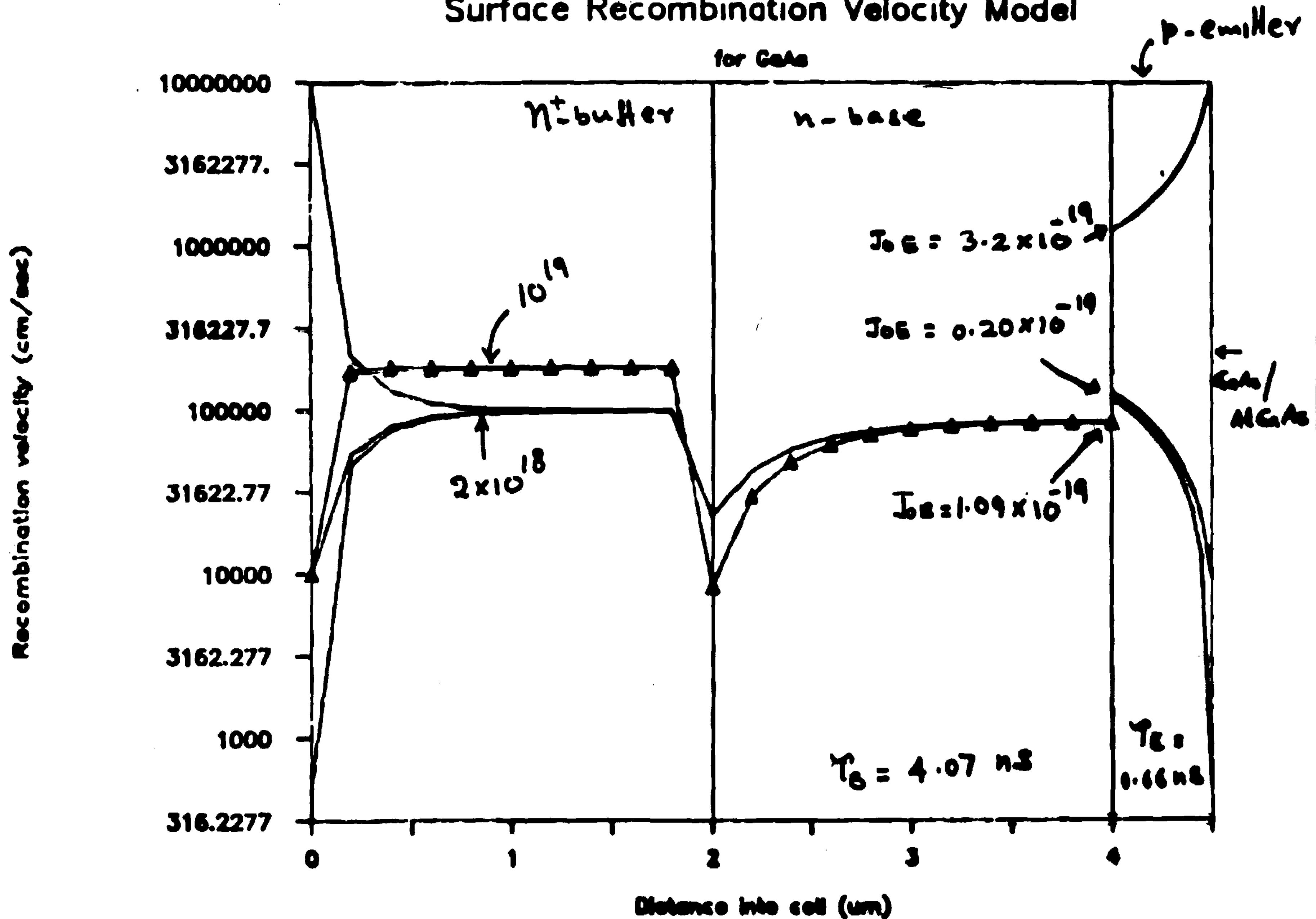

Figure 5: Variation of S throughout MOCVD device of Figure 1a for various values of S at front and back surfaces. The line with Δ marks is for a higher buffer doping as indicated.

RESEARCH ON AlGaAs/GaAs INTERFACES IN GaAs SOLAR CELLS

A. Rohatgi

Ninth Monthly Report for the Period
August 1 to August 31, 1987

Sandia National Laboratories
Contract No. 02-2255

GEORGIA INSTITUTE OF TECHNOLOGY
SCHOOL OF ELECTRICAL ENGINEERING
ATLANTA, GEORGIA 30332

Positron Annihilation Spectroscopy of AlGaAs/GaAs Interfaces in MOCVD-Grown GaAs Heterojunction Solar Cells

Abstract

The defect density profile of high efficiency epitaxial MOCVD-grown GaAs heterojunction solar cell structures has been characterized using a variable-energy positron beam. By control of the implantation depth of positrons, spatial defect changes, film thickness variations, and possibly interfacial space charge and disorder may be resolved from annihiliation characteristics. Correlations have been made relating positron annihilation spectroscopy (PAS) measurements to SPV data, band bending, and known MOCVD growth parameter variations. Based upon these correlations, it is expected that PAS may provide a valuable means for probling process-induced defect profiles which may affect the electrical and optical response of MOCVD-grown semiconductor materials.

I. INTRODUCTION

A major objective in the characterization of heterojunction semiconductors grown via MOCVD, MBE, or PECVD is the development of techniques for probing defect and impurity distributions affecting the electrical response. Thus, methodologies can be developed for adjusting deposition parameters, layer thickness, and/or dopant density to enhance the electrical properties of the semiconductor. Furthermore, from a quality assurance viewpoint, it is desireable that techniques for characterizing the atomic defect and/or impurity structure of a semiconductor be non-contact (NC) and nondestructive (ND). One relatively new technique that satifies the NC and ND constraints and is capable of profiling the defect density, detailing interfacial disorder, and detecting impurity complexes is Slow Positron Annihilation Spectroscopy (SPAS).[1-5]

By measuring the energy distribution of positron/electron annihilation events it is possible to probe a material's electron momentum distribution with a variable-energy positron beam. As a first order approximation, the intensity of the parabolic and Gaussian components of the annihilation energy distribution can be related to the respective fractions of positrons annihilating with valence electrons and those annihilating with the more tightly bound core electrons. If a positron becomes spatially localized due to defect trapping or to strong space charge effects, the fraction of annihilation events with valence electrons will be altered relative to core electrons, thus

narrowing or broadening the energy distribution curve.

A series of experiments was carried out to determine the potential applications of SPAS to heterojunction semiconductors by investigating the relative positron-sensitive defect profile for different MOCVD grown solar cell structures. Validation of any new microanalytical tool requires extensive comparisons with other more established techniques, wherever possible. The SPAS data has been subsequently compared to Surface Photo-Voltage (SPV), a destructive defect profiling technique, qualitative MOCVD growth variations, and band bending arguments.

II. EXPERIMENT

The MOCVD grown solar cell structures investigated are summarized in Table I, in terms of layer function, material, semiconductor type, and dopant density. These devices were grown in a Spire MO-450 reactor using trimethyl gallium, trimethyl aluminum, and arsine as reactants. The dopants are Zn for p-type regions and Si for the n-type regions.

The variable-energy positron beam (0 - 100 keV) used for analysis of the heterojunction solar cells has been previously described elsewhere.[8] In brief, the system consists of a Na-22 positron source moderated by a tungsten crystal with efficiency 5×10^{-4} and focused magnetically to the target, all of which is under UHV conditions (10^{-10} Torr). At each incident energy, 10^{6} counts (annihilation events) are collected with a count rate of 2 kHz. The change in lineshape of the annihilation energy

distribution has been calculated using the standard Doppler S-parameter[7], which is defined as the number of counts in some fixed central energy window divided by the total number of counts in the energy spectrum.

A Biorad Polaron PN4200 electrochemical profiler has been used in conjunction with a Polaron PN4250 SPV attachment to study the defect non-uniformity from the surface through the p-n junction interface. A detailed description on the operation of the depth-resolved SPV technique is to be published elsewhere.[9] By collecting SPV spectra taken at different etch depths, comparative ratios of one SPV spectrum divided throughout the wavelength scan yield information about the presence of localized defect regions in the emitter and base of the solar cell.[9,10]

III. SPAS MODELING

The deconvolution of the positron energy dependent (depth dependent) Doppler lineshape parameter, S(E) has been premised upon a previously developed multilayer model.[6] Each layer is assumed to be homogeneous and well-defined, therefore possessing a characteristic lineshape parameter S_i, where i is the layer designation. The characteristic value of S_i is functionally dependent upon the layer material, deposition conditions, and dopant density. S(E) is defined as the superposition of S_i weighted by the probability, $g(E)_i$, that positrons of energy E will annihilate in layer i such that

$$S(E) = \sum_i g(E)_i * S_i \quad (1)$$

where

$$g(E)_i = \int_{a_i}^{b_i} P(z,E)dz \quad (2)$$

and P(z,E) is the positron implantation profile integrated over the boundaries of the layer i from a_i to b_i. The mean positron implantation depth is functionally dependent upon the material mass density and two material Gaussian fitting parameters. As yet, no detailed experimental investigation has been performed to determine the best Gaussian fitting parameters for each of the MOCVD-grown layers. These parameters were chosen to best approximate the general S(E) behaviour and are within the range of previous SPAS studies (although on different materials).

While the above model is useful in delineating the layer boundaries and the relative layer defectiveness, the effects of material density (positron backscattering), localized trapping (e.g., at interfaces or at defect inclusions), and positron diffusion length have been neglected. In the current analysis, material density effects may be important since the $Al_xGa_{(1-x)}As$ (x=0.9) is less dense than adjacent GaAs layers. If the AlGaAs layer were sandwiched between two GaAs layers, an apparent enhancement of S_i for the AlGaAs layer relative to the GaAs layers could result.

Differential positron trapping across interfaces has been shown to be important for an SiO_2/Si interface[5] since the positron diffusion length in Si is substantially greater than in SiO_2. As yet, the positron diffusion lengths have not been

experimentally measured for the layer materials, thus the current modeling effort fails to explain local minimums and maximums in S(E). However, away from the interfaces, it has been assumed that localized defects may be approximated by the superposition of characteristic defect values, S_d, as exhibited in Figure 1. Nonetheless, competitive trapping between localized defects within the layers or between localized defects and nearby interfaces will accentuate the experimental S(E) minimums and maximums, whereas the model approximation has been shown to raise or lower S(E) in a more gradual manner.

IV. RESULTS AND DISCUSSION

Annihilation lineshape measurements have been obtained for the solar cell heterojunctions previously described in Table I. The variable-energy positron beam has been confined to sampling S(E) spectra with energies of ~250 eV to ~25 keV which is sufficient to probe through the p-n junction region. Initially, two SPAS S(E) spectra were obtained for two different specimens of MOCVD Run #872 (Figure 2). Both specimens were cut from the same wafer, except that 872A is representative of the center and 872B is representative of the edge. The general features of both specimens are similar; however, two major differences are apparent: (1) the 872B specimen S(E) spectrum is shifted to higher energies with respect to the 872A, and (2) the finer details of the 872A specimen tend to be absent from the 872B specimen.

Before explaining the apparent differences between the two specimens, a number of the features of 872A are first discussed. According to current theoretical model predictions, the depth resolution of the heterojunction layers is as shown in Figure 2. The model predicts the general shape of the convoluted S(E) curve; however, it fails to correctly place the AlGaAs layer and fails to correlate with the finer details of the S(E) spectrum (i.e., the localized minima and maxima). The twin maxima between 5 and 8 keV suggest that positron backscattering may be significant. It is anticipated that the incorporation of backscattering into the theoretical model will shift the predicted position of the AlGaAs layer toward the surface and predict the local maxima near the AlGaAs/GaAs interfaces.

Within the emitter p-GaAs layer, a number of local lineshape maxima exist which have been directly correlated with SPV data. For example, the SPAS data shows a maximum between positron energies of 8.5 keV and 9.5 keV (positron implantation range of .27 to .31 microns). The SPV data clearly shows a defect to exist between .28 and .32 microns (Figure 3). An interpretation of the SPV data is as follows:[10]

(a) the spectra ratio between .22 and .21 microns is indicative of a defective region below the surface in comparison to the material that has just been removed;

(b) the spectra ratio of .28/.22 microns shows that a defective region exists near the surface, but further into the emitter layer, the p-GaAs is less defective;

(c) the spectra ratio of .32/.30 being relatively flat and equal

to unity indicates that the defective region has been completely traversed.

When the existence of a local defect region (layer) is incorporated into the model calculation the agreement between the predicted curve and the experimental data is improved. However, the model is still incapable of predicting abrupt changes in S(E). As the synergistic effects of positron diffusion and trapping are folded into the model, it is anticipated that these sharp interfaces will be explained.

Another significant characteristic of the S(E) spectrum is the apparent broad troughs (minima) located between energies 7.5 and 8.5 keV and between energies 12.5 and 14 keV which correspond to the depth ranges of .21 to .27 microns and .50 to .60 microns, respectively. These depth ranges coincide with the AlGaAs/GaAs emitter interface and the p-n junction. Thus, a number of possibilities exist to explain the local minima in S(E). First, a strong electric field is present at the interfaces as a result of band bending. Hence, it is possible that positrons implanted in the space charge depletion region (or within a diffusion length of this region) are swept across the depletion region before an annihilation event is probable. Such an effect would decrease the S-parameter in the proximity of the depletion zone.

Alternatively, the local minimum may be related to the presence or absence of interfacial defect phenomena. In a previous study of SiO_2/Si interfaces[5], it has been shown that differential positron diffusion lengths across an interfacial

trap may result in a lower lineshape parameter than either SiO_2 or Si, indicative of higher electron momenta.

Another possible cause of the observed local minimum in the S-parameter may be drawn from the SPV data of Figure 3, where the .22/.21 ratio indicates that the previously etched material (closer to the AlGaAs/GaAs emitter interface) was of superior quality.[10]

The explanation for the S(E) spectrum differences between 872A and 872B can be correlated with the MOCVD growth rate difference at the edge of the wafer versus the center of the wafer. It has been observed by Spire[11] that the thickness of the heterojunction structure is "substantially" greater at the edge, most probably due to a temperature gradient which leads to enhanced nucleation rates at the wafer edge. This effect is sufficient to explain the S(E) spectrum shift of 872B edge specimen in comparison to 872A center specimen. In addition, by increasing the layer thicknesses, higher energy positrons are necessary to penetrate the individual material layers. Thus, localized minima and maxima of the S(E) spectrum should be reduced for 872B in comparison to 872A since the positron stopping profile is approximated by the derivative of a Gaussian function.[2] Another possible result of differential nucleation rates may be enhanced interdiffusion at the interfacial regions between layers, thus broadening the transition region between the heterojunction layers and thereby diminishing the finer details of the S(E) spectrum. SIMS data is currently being obtained in an effort to verify this hypothesis.

Two sets of SPAS data have been taken of MOCVD Run #1053 and subsequently averaged resulting in the S(E) spectrum shown in Figure 4. The 1053 S(E) spectrum is noticeably different from both of the 872 S(E) spectra, and of major significance is the absence of large contrast between the AlGaAs and adjacent GaAs layers. This difference is largely explained by the thicker cap layer, resulting in an AlGaAs window that is translated an additional .157 microns below the surface (see Table I). The theoretical convoluted S(E) behaviour shows a significantly suppressed AlGaAs spectrum for the 1053 specimen when using the identical characteristic S_1 parameters of the 872 specimens (Figure 4). However, the model placement of the AlGaAs layer appears to be dubious, and the general experimental features, namely the broad maxima and minima, are not predicted. It is possible that the GaAs cap is thicker than the prescribed dimensions in Table I, thus translating the predicted positions of the subsequent layers. Auger and ESCA data are currently being obtained to substantiate this hypothesis. If the GaAs cap is .475 microns thick (translation of .175 Angstroms), then the proposed energy positioning of the AlGaAs/GaAs and p-n junction interfaces is as shown in Figure 4. The troughs of 1053 can then be explained in terms of the previous arguments applied to the 872 specimens: band bending, differential diffusion lengths across an interfacial trap, and the absence of electrically active defects.

CONCLUSIONS

In conclusion, it has been shown that SPAS has potential as a ND profiling tool for high quality epitaxial films and interfaces. The SPAS experimental data provides a profile of distributed material defects that has a strong correlation to SPV results. Also, SPAS appears to possess the capability of performing a three-dimensional characterization of multiple layered structures, as indicated by the differentiation of wafer edge effects resulting from nonuniform film growth temperatures. Finally, SPAS appears to be sensitive to strong localized electric field regions at the AlGaAs/GaAs heterojunctions and the p-n homojunctions.

To fully realize the potential of SPAS, correlations with other established techniques, improvements in the deconvolution modeling of the S(E) lineshape parameter, an analyses of systematic experimental error, and gains in the statistical data collection rate need to be obtained. Also, more in-depth investigations of dopant density, depletion zone thickness, interfacial disorder, positron diffusion length, and other processing parameters such as deposition rate and surface temperature are required, in order to resolve the PAS characteristics of the individual material layer types. A number of ongoing experimental and theoretical efforts are expected to address the above outstanding issues within the near future.

ACKNOWLEDGMENTS

This research was supported in part by Sandia National Laboratories under contract No. 02-2255 and in part by the U.S. Department of Energy, Division of Material Sciences, Office of Basic Energy Sciences under contract No. DE/AC02-76CH00016.

References

[1] P.J. Schultz, K.G. Lynn, W.E. Frieze, and A. Vehanen, Phys. Rev. B, **27**, 6626 (1983).

[2] A. Vehanen, T. Makinen, P. Hautojarvi, H. Huomo, T. Lahtinen, R.M. Nieminen, and S. Valkealhti, Phys. Rev. B **32**, 7561 (1985).

[3] K.G. Lynn, D.M. Chen, B. Nielsen, R. Pareja, and S. Myers, Phys. Rev. B, **34**, 1449 (1986).

[4] A. Vehanen, P. Huttunen, T. Maikenen, and P. Hautojarvi, J. Vac. Sci. Technol. A, **5**, 1142 (1987).

[5] B. Nielsen, K.G. Lynn, Y.C. Chen, and D.O. Welch, Appl. Phys. Lett., **51**, 1022 (1987).

[6] A. Vehanen, K. Saarinen, P. Hautojarvi, and H. Huomo, Phys. Rev. B, **35**, 4606 (1987).

[7] MacKenzie, I.K., Eady, J.A.,and Gingerich, R.R., Phys. Lett., 33A, **5**, 279, 1970.

[8] K.G. Lynn, B. Neilsen, and T.H. Quateman, Appl. Phys. Lett. **47**, 239 (1985).

[9] S.A. Ringel, A. Rohatgi, and S.P. Tobin, in preparation.

[10] S.A. Ringel and A. Rohatgi, in preparation.

[11] S.P. Tobin, private communication.

TABLE I

SOLAR CELL HETEROJUNCTION STRUCTURES

LAYER	MATERIAL	THICKNESS (um)	TYPE	DOPING (cm^3)
MOCVD Run #872				
Cap	GaAs	0.143	p^+	8.0×10^{19}
Window	AlGaAs	0.05	p^+	1.0×10^{18}
Emitter	GaAs	0.5	p	1.5×10^{18}
Base	GaAs	2.0	n	2.0×10^{17}
Buffer	GaAs	2.0	n	2.0×10^{18}
Substrate	GaAs			
MOCVD Run #1053				
Cap	GaAs	0.31	p^+	8.0×10^{19}
Window	AlGaAs	0.03	p^+	1.0×10^{18}
Emitter	GaAs	0.5	p^+	2.0×10^{18}
Base	GaAs	3.0	n	8.0×10^{17}
BSF	AlGaAs	1.0	n^+	2.0×10^{18}
Buffer	GaAs	1.0	n^+	2.0×10^{18}
Substrate	GaAs			

Figure Captions

Figure 1. Example of a deconvoluted characteristic lineshape parameter as a function of the material layer for each layer incorporating the superposition of the layer contributions, S_1, (solid lines) and the local defect contributions, S_d (dashed lines).

Figure 2. Lineshape parameter, S(E), as a function of incident energy, E, for MOCVD Runs (a) #872A and (b) #872B. Experimental data connected by triangles. Theoretical approximations to the experimental data (with and without defects) are shown by the smooth solid curves.

Figure 3. SPV spectrum ratios as a function of wavelength taken at etch depths of (a) .22/.21 microns, (b) .28/.22 microns, and (c) .32/.28 microns.

Figure 4. Lineshape parameter, S(E), as a function of incident energy, E, for MOCVD Run #1053 averaged over two profiles of the same specimen.

FIGURE 1

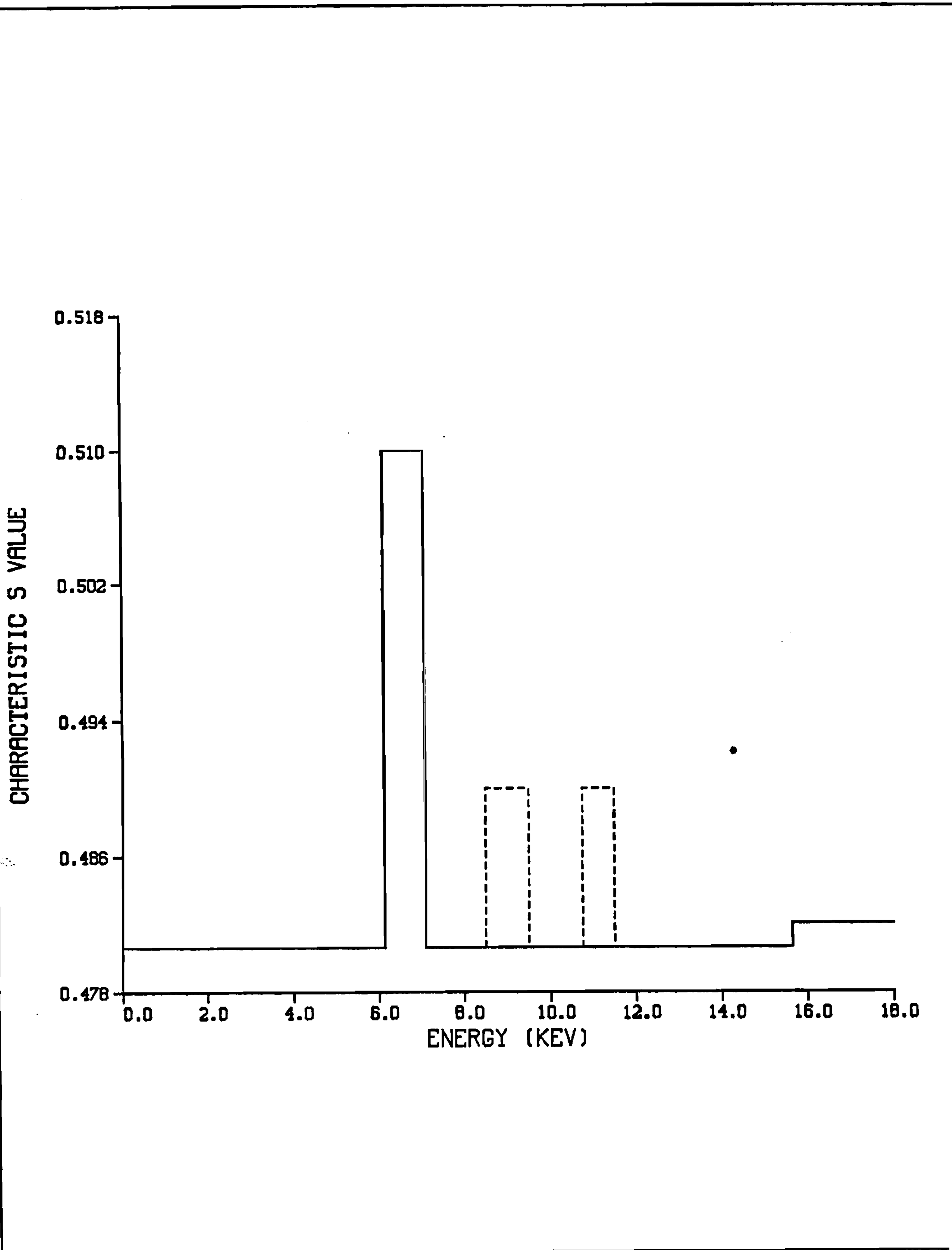

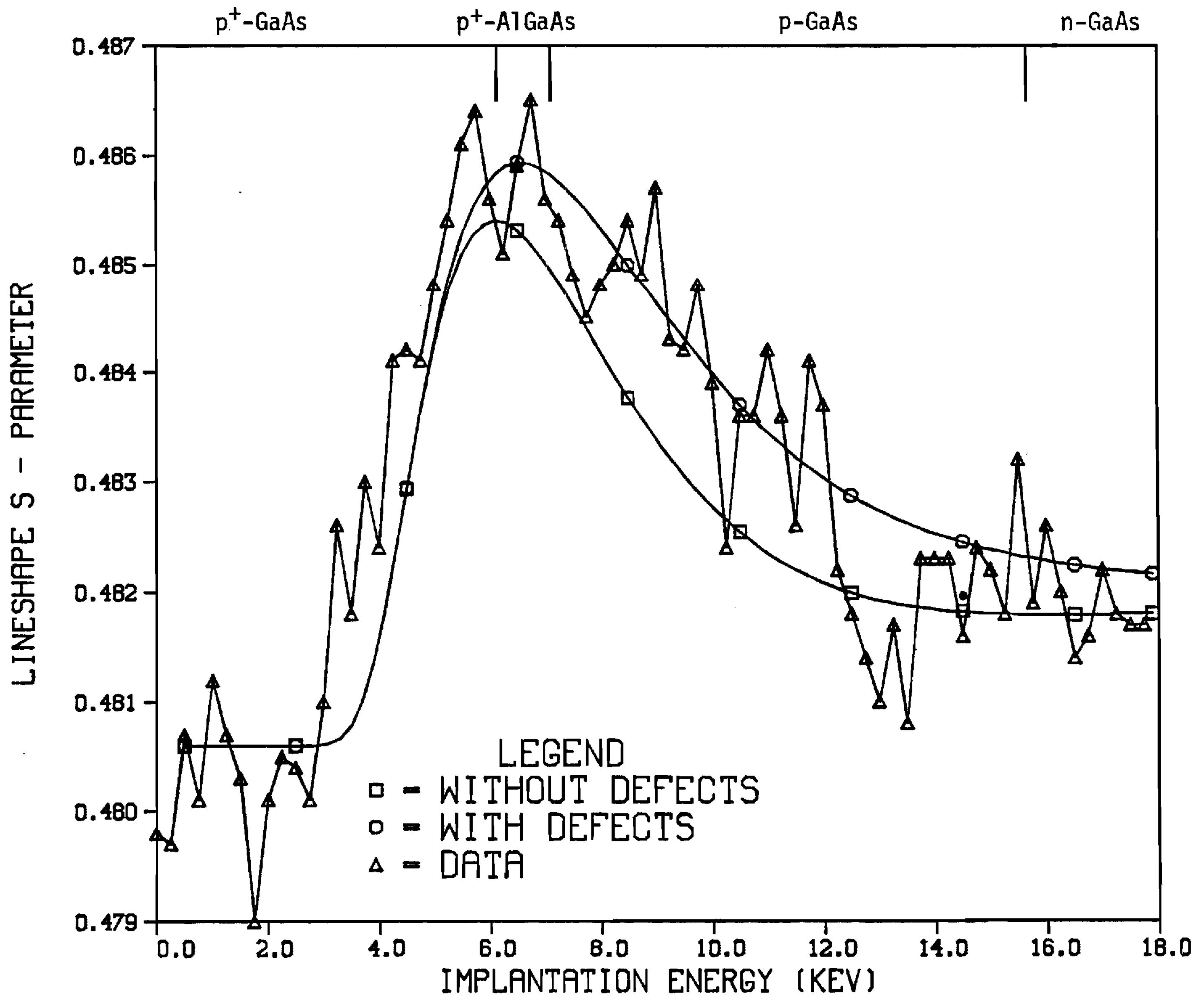
(A)
MOCVD RUN #872A - CENTER
p+-GaAs
p+-AlGaAs
p-GaAs
n-GaAs
LINESHAPE S - PARAMETER
0.487
0.486
0.485
0.484
0.483
0.482
0.481
0.480
0.479
0.0
2.0
4.0
6.0
8.0
10.0
12.0
14.0
16.0
18.0
IMPLANTATION ENERGY (KEV)
LEGEND
□ = WITHOUT DEFECTS
○ = WITH DEFECTS
△ = DATA

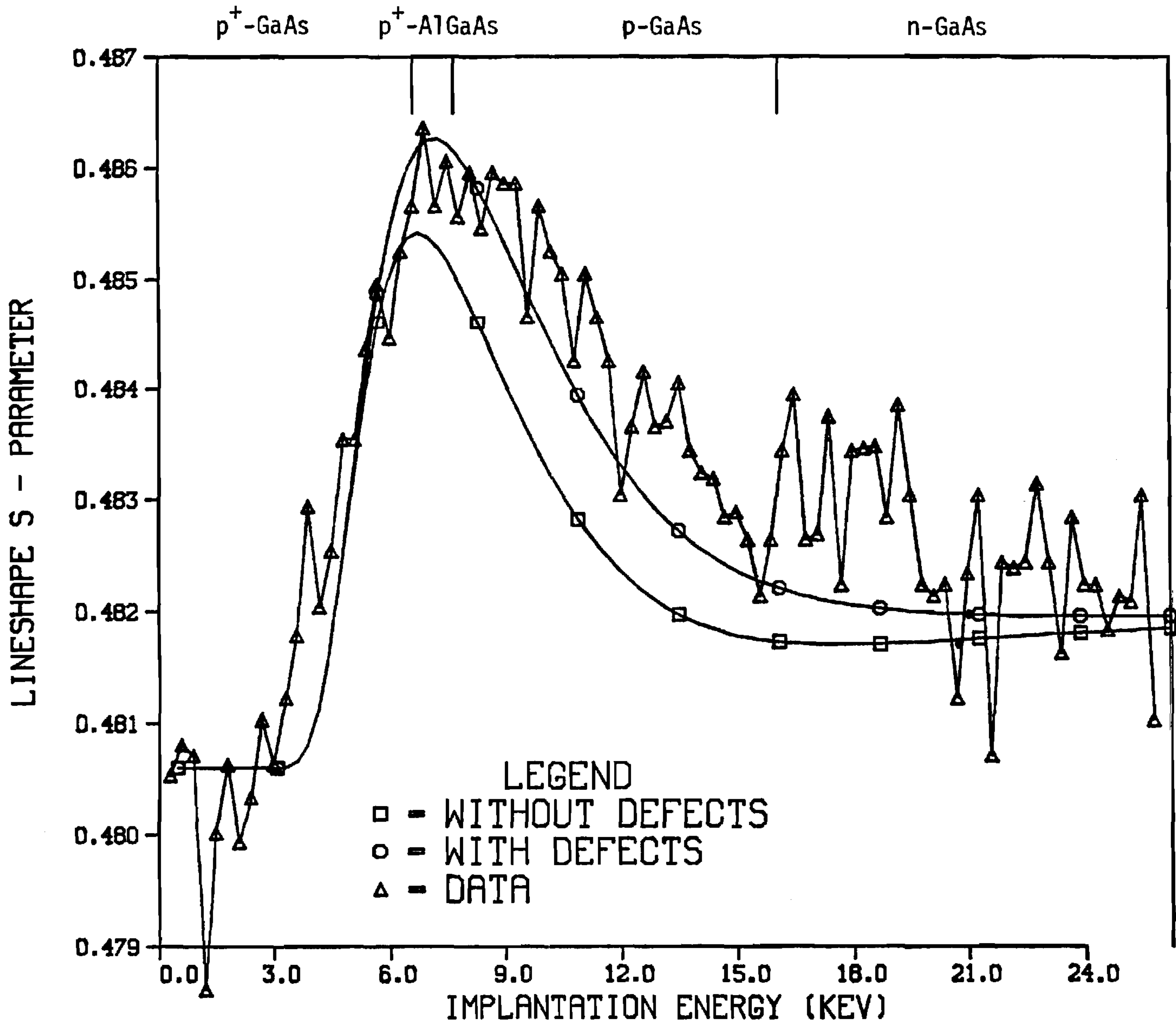
(B)
MOCVD RUN #872B - EDGE
p+-GaAs
p+-AlGaAs
p-GaAs
n-GaAs
LINESHAPE S - PARAMETER
0.487
0.486
0.485
0.484
0.483
0.482
0.481
0.480
0.479
0.0
3.0
6.0
9.0
12.0
15.0
18.0
21.0
24.0
IMPLANTATION ENERGY (KEV)
LEGEND
□ = WITHOUT DEFECTS
○ = WITH DEFECTS
Δ = DATA

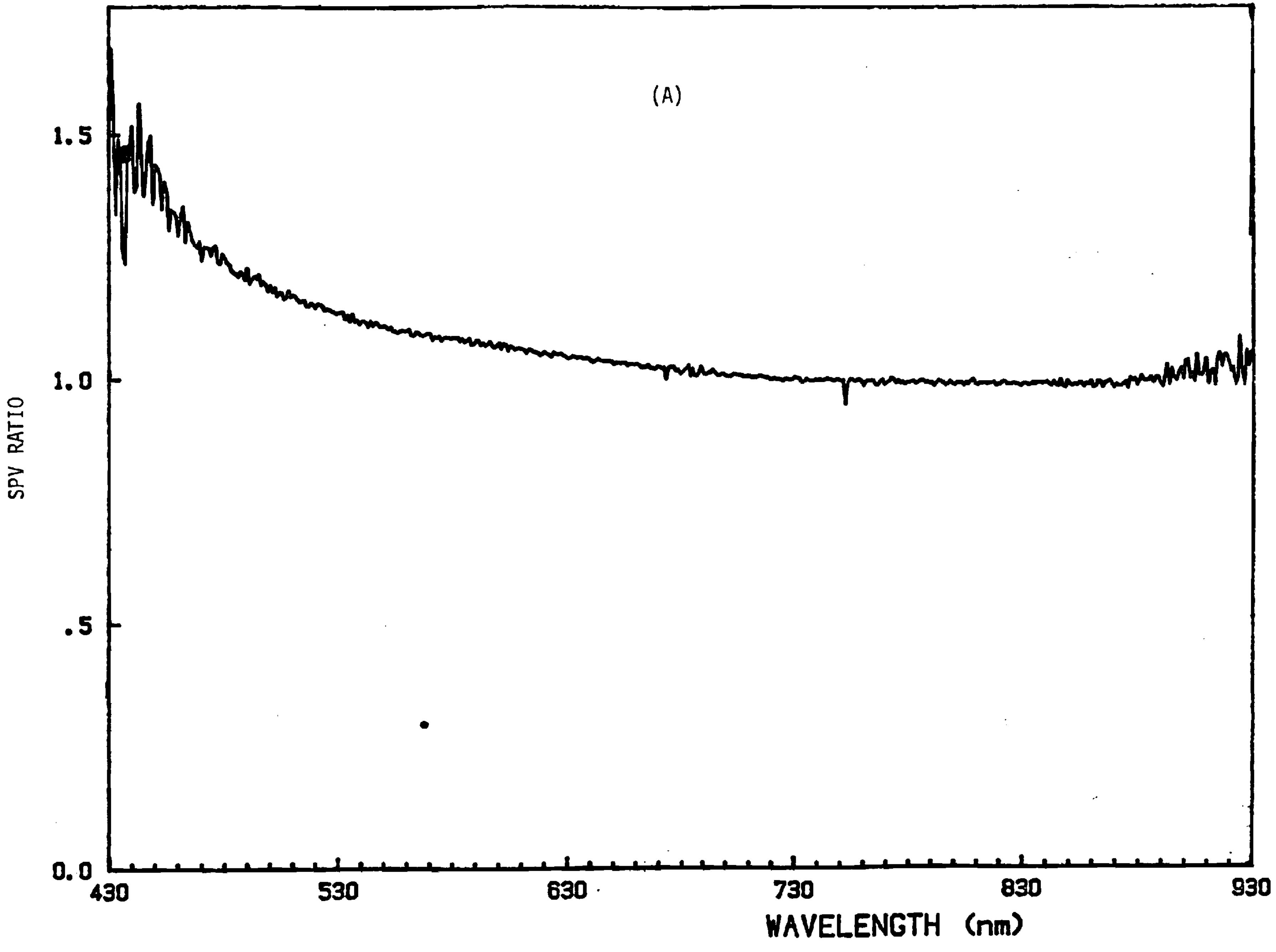

Figure 3

Figure 3

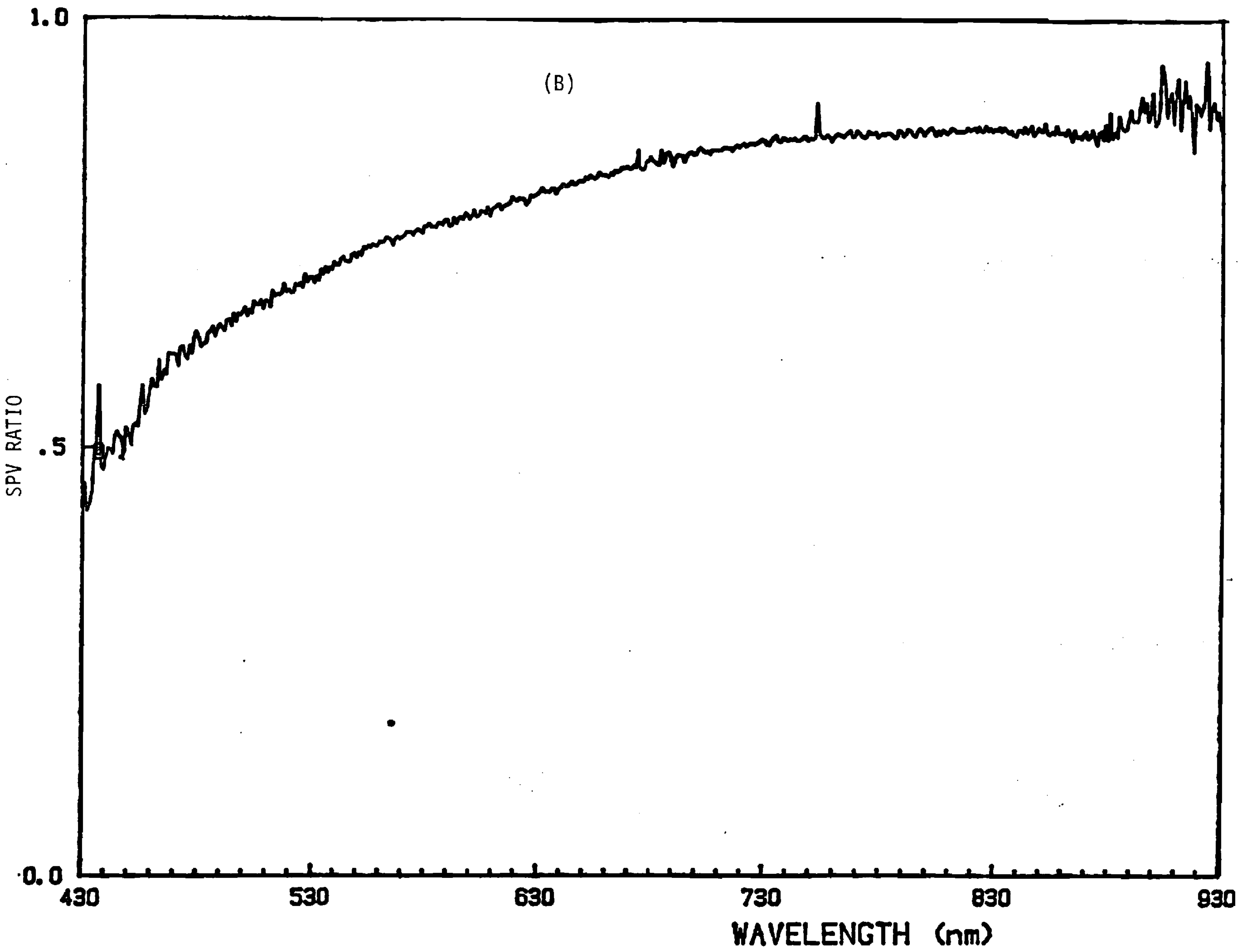

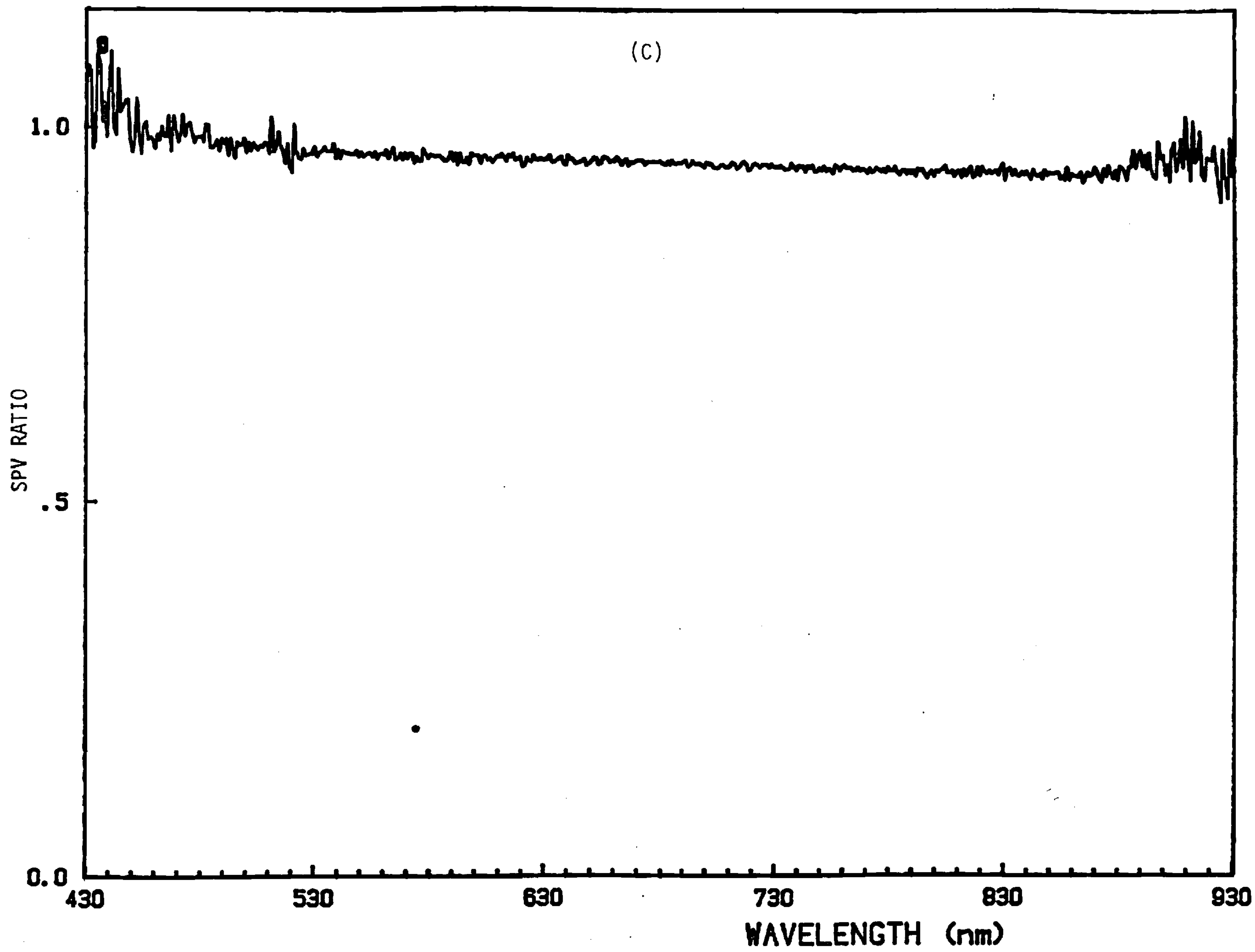

Figure 3

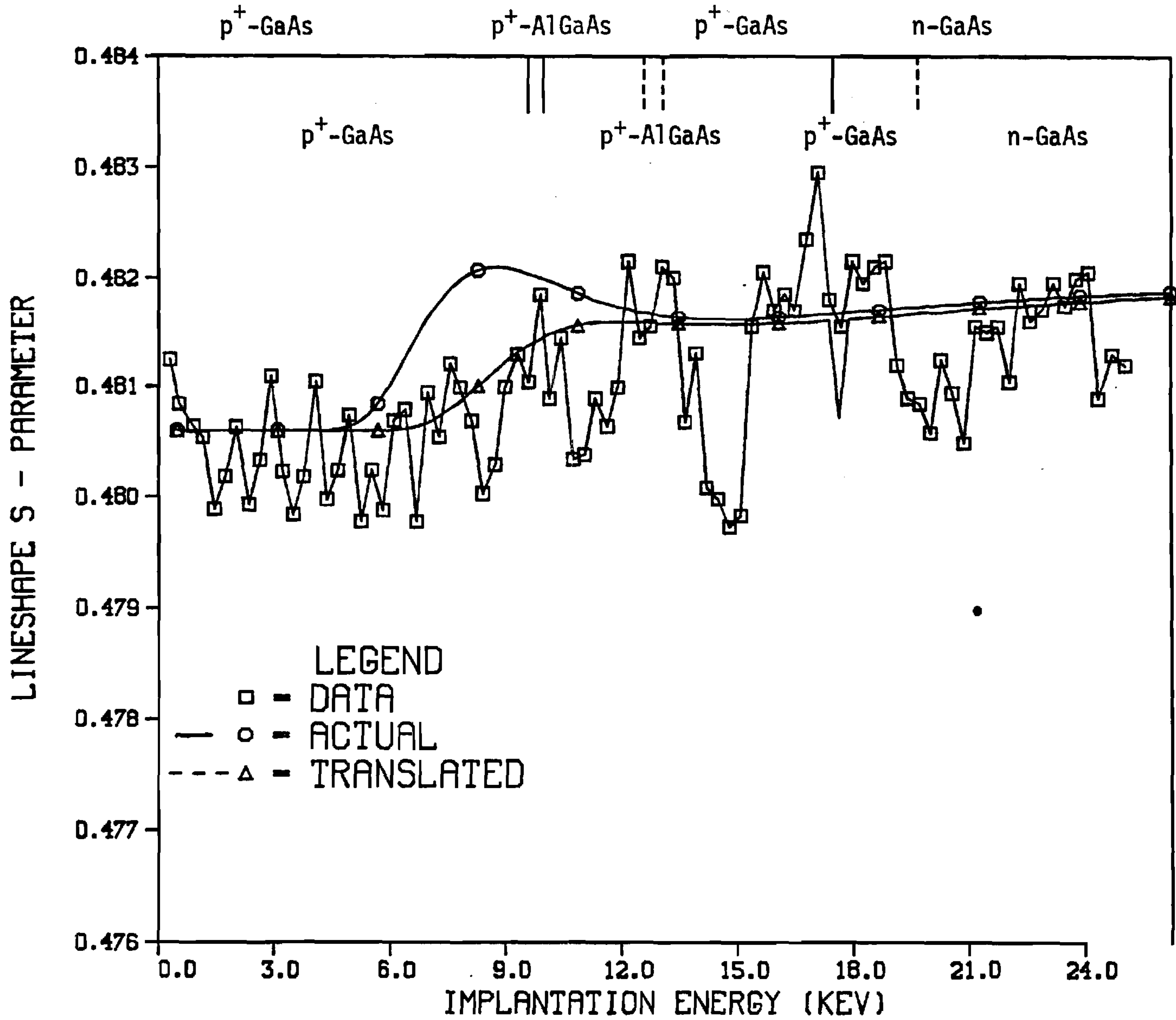
MOCVD RUN #1053
p+-GaAs
p+-AlGaAs
p+-GaAs
n-GaAs
p+-GaAs
p+-AlGaAs
p+-GaAs
n-GaAs
0.484
0.483
0.482
0.481
0.480
0.479
0.478
0.477
0.476
LINESHAPE S - PARAMETER
LEGEND
□ = DATA
—○ = ACTUAL
---△ = TRANSLATED
0.0
3.0
6.0
9.0
12.0
15.0
18.0
21.0
24.0
IMPLANTATION ENERGY (KEV)

RESEARCH ON AlGaAs/GaAs INTERFACES IN

GaAs SOLAR CELLS

A. Rohatgi

Tenth Monthly Report for the Period

September 1, to September 30, 1987

Sandia National Laboratories

Contract No. 02-2255

GEORGIA INSTITUTE OF TECHNOLOGY
SCHOOL OF ELECTRICAL ENGINEERING
ATLANTA, GA 30332

CHARACTERIZATION, MODELING, AND OPTIMIZATION OF HIGH EFFICIENCY GaAs SOLAR CELLS

S. A. Ringel and A. Rohatgi
School of Electrical Engineering
Georgia Institute of Technology
Atlanta, Georgia

ABSTRACT

To increase GaAs solar cell efficiencies to 24% and beyond, it is crucial to understand internal loss mechanisms, particularly their origin and their ultimate influence on design criteria. Only recently have attempts been made to quantify the impact of both interface and bulk quality in dictating cell performance. It is the objective of this paper to improve the basic understanding of internal recombination mechanisms in GaAs solar cells through a combination of experimental characterization and device modeling. A methodology is developed to measure and evaluate minority carrier transport properties, such as lifetime and recombination velocity throughout the device structure in a 21.2% GaAs cell. The cell performance is evaluated on the basis of these internal recombination effects through extensive computer modeling. Guidelines are presented to increase the efficiency of this cell to >24%. Device modeling is performed to show how a complete understanding of the lifetime limiting mechanisms in GaAs and careful growth can produce cell efficiencies approaching 25% with standard heteroface cell design.

CHARACTERIZATION, MODELING, AND OPTIMIZATION OF HIGH EFFICIENCY GaAS SOLAR CELLS

S. A. Ringel and A. Rohatgi
School of Electrical Engineering
Microelectronics Research Center
Georgia Institute of Technology
Atlanta, Georgia 30332-0250

EXTENDED ABSTRACT

To increase GaAs solar cell efficiencies to 24% and beyond, it is crucial to understand internal loss mechanisms, particularly their origin and their ultimate influence on design criteria. Only recently have attempts been made to quantify the impact of both interface and bulk quality in dictating cell performance [1,2]. It is the objective of this paper to improve the basic understanding of internal recombination mechanisms in GaAs solar cells through a combination of experimental characterization and device modeling. A methodology is developed to measure and evaluate minority carrier transport properties, such as lifetime and recombination velocity throughout the device structure in a 21.2% GaAs cell. The cell performance is evaluated on the basis of these internal recombination effects through extensive computer modeling. Guidelines are presented to increase the efficiency of this cell to >24%. Device modeling is performed to show how a complete understanding of the lifetime limiting mechanisms in GaAs and careful growth can produce cell efficiencies approaching 25% with standard heteroface cell design.

MOCVD-grown p-n heteroface GaAs cells were subjected to depth-resolved SPV, DLTS, I-V-T, spectral response, light and dark I-V measurements, followed by PC-1D and surface recombination velocity models to provide guidelines for higher efficiency cells. The cell structure consisted of 0.5 um p-type emitter (2×10^{18} cm^{-3}) on a 2 um n-type base (2×10^{17} cm^{-3}) with an n^+ buffer layer and a p^+ $Al_xGa_{1-x}As$ ($x = 0.90$) passivating window layer. This particular cell had an efficiency of 21.2%.

The DLTS spectrum in Figure 1 revealed a hole trap at $E_v + 0.91$ eV in the depletion region of the n-type base. Trap profile measurements showed a rise in the trap density as the p-n interface is approached. This was supported by comparing the magnitude of the SPV response at different etch depths using an electrochemical etching profiler. The reverse leakage current at a fixed voltage was measured as a function of temperature to establish that this deep level is controlling the leakage current of the cell. The Arrhenius plot in Figure 2 shows an activation energy of

~0.4523 eV which, when added to the activation energy of the DLTS level (0.91 eV), gives ~ the bandgap (1.36 eV) of GaAs. This verifies that the E_v + 0.91 eV trap is indeed limiting the space charge leakage current of this cell. Transformed dark I-V data indicated tha $J_{01} \sim J_{02}$ at the cell operating point (~1 volt) so removal of this hole trap can reduce the leakage current and improve cell performance.

In order to assess the surface recombination velocity and lifetime in this cell, first the PC-1D model was used to match the spectral response. It was found that a net base lifetime of ~8 ns along with a front surface recombinaton velocity (FSRV) of ~1.25×10^5 cm/s was necessary to match the actual response as shown in Figure 3. The consistency of these choices was checked using an effective recombination velocity (S) model which was developed for silicon devices [3], but modified to incorporate GaAs cells. S is calculated everywhere within the cell based on a lifetime profile, FSRV and BSRV, so that the J_{0b} and J_{0e} were found to be 0.89×10^{-19} and 0.51×10^{-19} A/cm^2, respectively. The calculated $J_{01} = J_{0b} + J_{0e} =$ ~1.40×10^{-19} A/cm^2, in close agreement with the measured J_{01} (~1.30×10^{-19} A/cm^2, supporting the selection of FSRV and lifetime. This suggests that J_{01} or V_{0c} of this cell is predominantly but not entirely base limited. The large emitter contribution indicates that this cell can benefit from improved emitter design or lower FSRV. These inputs (S, τ_b) were fed into the PC-1D model to calculate the cell data for this device, which is shown in Table 1 along with the measured cell data. An excellent match between the model and actual data reinforces our analysis of this cell. This analysis is extended further using PC-1D to show how to take this cell to >24% efficiency by simple design modifications stated in Table 1.

In conclusion, a characterization and modeling methodology to analyze the recombination mechanisms in a GaAs cell is presented. Guidelines for cell optimization toward 25% efficiency are discussed.

REFERENCES

1. P. D. Demoulin, C. S. Kyono, M. S. Lundstrom, and M. R. Melloch, Proceedings 19th IEEE Photovoltaic Specialists Conference, pp. 93-97 (1987).

2. S. A. Ringel et al., to be published in IEEE Trans. Electron. Dev., 1988.

3. A. Rohatgi and P. Rai-Choudhury, IEEE Trans. Electron. Dev., vol. ED-31, no. 5, pp. 596-601, 1984.

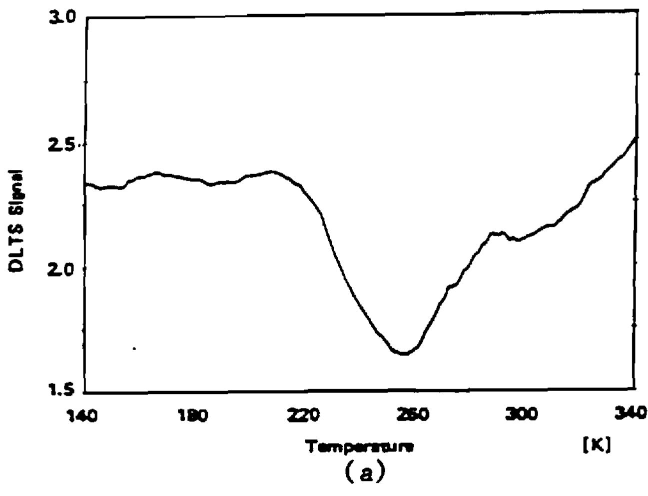

(a)

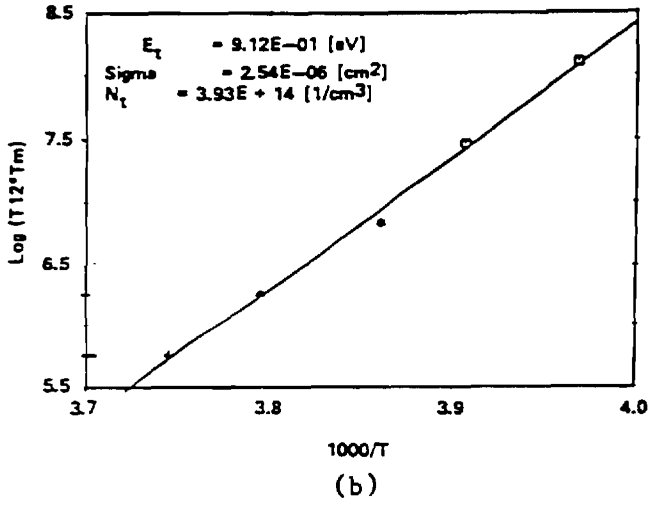

(b)

Figure 1: DLTS Scan (a) and Associated Arrhenius Plot (b) for Hole Trap in Base Depletion Region.

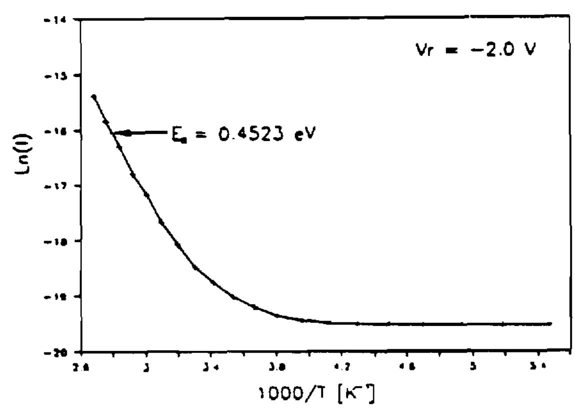

Figure 2: I-V-T Plot Indicating Deep Level Activation Energy

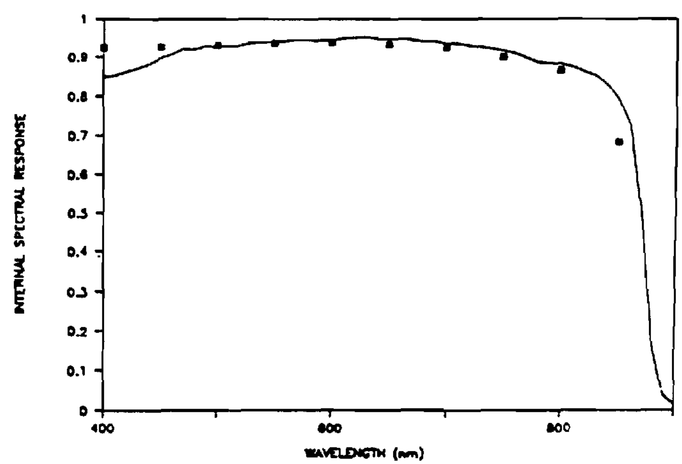

Figure 3: Comparison of Modeled (Solid Squares) and Actual (Line) Spectral Response for this Cell

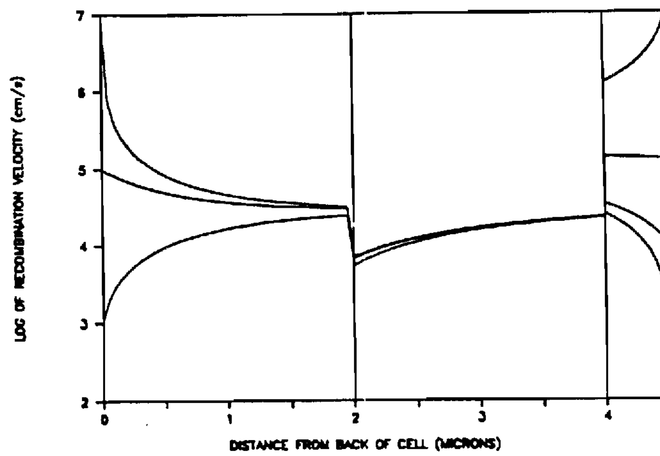

Figure 4: Effective Recombination Velocity Plot for Various Values of FSRV and BSRV

Table 1: Comparison of Measured and Modeled Cell Data with Design Guidelines for Improved Efficiencies

ID	FSRV (cm/s)	BSRV (cm/s)	N_A (cm^{-3})	N_D (cm^{-3})	τ_B (sec)	J_{sc} (A/cm^2)	V_{oc} (V)	EFF (%)
Actual			$2x10^{18}$	$2x10^{17}$		24.5	1.013	21.2
Match	$1.25x10^5$	$1.0x10^6$	$2x10^{18}$	$2x10^{17}$	$8x10^{-9}$	24.56	1.009	21.39
	$1.0 x10^4$	$1.0x10^4$	$2x10^{18}$	$2x10^{17}$	$8x10^{-9}$	26.71	1.017	23.13
	$1.0x10^4$	$1.0x10^4$	$2x10^{18}$	$2x10^{17}$	$15x10^{-9}$	27.108	1.032	24.17
	$1.0x10^4$	$1.0x10^4$	$2x10^{18}$	$5x10^{17}$	$15x10^{-9}$	26.78	1.048	24.34

G-21-602

RESEARCH ON ALGaAs/GaAs INTERFACES IN GaAs SOLAR CELLS

A. Rohatgi and S. A. Ringel

Technical Progress Report

October 1, 1987 - January 31, 1988

Sandia National Laboratories

Contract No. 02-2255

GEORGIA INSTITUTE OF TECHNOLOGY
School of Electrical Engineering
Atlanta, GA 30332

Introduction

As the conversion efficiencies of GaAs solar cells continue to increase, the ability to detect, analyze, and assess the importance of defects and other lifetime limiting mechanisms become critical to advance cell performance further. Most research to date has been devoted to the study of topics such as recombination centers in bulk GaAs [1,2] and at surfaces and interfaces using specialized test structures in which the interplay of interfacial effects with bulk properties such as minority carrier lifetime is not obvious [3-5]. Hence it is important to develop measurement techniques in conjunction with device modeling to separate those material parameters that dictate the performance of solar cells and other GaAs devices in which the carrier transport mechanisms are not well understood. Recently, a few attempts have been made to address this issue for GaAs solar cells [6-8].

This paper presents a combination of an electronic characterization methodology and device modeling to improve solar cell design by detecting and evaluating important material parameters such as lifetime, interface recombination velocity, and deep levels within a state-of-the-art MOCVD grown GaAs p-n heteroface solar cell. First, a number of standard semiconductor characterization techniques, such as DLTS (Deep Level Transient Spectroscopy) and dark I-V (current-voltage) and I-V-T were used to determine the carrier recombination and generation lifetimes separately. Then dopant profile and depth-resolved surface photovoltage measurements were performed with the help of an electrochemical etching profiler to provide necessary inputs to the device modeling programs used in this investigation. A combination of a one dimensional computer model and the experimental data obtained through the above

techniques was used to reveal the variation in the effective recombination velocity (S_e) throughout the device. S_e is indicative of net recombination anywhere within the device and can be used to guide the optimization of high efficiency cell design. A second device modeling program (PC-1D) was used to calculate cell parameters J_{sc}, V_{oc}, and efficiency along with the spectral response of the cell. The calculated values were correlated with the measured cell data to assess the accuracy of the characterization methodology to analyze the lifetime limiting mechanisms in the bulk and interfaces of GaAs structures. Finally, improved understanding of the loss mechanisms coupled with device modeling was used to provide guidelines for attaining GaAs cell efficiencies approaching 25% under AM1.5 conditions.

Experimental Methods

Device Structure

Figure 1 shows the device structure of the MOCVD grown GaAs heteroface solar cell used in this study, along with the measured cell data. The GaAs layers were grown at 700°C using trimethyl gallium and arsine as reactants. The AlGaAs was grown at 800°C using trimethyl aluminum for the Al source. The mole fraction of Al in the AlGaAs window layer was 0.90. Zn and Si were the p-type and n-type dopants, respectively, used throughout the structure.

For DLTS, I-V and I-V-T measurements, 50 mil diameter mesa dots were formed by evaporating Au/Zn ohmic contacts on the structure. The back surface was covered with evaporated Au/Zn ohmic contacts to facilitate the electrical measurements.

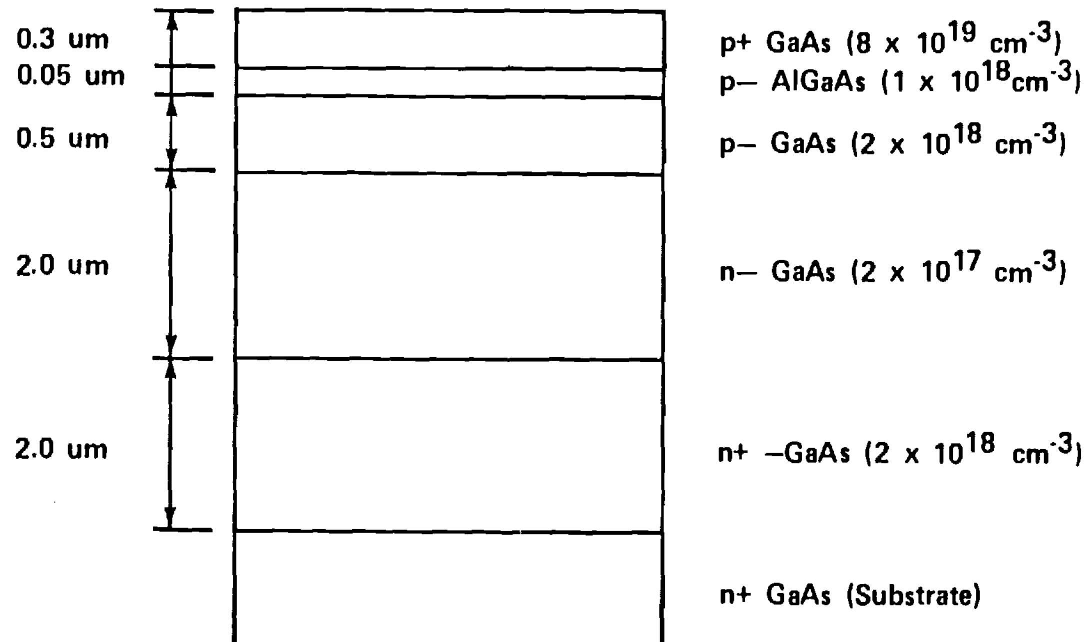

Figure 1. Device structure and measured cell data of the MOCVD GaAs heteroface cell used in this study.

Depth-Resolved SPV/C-V Measurements

Attempts were made to determine the carrier concentration profile and the spatial variation in the electro-optical response of the cell using a depth-resolved C-V and surface photovoltage (SPV) measurement. Both these measurements were performed in an automated electrochemical etching profiler in which an electrolyte is used to perform precise step-by-step etching coupled with I-V, C-V, and SPV measurements after each step [9]. A Schottky barrier formed between the electrolyte and the semiconductor facilitates both C-V and SPV measurements. The doping concentration is found from the C-V data at each depth. SPV measurements were performed in the wavelength range of 400 to 900 nm to accomodate both the GaAs and AlGaAs absorption edges. The SPV signal is measured at the surface under open circuit conditions to avoid electrochemical etching or deposition during the measurement. The choice of electrolyte is dictated by the properties of the semiconductor. For this study, a solution of 0.2 M NaOH + 0.1M EDTA (ethylenediamminetetraacetic acid) was found to be an adequate electrolyte for Schottky barrier formation and electrochemical etching and showed no signs of surface degradation.

DLTS Studies

A combination of DLTS and I-V-T measurements was used to determine the trap which controls the leakage current of the solar cell. The DLTS technique reveals all the detectable traps, regardless of their influence on the leakage current. DLTS measurements were made using an automated wafer analyzer system which obtains data via a modified lock-in amplifier type DLTS setup. Nonuniformity in deep level distribution near the p-n junction of the solar cell was investigated by varying the steady reverse bias level from -5 volts to -1 volt

but keeping the sum of the reverse bias and forward bias pulse height constant at -0.5 volts. In this way, the edge of the depletion region is steadily stepped toward the metallurgical junction as the reverse bias is decreased and a spatial trap profile of the depletion region is obtained. DLTS measurements were also performed in a forward bias mode (the sum of the steady reverse bias and the injection pulse height > the built-in voltage of the p-n junction) to detect both majority and minority carrier traps in the depletion region. It should be noted that the detection limit of our DLTS set-up is about 0.01% of the background doping concentration and hence defects with concentrations of less than 2×10^{13} cm^{-3} in the base region will not be detected.

I-V-T Analysis

The I-V-T technique, in contrast to DLTS, identifies only the activation energy of that deep level which limits the reverse leakage current as well as the generation/recombination lifetimes associated with it [10,11]. In addition, it does not suffer from the same doping dependent detection limit as DLTS, allowing information to be extracted from heavily doped device structures provided the trap is the dominant source of leakage. The carriers decay back to their equilibrium concentration by recombining at the deep level after an injection process. The generation lifetime associated with a deep level, τ_g, is the inverse of the decay process and becomes important where carrier concentration is low, such as the depletion region of a p-n junction.

The method is based on the assumption that the total reverse leakage current, J_o, is dominated by the space charge generation current, J_{o2}, and the diffusion component, J_{o1}, can be neglected under reverse bias. This is routinely observed in GaAs. From SRH (Schockly-Read-Hall) theory, the total carrier recombination rate, R, under steady state conditions is given by

$$R = \frac{np - n_i^2}{\tau_{po}(n + n_1) + \tau_{no}(p + p_1)} \qquad (1)$$

where

$$\tau_{po} = (\sigma_p N_T v_{TH})^{-1} \qquad (2)$$

$$\tau_{no} = (\sigma_n N_T v_{TH})^{-1} \qquad (3)$$

$$n_1 = n_i \exp[\frac{(E_t - E_i)}{kT}] \qquad (4)$$

$$p_1 = n_i \exp[\frac{-(E_t - E_i)}{kT}] \qquad (5)$$

Under reverse bias conditions the excess carrier concentration in the space charge region can be neglected so that equation (1) reduces to

$$R = -n_i/\tau_g \qquad (6)$$

with

$$\tau_g = \tau_{po} \exp[\frac{(E_t - E_i)}{kT}] + \tau_{no} \exp[\frac{-(E_t - E_i)}{kT}] \qquad (7)$$

where E_t is the energy level of the recombination center within the bandgap and E_i is the position of the intrinsic Fermi level. If the capture cross section for holes (σ_p) and electrons (σ_n) are comparable then τ_g reduces to

$$\tau_g = \tau_{po} \exp[\frac{(E_t - E_i)}{kT}] \qquad \text{for } E_t > E_i \qquad (8)$$

or

$$\tau_g = \tau_{no} \exp[\frac{-(E_t - E_i)}{kT}] \qquad \text{fpr } E_t < E_i \qquad (9)$$

but more generally,

$$\tau_g = \tau_r \exp\left[\frac{(E_t - E_i)}{kT}\right] \tag{10}$$

Using the definition of leakage current in a reverse-biased diode [12] and recalling the assumption which neglects the J_{o1} component of J_o,

$$J_{rev} = J_{o2} = \frac{qn_i W}{\tau_g} \tag{11}$$

where W is the width of the depletion region, then

$$J_{o2} \propto \exp\left[\frac{-(E_t - E_v)}{kT}\right] \qquad \text{for } E_t > E_i \tag{12}$$

or

$$J_{o2} \propto \exp\left[\frac{-(E_c - E_t)}{kT}\right] \qquad \text{for } E_t < E_i \tag{13}$$

Hence, the activation energy of the generation center which controls the leakage current can be determined from the slope of the $\ln(J_{o2})$ vs. 1000/T plot under constant applied reverse bias. It is important to note that the I-V-T method gives an activation energy of the trap which controls the leakage current but it does reveal the band edge with respect to which that activation energy is measured, unless the trap location is known. Therefore, this method must be supplemented by other measurements such as DLTS which gives all the traps present but does not reveal which one controls the leakage current.

Transformed I-V Analysis

The I-V characteristic of the mesa diode structure was measured in the dark and analyzed using an automated setup to separate the resistance, bulk and junction region effects. The I-V characteristic of a solar cell is a composite of two exponential functions including series and shunt resistance effects. The transformed I-V program first measures and subtracts the resistance effects from the measured data and then fits the rest to a double exponential equation given by

$$J = J_1 + J_2 = J_{o1}\left[\exp\left(\frac{qV}{kT}\right) - 1\right] + J_{o2}\left[\exp\left(\frac{qV}{nkT}\right) - 1\right] \quad (14)$$

where J_{o1} and J_{o2} are the saturation current densities for the diffusion (n=1) and space charge generation (n) current components, respectively. The computer program fits the data and provides values of J_{o1} and J_{o2}.

Results and Discussion

The doping profile throughout the device structure, Figure 1, was confirmed by depth-resolved C-V measurements. Since the doping level in the AlGaAs window layer is similar to that of the emitter, the AlGaAs layer was not evident. Presence of the AlGaAs layer was confirmed by far infrared reflectance measurements which also revealed the mole fraction of Al to be 0.87, close to the target composition. The AlGaAs thickness was found to be 50 nm by reflectance measurements.

Spatial variations in the material properties were investigated by depth-resolved SPV measurements in an electrochemical profiler. Figure 2 shows photovoltage spectra taken at various etch depths. This data was not taken on

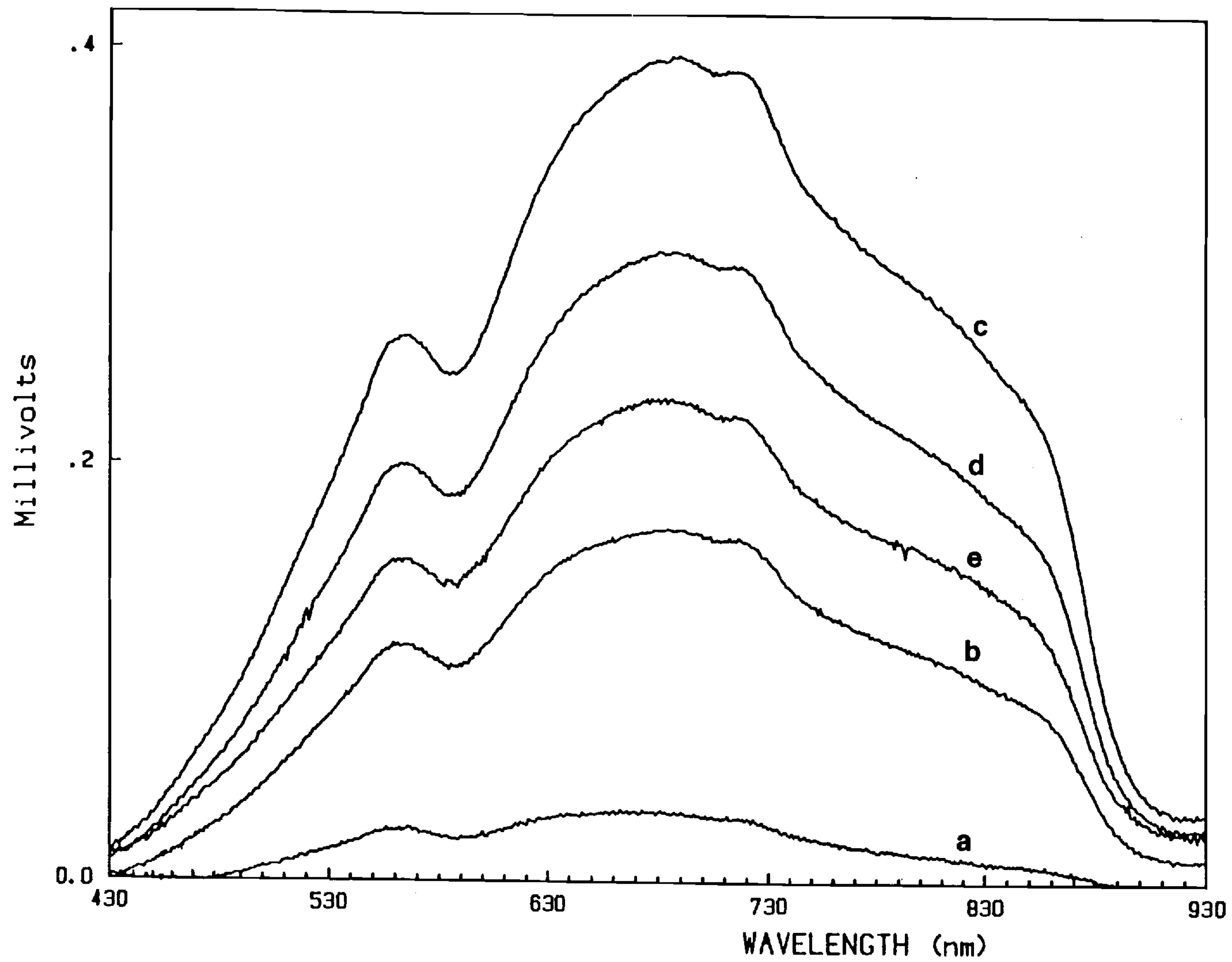

Figure 2. Variation of SPV response as the device is etched through. The measurements were taken at etch depths of (a) 0.12 um, (b) 0.17 um, (c) 0.21 um, (d)0.3 um, and (e) 0.42 um.

the actual cell but on a piece adjacent to it, which has the p^+ GaAs cap layer intact. The initial (0.12-0.21 um) increase in the response with increasing etch depth is due to the successive removal of the heavily doped cap layer which has high absorption and recombination. The two humps at 560 nm and 720 nm are the characteristic response of the SPV optics. The etch depths at which these measurements were made are indicated in the figure. Both the overall shape and magnitude of SPV response are related to the properties of the material being probed. As we etch through the emitter region (0.21-0.42 um) the response gradually drops. This does not necessarily indicate defects or nonuniformity in the emitter region, but instead could be the result of enhanced competition from the p-n junction for the carriers generated within the emitter region. Notice that the overall open-circuit signal represents the spectrally resolved sum of the opposing photovoltages generated at the front electrolyte/GaAs Schottky barrier and at the p-n junction [9]. At present it is not known how to quantitatively account for the effect of the p-n junction influence on the measured response.

A qualitative picture of material uniformity can be obtained from spectrally resolved divisions of consecutive SPV spectra. Figure 3 shows a series of ratios taken while the device is being etched through the emitter. SPV ratio curve "a" indicates that a fraction of the carriers generated at longer wavelengths are either being lost to the p-n junction or to a defective layer near it since the ratio there is less than unity. The sign change in the SPV ratio curve "b" of Figure 3 taken just before the p-n interface, indicates that for photons with wavelength greater than ~ 530 nm the p-n junction becomes the dominant carrier collecting junction. Up to this point, the effect of the presence of a defective region of material could be masked by

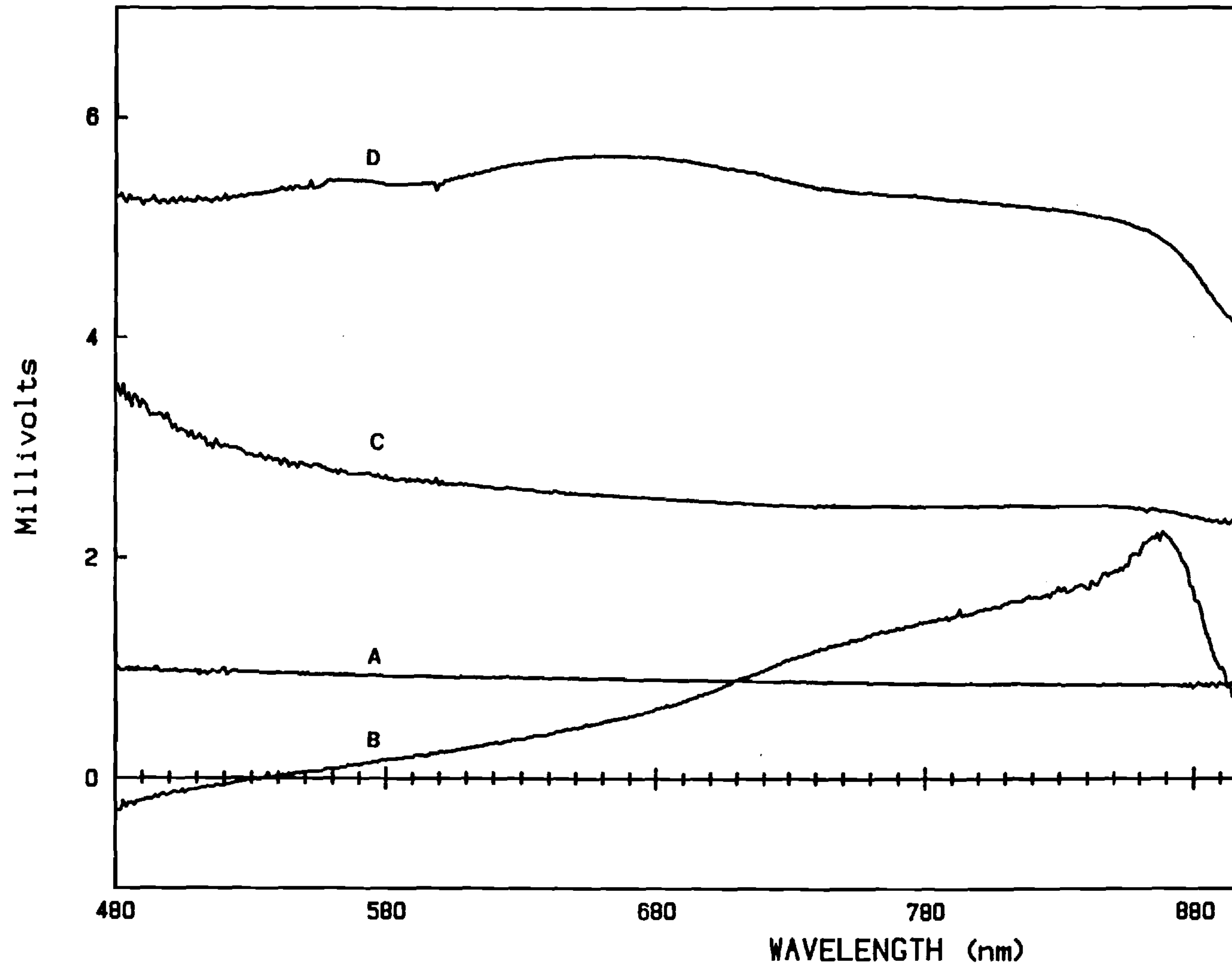

Figure 3. Ratios between SPV spectra taken at: (a) front of emitter; (b) just before p-n junction; (c) just after p-n junction; (d) 0.1 um after curve (c).

the competition from the p-n junction. However, the SPV ratio curves"c" and "d", obtained by etching through the p-n junction and another slice 0.1 um later, respectively, do not suffer from this complication. The ratio curves c and d suggest that near the p-n junction, the material quality is improving in the base as we move away from the junction edge because the ratios are not only greater than one but gradually increase with depth, in spite of the constant base doping.

From the depth-resolved SPV measurements, it appears that the defect density may be increasing as we approach the p-n junction. To investigate this further, depth-resolved DLTS measurements were performed on the same wafer using the mesa structure described earlier. The DLTS primarily probes the n-base side of the p^+-n junction. Figure 4 shows that a deep level was detected only when the probed depletion region got close to the p-n interface. This minority carrier trap had an activation energy of E_V + 0.912 eV and a concentraton of 3.93 + $10^{14}cm^{-3}$. The fact that this level was not detected for wider depletion widths supports the nonuniform defect distribution seen by the SPV response near the p-n junction. The ln(J) vs T plot from the I-V-T measurement, Figure 5, gave an activation energy of E_a = 0.4523 eV for the J_{o2} component. Since the sum of the DLTS and I-V-T activation energies is close to the bandgap of GaAs (0.4523 + 0.912 = 1.36 eV), it is reasonable to conclude that the level detected by DLTS and I-V-T is the same and is also responsible for the excess leakage current.

While the DLTS and I-V-T measurements yield the characteristics of the space charge region, they offer no information about the bulk material properties. In order to assess the bulk properties the transformed I-V technique was used to separate the bulk and junction effects. Figure 6 shows the trans-

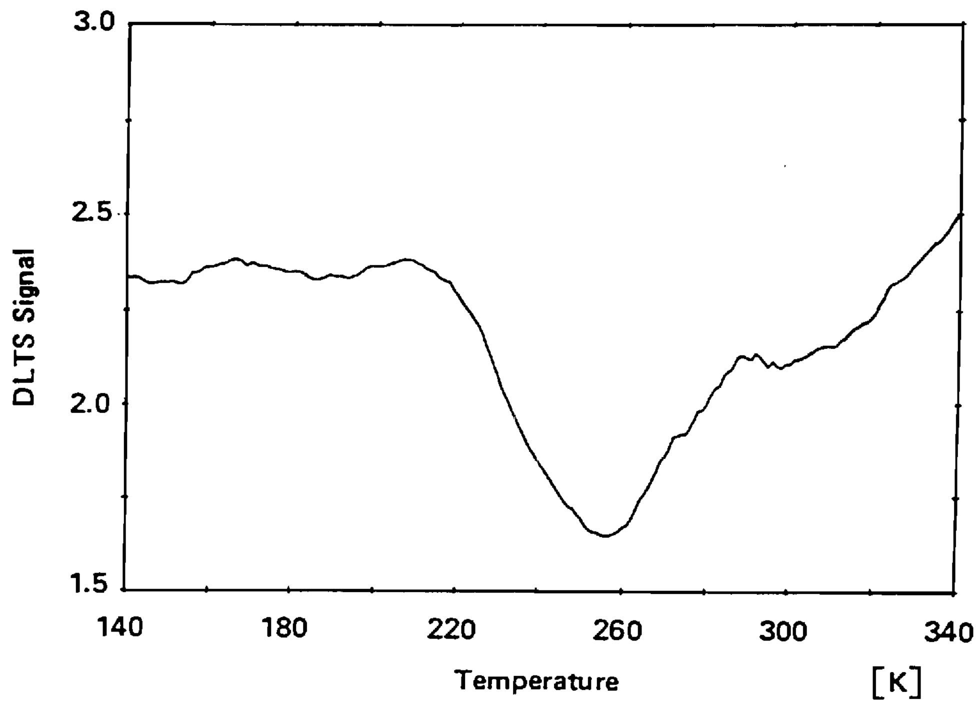

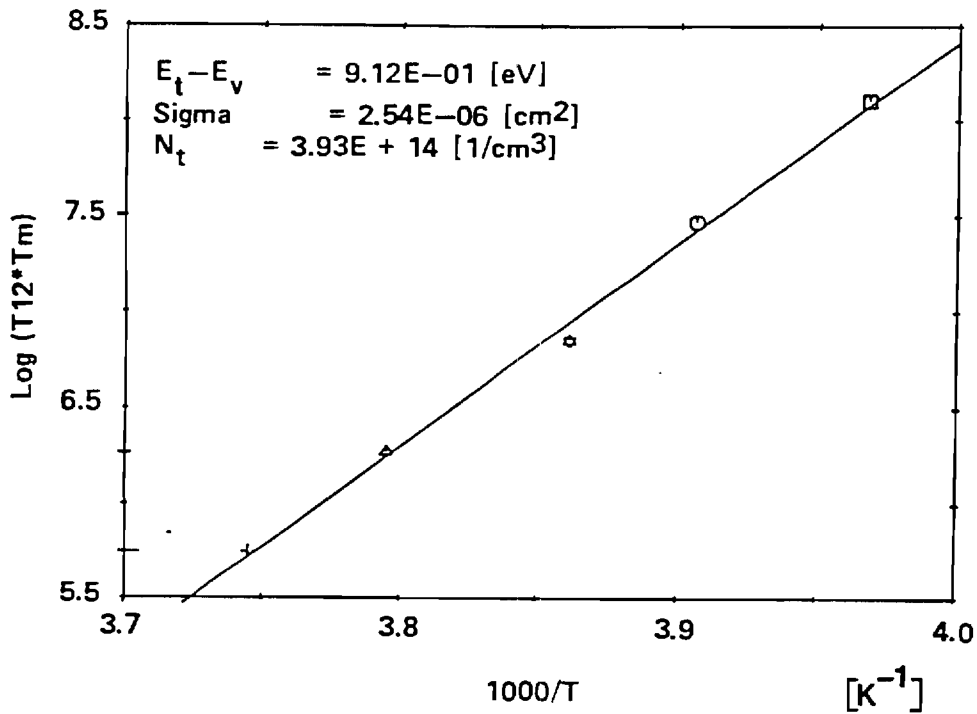

Figure 4. DLTS scan and activation energy plot indicating the presence of a hole trap in the n-type base depletion region.

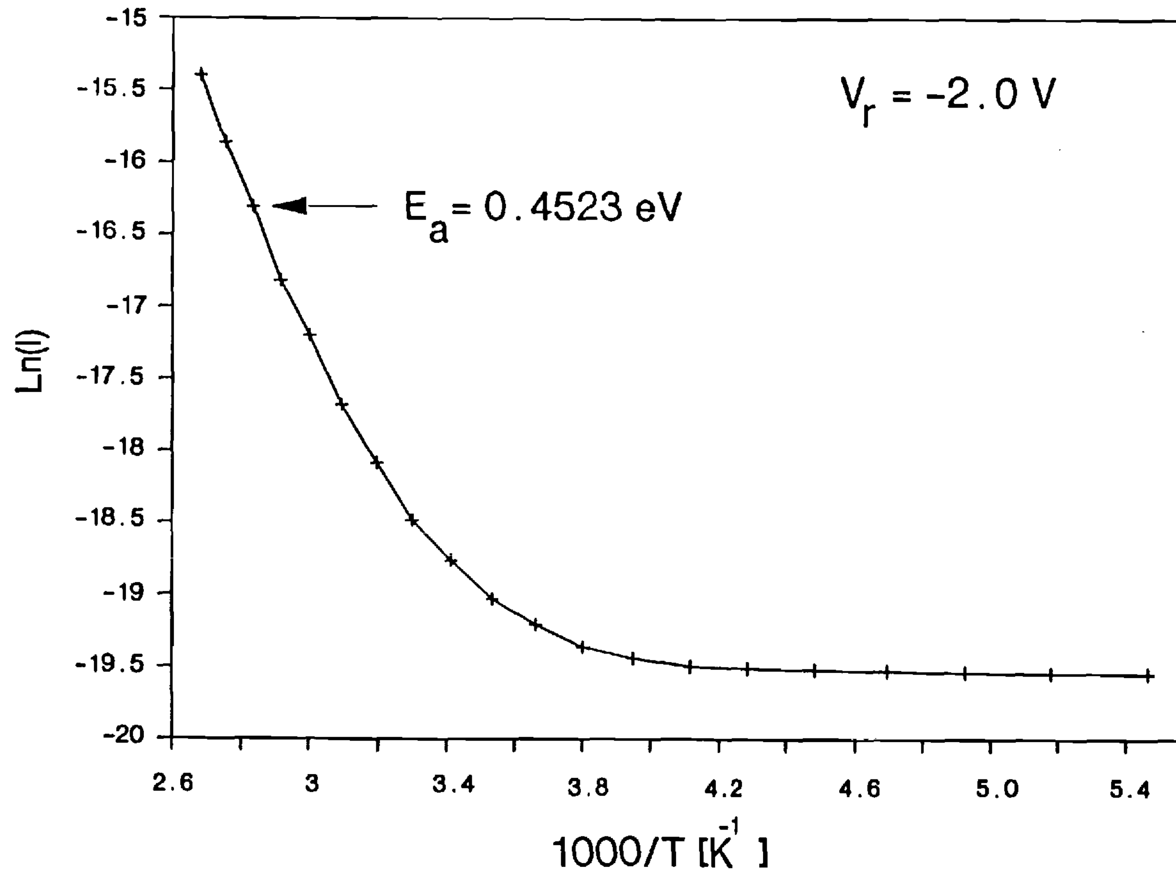

Figure 5. LN(J) vs. T plot measured at 2 volts constant reverse bias. Trap activation energy is shown in the figure.

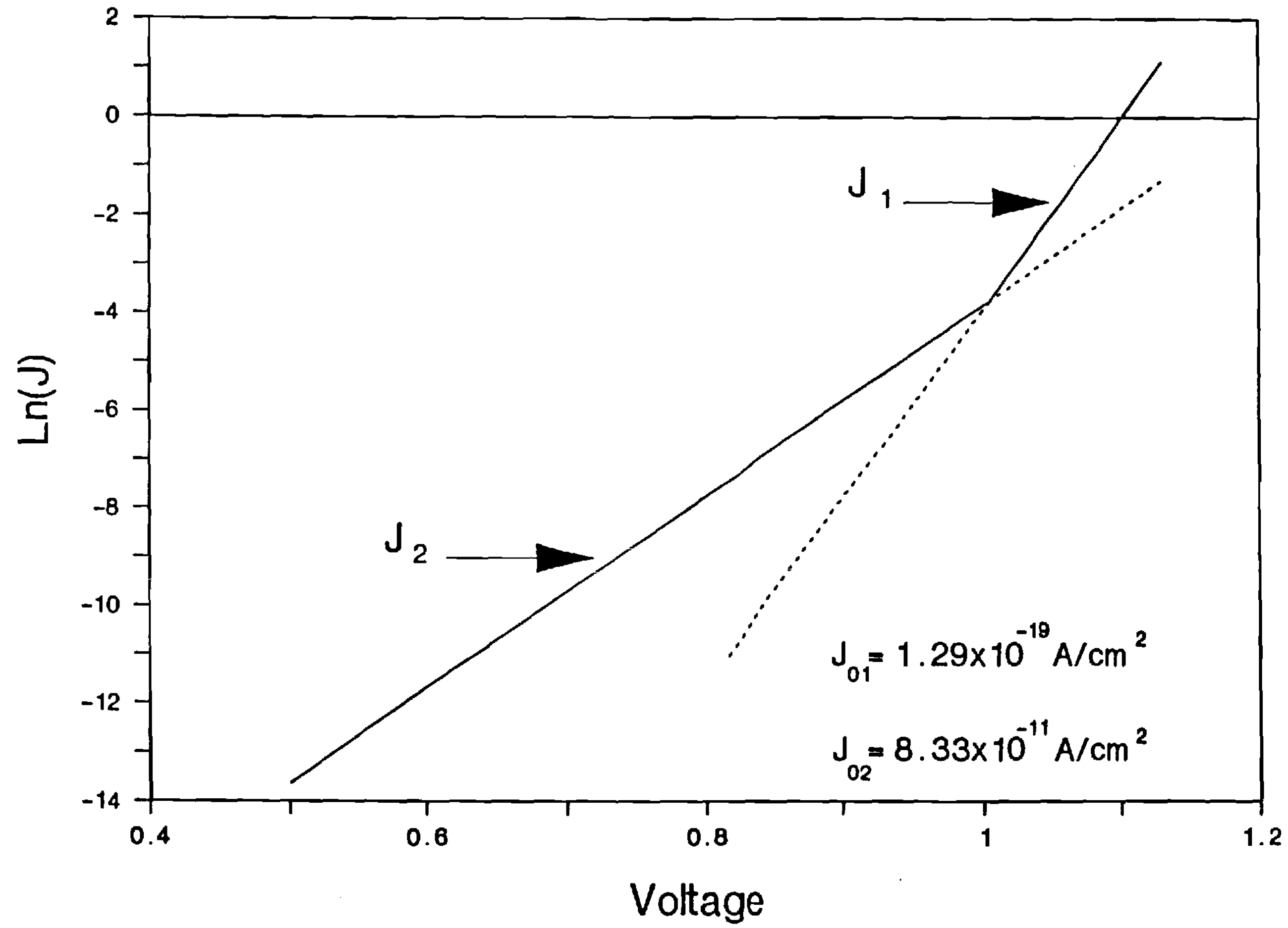

Figure 6. Transformed I-V characteristic for cell. J_1 (diffusion) and J_2 (space charge) current density components are indicated.

formed I-V curve for this device at room temperature. J_{o1} and J_{o2} components were found to be 1.29 E - 19 A/cm^2 and 8.33 E - 11 A/cm^2, respectively, while the corresponding n-factors were 1.00 and 1.97, consistent with theory.

Even though the trap detected by I-V-T and DLTS could not be seen deeper in the base, the leakage current produced in the depletion region of this cell degrades the cell performance because the J_{o1} and J_{o2} components are nearly equal at the cell operating point (~1 volt), Figure 6. Since the J_{o2} component at the operating point represents the current that does not make it to the load, performance of this particular cell can be appreciably improved by eliminating the E_v + 0.912 eV trap.

Computer Modeling

To test the experimental data and the validity of the above analyses, the solar cell was modeled with the help of two computer programs, one of which calculates the cell parameters V_{oc}, J_{sc}, efficiency, and spectral response, and the other which calculates an effective recombination velocity anywhere within the structure.

The PC-1D model, described elsewhere (13), was used first to model the spectral response. A net base lifetime of 8 ns with a front surface recombination velocity of 1.25 E5 cm/s was required to obtain a good match between the model calculations and the experimental data, Figure 7. Back surface passivation was found to have negligible effect on the spectral response. The emitter and buffer lifetimes were determined from the SRH lifetime in the base which was calculated from

$$\frac{1}{\tau} = \frac{1}{\tau_{srh}} + BN + CN^2 \qquad (15)$$

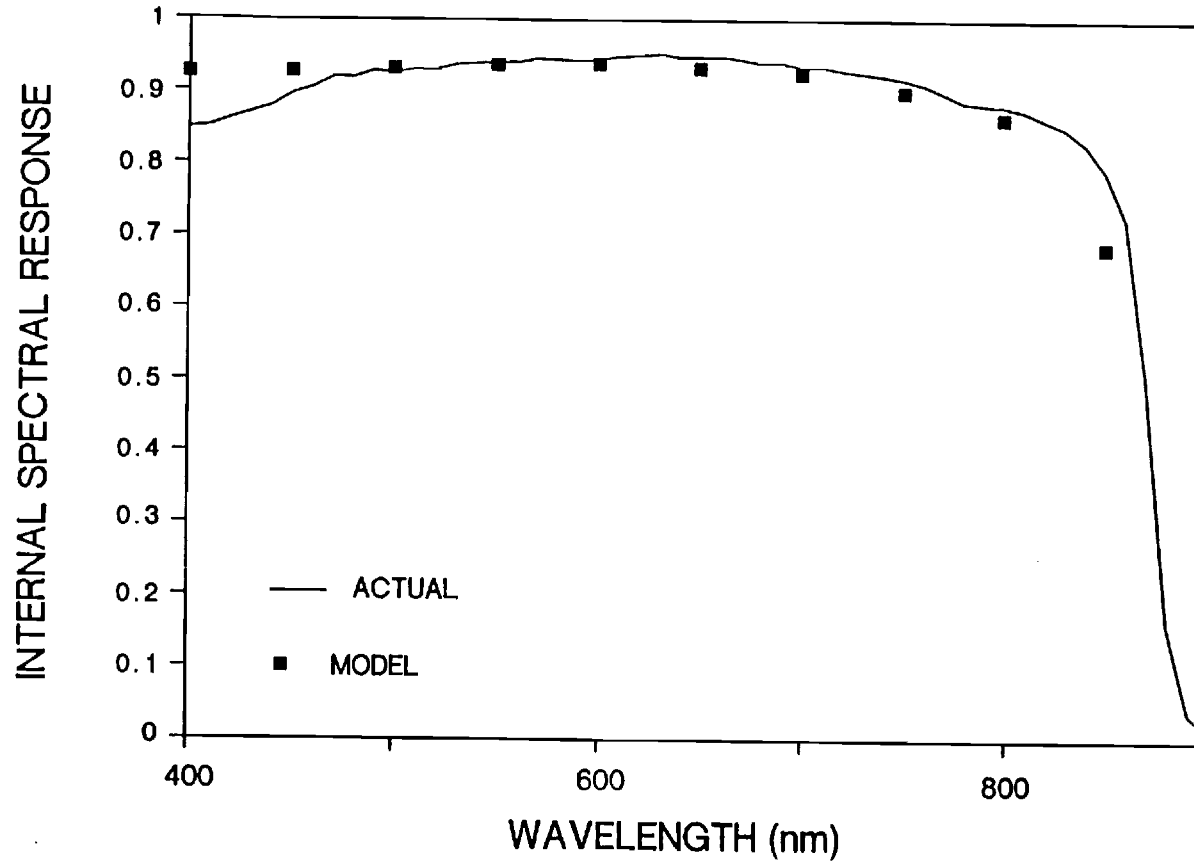

Figure 7. Comparison of actual spectral response (solid line) with modeled spectral response (blocks) as calculated from PC-1D for the given device structure.

where B is the radiative recombination coefficient and C is the Auger recombination coefficient for GaAs. Using B = 2.5 E - 11 cm^3 [14], C = 1.60 E - 29 cmI.^{6} [15], and τ_B = 8 ns in the base, we obtain τ_{srh} = 8.33 ns. Assuming defect dominated τ_{srh} to be constant throughout the device, equation (15) gave emitter and buffer lifetimes of 2.08 ns and 5.49 ns, respectively, by substituting the proper values for B and C in each region.

The numerical values of the spectral response, Figure 7, were found from the calculated J_{sc} and measured reflectivity as a function of wavelength using the AM1.5 energy content of the incident radiation. A shadow loss of 5% was used for the modeling. Figure 7 shows a good match between the calculated and measured values with only a slight difference in the short and long wavelengths. The lower measured response in the short wavelength, seen in Figure 7, can be attributed to absorption in the AlGaAs passivation layer which is not considered in the model. The AlGaAs acts to decrease the photon flux incident on the GaAs at the shorter wavelengths until the absorption edge of the AlGaAs at ~2 eV is reached. At long wavelengths (850 nm), the simulated response is somewhat lower than the actual probably because the increase in absorption coefficient due to doping near the band edge [16] is not included in the PC-1D model. This additional absorption allows more photons to be absorbed closer to the collecting junction and hence increase J_{sc} at these long wavelengths due to an increase in collection probability.

In order to test the estimated lifetime profile (τ_e, τ_b, τ_{buff}) and recombination velocities, an effective recombination velocity (S_e) model was used to calculate the reverse leakage current. S_e is a measure of the minority carrier losses in the various regions of the device which directly

provides the reverse saturation current density (J_{o1}). This model, which is described in detail elsewhere for silicon cell design and analysis [17], includes the effects of bandgap narrowing, Auger and radiative recombination, and recombination at surfaces and interfaces. The internal recombination velocity S_e throughout the cell can be calculated using the front surface recombination velocity at the emitter/AlGaAs interface, FSRV, the back surface recombination velocity at the back of the buffer layer, BSRV, the diffusion length, doping profile, and cell dimensions as input parameters. Each region of the cell (buffer, base, and emitter) is subdivided into a number of elements, all of the same width. S_e is calculated iteratively from FSRV and BSRV until the p-n junction edge is reached on each side. The recombination velocity S_{e2} at one boundary of any element is calculated in terms of velocity S_{e1} at the other boundary by

$$S_{e2} = \frac{N_2}{N_1} \frac{D}{L} \left[\frac{S_{e1} \frac{D}{L} + \tanh(\frac{W}{L})}{1 + S_{e1} \frac{D}{L} \tanh(\frac{W}{L})}\right] \exp\left[\frac{\Delta E_{g2} - \Delta E_{g1}}{kT}\right] \qquad (16)$$

where

W = element width

D,L = diffusion coefficient and diffusion length of minority carriers within the element

$N_{1,2}$ = doping densities at boundaries of element

ΔE_{g1}, ΔE_{g2} = bandgap narrowing due to doping densities N_1 and N_2.

The base and emitter components of the leakage current can then be determined from

$$J_{OB} = \frac{qn_i^2}{N_D} \cdot S_{ejb} \qquad (17)$$

and

$$J_{0E} = \frac{qn_i^2}{N_A} \cdot S_{eje} \tag{18}$$

where S_{ejb} and S_{eje} are the recombination velocities at the base edge and emitter edge of the p-n junction, respectively.

Figure 8 shows a plot of S_e versus depth for the GaAs heteroface cell for various values of FSRV and BSRV which support the spectral response conclusion that back-surface passivation has little or no effect on J_{0B} in this cell. The model calculations reveal that recombination velocity at the base side of the p-n junction is pinned so that $J_{0B} = \sim 0.85 + 10^{-19}$ A/cm^2 for all values of back surface recombination velocity. For FSRV = 1.25 X 10^5cm/s and τ_e = 2.08 ns, which gave the best match for the spectral response, the S_e-model gives J_{0E} = 0.55 X 10^{-19}A/cm^2 so that the simulated $J_{o1} = J_{0E}$ X J_{0B} = 1.40 + 10^{-19} A/cm^2. This is in good agreement with the measured J_{o1} of 1.29 X 10^{-19} A/cm^2. This supports the selection of FSRV and lifetime for the simulated spectral response and indicates that J_{o1} or V_{oc} of this cell is limited by both the base and emitter with the emitter contributing ~ 33% of J_{o1}.

A few more revealing observations can be made from Figure 8. Contrary to the back surface, front surface passivation is critical for this cell because an FSRV of 1 X 10^7cm/s, which is typical of the free GaAs surface, results in a large increase in J_{0E} and hence a lower V_{oc}. However, the AlGaAs passivation needs to limit FSRV only to ~1 X 10^4cm/s since in this cell FSRV below this value has very little impact on S_{eje} or J_{0E} as seen in Figure 8. Note also from this figure that the design rule for the emitter changes with the magnitude of FSRV. For devices with any reasonable amount of surface passivation a lower J_{0E} is accomplished by thinning the emitter, but for unpassivated surfaces, emitter thinning would actually increase J_{0E}. Thus, the AlGaAs passivation is most critical for thin emitters.

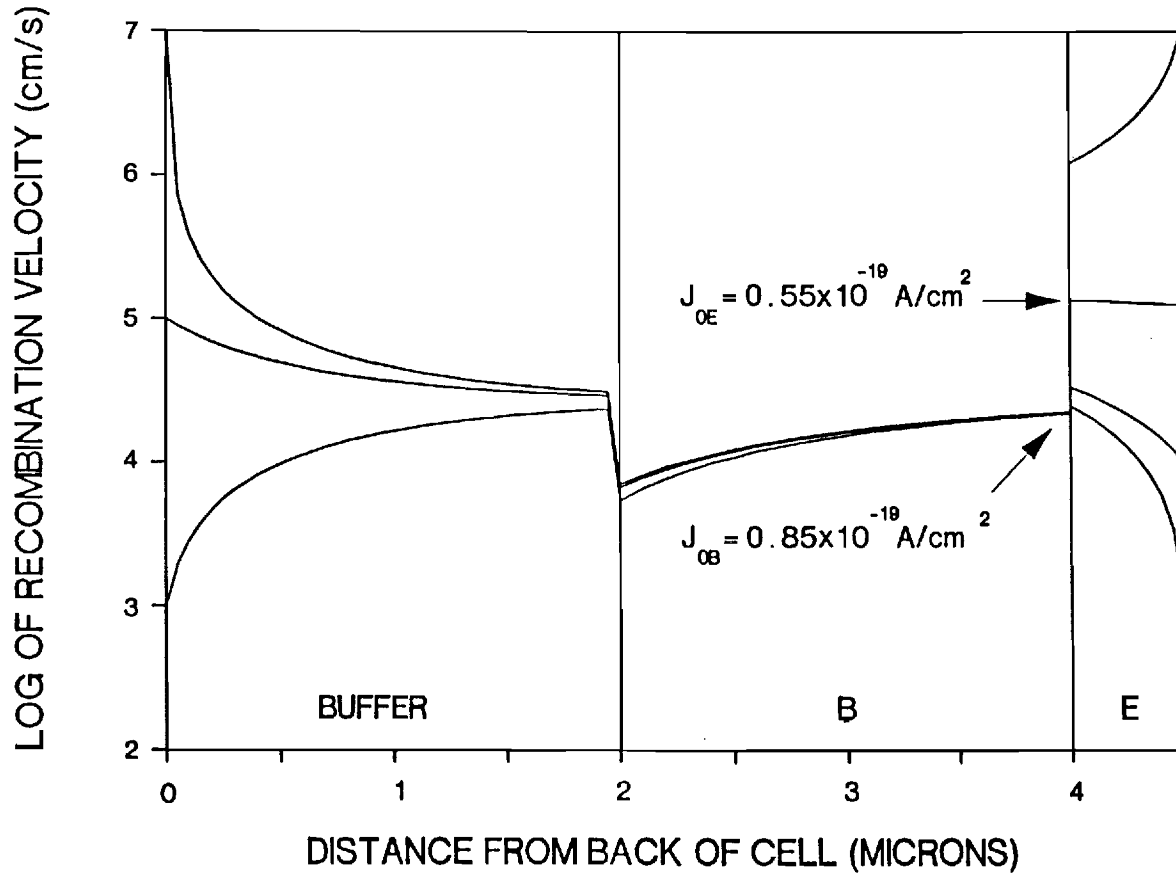

Figure 8. Plot of effective recombination velocity, S_e, for various values of front and back surface recombination velocities. Emitter and base leakage current components are indicated for the cell-matching S_e plot.

As a final confirmation of the lifetime profile and the S values derived above, the cell J_{sc}, V_{oc}, and efficiency were calculated using PC-ID. Table 1 shows a very good agreement between the measured and modeled values confirming the validity of the above procedure. Having established the match, the PC-1D model was used to provide guidelines for improving the efficiency of this cell and to optimize the p-n heteroface cell design. Model calculations in Table 1 show that a significant improvement in cell efficiency (23%) can be realized by properly passivating the front surface of this cell so that the FSRV = 1 + 10^4cm/s. Only a slight improvement is found by back surface passivation for the lifetime profile of this device structure. However, if the effective base lifetime can be improved to 15 ns the efficiency of this cell can reach ~24.17% with passivated front and back surfaces. This improvement is clearly understood upon inspection of Figure 9 which shows that longer lifetimes decrease the magnitudes of S_{eje} and S_{ejb} resulting in higher V_{oc}, in additon to raising J_{sc} via reduced recombination throughout the device. Further gain in efficiency can be obtained by optimizing the thickness and doping profile of the device. Since in n-type GaAs the net lifetime is dominated by defects up to a doping level of ~1 X 10^{18} cm^{-3} [7], an efficiency of ~24.40% can be obtained simply by changing the base doping to 5 X $10^{17}cm^{-3}$ and the buffer doping to 2.5 X $10^{18}cm^{-3}$. These doping levels represent the optimum trade-off between an increase in V_{oc} due to the heavier base doping and a decrease in J_{sc} resulting from higher S_e in the base due to a reduced doping discontinuity (N_1/N_2) at the buffer/base interface. It should be recognized that these calculations are easily deduced from S_e-plots which signify the importance of such analysis. The cell efficiency tends to saturate near the 24.40% level unless the base material quality is improved

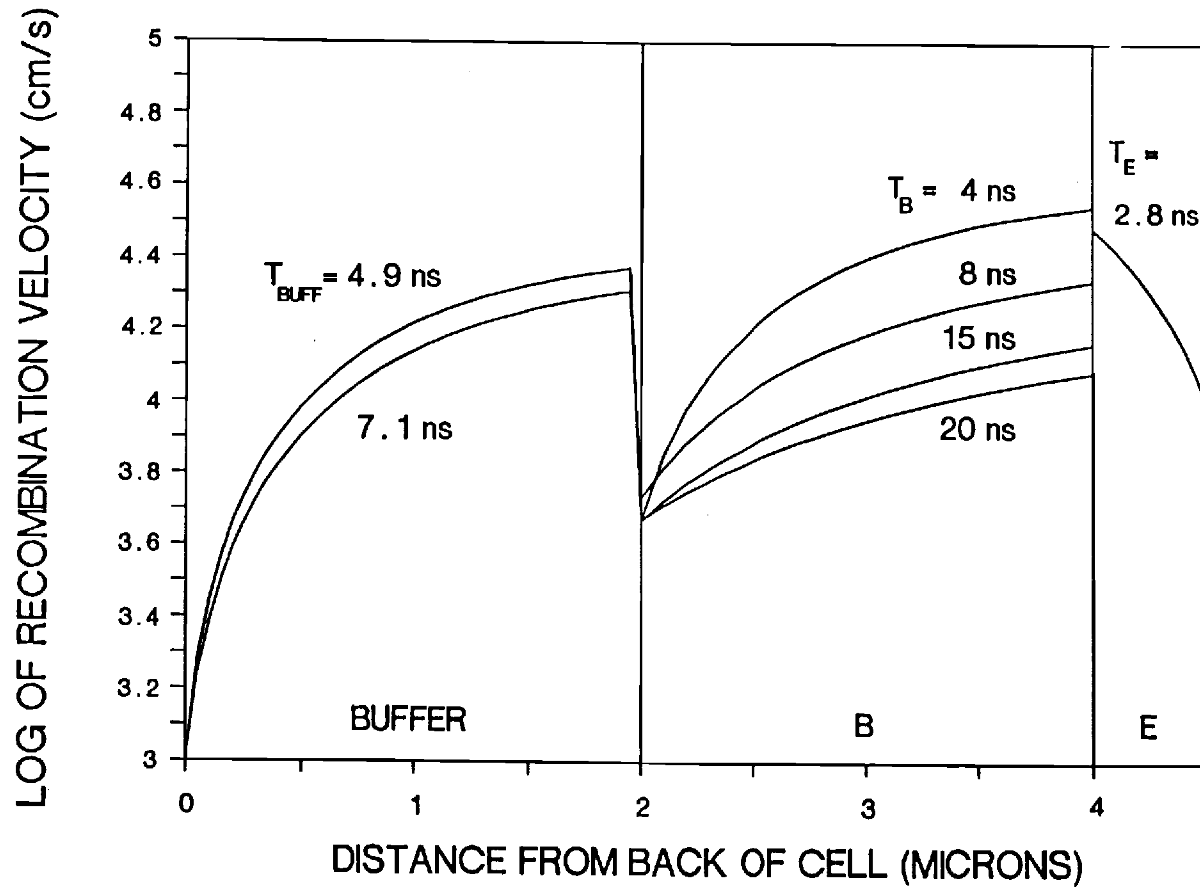

Figure 9. Plot of effective recombination velocity, S_e, showing the influence of minority carrier lifetime on recombination throughout the device. The net lifetimes in each layer are indicated.

further. Table 1 shows an efficiency of 24.76% can be obtained with a lifetime of 20 ns, which is still well below the intrinsic lifetime limit of GaAs at a doing level of 5 X $10^{17}cm^{-3}$. This represents the highest efficiency found for our simulations of this particular p-n heteroface structure.

Further optimization is possible only by modifying the device structure. Table 1 shows that a 24.74% efficient cell can be achieved with only a 15 ns base lifetime by thinning the base to 1.2 um. This improvement comes as a result of the trade-off between low S_e in the base and increased photon absorption in the buffer. For this device structure, it is necessary to have a passivated back surface and reasonable lifetime in the buffer. The doping and thickness of the base and buffer layers become critical to the performance of such a device since there exists a sensitive trade-off between greatly increased carrier collection in the thinned based due to reduced recombination in the base resulting from the proximity of the base/buffer interface to the collecting junction, and the amount of carriers generated in the buffer layer that do not make it to the p-n junction. The V_{oc} is greatly increased due to the lower S_{ejb} while the J_{sc} benefits from the higher collection efficiency of photogenerated carriers in the thin base. Model calculations in Table 1 indicate efficiencies as high as ~25.04% are possible for a device with a base width of 1.2 um, buffer thickness of 1.3 um, base doping of 6 X $10^{17}cm^{-3}$, buffer doping of 2.5 X $10^{18}cm^{-3}$, base lifetime of 20 ns, FSRV = 1 X 10^4cm/s and BSRV = 1 X 10^3cm/s. It should be noted that the buffer thickness now becomes important since the effectiveness of the back surface passivation would be reduced if the buffer were too thick. In essence, the buffer here acts as part of a two-step base layer which suggests that further gains in efficiency can be realized by multi-step or even graded base regions.

Table 1: Guideline for cell optimization using PC-1D and effective recombination velocity modeling. Actual cell data and best match are shown. Cells 6 and 7 (starred entries) are thinnned base and buffer structures.

cell ID	N_d (cm^{-3})	N_a (cm^{-3})	N_b (cm^{-3})	FSRV (cm/s)	BSRV (cm/s)	T_b (ns)	V_{oc} (Volts)	J_{sc} (A/cm^2)	Eff
actual	2×10^{17}	2×10^{18}	2×10^{18}				1.013	24.5	21.2
match	2×10^{17}	2×10^{18}	2×10^{18}	1.25E5	1.0E6	8	1.01	24.56	21.39
1	2×10^{17}	2×10^{18}	2×10^{18}	1.0E4	1.0E6	8	1.016	26.59	23.02
2	2×10^{17}	2×10^{18}	2×10^{18}	1.0E4	1.0E4	8	1.017	26.71	23.13
3	2×10^{17}	2×10^{18}	2×10^{18}	1.0E4	1.0E4	15	1.032	27.11	24.17
4	5×10^{17}	2×10^{18}	2.5E18	1.0E4	1.0E4	15	1.048	26.83	24.40
5	5×10^{17}	2×10^{18}	2.5E18	1.0E4	1.0E4	20	1.054	26.95	24.76
6*	6×10^{17}	2×10^{18}	2.5E18	1.0E4	1.0E3	15	1.055	27.04	24.74
7*	6×10^{17}	2×10^{18}	2.5E18	1.0E4	1.0E3	20	1.0596	27.10	25.04

REFERENCES

1. R. J. Nelson and R. G. Sobers, "Minority-carrier lifetime and internal quantum efficiency of surface-free GaAs," Appl. Phys., vol. 49, no. 12, pp. 6103-6108, 1978.

2. C. J. Hwang, "Doping dependence of hole lifetime in n-type GaAs," J. Appl. Phys., vol. 42, no. 11, pp. 4408-4413, 1971.

3. R. J. Nelson, "Interfacial recombination in GaAlAs-GaAs heterostructures," J. Vac. Sci. Technol., vol. 15, no. 4, pp. 1475-1477, 1978.

4. P. Dawson and K. Woodbridge, "Effects of prelayers on minority-carrier lifetime in GaAs/AlGaAs double heterostructures grown by molecular beam epitaxy," Appl. Phys. Lett., vol. 45, no. 11, pp. 1227-1229, 1984.

5. J. M. Woodall and J. L. Freeouf, J. Vac. Sci. Technol., vol. 19, p. 794, 1981.

6. P. D. DeMoulin, C. S. Kyono, M. S. Lundstrom, and M. R. Melloch, "Dark I/V characterization of GaAs p.n heteroface cells, Proc. of Nineteenth IEEE Photovoltaic Specialits Conf., pp. 93-97, 1987.

7. P. D. DeMoulin and M. S. Lundstrom, "Theoretical comparison of conventional and unconventional GaAs cell design," Proc. of Nineteenth Photovoltaic Specialists Conf., pp. 925-930, 1987.

8. M. S. Lundstrom, "Device physics of crystalline solar cells," presented at Eight Photovoltaic Advanced Res. Dev. Project Rev. Meeting, Nov. 1987.

9. P. Blood, "Measurement of optical absorption in epitaxial semiconductor layers by a photovoltage method," J. Appl. Phys., vol. 58, no. 6, pp. 2288-2295, 1985.

10. D. K. Schroder, "The concept of generation and recombination lifetimes in semiconductors," IEEE Trans. Electron. Dev., vol. ED-29, no. 8, pp. 1336-1338, 1982.

11. K. W. Loh, D. K. Schroder, R. C. Clarke, A. Rohatgi, and G. W. Eldridge, "Low leakage current GaAs diodes," IEEE Trans. Electron Dev., vol. ED-28, no. 7, pp. 796-800, 1981.

12. A. S. Grove, "Physics and technology of semiconductor devices," Wiley, New York, 1967.

13. D. Rover, P. Basore, and G. Thorson, "Solar cell modeling on personal computers," Conf. Proc. of the Eighteenth Photovoltaic Spec. Conf., Las Vegas, Oct. 1985.

14. C. J. Hwang, Phys. Rev. B., vol. 6, pp. 1355-1359, 1972.

15. A. Haug, "Auger recombination in direct-gap semiconductors: band structure effects," J. Phys. C: Solid State Phys., vol. 16, pp. 4159-4172, 1983.

16. J. S. Blakemore, "Semiconducting and other major properties of gallium arsenide," J. Appl. Phys., vol. 53, no. 10, pp. R123-R181, 1982.

17. A. Rohatgi and P. Rai-Choudhury, "Design, fabrication and analysis of 17-18 percent efficient surface-passivated silicon solar cells," IEEE Trans. Electron Dev., vol. ED-31, no. 5, pp. 596-601, 1984.

ACKNOWLEDGEMENTS

The authors would like to thank Steve Tobin of Spire Corporation and Bob Loo of Hughes Research Labs. for their helpful discussions and samples, and Jim Welch of Georgia Tech, MRC, for assistance in the computer modeling, A. B. Dewald and Robert Frost for PAS measurements and analysis, B. Neilson and K. G. Lynn of Brookhaven National Labs for the help in SPAS measurements, and James Gee of Sandia Labs for the valuable discussions and help in arranging the samples.

E-21-603

RESEARCH ON ALGaAs/GaAs INTERFACES IN GaAs SOLAR CELLS

A. Rohatgi and S. A. Ringel

Draft of Final Report for the Period

October 28, 1986 - February 28, 1988

Sandia National Laboratories

Contract No. 02-2255

GEORGIA INSTITUTE OF TECHNOLOGY
School of Electrical Engineering
Atlanta, GA 30332

TABLE OF CONTENTS

	Page
1. INTRODUCTION	1
2. TECHNICAL PROGRESS	2
2.1 Electrical Characterization, Modeling, and Optimization of High Efficiency GaAs Solar Cells	2
2.11 Introduction	2
2.12 Experimental Methods	3
2.12(a) Device Structure	3
2.12(b) Depth-Resolved SPV/C-V Measurements	5
2.12(c) DCTS Studies	5
2.12(d) I-V-T Analysis	6
2.12(e) Transformed I-V Analysis	9
2.13 Results and Discussion	9
2.14 Computer Modeling	16
2.2 Positron Annihilation Spectroscopy of AlGaAs/GaAs Interfaces in MOCVD-Grown Heterojunction Solar Cells	27
2.21 Introduction	27
2.22 Experiment	28
2.23 SPAS Modeling	30
2.24 Results and Discussion	33
2.3 Measurements and Analyses on Additional Device Structures	43
2.31 LPE-Grown GaAs Heteroface Solar Cells	43
2.32 LPE-Grown AlGaAs Layers on GaAs	43
3. CONCLUSIONS	48
4. REFERENCES	50
5. ACKNOWLEDGEMENTS	52

LIST OF FIGURES

Figure		Page
Figure 1.	Device structure and measured cell data of the MOCVD GaAs heteroface cell used in this study...............	4
Figure 2.	Variation of SPV repsonse as the device is etched through. The measurements were taken at etch depths of (a) 0.12 um, (b) 0.17 um, (c) 0.21 um, (d) 0.3 um, and (e) 0.42 um..	11
Figure 3.	Ratios between SPV spectra taken at: (a) front of emitter; (b) just before p-n junction; (c) just after p-n junction; (d) 0.1 um after curve (c)..............	12
Figure 4.	DLTS scan and activation energy plot indicating the presence of a hole trap in the n-type base depletion region..	14
Figure 5.	LN(J) vs. T plot measured at 2 volts constant reverse bias. Trap activation energy is shown in the figure..	15
Figure 6.	Transformed I-V characteristic for cell. J_1 (diffusion) and J_2 (space charge) current density components are indicated...........................	17
Figure 7.	Comparison of actual spectral response (solid line) with modeled spectral response (blocks) as calculated from PC-ID for the the given device structure...	18
Figure 8.	Plot of effective recombination velocity, S_e for various values of front and back surface recombination velocities. Emitter and base leakage current components are indicated for the cell-matching S_e plot....................................	22
Figure 9.	Plot of effective recombination velocity, S_e, showing the influence of minority carrier lifetime on recombination throughout the device. The net lifetimes in each layer are indicated......................	25
Figure 10.	Example of a deconvoluted characteristic lineshape parameter as a function of the material layer for each layer incorporating the superposition of the layer contributions, S_i, (solid lines) and the local defect contributions, S_d (dashed lines)..............	32

Figure 11. Lineshape parameter, S(E), as a function of incident energy, E, for MOCVD Runs (a) #872A and (b) #872B. Experimental data connected by triangles. Theoretical approximations to the experimental data (with and without defects) are shown by the smooth solid curves.. 34

Figure 12. SPV spectrum ratios as a function of wavelength taken at etch depths of (a) .22/.21 microns, (b) .28/.22 microns, and (c) .32/.28 microns.................... 38

Figure 13. Lineshape parameter, S(E), as a function of incident energy, E, for MOCVD Run #1053 averaged over two profiles of the same specimen.............................. 42

Figure 14. Hughes Mesa Diode Structure used for DLTS Measurements.. 44

Figure 15. DLTS Spectrum for Hughes Mesa diode (a) and associated Arrhenius plot (b) for deep level................ 45

Figure 16. Photovoltage spectra fro x = 0.20 and x = 0.38 $Al_xGa_{1-x}As$.. 46

Figure 17. Dopant profiles as determined by the Polaron PN4200 Electrochemical Profiler for (a) x = 0.20 and (b) x = 0.38 AlGaAs.................................. 47

LIST OF TABLES

Table | Page

Table 1. Guideline for cell optimization using PC-1D and effective recombination velocity modeling. Actual cell data and best match are shown. Cells 6 and 7 (starred entries) are thinned base and buffer structures.. 24

Table 2. Solar cell heterojunction structures........................ 29

1. INTRODUCTION

GaAs solar cells have been fabricated with efficiencies of 22% at one-sun and 26% under concentration, which are comparable to the best silicon cell efficiencies reported. However, very little is understood about the internal recombination mechanisms in III-V solar cells. For instance, peak internal quantum efficiencies in the best GaAs cells are only around 95% and decrease in the short wavelength part of the spectrum. High efficiency silicon cells have demonstrated internal quantum efficiencies near 100% over the entire useable spectrum. Identification of the internal recombination mechanisms in GaAs cells is necessary for further improvements in GaAs technology.

The objective of this research is to improve the basic understanding of internal loss mechanisms in GaAs solar cells, particularly their origin and ultimate influence on design criteria. The development of characterization techniques coupled with computer modeling was found essential to achieve the goal. A methodology consisting of electrical characterization, nondestructive defect profiling (SPAS), and computer modeling which allows the determination of internal loss mechanisms in an MOCVD grown GaAs p-n heteroface solar cell is presented. Parameters of particular interest are minority carrier lifetimes, bulk and interfacial recombination velocities, and deep levels. The cell performance is evaluated on the basis of these internal recombination parameters through extensive computer modeling. Device modeling is also used to show how a complete understanding of lifetime limiting mechanisms in GaAs coupled with clever cell design can result in cell efficiencies in excess of 25%.

2. TECHNICAL PROGRESS

2.1 Characterization, Modeling, and Optimization of High Efficiency GaAs Solar Cells

2.11 Introduction

As the conversion efficiencies of GaAs solar cells continue to increase, the ability to detect, analyze, and assess the importance of defects and other lifetime limiting mechanisms become critical to advance cell performance further. Most research to date has been devoted to the study of topics such as recombination centers in bulk GaAs [1,2] and at surfaces and interfaces using specialized test structures in which the interplay of interfacial effects with bulk properties such as minority carrier lifetime is not obvious [3-5]. Hence it is important to develop measurement techniques in conjunction with device modeling to separate those material parameters that dictate the performance of solar cells and other GaAs devices in which the carrier transport mechanisms are not well understood. Recently, a few attempts have been made to address this issue for GaAs solar cells [6-8].

This paper presents a combination of an electronic characterization methodology and device modeling to improve solar cell design by detecting and evaluating important material parameters such as lifetime, interface recombination velocity, and deep levels within a state-of-the-art MOCVD grown GaAs p-n heteroface solar cell. First, a number of standard semiconductor characterization techniques, such as DLTS (Deep Level Transient Spectroscopy) and dark I-V (current-voltage) and I-V-T were used to determine the carrier recombination and generation lifetimes separately. Then dopant profile and depth-

resolved surface photovoltage measurements were performed with the help of an electrochemical etching profiler to provide necessary inputs to the device modeling programs used in this investigation. A combination of a one dimensional computer model and the experimental data obtained through the above techniques was used to reveal the variation in the effective recombination velocity (S_e) throughout the device. S_e is indicative of net recombination anywhere within the device and can be used to guide the optimization of high efficiency cell design. A second device modeling program (PC-1D) was used to calculate cell parameters J_{sc}, V_{oc}, and efficiency along with the spectral response of the cell. The calculated values were correlated with the measured cell data to assess the accuracy of the characterization methodology to analyze the lifetime limiting mechanisms in the bulk and interfaces of GaAs structures. Finally, improved understanding of the loss mechanisms coupled with device modeling was used to provide guidelines for attaining GaAs cell efficiencies approaching 25% under AM1.5 conditions.

2.12 Experimental Methods

2.12(a) Device Structure

Figure 1 shows the device structure of the MOCVD grown GaAs heteroface solar cell used in this study, along with the measured cell data. The GaAs layers were grown at 700°C using trimethyl gallium and arsine as reactants. The AlGaAs was grown at 800°C using trimethyl aluminum for the Al source. The mole fraction of Al in the AlGaAs window layer was 0.90. Zn and Si were the p-type and n-type dopants, respectively, used throughout the structure.

For DLTS, I-V and I-V-T measurements, 50 mil diameter mesa dots were formed by evaporating Au/Zn ohmic contacts on the structure. The back surface

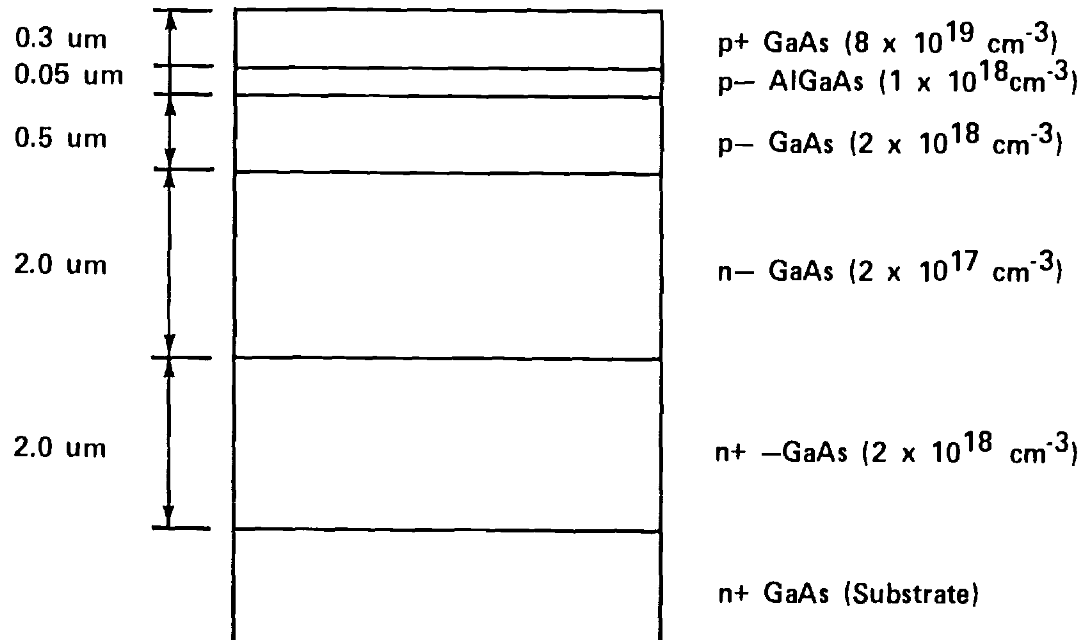

GaAs solar cell structure used in these experiments

V_{oc} = 1.013V J_{sc} = 24.5 mA/cm^2

F.F. = 0.867 Eff = 21.2%

Figure 1. Device structure and measured cell data of the MOCVD GaAs heteroface cell used in this study.

was covered with evaporated Au/Zn ohmic contacts to facilitate the electrical measurements.

2.12(b) Depth-Resolved SPV/C-V Measurements

Attempts were made to determine the carrier concentration profile and the spatial variation in the electro-optical response of the cell using a depth-resolved C-V and surface photovoltage (SPV) measurement. Both these measurements were performed in an automated electrochemical etching profiler in which an electrolyte is used to perform precise step-by-step etching coupled with I-V, C-V, and SPV measurements after each step [9]. A Schottky barrier formed between the electrolyte and the semiconductor facilitates both C-V and SPV measurements. The doping concentration is found from the C-V data at each depth. SPV measurements were performed in the wavelength range of 400 to 900 nm to accomodate both the GaAs and AlGaAs absorption edges. The SPV signal is measured at the surface under open circuit conditions to avoid electrochemical etching or deposition during the measurement. The choice of electrolyte is dictated by the properties of the semiconductor. For this study, a solution of 0.2 M NaOH + 0.1M EDTA (ethylenediamminetetraacetic acid) was found to be an adequate electrolyte for Schottky barrier formation and electrochemical etching and showed no signs of surface degradation.

2.12(c) DLTS Studies

A combination of DLTS and I-V-T measurements was used to determine the trap which controls the leakage current of the solar cell. The DLTS technique reveals all the detectable traps, regardless of their influence on the leakage current. DLTS measurements were made using an automated wafer analyzer system

which obtains data via a modified lock-in amplifier type DLTS setup. Nonuniformity in deep level distribution near the p-n junction of the solar cell was investigated by varying the steady reverse bias level from -5 volts to -1 volt but keeping the sum of the reverse bias and forward bias pulse height constant at -0.5 volts. In this way, the edge of the depletion region is steadily stepped toward the metallurgical junction as the reverse bias is decreased and a spatial trap profile of the depletion region is obtained. DLTS measurements were also performed in a forward bias mode (the sum of the steady reverse bias and the injection pulse height > the built-in voltage of the p-n junction) to detect both majority and minority carrier traps in the depletion region. It should be noted that the detection limit of our DLTS set-up is about 0.01% of the background doping concentration and hence defects with concentrations of less than 2×10^{13} cm^{-3} in the base region will not be detected.

2.12(d) I-V-T Analysis

The I-V-T technique, in contrast to DLTS, identifies only the activation energy of that deep level which limits the reverse leakage current as well as the generation/recombination lifetimes associated with it [10,11]. In addition, it does not suffer from the same doping dependent detection limit as DLTS, allowing information to be extracted from heavily doped device structures provided the trap is the dominant source of leakage. The carriers decay back to their equilibrium concentration by recombining at the deep level after an injection process. The generation lifetime associated with a deep level, τ_g, is the inverse of the decay process and becomes important where carrier concentration is low, such as the depletion region of a p-n junction.

The method is based on the assumption that the total reverse leakage current, J_o, is dominated by the space charge generation current, J_{o2}, and the diffusion component, J_{o1}, can be neglected under reverse bias. This is routinely observed in GaAs. From SRH (Schockly-Read-Hall) theory, the total carrier recombination rate, R, under steady state conditions is given by

$$R = \frac{np - n_i^2}{\tau_{po}(n + n_1) + \tau_{no}(p + p_1)} \tag{1}$$

where

$$\tau_{po} = (\sigma_p N_T v_{TH})^{-1} \tag{2}$$

$$\tau_{no} = (\sigma_n N_T v_{TH})^{-1} \tag{3}$$

$$n_1 = n_i \exp[\frac{(E_t - E_i)}{kT}] \tag{4}$$

$$p_1 = n_i \exp[\frac{-(E_t - E_i)}{kT}] \tag{5}$$

Under reverse bias conditions the excess carrier concentration in the space charge region can be neglected so that equation (1) reduces to

$$R = -n_i/\tau_g \tag{6}$$

with

$$\tau_g = \tau_{po} \exp[\frac{(E_t - E_i)}{kT}] + \tau_{no} \exp[\frac{-(E_t - E_i)}{kT}] \tag{7}$$

where E_t is the energy level of the recombination center within the bandgap and E_i is the position of the intrinsic Fermi level. If the capture cross section for holes (σ_p) and electrons (σ_n) are comparable then τ_g reduces to

$$\tau_g = \tau_{po} \exp\left[\frac{(E_t - E_i)}{kT}\right] \qquad \text{for } E_t > E_i \tag{8}$$

or

$$\tau_g = \tau_{no} \exp\left[\frac{-(E_t - E_i)}{kT}\right] \qquad \text{fpr } E_t < E_i \tag{9}$$

but more generally,

$$\tau_g = \tau_r \exp\left[\frac{(E_t - E_i)}{kT}\right] \tag{10}$$

Using the definition of leakage current in a reverse-biased diode [12] and recalling the assumption which neglects the J_{o1} component of J_o,

$$J_{rev} = J_{o2} = \frac{qn_i W}{\tau_g} \tag{11}$$

where W is the width of the depletion region, then

$$J_{o2} \propto \exp\left[\frac{-(E_t - E_v)}{kT}\right] \qquad \text{for } E_t > E_i \tag{12}$$

or

$$J_{o2} \propto \exp\left[\frac{-(E_c - E_t)}{kT}\right] \qquad \text{for } E_t < E_i \tag{13}$$

Hence, the activation energy of the generation center which controls the leakage current can be determined from the slope of the $\ln(J_{o2})$ vs. 1000/T plot under constant applied reverse bias. It is important to note that the I-V-T method gives an activation energy of the trap which controls the leakage current but it does reveal the band edge with respect to which that activation energy is measured, unless the trap location is known. Therefore, this method

must be supplemented by other measurements such as DLTS which gives all the traps present but does not reveal which one controls the leakage current.

2.12(e) Transformed I-V Analysis

The I-V characteristic of the mesa diode structure was measured in the dark and analyzed using an automated setup to separate the resistance, bulk and junction region effects. The I-V characteristic of a solar cell is a composite of two exponential functions including series and shunt resistance effects. The transformed I-V program first measures and subtracts the resistance effects from the measured data and then fits the rest to a double exponential equation given by

$$J = J_1 + J_2 = J_{o1}\left[\exp\left(\frac{qV}{kT}\right) - 1\right] + J_{o2}\left[\exp\left(\frac{qV}{nkT}\right) - 1\right] \qquad (14)$$

where J_{o1} and J_{o2} are the saturation current densities for the diffusion (n=1) and space charge generation (n) current components, respectively. The computer program fits the data and provides values of J_{o1} and J_{o2}.

2.13 Results and Discussion

The doping profile throughout the device structure, Figure 1, was confirmed by depth-resolved C-V measurements. Since the doping level in the AlGaAs window layer is similar to that of the emitter, the AlGaAs layer was not evident. Presence of the AlGaAs layer was confirmed by far infrared reflectance measurements which also revealed the mole fraction of Al to be 0.87, close to the target composition. The AlGaAs thickness was found to be 50 nm by reflectance measurements.

Spatial variations in the material properties were investigated by depth-resolved SPV measurements in an electrochemical profiler. Figure 2 shows photovoltage spectra taken at various etch depths. This data was not taken on the actual cell but on a piece adjacent to it, which has the p^+ GaAs cap layer intact. The initial (0.12-0.21 um) increase in the response with increasing etch depth is due to the successive removal of the heavily doped cap layer which has high absorption and recombination. The two humps at 560 nm and 720 nm are the characteristic response of the SPV optics. The etch depths at which these measurements were made are indicated in the figure. Both the overall shape and magnitude of SPV response are related to the properties of the material being probed. As we etch through the emitter region (0.21-0.42 um) the response gradually drops. This does not necessarily indicate defects or nonuniformity in the emitter region, but instead could be the result of enhanced competition from the p-n junction for the carriers generated within the emitter region. Notice that the overall open-circuit signal represents the spectrally resolved sum of the opposing photovoltages generated at the front electrolyte/GaAs Schottky barrier and at the p-n junction [9]. At present it is not known how to quantitatively account for the effect of the p-n junction influence on the measured response.

A qualitative picture of material uniformity can be obtained from spectrally resolved divisions of consecutive SPV spectra. Figure 3 shows a series of ratios taken while the device is being etched through the emitter. SPV ratio curve "a" indicates that a fraction of the carriers generated at longer wavelengths are either being lost to the p-n junction or to a defective layer near it since the ratio there is less than unity. The sign change in the SPV ratio curve "b" of Figure 3 taken just before the p-n interface, indicates

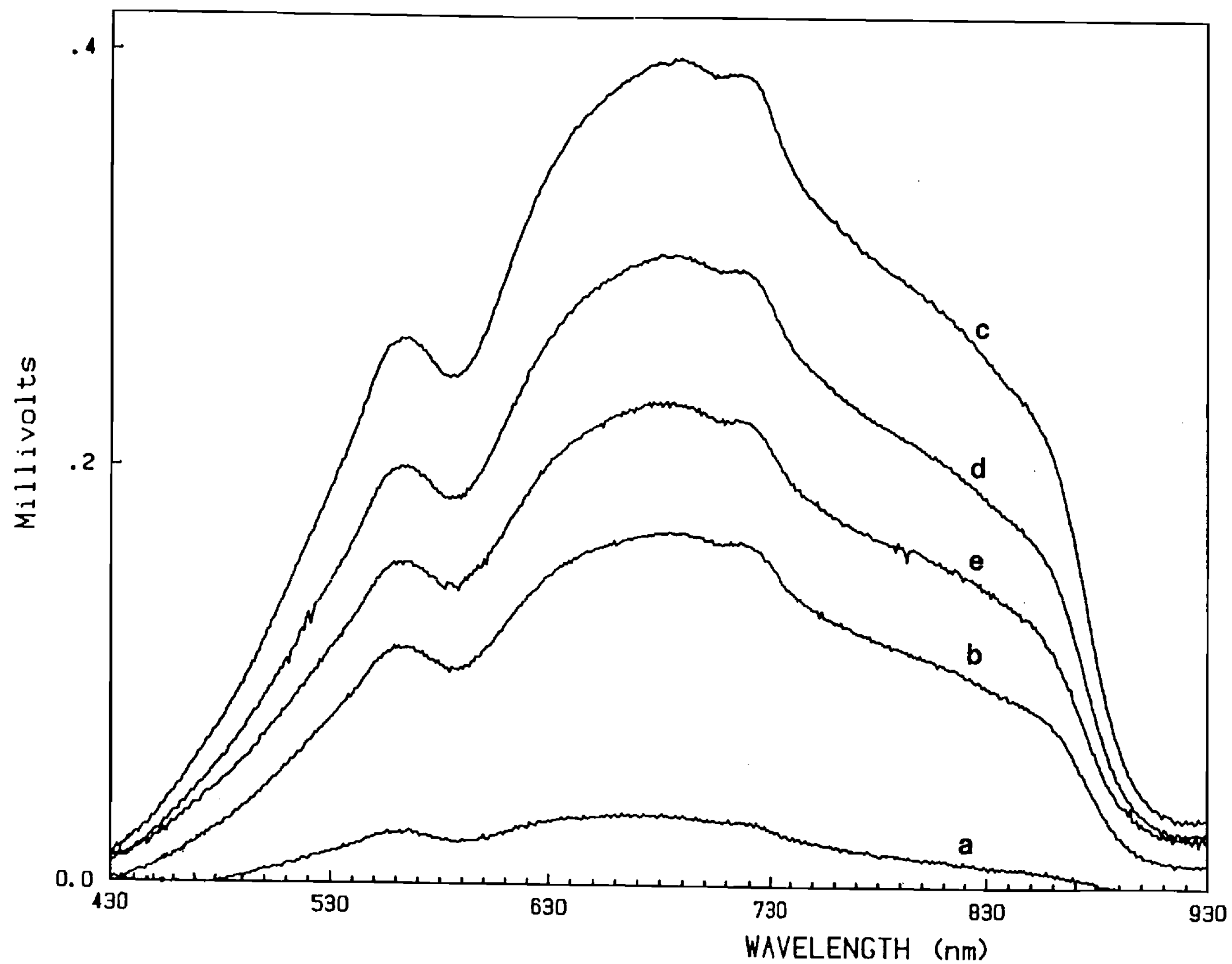

Figure 2. Variation of SPV response as the device is etched through. The measurements were taken at etch depths of (a) 0.12 um, (b) 0.17 um, (c) 0.21 um, (d) 0.3 um, and (e) 0.42 um.

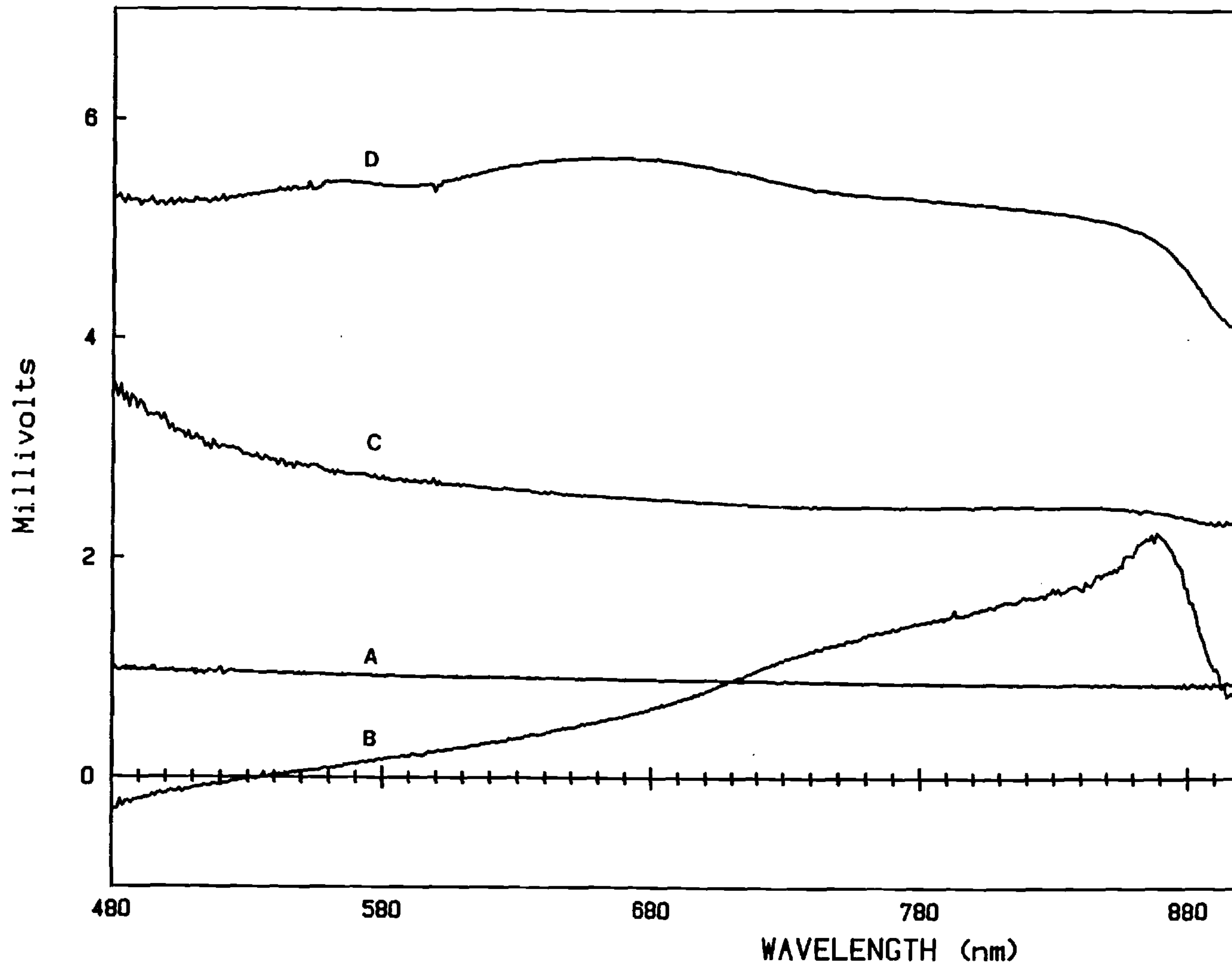

Figure 3. Ratios between SPV spectra taken at: (a) front of emitter; (b) just before p-n junction; (c) just after p-n junction; (d) 0.1 um after curve (c).

that for photons with wavelength greater than ~ 530 nm the p-n junction becomes the dominant carrier collecting junction. Up to this point, the effect of the presence of a defective region of material could be masked by the competition from the p-n junction. However, the SPV ratio curves"c" and "d", obtained by etching through the p-n junction and another slice 0.1 um later, respectively, do not suffer from this complication. The ratio curves c and d suggest that near the p-n junction, the material quality is improving in the base as we move away from the junction edge because the ratios are not only greater than one but gradually increase with depth, in spite of the constant base doping.

From the depth-resolved SPV measurements, it appears that the defect density may be increasing as we approach the p-n junction. To investigate this further, depth-resolved DLTS measurements were performed on the same wafer using the mesa structure described earlier. The DLTS primarily probes the n-base side of the p^+-n junction. Figure 4 shows that a deep level was detected only when the probed depletion region got close to the p-n interface. This minority carrier trap had an activation energy of E_V + 0.912 eV and a concentraton of 3.93 + $10^{14}cm^{-3}$. The fact that this level was not detected for wider depletion widths supports the nonuniform defect distribution seen by the SPV response near the p-n junction. The ln(J) vs T plot from the I-V-T measurement, Figure 5, gave an activation energy of E_a = 0.4523 eV for the J_{o2} component. Since the sum of the DLTS and I-V-T activation energies is close to the bandgap of GaAs (0.4523 + 0.912 = 1.36 eV), it is reasonable to conclude that the level detected by DLTS and I-V-T is the same and is also responsible for the excess leakage current.

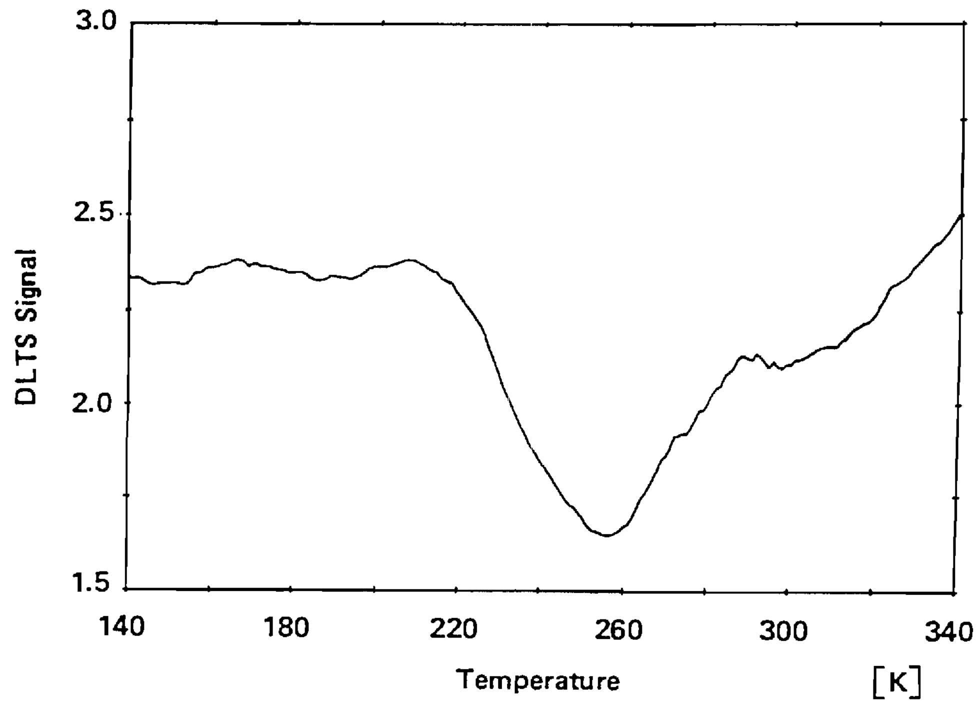

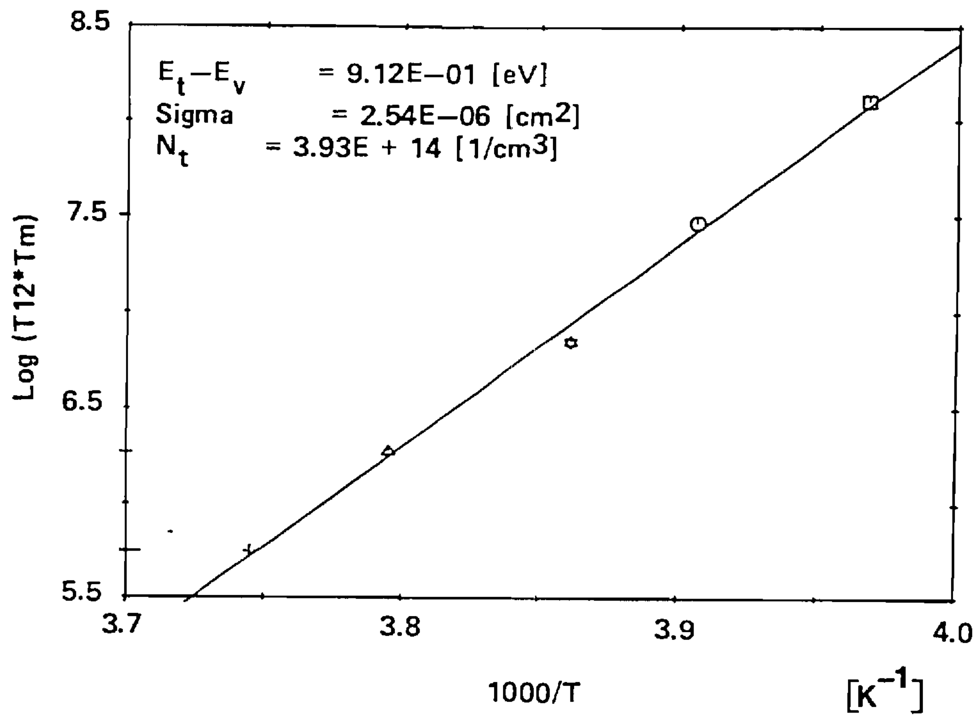

Figure 4. DLTS scan and activation energy plot indicating the presence of a hole trap in the n-type base depletion region.

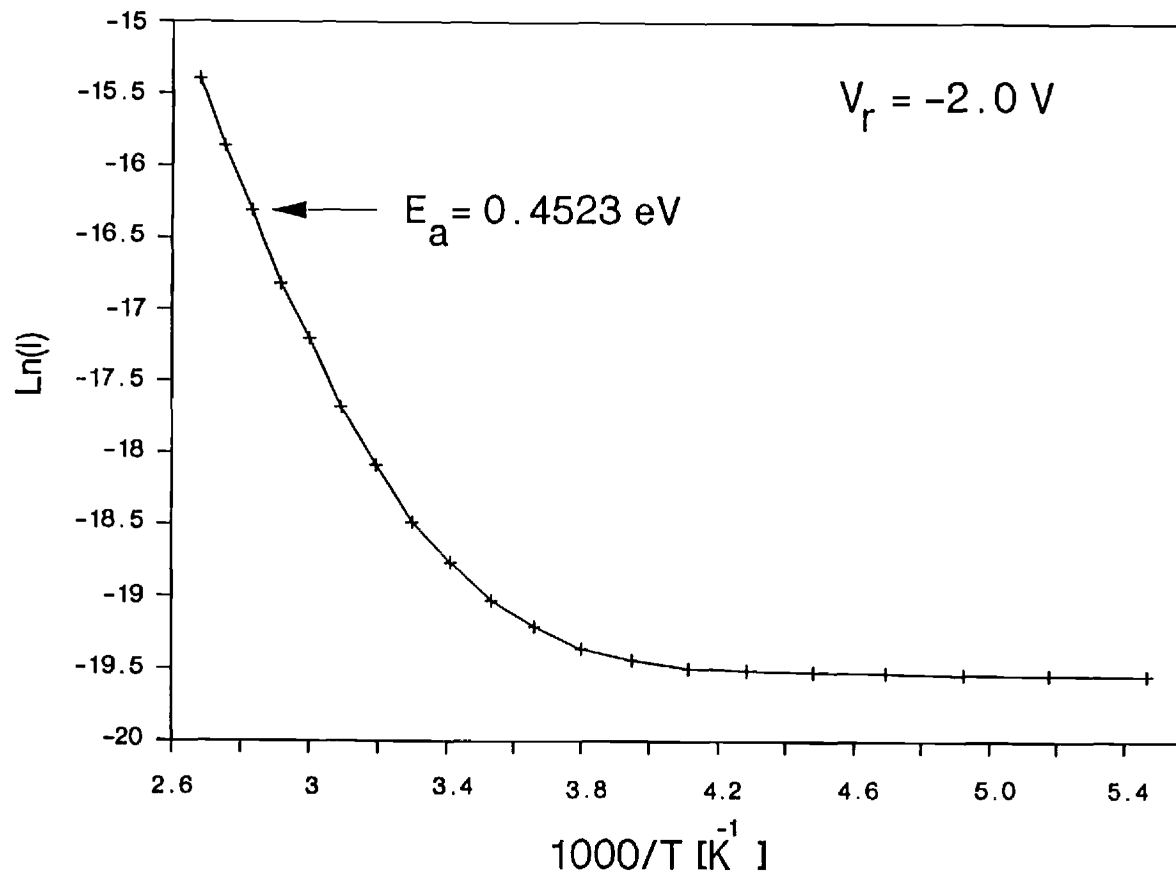

Figure 5. LN(J) vs. T plot measured at 2 volts constant reverse bias. Trap activation energy is shown in the figure.

While the DLTS and I-V-T measurements yield the characteristics of the space charge region, they offer no information about the bulk material properties. In order to assess the bulk properties the transformed I-V technique was used to separate the bulk and junction effects. Figure 6 shows the transformed I-V curve for this device at room temperature. J_{o1} and J_{o2} components were found to be 1.29 E - 19 A/cm^2 and 8.33 E - 11 A/cm^2, respectively, while the corresponding n-factors were 1.00 and 1.97, consistent with theory.

Even though the trap detected by I-V-T and DLTS could not be seen deeper in the base, the leakage current produced in the depletion region of this cell degrades the cell performance because the J_{o1} and J_{o2} components are nearly equal at the cell operating point (~1 volt), Figure 6. Since the J_{o2} component at the operating point represents the current that does not make it to the load, performance of this particular cell can be appreciably improved by eliminating the E_V + 0.912 eV trap.

2.14 Computer Modeling

To test the experimental data and the validity of the above analyses, the solar cell was modeled with the help of two computer programs, one of which calculates the cell parameters V_{oc}, J_{sc}, efficiency, and spectral response, and the other which calculates an effective recombination velocity anywhere within the structure.

The PC-1D model, described elsewhere (13), was used first to model the spectral response. A net base lifetime of 8 ns with a front surface recombination velocity of 1.25 E5 cm/s was required to obtain a good match between the model calculations and the experimental data, Figure 7. Back surface passivation was found to have negligible effect on the spectral response. The

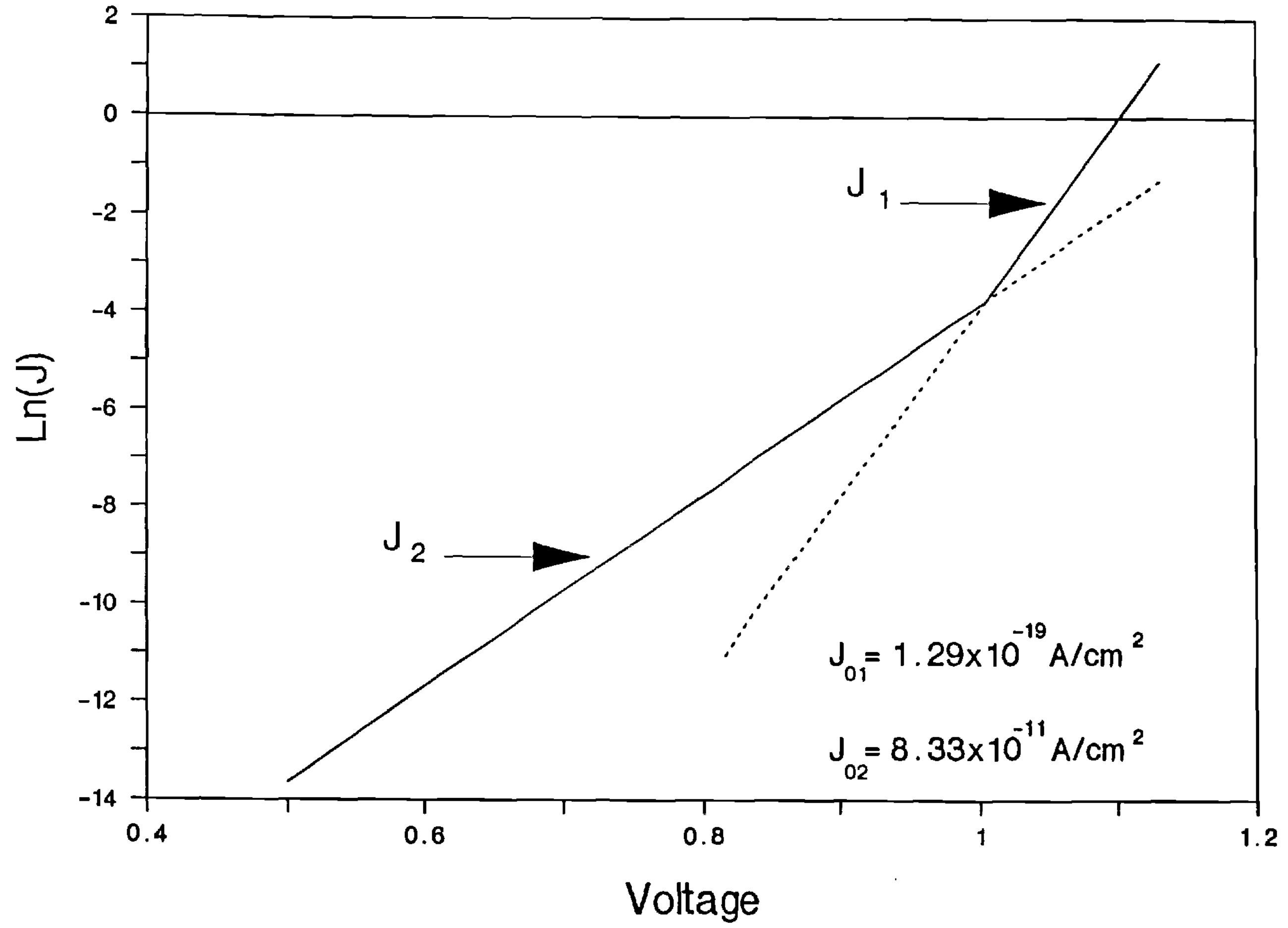

Figure 6. Transformed I-V characteristic for cell. J_1 (diffusion) and J_2 (space charge) current density components are indicated.

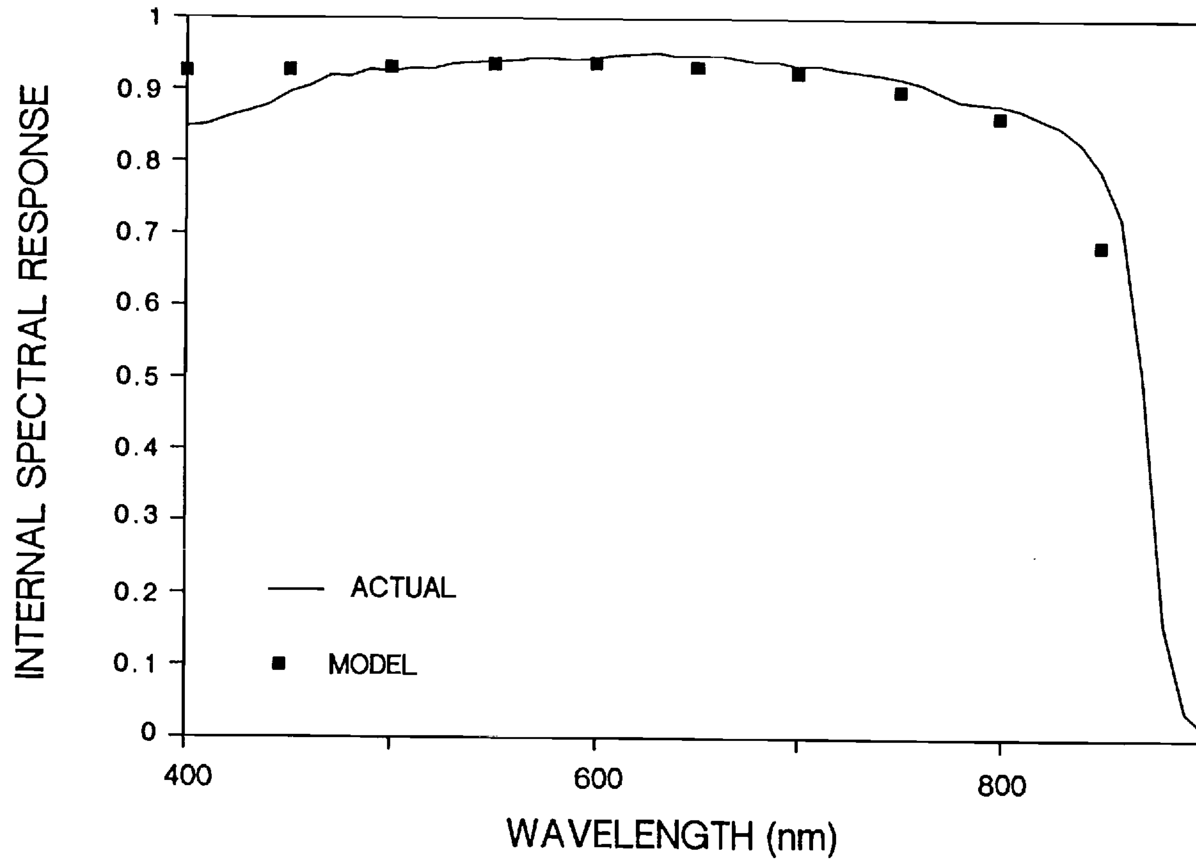

Figure 7. Comparison of actual spectral response (solid line) with modeled spectral response (blocks) as calculated from PC-1D for the given device structure.

emitter and buffer lifetimes were determined from the SRH lifetime in the base which was calculated from

$$\frac{1}{\tau} = \frac{1}{\tau_{srh}} + BN + CN^2 \qquad (15)$$

where B is the radiative recombination coefficient and C is the Auger recombination coefficient for GaAs. Using B = 2.5 E - 11 cm^3 [14], C = 1.60 E - 29 $cmI.^6$ [15], and τ_B = 8 ns in the base, we obtain τ_{srh} = 8.33 ns. Assuming defect dominated τ_{srh} to be constant throughout the device, equation (15) gave emitter and buffer lifetimes of 2.08 ns and 5.49 ns, respectively, by substituting the proper values for B and C in each region.

The numerical values of the spectral response, Figure 7, were found from the calculated J_{sc} and measured reflectivity as a function of wavelength using the AM1.5 energy content of the incident radiation. A shadow loss of 5% was used for the modeling. Figure 7 shows a good match between the calculated and measured values with only a slight difference in the short and long wavelengths. The lower measured response in the short wavelength, seen in Figure 7, can be attributed to absorption in the AlGaAs passivation layer which is not considered in the model. The AlGaAs acts to decrease the photon flux incident on the GaAs at the shorter wavelengths until the absorption edge of the AlGaAs at ~2 eV is reached. At long wavelengths (850 nm), the simulated response is somewhat lower than the actual probably because the increase in absorption coefficient due to doping near the band edge [16] is not included in the PC-1D model. This additional absorption allows more photons to be absorbed closer to the collecting junction and hence increase J_{sc} at these long wavelengths due to an increase in collection probability.

In order to test the estimated lifetime profile (τ_e, τ_b, τ_{buff}) and recombination velocities, an effective recombination velocity (S_e) model was used to calculate the reverse leakage current. S_e is a measure of the minority carrier losses in the various regions of the device which directly provides the reverse saturation current density (J_{o1}). This model, which is described in detail elsewhere for silicon cell design and analysis [17], includes the effects of bandgap narrowing, Auger and radiative recombination, and recombination at surfaces and interfaces. The internal recombination velocity S_e throughout the cell can be calculated using the front surface recombination velocity at the emitter/AlGaAs interface, FSRV, the back surface recombination velocity at the back of the buffer layer, BSRV, the diffusion length, doping profile, and cell dimensions as input parameters. Each region of the cell (buffer, base, and emitter) is subdivided into a number of elements, all of the same width. S_e is calculated iteratively from FSRV and BSRV until the p-n junction edge is reached on each side. The recombination velocity S_{e2} at one boundary of any element is calculated in terms of velocity S_{e1} at the other boundary by

$$S_{e2} = \frac{N_2}{N_1} \frac{D}{L} \left[\frac{S_{e1} \frac{D}{L} + \tanh(\frac{W}{L})}{1 + S_{e1} \frac{D}{L} \tanh(\frac{W}{L})}\right] \exp\left[\frac{\Delta E_{g2} - \Delta E_{g1}}{kT}\right] \qquad (16)$$

where

W = element width

D,L = diffusion coefficient and diffusion length of minority carriers within the element

$N_{1,2}$ = doping densities at boundaries of element

ΔE_{g1}, ΔE_{g2} = bandgap narrowing due to doping densities N_1 and N_2.

The base and emitter components of the leakage current can then be determined from

$$J_{OB} = \frac{qn_i^2}{N_D} \cdot S_{ejb} \tag{17}$$

and

$$J_{OE} = \frac{qn_i^2}{N_A} \cdot S_{eje} \tag{18}$$

where S_{ejb} and S_{eje} are the recombination velocities at the base edge and emitter edge of the p-n junction, respectively.

Figure 8 shows a plot of S_e versus depth for the GaAs heteroface cell for various values of FSRV and BSRV which support the spectral response conclusion that back-surface passivation has little or no effect on J_{OB} in this cell. The model calculations reveal that recombination velocity at the base side of the p-n junction is pinned so that $J_{OB} = \sim 0.85 + 10^{-19}$ A/cm^2 for all values of back surface recombination velocity. For FSRV = 1.25 X 10^5cm/s and τ_e = 2.08 ns, which gave the best match for the spectral response, the S_e-model gives J_{OE} = 0.55 X 10^{-19}A/cm^2 so that the simulated $J_{o1} = J_{OE}$ X J_{OB} = 1.40 + 10^{-19} A/cm^2. This is in good agreement with the measured J_{o1} of 1.29 X 10^{-19} A/cm^2. This supports the selection of FSRV and lifetime for the simulated spectral response and indicates that J_{o1} or V_{oc} of this cell is limited by both the base and emitter with the emitter contributing ~ 33% of J_{o1}.

A few more revealing observations can be made from Figure 8. Contrary to the back surface, front surface passivation is critical for this cell because an FSRV of 1 X 10^7cm/s, which is typical of the free GaAs surface, results in a large increase in J_{OE} and hence a lower V_{oc}. However, the AlGaAs passivation needs to limit FSRV only to ~1 X 10^4cm/s since in this cell FSRV

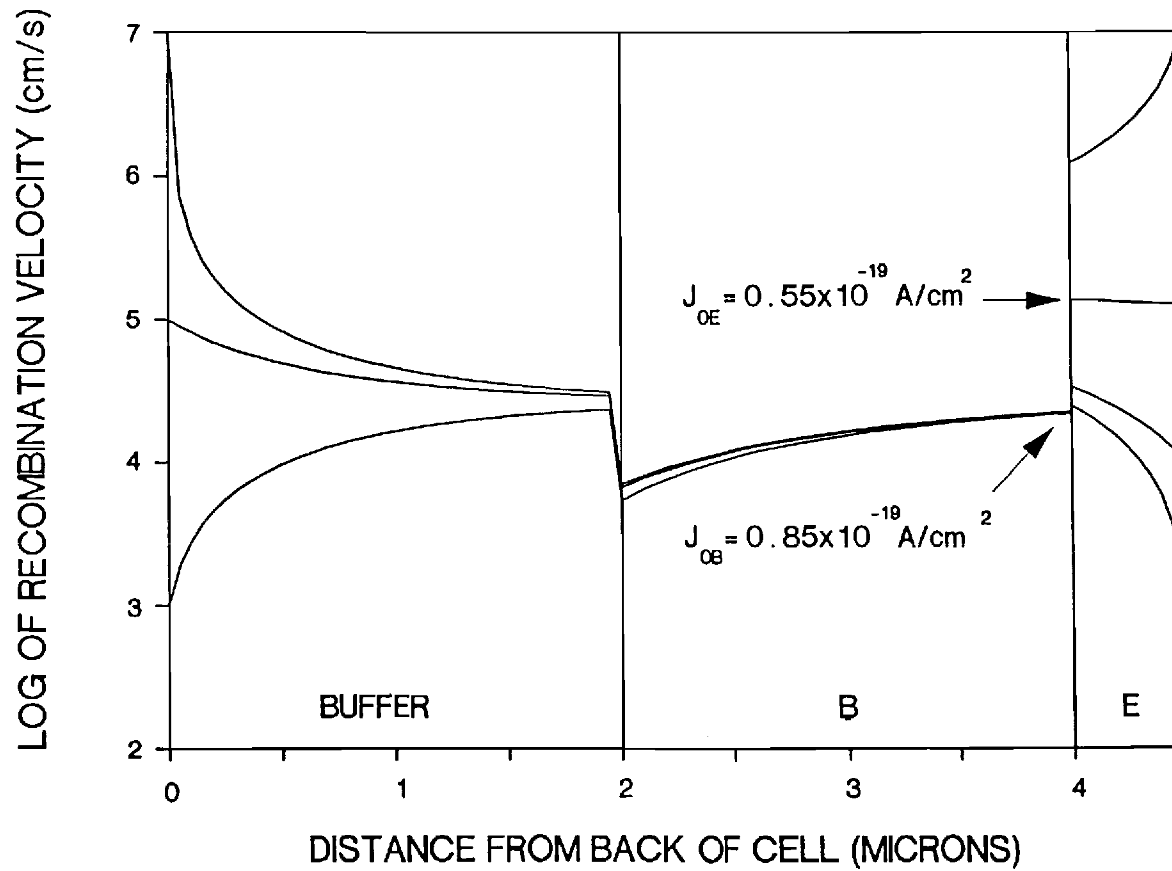

Figure 8. Plot of effective recombination velocity, S_e, for various values of front and back surface recombination velocities. Emitter and base leakage current components are indicated for the cell-matching S_e plot.

below this value has very little impact on S_{eje} or J_{0E} as seen in Figure 8. Note also from this figure that the design rule for the emitter changes with the magnitude of FSRV. For devices with any reasonable amount of surface passivation a lower J_{0E} is accomplished by thinning the emitter, but for unpassivated surfaces, emitter thinning would actually increase J_{0E}. Thus, the AlGaAs passivation is most critical for thin emitters.

As a final confirmation of the lifetime profile and the S values derived above, the cell J_{sc}, V_{oc}, and efficiency were calculated using PC-1D. Table 1 shows a very good agreement between the measured and modeled values confirming the validity of the above procedure. Having established the match, the PC-1D model was used to provide guidelines for improving the efficiency of this cell and to optimize the p-n heteroface cell design. Model calculations in Table 1 show that a significant improvement in cell efficiency (23%) can be realized by properly passivating the front surface of this cell so that the FSRV = 1 + 10^4cm/s. Only a slight improvement is found by back surface passivation for the lifetime profile of this device structure. However, if the effective base lifetime can be improved to 15 ns the efficiency of this cell can reach ~24.17% with passivated front and back surfaces. This improvement is clearly understood upon inspection of Figure 9 which shows that longer lifetimes decrease the magnitudes of S_{eje} and S_{ejb} resulting in higher V_{oc}, in additon to raising J_{sc} via reduced recombination throughout the device. Further gain in efficiency can be obtained by optimizing the thickness and doping profile of the device. Since in n-type GaAs the net lifetime is dominated by defects up to a doping level of ~1 X 10^{18} cm^{-3} [7], an efficiency of ~24.40% can be obtained simply by changing the base doping to 5 X $10^{17}cm^{-3}$ and the buffer doping to 2.5 X $10^{18}cm^{-3}$. These doping levels represent the

Table 1: Guideline for cell optimization using PC-1D and effective recombination velocity modeling. Actual cell data and best match are shown. Cells 6 and 7 (starred entries) are thinnned base and buffer structures.

cell ID	N_d (cm^{-3})	N_a (cm^{-3})	N_b (cm^{-3})	FSRV (cm/s)	BSRV (cm/s)	T_b (ns)	V_{oc} (Volts)	J_{sc} (A/cm^2)	Eff
actual	$2x10^{17}$	$2x10^{18}$	$2x10^{18}$				1.013	24.5	21.2
match	$2x10^{17}$	$2x10^{18}$	$2x10^{18}$	1.25E5	1.0E6	8	1.01	24.56	21.39
1	$2x10^{17}$	$2x10^{18}$	$2x10^{18}$	1.0E4	1.0E6	8	1.016	26.59	23.02
2	$2x10^{17}$	$2x10^{18}$	$2x10^{18}$	1.0E4	1.0E4	8	1.017	26.71	23.13
3	$2x10^{17}$	$2x10^{18}$	$2x10^{18}$	1.0E4	1.0E4	15	1.032	27.11	24.17
4	$5x10^{17}$	$2x10^{18}$	2.5E18	1.0E4	1.0E4	15	1.048	26.83	24.40
5	$5x10^{17}$	$2x10^{18}$	2.5E18	1.0E4	1.0E4	20	1.054	26.95	24.76
6*	$6x10^{17}$	$2x10^{18}$	2.5E18	1.0E4	1.0E3	15	1.055	27.04	24.74
7*	$6x10^{17}$	$2x10^{18}$	2.5E18	1.0E4	1.0E3	20	1.0596	27.10	25.04

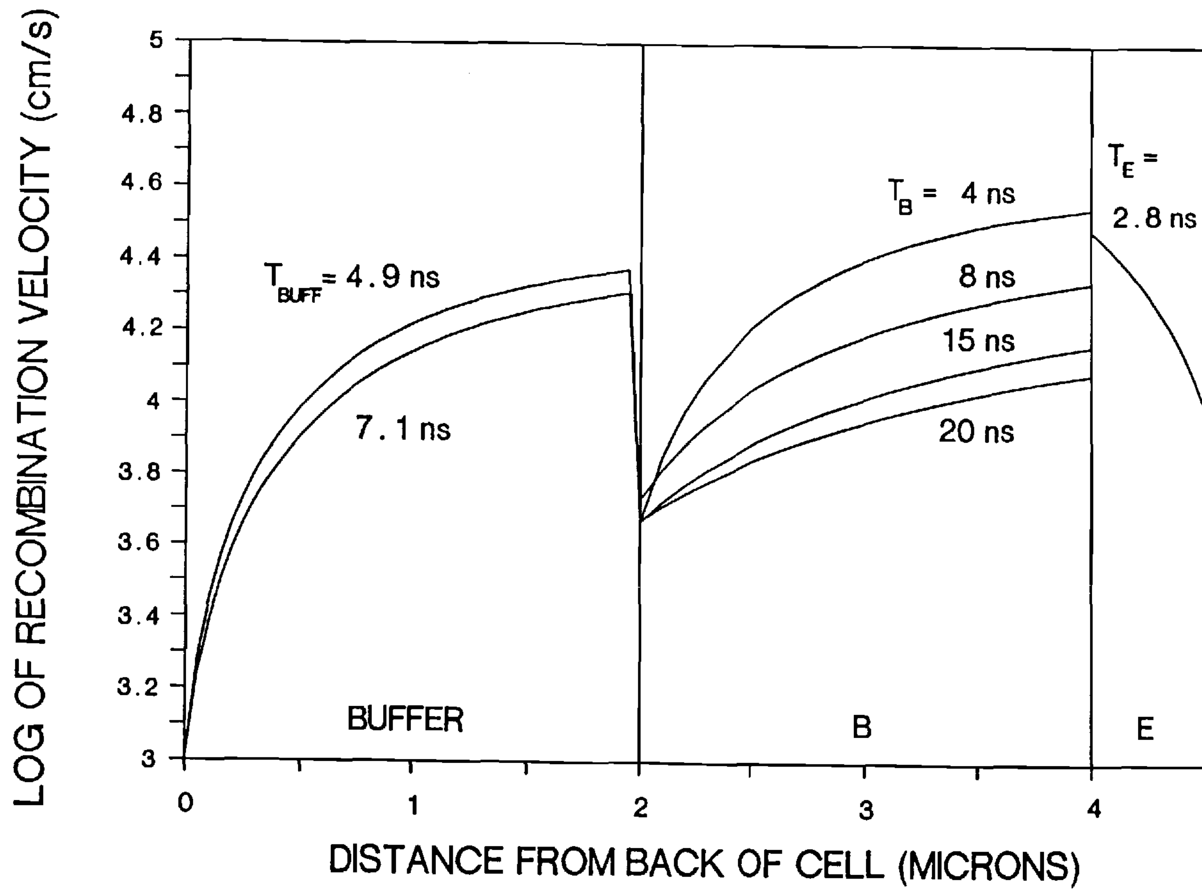

Figure 9. Plot of effective recombination velocity, S_e, showing the influence of minority carrier lifetime on recombination throughout the device. The net lifetimes in each layer are indicated.

optimum trade-off between an increase in V_{oc} due to the heavier base doping and a decrease in J_{sc} resulting from higher S_e in the base due to a reduced doping discontinuity (N_1/N_2) at the buffer/base interface. It should be recognized that these calculations are easily deduced from S_e-plots which signify the importance of such analysis. The cell efficiency tends to saturate near the 24.40% level unless the base material quality is improved further. Table 1 shows an efficiency of 24.76% can be obtained with a lifetime of 20 ns, which is still well below the intrinsic lifetime limit of GaAs at a doing level of 5 X $10^{17}cm^{-3}$. This represents the highest efficiency found for our simulations of this particular p-n heteroface structure.

Further optimization is possible only by modifying the device structure. Table 1 shows that a 24.74% efficient cell can be achieved with only a 15 ns base lifetime by thinning the base to 1.2 um. This improvement comes as a result of the trade-off between low S_e in the base and increased photon absorption in the buffer. For this device structure, it is necessary to have a passivated back surface and reasonable lifetime in the buffer. The doping and thickness of the base and buffer layers become critical to the performance of such a device since there exists a sensitive trade-off between greatly increased carrier collection in the thinned based due to reduced recombination in the base resulting from the proximity of the base/buffer interface to the collecting junction, and the amount of carriers generated in the buffer layer that do not make it to the p-n junction. The V_{oc} is greatly increased due to the lower S_{ejb} while the J_{sc} benefits from the higher collection efficiency of photogenerated carriers in the thin base. Model calculations in Table 1 indicate efficiencies as high as ~25.04% are possible for a device with a base width of 1.2 um, buffer thickness of 1.3 um, base doping of 6 X $10^{17}cm^{-3}$,

buffer doping of 2.5 X $10^{18} cm^{-3}$, base lifetime of 20 ns, FSRV = 1 X 10^4 cm/s and BSRV = 1 X 10^3 cm/s. It should be noted that the buffer thickness now becomes important since the effectiveness of the back surface passivation would be reduced if the buffer were too thick. In essence, the buffer here acts as part of a two-step base layer which suggests that further gains in efficiency can be realized by multi-step or even graded base regions.

2.2 Positron Annihilation Spectroscopy of AlGaAs/GaAs Interfaces in MOCVD-Grown GaAs Heterojunction Solar Cells

2.21 Introduction

A major objective in the characterization of heterojunction semiconductors grown via MOCVD, MBE, or PEVD is the development of techniques for probing defect and impurity distributions affecting the electrical response. Thus, methodologies can be developed for adjusting deposition parameters, layer thickness, and/or dopant density to enhance the electrical properties of the semiconductor. Furthermore, from a quality assurance viewpoint, it is desirable that techniques for characterizing the atomic defect and/or impurity structure of a semiconductor be non-contact (NC) and nondestructive (ND). One relatively new technique that satisfies the NC and ND constraints and is capable of profiling the defect density, detailing interfacial disorder, and detecting impurity complexes is Slow Positron Annihilation Spectroscopy (SPAS) [17-21].

By measuring the energy distribution of positron/electron annihilation events it is possible to probe a material's electron momentum distribution with a variable-energy positron beam. As a first order approximation, the intensity of the parabolic and Gaussian components of the annihilation energy

distribution can be related to the respective fractions of positrons annihilating with valence electrons and those annihilating with the more tightly bound core electrons. If a positron becomes spatially localized due to defect trapping or to strong space charge effects, the fraction of annihilation events with valence electrons will be altered relative to core electrons, thus narrowing or broadening the energy distribution curve.

A series of experiments was carried out to determine the potential applications of SPAS to heterojunction semiconductors by investigating the relative positron-sensitive defect profile for different MOCVD grown solar cell structures. Validation of any new microanalytical tool requires extensive comparisons with other more established techniques, wherever possible. The SPAS data has been subsequently compared to Surface Photo-Voltage (SPV), a destructive defect profiling technique, qualitative MOCVD growth variations, and band bending arguments.

2.22 Experiment

The MOCVD grown solar cell structures investigated are summarized in Table 2, in terms of layer function, material, semiconductor type, and dopant density. These devices were grown in a Spire MO-450 reactor using trimethyl gallium, trimethyl aluminum, and arsine as reactants. The dopants are Zn for p-type regions and Si for the n-type regions.

The variable-energy positron beam (0 - 100 keV) used for analysis of the heterojunction solar cells has been previously described elsewhere [24]. In brief, the system consists of a Na-22 positron source moderated by a tungsten crystal with efficiency 5×10^{-4} and focused magnetically to the target, all of which is under UHV conditions (10^{-10} Torr). At each incident energy,

TABLE 2. SOLAR CELL HETEROJUNCTION STRUCTURES

LAYER	MATERIAL	THICKNESS (um)	TYPE	DOPING (cm^3)
MOCVD Run #872				
Cap	GaAs	0.143	p^+	8.0×10^{19}
Window	AlGaAs	0.05	p^+	1.0×10^{18}
Emitter	GaAs	0.5	p	1.5×10^{18}
Base	GaAs	2.0	n	2.0×10^{17}
Buffer	GaAs	2.0	n	2.0×10^{18}
Substrate	GaAs			
MOCVD Run #1053				
Cap	GaAs	0.31	p^+	8.0×10^{19}
Window	AlGaAs	0.03	p^+	1.0×10^{18}
Emitter	GaAs	0.5	p^+	2.0×10^{18}
Base	GaAs	3.0	n	8.0×10^{17}
BSF	AlGaAs	1.0	n^+	2.0×10^{18}
Buffer	GaAs	1.0	n^+	2.0×10^{18}
Substrate	GaAs			

counts (annihilation events) are collected with a count rate of 2 kHz. The change in lineshape of the annihilation energy distribution has been calculated using the standard Doppler S-parameter [23], which is defined as the number of counts in some fixed central energy window divided by the total number of counts in the energy spectrum.

A Biorad Polaron PN4200 electrochemical profiler has been used in conjunction with a Polaron PN 4250 SPV attachment to study the defect nonuniformity from the surface through the p-n junction interface. A detailed description on the operation of the depth-resolved SPV technique is to be published elsewhere [25]. By collecting SPV spectra taken at different etch depths, comparative ratios of one SPV spectrum divided throughout the wavelength scan yield information about the presence of localized defect regions in the emitter and base of the solar cell [25,26].

2.23 SPAS Modeling

The deconvolution of the positron energy dependent (depth dependent) Doppler lineshape parameter, S(E) has been premised upon a previously developed multilayer model [22]. Each layer is assumed to be homogeneous and well-defined, therefore possesing a characteristic lineshape parameter S_i, where i is the layer dependent upon the layer material, deposition conditions, and dopant density. S(E) is defined as the superposition of S_i weighted by the probability, $g(E)_i$, that positrons of energy E will annihilate in layer i such that

$$S(E) = \sum_i g(E)_i * S_i \qquad (1)$$

where

$$g(E)_i = \int_{a_i}^{b_i} P(z,E)dz \qquad (2)$$

and P(z,E) is the positron implantation profile integrated over the boundaries of the layer i from a_i to b_i. The mean positron implantation depth is functionally dependent upon the material mass density and two material Gaussian fitting parameters. As yet, no detailed experimental investigation has been performed to determine the best Gaussian fitting parameters for each of the MOCVD-grown layers. These parameters were chosen to best approximate the general S(E) behavior and are within the range of previous SPAS studies (although on different materials).

While the above model is useful in delineating the layer boundaries and the relative layer defectiveness, the effects of material density (positron backscattering), localized trapping (e.g., at interfaces or at defect inclusions), and positron diffusion length have been neglected. In the current analysis, material density effects may be important since the $Al_xGa_{(1-x)}As$ (x = 0.9) is less dense than adjacent GaAs layers. If the AlGaAs layer were sandwiched between two GaAs layers, an apparent enhancement of S_i for the AlGaAs layer relative to the GaAs layers could result.

Differential positron trapping across interfaces has been shown to be important for an SiO_2/Si interface [21] since the positron diffusion length in Si is substantially greater than in SiO_2. As yet, the positron diffusion lengths have not been experimentally measured for the layer materials, thus the current modeling effort fails to explain local minimums and maximums in S(E). However, away from the interfaces, it has been assumed that localized defects may be approximated by the superposition of characteristic defect values, S_a, as exhibited in Figure 10. Nonetheless, competitive trapping

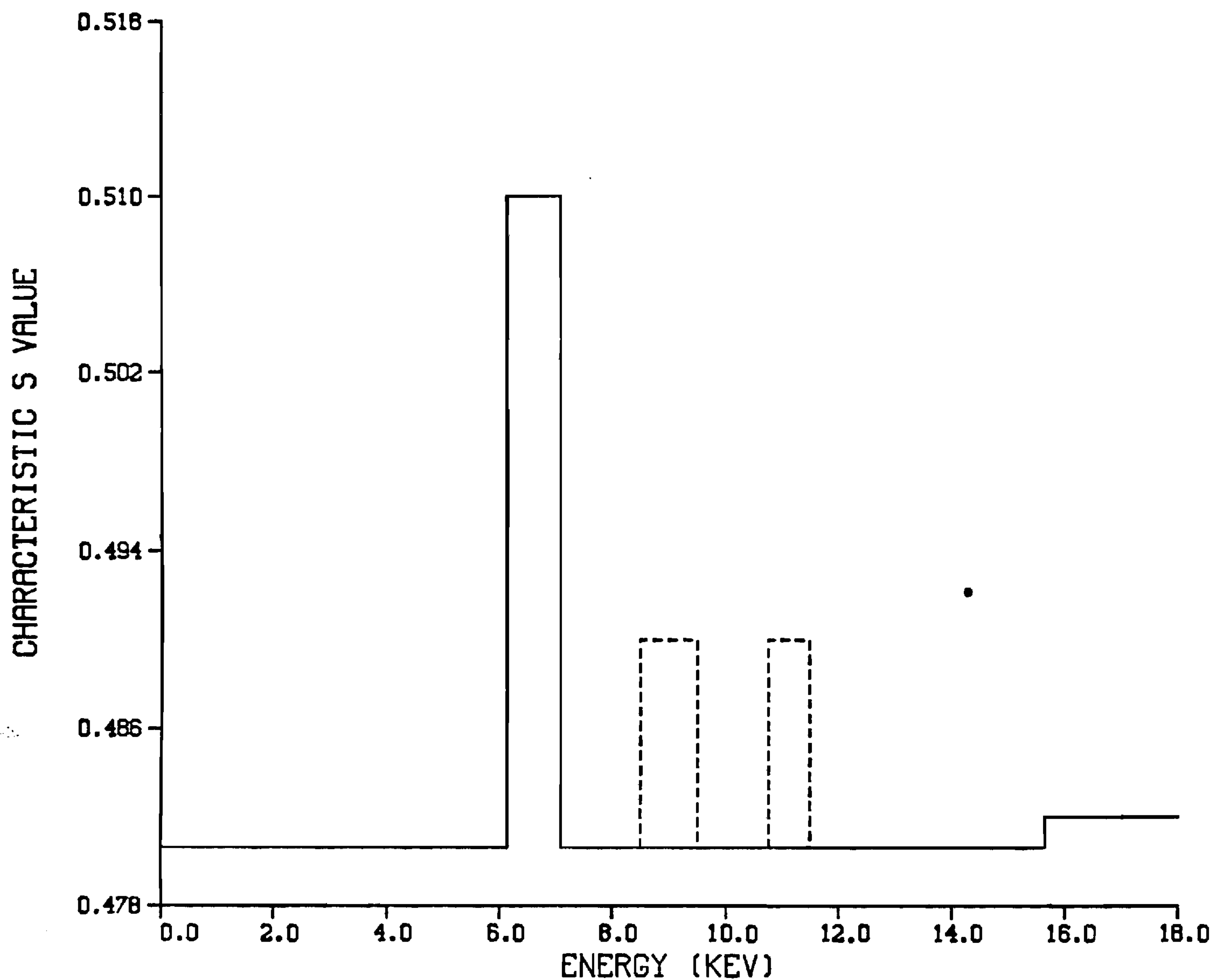

Figure 10. Example of a deconvoluted characteristic lineshape parameter as a function of the material layer for each layer incorporating the superposition of the layer contributions, S_i, (solid lines) and the local defect contributions, S_d (dashed lines).

between localized defects within the layers or between localized defects and nearby interfaces will accentuate the experimental S(E) minimums and maximums, whereas the model approximation has been shown to raise or lower S(E) in a more gradual manner.

2.24 Results and Discussion

Annihilation lineshape measurements have been obtained for the solar cell heterojunctions previously described in Table 2. The variable-energy positron beam has been confined to sampling S(E) spectra with energies of -250 eV to -25 keV which is sufficient to probe through the p-n junction region. Initially, two SPAS S(E) spectra were obtained for two different specimens of MOCVD Run #872 (Figure 11). Both specimens were cut from the same wafer, except that 872A is representative of the center and 872B is representative of the edge. The general features of both specimens are similar; however, two major differences are apparent: (1) the 872B specimen S(E) spectrum is shifted to higher energies with respect to the 872A, and (2) the finer details of the 872A specimen tend to be absent from the 872B specimen.

Before explaining the apparent differences between the two specimens, a number of the features of 872A are first discussed. According to current theoretical model predictions, the depth resolution of the heterojunction layers is as shown in Figure 11. The model predicts that general shape of the convoluted S(E) curve; however, it fails to correctly place the AlGaAs layer and fails to correlate with the finer details of the S(E) spectrum (i.e., the localized minima and maxima). The twin maxima between 5 and 8 keV suggest that positron backscattering may be significant. It is anticipated that the incorporation of backscattering into the theoretical model will shift the

(A)

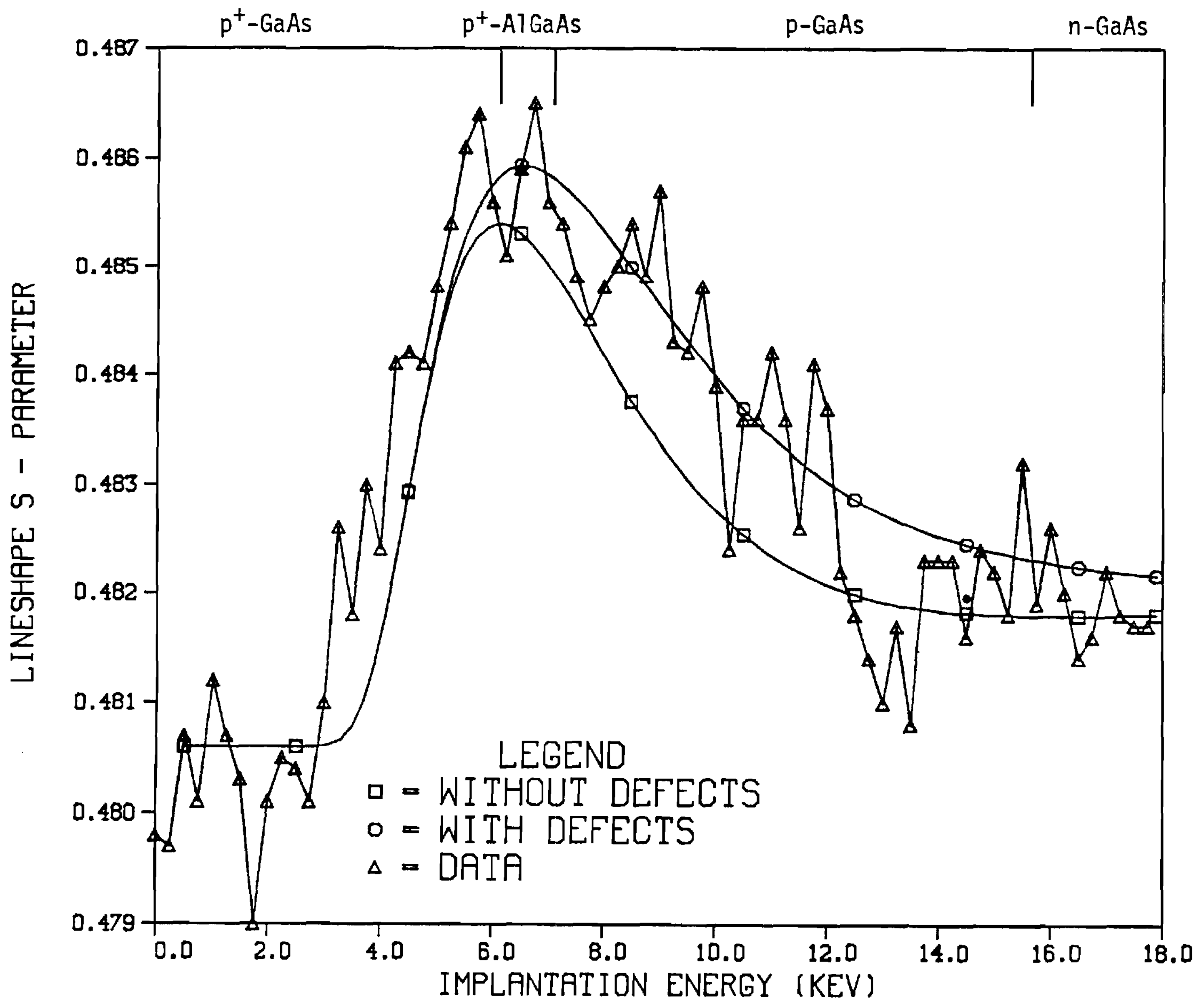

Figure 11.(a) Lineshape parameter, S(E), as a function of incident energy, E, for MOCVD Runs. (a) #872A experimental data connected by triangles. Theoretical approximations to the experimental data (with and without defects) are shown by the smooth solid curves.

(B)

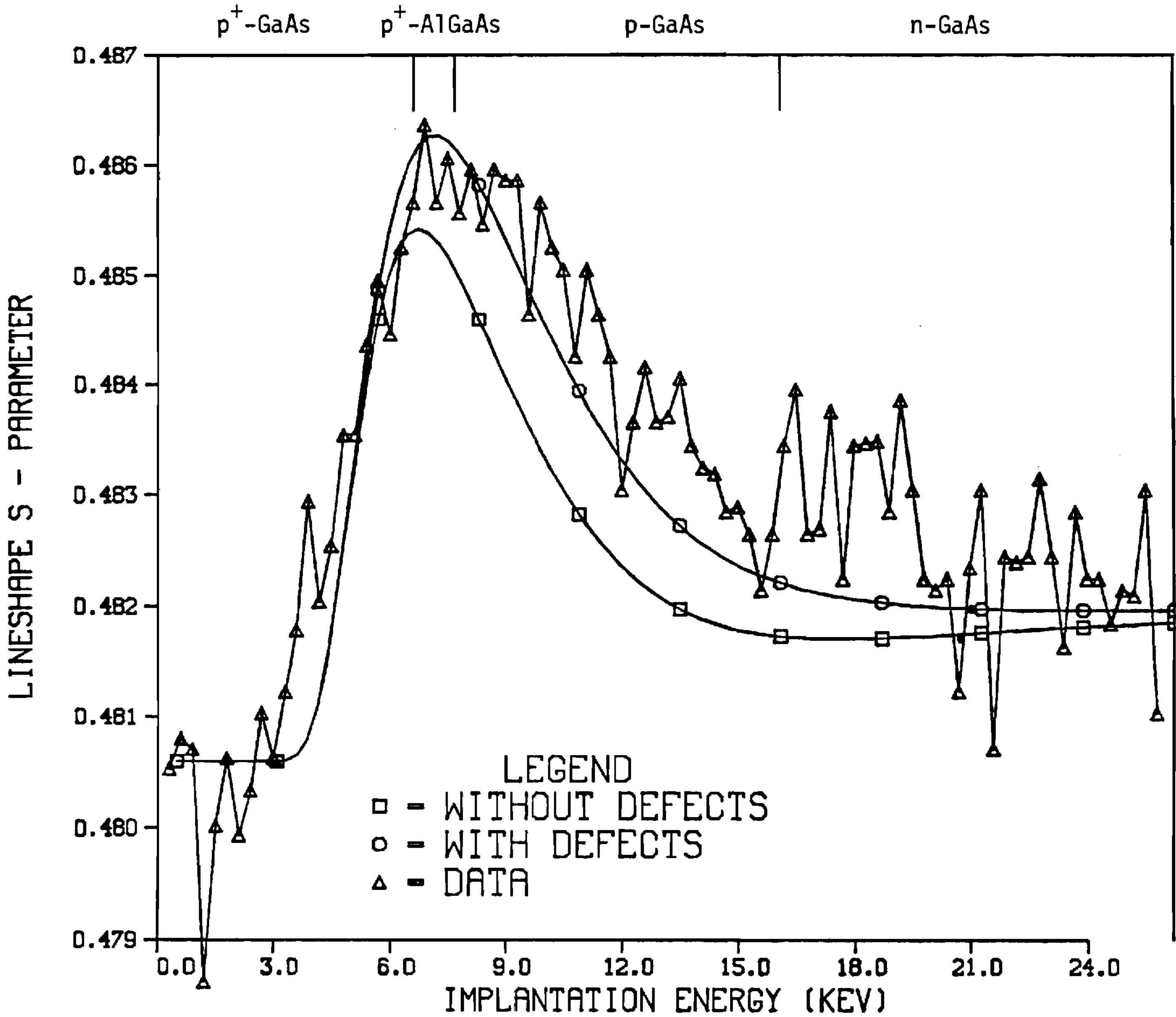

Figure 11.(b) Lineshape parameter, S(E), as a function of incident energy, E, for MOCVD Runs. (b) #872B experimental data connected by triangles. Theoretical approximations to the experimental data (with and without defects) are shown by the smooth solid curves.

predicted position of the AlGaAs layer toward the surface and predict the local maxima near the AlGaAs/GaAs interfaces.

Within the emitter p-GaAs layer, a number of local lineshape maxima exist which have been directly correlated with SPV data. For example, the SPAS data shows a maximum between positron energies of 8.5 keV and 9.5 keV (positron implantation range of .27 to .31 microns). The SPV data clearly shows a defect to exist between .28 and .32 microns (Figure 12). An interpretation of the SPV data is as follows [26]:

(a) the spectra ratio between .22 and .21 microns is indicative of a defective region below the surface in comparison to the material that has just been removed;

(b) the spectra ratio of .28/.22 microns shows that a defective region exists near the surface, but further into the emitter layer, the p-GaAs is less defective;

(c) the spectra ratio of .32/.30 being relatively flat and equal to unity indicates that the defective region has been completely traversed.

When the existence of a local defect region (layer) is incorporated into the model calculation the agreement between the predicted curve and the experimental data is improved. However, the model is still incapable of predicting abrupt changes in S(E). As the synergistic effects of positron diffusion and trapping are folded into the model, it is anticipated that these sharp interfaces will be explained.

Another significant characteristic of the S(E) spectrum is the apparent broad troughs (minima) located between energies 7.5 and 8.5 keV and between energies 12.5 and 14 keV which correspond to the depth ranges of .21 to .27

microns and .50 and .60 microns, respectively. These depth ranges coincide with the AlGaAs/GaAs emitter interface and the p-n junction. Thus, a number of possibilities exist to explain the local minima in S(E). First, a strong electric field is present at the interfaces as a result of band bending. Hence, it is possible that positrons implanted in the space charge depletion region (or within a diffusion length of this region) are swept across the depletion region before an annihilation event is probable. Such an effect would decrease the S-parameter in the proximity of the depletion zone.

Alternatively, the local minimum may be related to the presence or absence of interfacial defect phenomena. In a previous study of SiO_2/Si interfaces [21], it has been shown that differential positron diffusion lengths across an interfacial trap may result in a lower lineshape parameter than either SiO_2 or Si, indicative of higher electron momenta.

Another possible cause of the observed local minimum in the S-parameter may be drawn from the SPV data of Figure 12, where the .22/.21 ratio indicates that the previously etched material (closer to the AlGaAs/GaAs emitter interface) was of superior quality [26].

The explanation for the S(E) spectrum differences between 872A and 872B can be correlated with the MOCVD growth rate difference at the edge of the wafer versus the center of the wafer. It has been observed by Spire [27] that the thicknes of the heterojunction structure is "substantially" greater at the edge, most probably due to a temperature gradient which leads to enhanced nucleation rates at the wafer edge. This effect is sufficient to explain the S(E) spectrum shift of 872B edge specimen in comparison to 872A center specimen. In addition, by increasing the layer thicknesses, higher energy positrons are necessary to penetrate the individual material layers. Thus, loca-

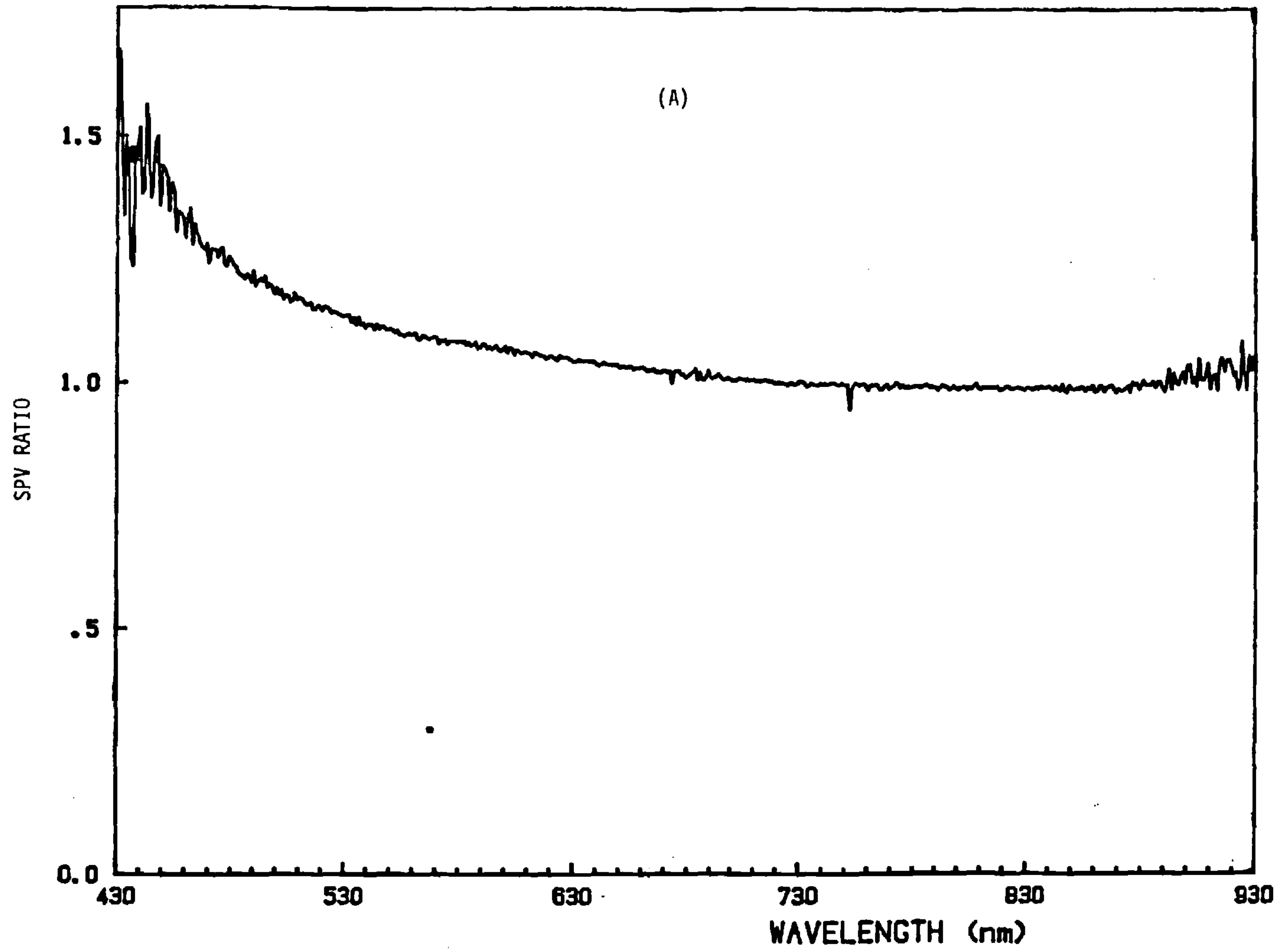

Figure 12.(a) SPV spectrum ratios as a function of wavelength taken at etch depths of (a) .22/.21 microns.

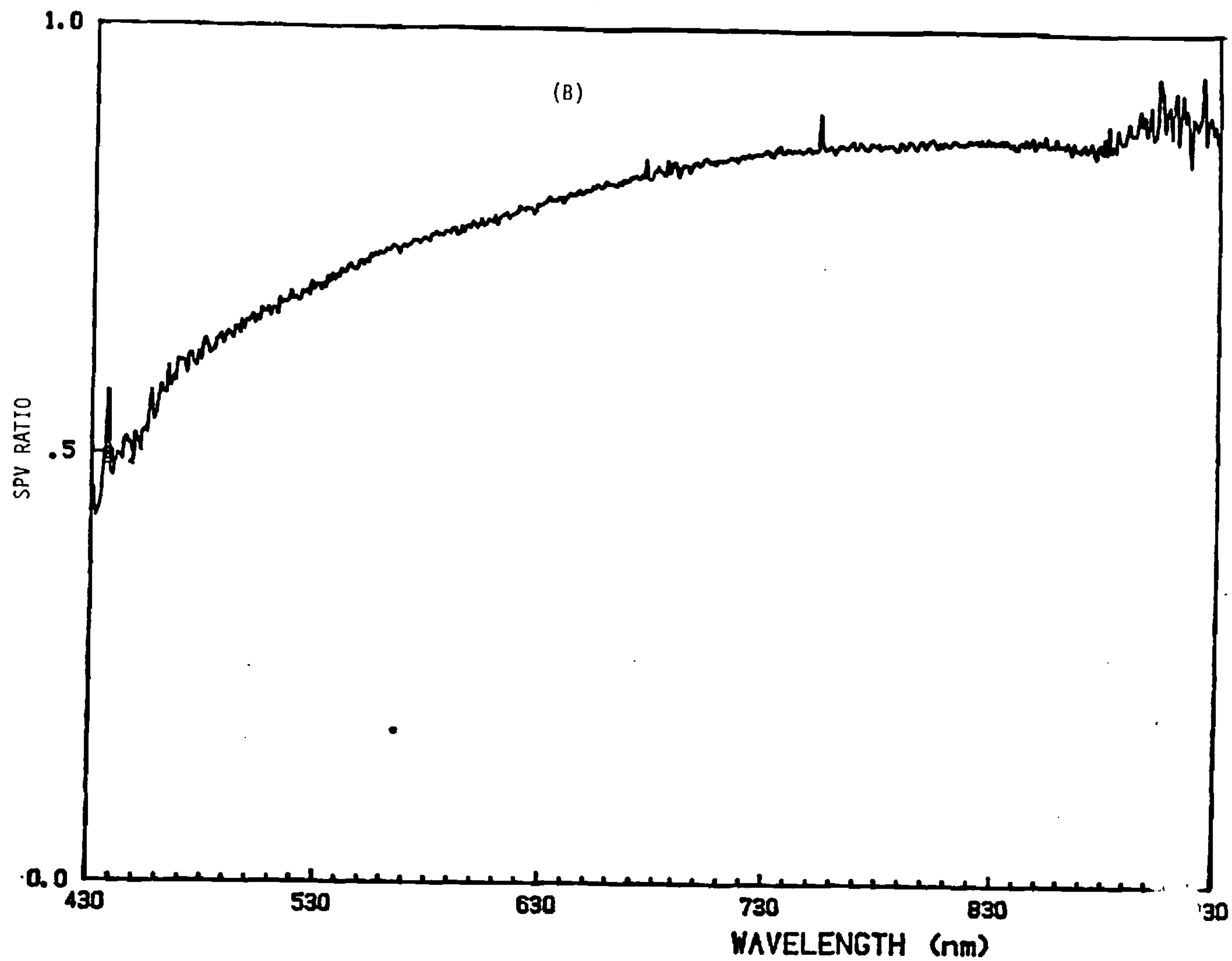

Figure 12.(b) SPV spectrum ratios as a function of wavelength taken at etch depths of (b) .28/.22 microns.

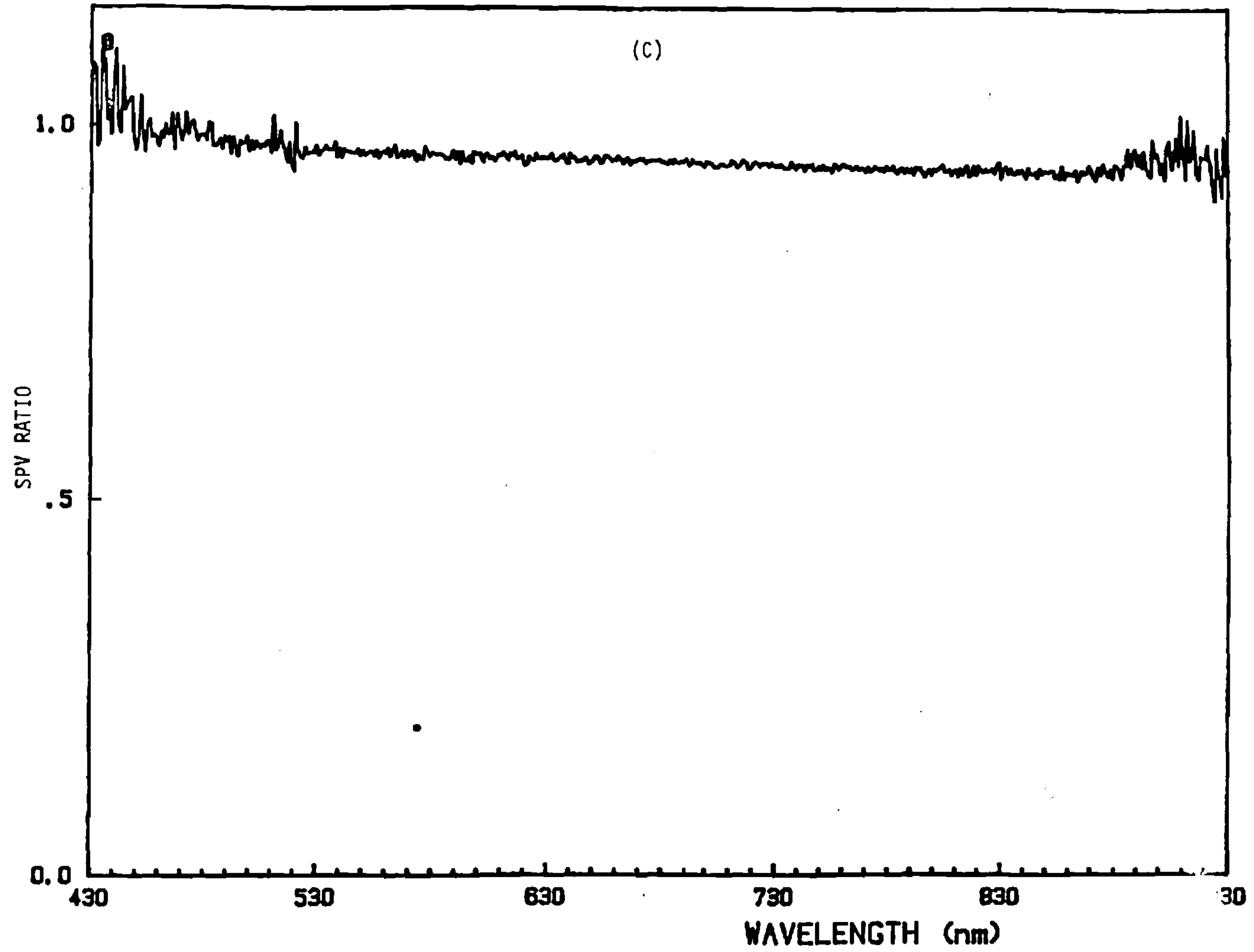

Figure 12(c) SPV spectrum ratios as a function of wavelength taken at etch depths of (c) .32/.28 microns.

lized minima and maxima of the S(E) spectrum should be reduced for 872B in comparison to 872A since the positron stopping profile is approximated by the derivative of a Gaussian function [18]. Another possible result of differential nucleation rates may be enhanced interdiffusion at the interfacial regions between layers, thus broadening the transition region between the heterojunction layers and thereby diminishing the finer details of the S(E) spectrum. SIMS data is currently being obtained in an effort to verify this hypothesis.

Two sets of SPAS data have been taken of MOCVD Run #1053 and subsequently averaged resulting in the S(E) spectrum shown in Figure 13. The 1053 S(E) spectrum is noticeably different from both of the 872 S(E) spectra, and of major significance is the absence of large contrast between the AlGaAs and adjacent GaAs layers. This difference is largely explained by the thicker cap layer, resulting in an AlGaAs window that is translated an additional .157 microns below the surface (see Table 2). The theoretical convoluted S(E) behavior shows a significantly suppressed AlGaAs spectrum for the 1053 specimen when using the identical characteristic S_i parameters of the 872 specimens (Figure 13). However, the model placement of the AlGaAs layer appears to be dubious, and the general experimental features, namely the broad maxima and minima, are not predicted. It is possible that the GaAs cap is thicker than the prescribed dimensions in Table 2, thus translating the predicted positions of the subsequent layers. Auger and ESCA data are currently being obtained to substantiate this hypothesis. If the GaAs cap is .475 microns thick (translation of .175 Angstroms), then the proposed energy positioning of the AlGaAs/GaAs and p-n junction interfaces is as shown in Figure 13. The troughs of 1053 can then be explained in terms of the previous arguments applied to

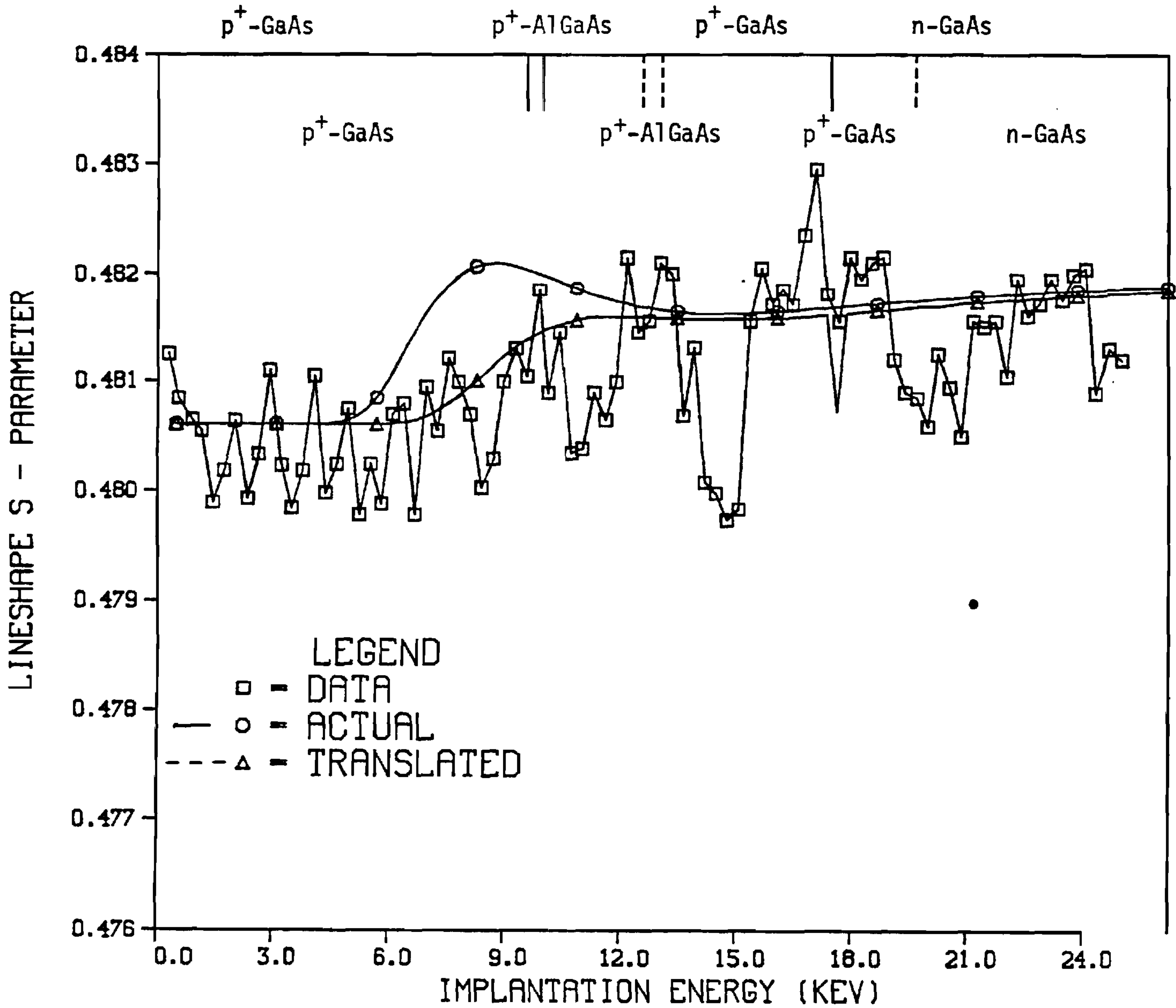

Figure 13. Lineshape parameter, S(E), as a function of incident energy, E, for MOCVD Run #1053 averaged over two profiles of the same specimen.

the 872 specimens: band bending, differential diffusion lengths across an interfacial trap, and the absence of electrically active defects.

2.3 Measurements and Analyses on Additional Device Structures

2.31 LPE-Grown GaAs Heteroface Solar Cells

LPE-grown p^{+}-n GaAs heteroface solar cell structures were obtained from Hughes Research Labs. The device structure, Figure 14 was mesa etched to provide isolation for electrical characterization. DLTS was successfully performed, identifying a hole trap in the n-GaAs base located 0.57 eV above Ev with a trap density of 3.5 X $10^{14}cm^{-3}$ as shown in Figure 15. Depth-resolved SPV measurements were attempted but were not successful due to the presence of contact grid and antireflection coating which were not possible to remove without damaging the underlying device structure.

2.32 LPE-Grown AlGaAs Layers on GaAs

Some properties of LPE-grown AlGaAs films on GaAs were studied as a function of Al content. Two target Al mole fractions, 0.20 and 0.38 were used for this study. Figure 16 shows SPV data for each film from which the bandgap values were found to be 1.97 eV and 1.71 eV, correlating well with the desired 0.38 and 0.20 compositions, respectively. The difference in response size can be attributed to both the difference in absorption coefficient (α) since $\alpha \sim (hf - Eg)^{1/2}$, and a smaller diffusion length in the higher bandgap AlGaAs due to a higher degree of alloy scattering. Free carrier effects were not a factor in the SPV variation since the doping profiles of each film were almost identical as determined by the depth-resolved C-V electrochemical profile data in Figure 17.

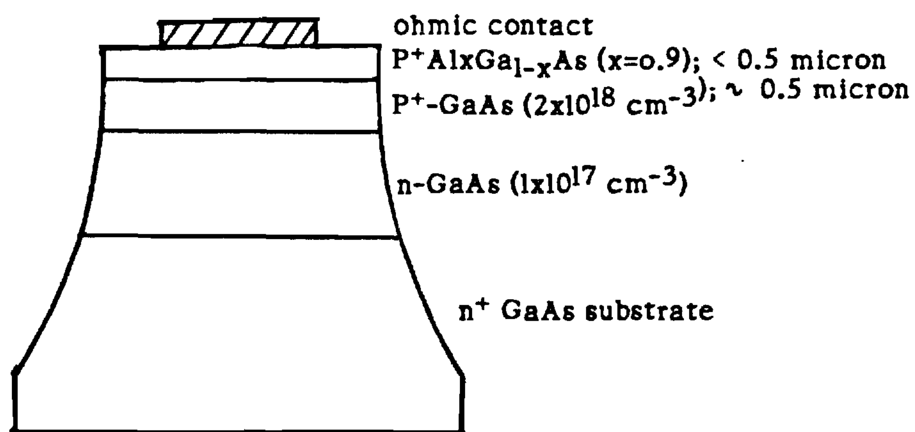

Figure 14. Hughes Mesa Diode Structure used for DLTS Measurements

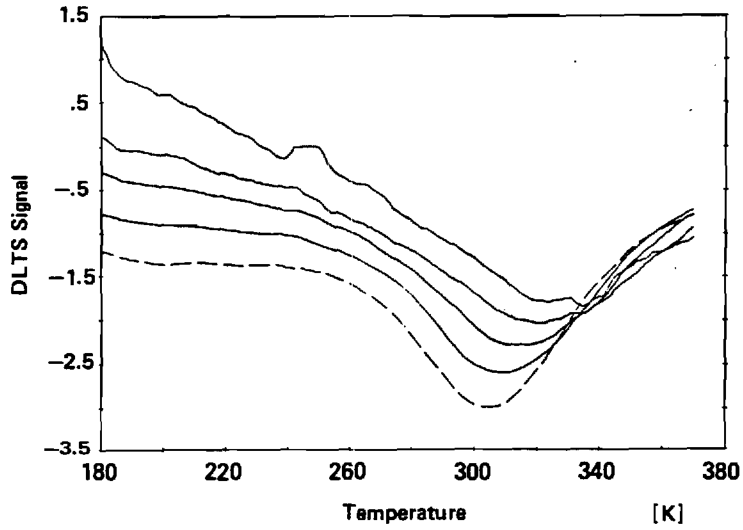

DLTS Spectrum for Hughes Mesa Diode

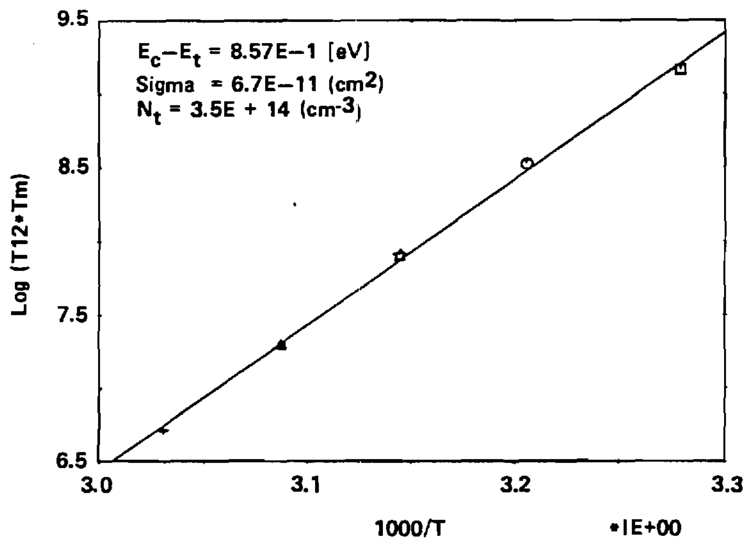

Arrhenius Plot for Deep Level Indicated in DLTS Spectrum

Figure 15. DLTS Spectrum for Hughes Mesa diode (a) and associated Arrhenius Plot (b) for deep level.

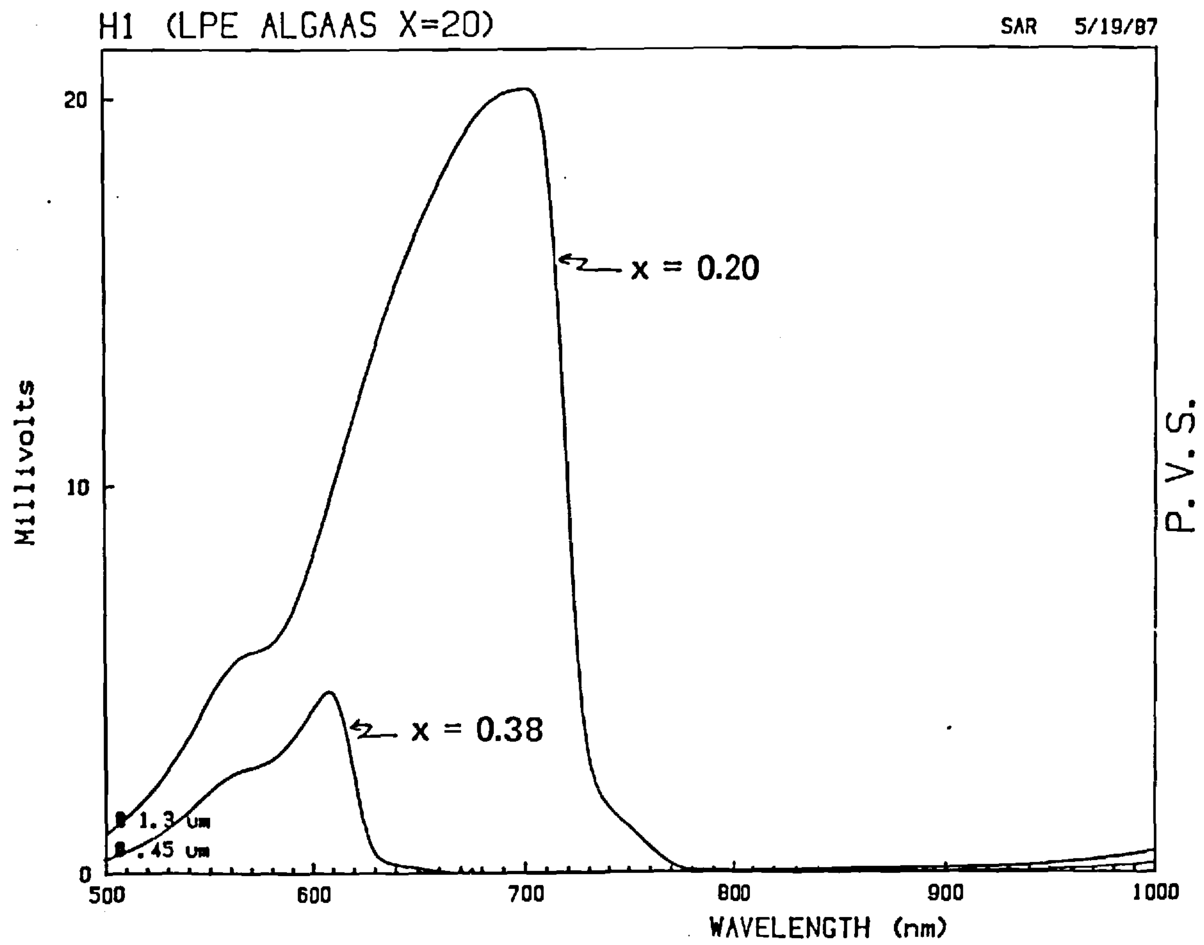

Figure 16. Photovoltage spectra for x = 0.20 and x = 0.38 $Al_xGa_{1-x}As$

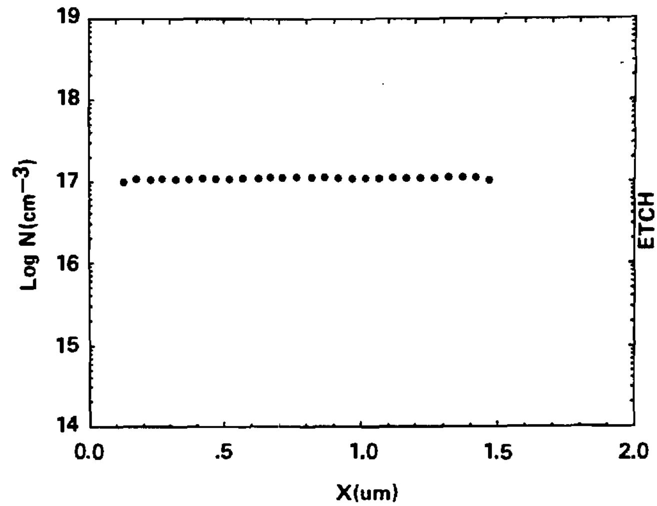

(a)

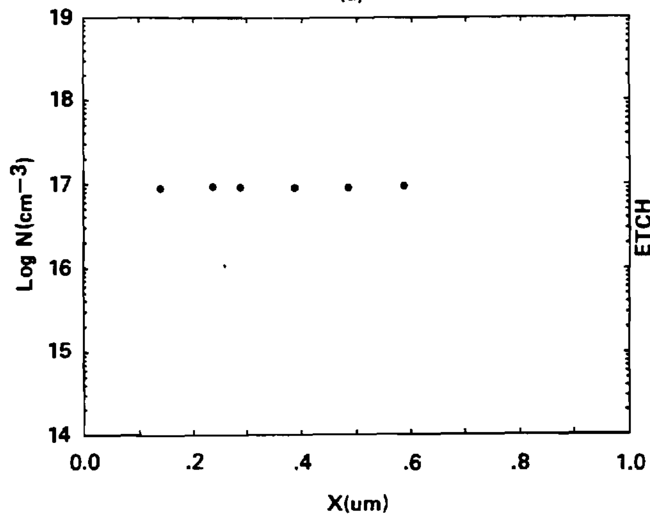

(b)

Figure 17. Dopant profiles as determined by the Polaron PN4200 Electrochemical Profiler for a) x = 0.20 and b) x = 0.38 AlGaAs.

3. CONCLUSIONS

A high efficiency, MOCVD grown, GaAs p-n heteroface solar cell has been characterized in order to understand loss mechanisms and optimized its design through extensive computer modeling. Recombination mechanisms were studied using dark I-V, I-V-T, and DLTS measurements which revealed a hole trap at E_v + 0.912 eV for being responsible for the space charge component of the leakage current. Depth-resolved DLTS and SPV measurements were performed to establish that this level was spatially localized near the p-n interface. Although the observed deep level does not effect J_{o1}, it still degrades the cell performance by making the J_{o2} component comparable to the J_{o1} component at the cell operating pont.

Additional defect profiling was accomplished nondestructively using SPAS. It has been shown that SPAS has potential as a profiling tool for high quality epitaxial films and interfaces. The SPAS experimental data provides a profile of distributed material defects that has a strong correlation to SPV results. Also, SPAS appears to possess the capability of performing a three-dimensional characterization of multiple layered structures, as indicated by the differentiation of wafer edge effects resulting from nonuniform film growth temperatures. Finally, SPAS appears to be sensitive to strong localized electric field regions at the AlGaAs/GaAs heterojunctions and the p-n homojunctions.

The internal recombination parameters (lifetime, J_{o1}, FSRV, BSRV) were determined by simulatenously matching the measured and simulated spectral response, J_{01}, and cell data (J_{sc}, V_{oc}, efficiency) with the help of PC-1D and effective recombination velocity models. It was found that a front surface

recombination velocity of 1.25 X 10^5cm/s and a net base lifetime of 8 ns were required to match the cell data. These values were further verified by a good match between the measured and calculated values of J_{o1} using the above FSRV and lifetime profile as inputs to the effective recombination velocity model. This model also gave the emitter and base components of J_{o1} which showed that the base exerted primary control over the leakage current, accounting for ~67% of the total J_{o1}.

Having matched the cell under investigation, guidelines were provided to optimize this structure. For the device studied here, the efficiency can be increased from 21.2% to over 24% by improved front surface passivation (FSRV ~1 X 10^4 cm/s) and base material quality (τ_o = 15 ns). Further efficiency improvement can be realized by thinning the base so that the buffer becomes an active part of the device, forming essentially a two-step base. This structure, however, requires back surface passivation to maximize cell efficiency. This device structure, with a net base lifetime of 20 ns, can result in efficiencies in excess of 25%.

4. REFERENCES

1. R. J. Nelson and R. G. Sobers, "Minority-carrier lifetime and internal quantum efficiency of surface-free GaAs," Appl. Phys., vol. 49, no. 12, pp. 6103-6108, 1978.

2. C. J. Hwang, "Doping dependence of hole lifetime in n-type GaAs," J. Appl. Phys., vol. 42, no. 11, pp. 4408-4413, 1971.

3R. J. Nelson, "Interfacial recombination in GaAlAs-GaAs heterostructures," J. Vac. Sci. Technol., vol. 15, no. 4, pp. 1475-1477, 1978.

4. P. Dawson and K. Woodbridge, "Effects of prelayers on minority-carrier lifetime in GaAs/AlGaAs double heterostructures grown by molecular beam epitaxy," Appl. Phys. Lett., vol. 45, no. 11, pp. 1227-1229, 1984.

5. J. M. Woodall and J. L. Freeouf, J. Vac. Sci. Technol., vol. 19, p. 794, 1981.

6. P. D. DeMoulin, C. S. Kyono, M. S. Lundstrom, and M. R. Melloch, "Dark I/V characterization of GaAs p.n heteroface cells, Proc. of Nineteenth IEEE Photovoltaic Specialits Conf., pp. 93-97, 1987.

7. P. D. DeMoulin and M. S. Lundstrom, "Theoretical comparison of conventional and unconventional GaAs cell design," Proc. of Nineteenth Photovoltaic Specialists Conf., pp. 925-930, 1987.

8. M. S. Lundstrom, "Device physics of crystalline solar cells," presented at Eight Photovoltaic Advanced Res. Dev. Project Rev. Meeting, Nov. 1987.

9. P. Blood, "Measurement of optical absorption in epitaxial semiconductor layers by a photovoltage method," J. Appl. Phys., vol. 58, no. 6, pp. 2288-2295, 1985.

10. D. K. Schroder, "The concept of generation and recombination lifetimes in semiconductors," IEEE Trans. Electron. Dev., vol. ED-29, no. 8, pp. 1336-1338, 1982.

11. K. W. Loh, D. K. Schroder, R. C. Clarke, A. Rohatgi, and G. W. Eldridge, "Low leakage current GaAs diodes," IEEE Trans. Electron Dev., vol. ED-28, no. 7, pp. 796-800, 1981.

12. A. S. Grove, "Physics and technology of semiconductor devices," Wiley, New York, 1967.

13. D. Rover, P. Basore, and G. Thorson, "Solar cell modeling on personal computers," Conf. Proc. of the Eighteenth Photovoltaic Spec. Conf., Las Vegas, Oct. 1985.

14. C. J. Hwang, Phys. Rev. B., vol. 6, pp. 1355-1359, 1972.

15. A. Haug, "Auger recombination in direct-gap semiconductors: band structure effects," J. Phys. C: Solid State Phys., vol. 16, pp. 4159-4172, 1983.

16. J. S. Blakemore, "Semiconducting and other major properties of gallium arsenide," J. Appl. Phys., vol. 53, no. 10, pp. R123-R181, 1982.

17. A. Rohatgi and P. Rai-Choudhury, "Design, fabrication and analysis of 17-18 percent efficient surface-passivated silicon solar cells," IEEE Trans. Electron Dev., vol. ED-31, no. 5, pp. 596-601, 1984.

18. P. J. Schultz, K. G. Lynn, W. E. Frieze, and A. Vehanen, Phys. Rev. B, 27, 6626, 1983.

19. A. Vehanen, T. Makinen, P. Hautojarvi, H. Huomo, T. Lahtinen, R. M. Nieminen, and S. Valkealhti, Phys. Rev. B, vol. 32, pp. 7561, 1985.

20. K. G. Lynn, D. M. Chen, B. Nielsen, R. Pareja, and S. Myers, Phys. Rev. B, vol. 34, pp. 1449, 1986.

21. A. Vehanen, P. Huttunen, T. Mikenen, and P. Hautojarvi, J. Vac. Sci. Technolo. A, vol. 5, pp. 1142, 1987.

22. B. Nielsen, K. G. Lynn, Y. C. Chen, and D. O. Welch, Appl. Phys. Lett., vol. 51, pp. 1022, 1987.

23. A. Vehanen, K. Saarinen, P. Hautojarvi, and H. Huomo, Phys. Rev. B, vol. 35, pp. 4606, 1987.

24. I. K. MacKenzie, J. A. Eady, and R. R. Gingerich, Phys. Let., vol. 33A, no. 5, pp. 279, 1970.

25. K. G. Lynn, B. Neilsen, and T. H. Quateman, Appl. Phys. Lett., vol. 47, pp. 239, 1985.

26. S. A. Ringel, A. Rohatgi, and S. P. Tobin, in preparation.

27. S. A. Ringel and A. Rohatgi, in preparation.

28. S. P. Tobin, private communication.

5. ACKNOWLEDGEMENTS

The authors would like to thank Steve Tobin of Spire Corporation and Bob Loo of Hughes Research Labs. for their helpful discussions and samples, and Jim Welch of Georgia Tech, MRC, for assistance in the computer modeling, A. B. Dewald and Robert Frost for PAS measurements and analysis, B. Neilson and K. G. Lynn of Brookhaven National Labs for the help in SPAS measurements, and James Gee of Sandia Labs for the valuable discussions and help in arranging the samples.